

1-1-1986

# The influence of drying on the structure and mechanics of poly (p-phenylene benzobisthiazole) fibers/

Lorelle A. Pottick

*University of Massachusetts Amherst*

Follow this and additional works at: [https://scholarworks.umass.edu/dissertations\\_1](https://scholarworks.umass.edu/dissertations_1)

---

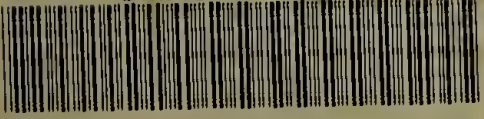
## Recommended Citation

Pottick, Lorelle A., "The influence of drying on the structure and mechanics of poly (p-phenylene benzobisthiazole) fibers/" (1986).  
*Doctoral Dissertations 1896 - February 2014*. 704.  
[https://scholarworks.umass.edu/dissertations\\_1/704](https://scholarworks.umass.edu/dissertations_1/704)

This Open Access Dissertation is brought to you for free and open access by ScholarWorks@UMass Amherst. It has been accepted for inclusion in Doctoral Dissertations 1896 - February 2014 by an authorized administrator of ScholarWorks@UMass Amherst. For more information, please contact [scholarworks@library.umass.edu](mailto:scholarworks@library.umass.edu).



UMASS/AMHERST



312066007000041



THE INFLUENCE OF DRYING ON THE STRUCTURE AND MECHANICS  
OF POLY (P-PHENYLENE BENZOBISTHIAZOLE) FIBERS

A Dissertation Presented

By

LORELLE ANN POTTICK

Submitted to the Graduate School of the  
University of Massachusetts in partial fulfillment  
of the requirements for the degree of

DOCTOR OF PHILOSOPHY

February 1986

Polymer Science and Engineering

© Lorelle Ann Pottick September 1985

All Rights Reserved

AFWAL/MLBP

Contract No.  
F33615-82-K-5068  
F33615-83-K-5001



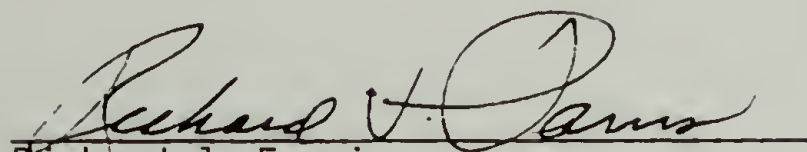
THE INFLUENCE OF DRYING ON THE  
STRUCTURE AND MECHANICS OF  
POLY(P-PHENYLENE BENZOBISTHIAZOLE) FIBERS

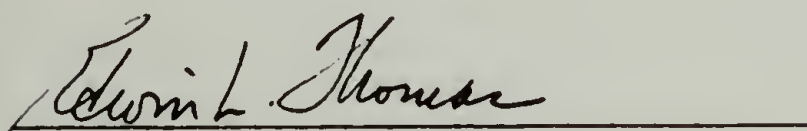
A Dissertation Presented

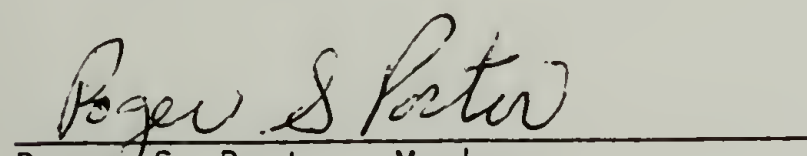
By

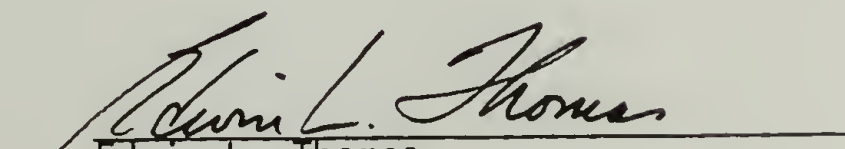
Lorelle Ann Pottick

Approved as to style and content by:

  
Richard J. Farris  
Chairperson of Committee

  
Edwin L. Thomas, Member

  
Roger S. Porter, Member

  
Edwin L. Thomas  
Department Head  
Polymer Science and Engineering  
Department

Date 9/20/85

To my sisters, Fran and Kathy,  
whose inspiration and love gave  
me the perseverance to attain  
this seemingly insurmountable  
goal.

## ACKNOWLEDGEMENTS

Mere words cannot adequately express my gratitude to Professor Richard Farris. As my advisor, he has not only introduced me to and guided me in the area of polymer mechanics, but has instilled in me a sense of confidence and intuition that will remain with me as I continue in my scientific endeavors. His appreciation of my work has enabled me to pursue this research with much enthusiasm, and I am very thankful for his continued support.

Professors Edwin Thomas and Roger Porter deserve special recognition as members of the dissertation committee. In addition to their continual advice and discussions, they, along with Professor Farris, have provided me with a sense of what it takes to succeed in this field. A special thanks is extended to Professor Thomas for the many additional discussions on the morphological aspects of this project. His commitment to this research was clearly beyond the responsibility of a committee member.

I would like to thank my dear friend and colleague Steven Allen for introducing me to the field of polymer mechanics. His instructions and advice as well as his friendship were invaluable.

Much of the research herein resulted from many fruitful discussions with my colleagues, most notably W. Wade Adams and Yachin Cohen. Both men provided considerable input on the morphological aspects of this work. I extend my thanks for their advice and support.



My sincere appreciation is extended to: Barbara Wood and Lori Colangelo for "experiencing" the writing of this dissertation chapter by chapter as well as their friendship; Ellen Rubinstein for making this work more enjoyable through her friendship; Norm Page and Richard Zisk for their technical support on numerous occasions; Dianne Peterson for her patience in the typing and retyping of this manuscript; and . . . my family, for their love and support from the beginning to the end.

## ABSTRACT

### The Influence of Drying on the Structure and Mechanics of Poly (p-phenylene benzobisthiazole) Fibers

(February 1986)

Lorelle Ann Pottick, B.A. University of Rochester

M.S., Ph.D., University of Massachusetts

Directed by: Professor Richard J. Farris

A study of the influence of the drying process in developing fiber properties during the dry-jet wet spinning of poly (p-phenylene benzobisthiazole) is undertaken. The fiber's structure and mechanical characteristics from the coagulated state through the drying process to the as-spun and heat treated state are investigated herein.

The wet fiber is composed of a swollen macro and microfibrillar network of highly oriented molecules with lateral but no longitudinal order and exhibits a high degree of mechanical anisotropy. The structural and mechanical features of the as-spun fiber appear to develop during coagulation.

The drying process during drying is characterized by a distinct radial contraction and axial elongation due to the porous and anisotropic nature of the coagulated fiber. Alterations in the structure and mechanics of PBT fibers are observed upon drying which is rationalized in terms of the collapse process. The drying process is a fiber modification phase.

High temperature and tension are employed to optimize the driving force toward property enhancement during the drying stage. Tension during drying straightens the wet fibrillar network while offsetting axial compressive internal stresses whereas the use of high temperature increases the extent of the lateral molecular order and increases molecular orientation resulting in enhanced tensile properties.

The compressive strength and shear modulus increase after drying suggesting that removal of water may serve to enhance lateral interactions within the swollen fibrillar network inhibiting shear and compressive deformation and the onset of buckling instabilities. Further increases in the compressive strength through high tension and temperature drying are not achieved since further enhancements in intermicrofibrillar and fibrillar associations are speculated to be minimal.

A force-temperature (F-T) technique is implemented to study thermal expansion characteristics of these rigid rod aromatic fibers through examination of the reversible F-T behavior. Subsequent mass loss and microstructural changes during the F-T experiment (an effective post processing heat treatment) is detected from irreversible F-T effects. An assessment of the effectiveness of the initial drying and heat treatment processing to induce thermal stability and material alterations is obtained through this F-T technique.



## TABLE OF CONTENTS

ACKNOWLEDGEMENTS . . . . .	v
ABSTRACT . . . . .	vii
LIST OF TABLES . . . . .	xi
LIST OF FIGURES . . . . .	xii
Chapter	
I. INTRODUCTION . . . . .	1
1.1 High Performance Fibers: A Chemical and Engineering Approach . . . . .	1
1.2 Fundamental Aspects of Fiber Formation During Solution Wet Spinning . . . . .	8
1.2.1 Coagulation Process in Flexible Chain Polymers . . . . .	8
1.2.2 Drying Process in Flexible Chain Polymers . . . . .	11
1.2.3 Post Processing Heat Treatment . . . . .	13
1.3 Rigid Rod Aromatic Fibers: Processing and Properties . . . . .	13
1.4 Dissertation Overview . . . . .	18
II. COAGULATED FIBER PROPERTIES: THE COLLAPSE PROCESS: MODIFICATIONS DURING DRYING . . . . .	21
2.1 Introduction . . . . .	21
2.2 Fiber Production . . . . .	21
2.3 Experimental . . . . .	25
2.3.1 Fiber Collapse Characterization . . . . .	25
2.3.2 Morphology Characterization . . . . .	26
2.3.3 Mechanics . . . . .	30
2.4 Wet Fiber Properties . . . . .	35
2.4.1 Morphology . . . . .	35
2.4.2 Mechanics . . . . .	44
2.5 Collapse Process . . . . .	53
2.5.1 Observations . . . . .	53
2.5.2 Molecular Considerations . . . . .	57
2.6 Fiber Property Alterations During Drying . . . . .	60
2.6.1 Structure . . . . .	60
2.6.2 Mechanics . . . . .	62
2.7 Shrinkage Behavior in a Cylindrically Orthotropic Material . . . . .	78
2.8 Summary and Conclusions . . . . .	93

III.	HIGH TENSION AND TEMPERATURE DRYING: POST PROCESSING HEAT TREATMENT INVESTIGATIONS . . . . .	96
3.1	Introduction . . . . .	96
3.2	Experimental . . . . .	97
3.3	Room Temperature Drying . . . . .	102
3.4	Elevated Temperature Drying . . . . .	127
3.5	Post Processing Heat Treatment Investigations . . . . .	138
3.6	Conclusions . . . . .	148
IV.	FORCE TEMPERATURE BEHAVIOR OF RIGID ROD POLYMERIC FIBERS . .	154
4.1	Introduction . . . . .	154
4.2	Experimental . . . . .	156
4.2.1	F-T Design and Procedures . . . . .	156
4.2.2	Fiber Physical and Mechanical Characterization . . . . .	157
4.2.3	Fiber Denier Characterization . . . . .	160
4.3	Reversible Thermal Elastic Behavior . . . . .	163
4.4	Irreversible Thermal Elastic Behavior . . . . .	174
4.5	Force-Temperature Processing Correlations . . . . .	188
4.6	Conclusions . . . . .	199
V.	CONCLUDING REMARKS AND RECOMMENDATIONS . . . . .	203
5.1	Overview . . . . .	203
5.2	Coagulation Process . . . . .	204
5.3	Drying Process . . . . .	205
5.4	Post Processing Heat Treatment . . . . .	211
5.5	Summary . . . . .	213
. . . . .		
	REFERENCES . . . . .	214
	BIBLIOGRAPHY . . . . .	222
	APPENDIX. LIST OF PUBLICATIONS . . . . .	230

## LIST OF TABLES

1.	Comparison between tensile moduli as theoretically calculated and experimentally determined for various synthetic high modulus/high strength fibers . . . . .	6
2.	Spinning conditions for PBT fibers . . . . .	24
3.	Mechanical properties of wet PBT fibers . . . . .	47
4.	Strain hardening effects versus spin draw ratio of wet PBT fibers . . . . .	50
5.	Diameter changes for various PBT fibers due to the drying Process . . . . .	55
6.	Air dried collapse of PBT coagulated by various non-solvents . . . . .	58
7.	Wide angle x-ray diffractometer data: Wet versus dry PBT . . . . .	61
8.	A comparison between the tensile properties of wet versus dry PBT fibers . . . . .	65
9.	Comparison between the strain hardening behavior of wet versus dry PBT at 1% strain . . . . .	70
10.	Torsion and compressive properties of wet and dry PBT fibers . . . . .	72
11.	Compliance coefficients and shrinkage behavior for various wood types . . . . .	89
12.	Tensile properties for differently drawn PBT fibers dried under various tensions . . . . .	106
13.	Strain hardening effects of the coagulated PBT fibers . . . . .	110
14.	Strain hardening behavior of PBT fiber (I) . . . . .	114
15.	Mechanical properties of PBT fibers dried at room temperature . . . . .	121
16.	Strain hardening effects of wet vs. dry PBT fiber (I) . . . . .	124
17.	Comparison of PBT fibers (VA) dried under various tensions at room temperature . . . . .	126
18.	Tensile properties of PBT fibers continuously dried at various temperatures . . . . .	131
19.	Transverse properties of PBT fibers (VB) dried at various temperatures . . . . .	136
20.	Comparison between the tensile properties of a "heat treated" wet and dry PBT fiber (VB) . . . . .	139
21.	Comparison between the transverse properties of a "heat treated" wet and dry PBT fiber (VB) . . . . .	143
22.	Summary of heat treated properties of tension versus non-tension room temperature dried fibers (VB) . . . . .	144
23.	Summary of heat treated properties of elevated temperature dried fibers (VB) . . . . .	146
24.	Overview of properties during PBT fiber spinning process . . . . .	151
25.	Compliance and thermal expansion coefficients for model single crystal graphite fibers . . . . .	173
26.	WAXS diffractometric data of as-spun PBT yarn . . . . .	180
27.	Mechanical properties of PBT and Kevlar <sup>R</sup> 29 before and after force temperature cycling . . . . .	181
28.	Calculated thermal expansion coefficients for differently processed PBT Fiber VB . . . . .	200
29.	Shear characteristics versus diameter size for PBT fiber . . . . .	210



## LIST OF FIGURES

1.	A comparison of specific tensile properties for various materials . . . . .	2
2.	Rod-like aromatic polymers . . . . .	4
3.	Schematic diagram of dry-jet wet spinning process . . . . .	23
4.	Experimental design for axial displacement measurement during drying . . . . .	28
5.	Schematic diagram of the torsion pendulum apparatus for wet PBT fibers . . . . .	32
6.	Mounting of hollow fibers for compression tests . . . . .	34
7.	Wide angle x-ray diffraction patterns of (1) wet PBT fiber, (2) water, (3) schematic of wet PBT fiber diffraction pattern without water scattering, (4) dry PBT fiber . . . . .	38
8.	Scanning electron micrograph of a critical point dried PBT fiber . . . . .	41
9.	Structural model for the coagulated (wet) PBT fiber . . . . .	43
10.	Typical stress-strain curve for wet PBT fiber . . . . .	45
11.	Tensile moduli for wet PBT fibers at different spin draw ratios . . . . .	48
12.	Relative enhancement in tensile moduli upon a 1% strain deformation for wet PBT fibers at different spin draw ratios . . . . .	51
13.	Radial changes for a PBT fiber during drying . . . . .	54
14.	Axial changes for a PBT fiber during drying . . . . .	56
15.	Typical stress-strain curves for wet vs. dry PBT fiber (I) . . . . .	63
16.	Typical force-strain curves for wet vs. dry PBT fiber (I) . . . . .	64
17.	Enhancement in tensile moduli as determined from the force deflection curves upon drying for PBT fibers of different spin draw ratios . . . . .	67
18.	Representation of a fibril before and after the fiber's collapse . . . . .	68
19.	Compressive force-strain behavior for hollow wet versus dry PBT fibers . . . . .	73
20.	Representation of a PBT fiber composed of 3 and 7 fibrils in the wet and dry state . . . . .	76
21.	Predicted radial, longitudinal and hoop stress distribution after unrestrained drying . . . . .	91
22.	Schematic diagram of PBT fiber drying apparatus . . . . .	99
23.	Typical stress-strain curves for as-spun PBT fiber (I): (A) tension dried (300 MPa); (B) tension dried (30 MPa); (C) non-tension dried . . . . .	103
24.	Tensile moduli of PBT fibers dried at various tensions at room temperature . . . . .	104
25.	Yield stresses of PBT fibers dried at various tensions at room temperature . . . . .	105
26.	WAXD patterns for PBT Fiber I: (a) non tension dried; (b) tension dried . . . . .	109

27.	Stress-strain curve displaying strain hardening effects for a non-tension room temperature dried PBT fiber . . . . .	112
28.	Stress-strain curve displaying strain hardening effects for a tension room temperature dried PBT fiber . . . . .	113
29.	Scanning electron micrographs of a non-tension dried fiber displaying surface undulations and a tension dried fiber void of dry buckling defects . . . . .	116
30.	Schematic representation of axial internal stress distribution during and after tension drying . . . . .	118
31.	Stress-strain behavior for PBT fiber I: (a) non-tension dried, (b) non-tension dried then subsequently tensioned, (c) tension dried . . . . .	120
32.	WAXD patterns of PBT Fiber I: (a) non-tension dried, (b) non-tension dried then subsequently tensioned, (c) tension dried . . . . .	123
33.	Typical stress-strain curves for PBT fibers (VA) dried at 150°C, 320°C and 500°C at (a) 45 MPa tension applied, (b) 440 MPa tension applied . . . . .	130
34.	Comparison of the stress strain behavior for PBT fibers (VA) dried under 45 MPa (minimal) tension at (a) 25°C, (b) 150°C, (c) 320°C, (d) 500°C . . . . .	132
35.	Comparison of the stress-strain behavior of PBT fibers (VA) dried under 440 MPa tension at (a) 25°C, (b) 150°C, (c) 320°C, (d) 500°C . . . . .	133
36.	Shear moduli and compressive strengths for PBT fibers (VB) dried at various temperatures . . . . .	137
37.	Scanning electron micrographs of a PBT fiber (VB) (A) dried at 320°C and (B) heat treated at 320°C . . . . .	142
38.	Thermal gravimetric behavior for (A) as-spun PBT fiber, (B) tension heat treated PBT fiber (800 MPa; 500°C) . . . . .	147
39.	Schematic diagram of force-temperature experiment . . . . .	159
40.	Schematic diagram of the force-temperature/denier-temperature apparatus . . . . .	162
41.	Force versus temperature profile for steel yarn . . . . .	164
42.	Stress-temperature profiles for tension heated treated PBT and Kevlar <sup>R</sup> 49 yarns (650°C) . . . . .	166
43.	Stress-temperature profiles for Kevlar <sup>R</sup> 49 yarn 24 hours after the first heating cycle . . . . .	167
44.	Lateral motion of an atom in an inextensible chain . . . . .	169
45.	Stress-temperature profile for as-spun PBT yarn . . . . .	175
46.	Stress-temperature profile for Kevlar <sup>R</sup> 29 yarn . . . . .	176
47.	Wide angle x-ray diffraction patterns of: (A) Kevlar <sup>R</sup> 29, (B) FTC-Kevlar <sup>R</sup> 29, (c) Kevlar <sup>R</sup> 49 . . . . .	179
48.	A comparison between force-temperature, denier temperature and thermal gravimetric profiles for as-spun PBT Fiber V . . . . .	184
49.	A comparison between the force-temperature, denier temperature and thermal gravimetric profiles for tension heat treated (800 MPa, 500°C) PBT Fiber V . . . . .	186

50.	Temperature of onset of stress drop, $T_T$ , versus applied stress during the F-T experiment . . . . .	189
51.	Typical stress-temperature profiles for PBT fiber dried at room temperature (A) no tension, (B) 40 MPa tension, (C) 800 MPa tension . . . . .	191
52.	Typical stress-temperature profiles for PBT fibers dried under minimal load at various temperatures . . . . .	192
53.	Typical stress-temperature profiles for PBT fibers initially non-tension dried then heat treated at 320°C and 500°C . . . . .	194
54.	Typical stress-temperature profiles for PBT fibers initially non tension dried then tension (800 MPa) heat treated at 320°C and 500°C . . . . .	195
55.	Typical stress-temperature profiles for PBT fibers (A) non-tension dried 320°C, (B) heat treated 320°C with no tension . . . . .	197
56.	Typical stress-temperature profiles for PBT fibers (A) non-tension dried 500°C, (B) heat treated 500°C with no tension . . . . .	198



# C H A P T E R I

## INTRODUCTION

### 1.1 High Performance Fibers: A Chemical and Engineering Approach

The technology of man-made fibers has been advancing since the first fibers based on modified cellulose were developed at the end of the 19th century. Recent advances in fiber science have focused on high modulus/high strength polymeric fibers with engineering properties comparable to structural metals (1-4). The specific tensile properties (per weight basis) for both organic fibers and materials such as steel and glass are compared in Figure 1. The organic fibers show superior properties revealing the potential advantage in using these materials where weight is of primary concern.

The molecular basis of high modulus/high strength behavior is the attainment of extended chain configurations along the polymer backbone. High performance fibers have been developed through both novel synthetic and fiber formation processes. Various processing techniques have been used to extend flexible chain polymers by either pulling out the folds in a polymer in a post extrusion process or by increasing the ratio of extended chain to folded chain polymer as the fiber forms from a flowing solution. Techniques such as solid state drawing (5), solid state extrusion (6), and gel spinning (7,8) have been used successfully to obtain high modulus properties (70-100 GPa) from flexible chain polymers. More recently, a combination of solid state extrusion followed by

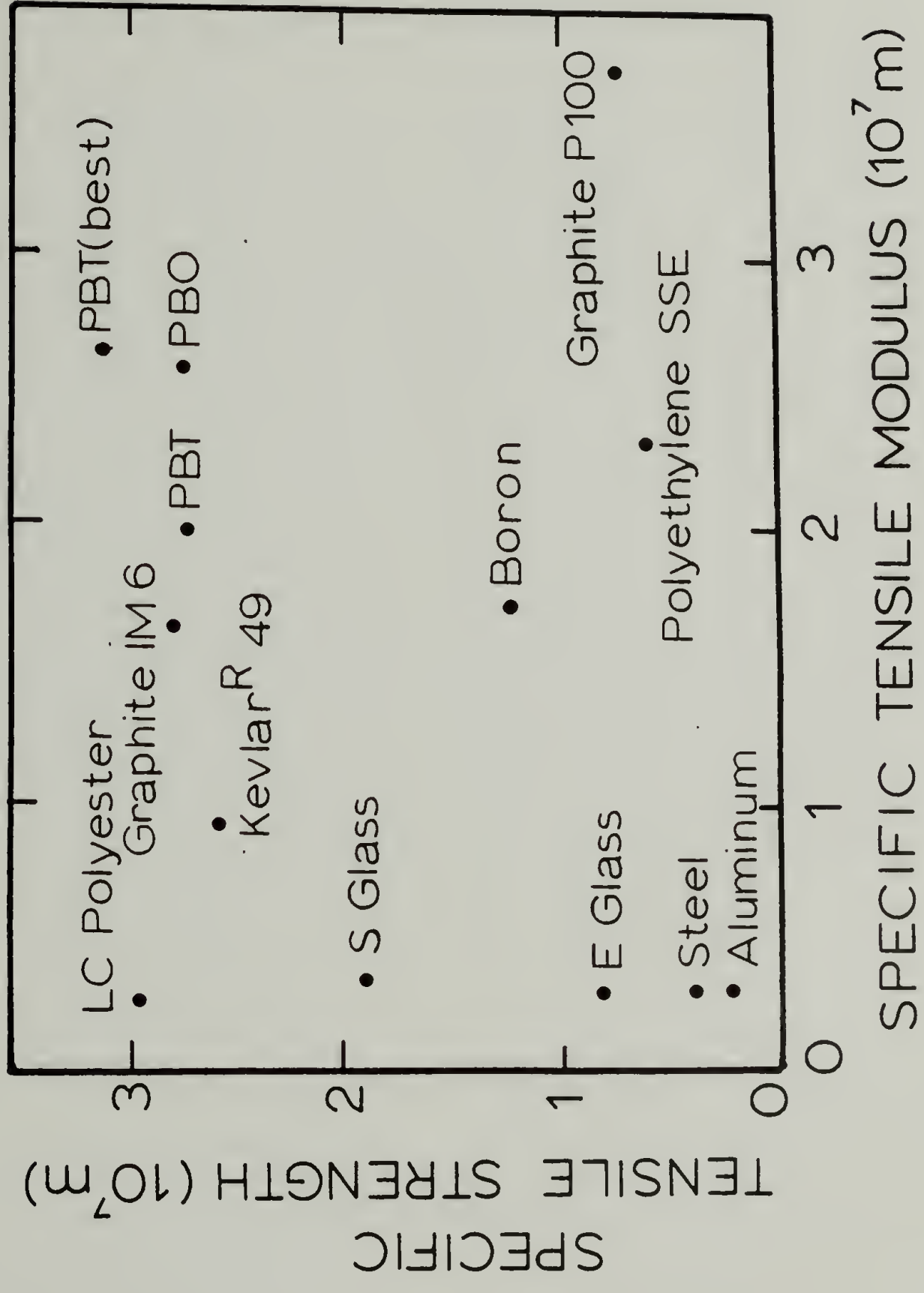


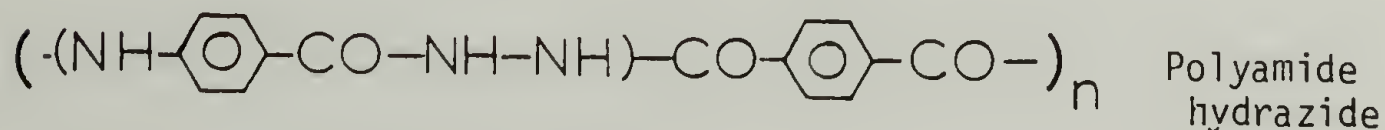
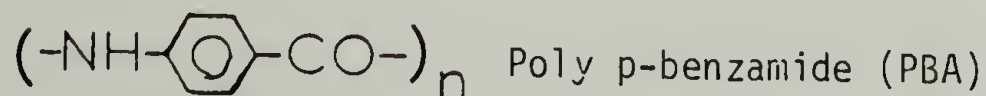
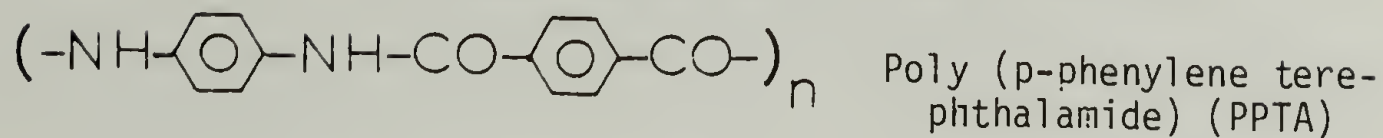
Figure 1. A comparison of specific tensile properties for various materials

tensile drawing has resulted in a draw ratio for polyethylene (PE) of 250 with a tensile modulus of 220 GPa (9).

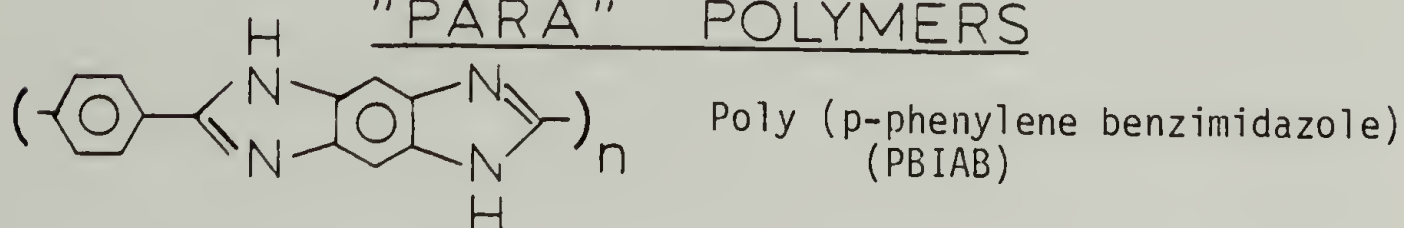
An alternative approach to attain extended chain polymers is to synthetically tailor their molecular architecture. By constructing linear stiff chain polymers which are sufficiently rigid due to steric hinderances along the backbone, chain folding becomes impossible. High molecular weight rigid rod aromatic polymers such as poly (p-phenylene terephthalamide) (PPTA/Kevlar<sup>R</sup>) (10), poly (p-benzamide) (11), and polyamide hydrazide (X-500) (12,13) have been successfully developed for high modulus and high strength materials. Another class of rodlike polymers, the "ladder" polymers and the "para" polymers (Figure 2) (14-18) have been synthesized for the Air Force Ordered Polymers Research Program (19). For these polymers, the condensation linkage imparts no flexibility of the type possible with amide or hydrazide linkages. As a result, high temperature resistant ultra high modulus fibers are obtained from these "ladder" and "para" polymers.

There has been a tremendous effort to adequately process these stiff chain aromatic polymers to maximize their potential as high performance materials. Since these rodlike polymers thermally decompose before they melt, the fibers must be spun from solution. During this process, the polymer is dissolved in a solvent and solidification occurs upon removal of the solvent. Solvents which are volatile can be removed by an evaporative process (solution dry spinning). The solvents for rigid rod molecules are not sufficiently volatile to be evaporated. Hence, solution wet spinning whereby the solvent is extracted by a non

## AROMATIC POLYAMIDES



## "PARA" POLYMERS



## "LADDER" POLYMER

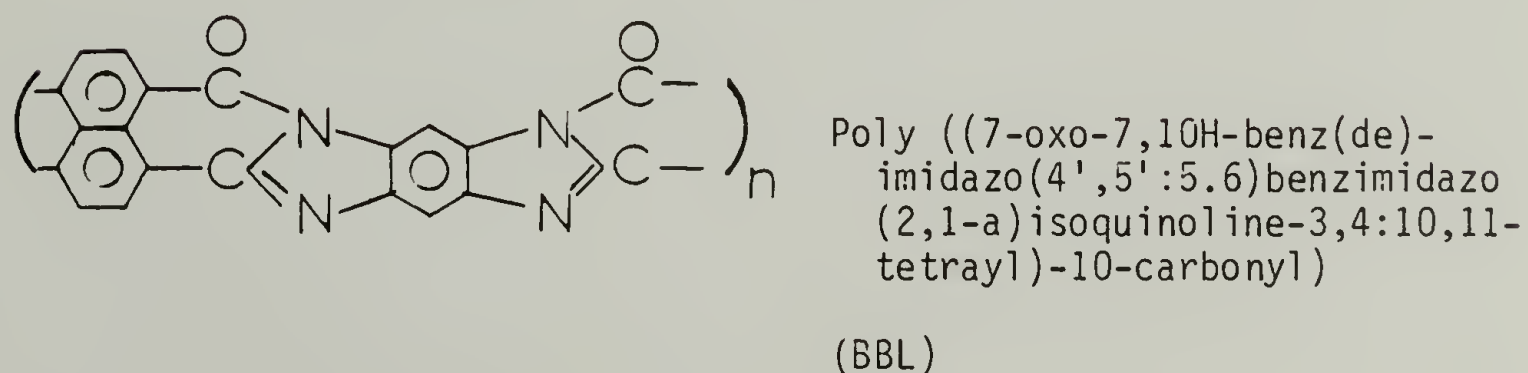


Figure 2. Rod-like aromatic polymers



solvent is the preferred process. After coagulation (the solidification process) the fiber is washed, subsequently dried and possibly heat treated.

The wet spinning of wholly para-oriented aromatic polymer solutions was first successfully done by researchers at Monsanto (20) and Dupont (21). Polyamide hydrazide fiber, spun from an isotropic solution, resulted in the attainment of a tensile modulus of 100 GPa with strengths over 2.5 GPa. In contrast to the spinning of X-500 fibers, anisotropic solutions of PPTA were used to spin Kevlar<sup>R</sup>. To further improve the orientation of the polymer chain in the spinning of Kevlar<sup>R</sup>, a dry-jet wet spinning process was developed by Blades (21,22). This process allows for the solution to be oriented as it is stretched in an air gap prior to coagulation. Fiber tensile moduli up to 124 GPa with strengths over 2.7 GPa are typical for commercial PPTA (Kevlar<sup>R</sup>) fibers (23).

Rigid rod heterocyclic polymers (PBO; PBT; PBIAB) have similarly been dry jet wet spun by Choe et al. and Chenevey et al. (17,24). These materials have been successfully spun from the polymerization medium, poly (phosphoric acid) (PPA) as well as from methane sulfonic acid (MSA). Tensile strengths over 3 GPa and tensile moduli as high as 300 GPa have been reported (25).

At present, the final fiber properties achieved for rigid rod aromatic fibers do not compare favorably to the theoretical estimations based on the fiber's chemical structure (26,27) since the calculated theoretical moduli for rigid rod aromatic fibers exceeds the experimentally determined tensile moduli (Table 1). However, for extended chain

Table 1. Comparisons between tensile moduli as theoretically calculated and experimentally determined for various synthetic high modulus/high strength fibers.

	Tensile modulus from macroscopic measurements (GPa)	Tensile modulus from X-ray determination of the crystal's elastic constants (GPa)	Tensile modulus from theoretical calculations of the molecules elastic modulus (GPa)
Kevlar	124 <sup>a</sup>	182 <sup>b</sup>	256 <sup>c</sup>
PBT	290 <sup>d</sup>	390 <sup>e</sup>	-
PE	220 <sup>f</sup>	255 <sup>b</sup>	290-358 <sup>b</sup>

<sup>a</sup>reference 23

<sup>b</sup>reference 28

<sup>c</sup>reference 26

<sup>d</sup>reference 25

<sup>e</sup>reference 27

<sup>f</sup>reference 9

polymers such as polyethylene (PE), the maximum experimental tensile modulus attained to date approaches the calculated theoretical tensile modulus (28). The discrepancies between the theoretical and experimental tensile properties may be attributed to deficiencies during the fiber processing although the possibility that the theoretical predictions may be in error cannot be overlooked. For the case of PE, fundamental research on the crystallization and subsequent deformation behavior of various morphologies by Kanamoto et al. (9) has been used to adequately engineer the material through a two stage drawing process. The result is a relatively high ratio of experimental tensile modulus to theoretical modulus. It is apparent that by adequately studying the physical processes during fiber formation, the processing of these materials may be carefully engineered, and the mechanical and physical potential of the fiber as determined by its chemical structure can be achieved.

The synthesis of novel polymers (the chemical approach) has and will continue to be very crucial in the development of high performance fibers. However, a deeper understanding of the spinning process and the implementation of this knowledge (the engineering approach) is necessary in order to fully exploit the capabilities of these rigid rod aromatic fibers.

Unfortunately, developments in fiber processing of solution spun polymers have traditionally been based on empirical studies without insight into the fiber formation process. However, due to the increasing requirements in fiber properties and the economics of fiber

production, fundamental studies in the area of wet spinning are now being undertaken (29).

## 1.2 Fundamental Aspects of Fiber Formation During Solution Wet Spinning

Fundamental studies of solution wet spinning involve the investigation of two problems: (1) the structure formation in various process conditions, and (2) the relationship between structure and macroscopic properties. The study of wet spinning is very complex since heat and mass transfer accompanied by phase transitions occur in the coagulation, drying and heat treatment processes. Consequently, structure formation during wet spinning and structure-property correlations in solution spun fibers are not well understood.

Most investigations to date have focused on the wet spinning of such flexible extended chain polymers as cellulosic materials (30), proteins (31,32), and polyacrylonitrile (PAN) (33-38). More recently, solution spun aliphatic polyamides and polyesters which are traditionally melt spun have been studied (31,39,40). Through a better understanding of the coagulation, drying and heat treatment processes in flexible chain polymers, fiber formation processes in the lyotropic liquid crystalline systems can be better assessed.

### 1.2.1 Coagulation Process in Flexible Chain Polymers

Solidification of the dissolved polymer occurs through the coagulation process. The spinning solution undergoes a change in composition depending on the outward flux of the solvent  $j_s$  and the inward flux of



the non-solvent  $j_n$ . The coagulation process and the resulting fiber morphology and mechanical properties are controlled by both thermodynamic effects, that is, the characteristic phase boundaries and kinetic effects, the ratio of the fluxes  $j_s/j_n$ .

The phase diagram and transport properties are, in part, influenced by the temperature of the spinning bath. With increasing temperature, the solubility of the system increases and the binodal will move to lower solvent concentrations. Furthermore, increasing the temperature of the system results in an increase in the diffusion coefficients and the fluxes  $j_s$  and  $j_n$ . For a PAN-DMF solution, Paul has found that the resulting flux ratio  $j_s/j_n$  increases with rising temperature (33).

The kinetics of mass transfer are also controlled by solvent concentration in the spinning bath and the polymer concentration in the spinning dope. With regard to the PAN-DMF system, an increase in DMF content in the water bath has been found by Groebe et al. to reduce the driving force for diffusion and the fluxes of the solvent and non-solvent (34). A more homogeneous fiber then results with increasing solvent concentration. This behavior may be attributed to the formation of a rigid skin which often accompanies phase separation. In addition, these researchers have determined that by increasing the polymer concentration in the spinning dope, the rate of diffusion of solvent and non-solvent is reduced producing a more homogeneous filament (34).

In wet spinning, the morphology of the fiber is strongly dependent on the mass transfer kinetics and the concentration dependent phase transitions. One pronounced morphological feature developed during

coagulation is the appearance of large voids and capillaries. In general, the formation of voids may be suppressed in one of the following ways: (1) using precipitating agents with a lower coagulation power, (2) by increasing the solvent content in the spinning bath, *this lowers conc?* (3) by lowering the coagulation bath temperature, or (4) by increasing *→ conc.* the polymer content in the spinning dope (31,35,39,40). Hancock et al. have proposed that the mechanism of void formation is the result of interfacial instabilities between the coagulant and the solvent (40). All of the above processing conditions serve to slow down the coagulation and thus probably reduce interfacial instabilities.

Materials such as coagulated cellulose, PAN, poly (amino acids), and wet wood possess an interconnected fibrillar structure (30,32,35, 36). For these materials, a distinct fibril/void structure with a lateral periodicity in the range of  $100 \text{ \AA}$  to  $1 \mu\text{m}$  is common. It is believed that the formation of the fibrillar structure is a direct result of the phase separation process. At present, there is considerable uncertainty as to whether this structure results from a nucleation and growth or a spinodal decomposition mechanism. Studies by Bell et al. on wet spun acrylic fibers reveal that as bath temperatures increase, the size of the fibrils and microvoids also increase (38). This behavior is most likely a consequence of a shift of the binodal to lower solvent concentrations with increasing bath temperature. Such alterations in the phase diagram may strongly influence the mechanism of phase separation and the resulting morphology.

The radial differentiation of the fiber structure is another feature found in wet spun systems. The structural nature of the skin and the mechanism of its formation are still unclear. In addition, little information is known on the effects of the coagulation conditions on skin formation and the relationship between the amount of skin and the final fiber properties.

The mechanical properties of wet spun fibers are, also, very sensitive to such coagulation conditions as the temperature and composition of the spin bath and the polymer concentration in the spinning dope. The influence of coagulation variables on acrylic fibers has been studied by Knudsen (35). The tenacity of acrylic fibers is reported to increase with increasing polymer content in the spinning dope, increasing solvent content in the spinning bath and decreasing bath temperature. In addition, at lower coagulation bath temperatures, the initial modulus increases with a decrease in elongation (35). By providing a more homogeneous fiber through alterations in the kinetics and thermodynamics of coagulation, an enhancement in the tensile properties may be achieved.

### 1.2.2 Drying Process in Flexible Chain Polymers

Due to the porous nature of coagulated cellulose, PAN, polyamino acids and wet wood, there is a dramatic structural collapse during the drying of these materials (30,35,37,38,41,42). Skaar suggests that this collapse process may be attributed to the capillary forces generated in the cavities, a consequence of the surface tension at the liquid/gas



interface (42). The material collapses when the capillary tension exceeds the lateral strength of the structure.

The nature of these dimensional changes has been studied most extensively for wood and other cellulosic materials (43-45). In wood, which is highly anisotropic, the dimensional changes during the collapse process are orthotropic. Longitudinal shrinkage is 1-2 orders of magnitude less than the transverse shrinkage. In addition, the radial shrinkage is usually half the tangential shrinkage. Several theories have been proposed to explain the anisotropic shrinkage based upon considerations of the gross wood structure and fibril alignment (43-46).

Because of these drastic dimensional changes during drying, residual stresses are known to develop in these extended flexible chain polymers (30,38,45-47). McMillen has proposed a mechanism for residual stress formation in wood (47). It has been suggested that the dried outside section of wood is initially in a state of axial tension thereby forcing the undried inner layers into a state of axial compression. As drying continues, the outside layers whose dimensions are permanently set are placed into axial compression as the inner layers shrink into a state of axial tension. This final distribution of longitudinal stresses in wood is characteristic of the internal stresses present in as-spun cellulose and PAN.

The influence of the drying process on the resulting mechanical properties has been examined for these flexible chain solution spun polymers. In general, with the removal of coagulants/residual solvents,



an enhancement in tensile properties has been found for both cellulose (30) and PAN (38).

### 1.2.3 Post Processing Heat Treatment

Mechanical treatments and solidification processes during fiber wet spinning introduce some instability into the fiber structure and properties. Consequently, a heat treatment process is often employed to stabilize the fibers against subsequent changes in fiber dimension, crystallinity, microporosity, molecular orientation, and internal stresses. In general, post processing heat treatment of solution processed fibers serves to improve the molecular order with a reduction in porosity resulting in improved tensile properties (29).

### 1.3 Rigid Rod Aromatic Fibers: Processing and Properties

As indicated in the previous section, the coagulation, drying and heat treatment processes strongly influence the characteristic structural and mechanical features of solution wet spun fibers. Consequently, for the development of rigid rod aromatic fibers, detailed studies on the processing of these stiff chain polymers and its effect on the resulting material properties are of interest.

During coagulation, fibers spun from a PBT/MSA solution undergo a large radial shrinkage whereas the diameters of fibers from PBT/PPA solution have been observed to undergo only small changes by Chenevey (48). Optical microscopy studies of coagulating PBT/MSA and PPTA/H<sub>2</sub>SO<sub>4</sub> solutions by Thomas et al. have shown that the materials drastically

shrink with the eventual formation of a void (49). It has been speculated that the formation of macrovoids is a result, in part, of the development of large internal shrinkage stresses during coagulation.

The coagulation process has a pronounced influence on the resulting tensile properties similar to solution spun flexible chain polymers. In general, an increase in the solvent content and a decrease in the temperature of the coagulation bath has previously been reported to cause an increase in fiber tenacity for PPTA/H<sub>2</sub>SO<sub>4</sub> and PBT/MSA solution spun fibers (21,39,48). Microscopic studies by Hancock et al. (39) reveal a decrease in void content in PPTA fibers with increasing coagulant acidity and decreasing coagulant temperature which contributes to the enhanced tensile strength. Similar results have been obtained for PBT/PPA solution spun fibers produced at DuPont (50). With increasing amounts of PPA and MeOH in the coagulant, the tensile properties and density of the final as-spun fibers are reported to increase. By modifying the kinetics and thermodynamics of coagulation through temperature and concentration effects, alterations in the fiber properties may be attained in these rigid rod aromatic fibers.

Jaffee et al. suggest that the rate of coagulation and the resulting fiber properties may be strongly influenced by the presence of the dry jet region during wet spinning (51). For PPTA spinning dopes, the air gap, in addition to developing high molecular orientation through a draw down process, is believed to facilitate the cooling of the hot spinning dope before it enters the frigid coagulation bath. The spinning solution then undergoes a low temperature (slow) coagulation.

During wet spinning hot PPTA dope is spun directly into the cold coagulant resulting in a high temperature (fast) coagulation. This reasoning has been proposed to explain the distinct differences in the morphology and mechanical properties which they observe between dry-jet wet spun and wet spun PPTA fibers (51).

During the drying process, fibers spun from a PBT/PPA solution undergo large macroscopic changes. Allen et al. have proposed that large residual stresses develop due to the fiber's dimensional changes during processing (25). They suggest that the longitudinal internal stresses developed are tensile on the inside and compressive on the fiber's outer edge. When the compressive shrinkage stresses are large enough, the outer fibrillar elements buckle upon drying. Scanning electron microscopy observations of PBT fibers by Allen et al. reveal the presence of buckled elements perpendicular to the fiber axis (52).

The macrostructure of both as-spun (dried) PBT and PPTA fibers is reported to be a void containing fibrillar structure characteristic of many flexible chain solution spun polymers (52-55). In addition, differences between the skin and core have been reported to exist in PPTA fibers (55,56). Although it is postulated that skin-core differentiation exists for PBO and PBT, no direct evidence has been reported to date.

Microstructural analysis through wide angle x-ray diffraction (WAXD) by various investigators indicates that both PBT and Kevlar<sup>R</sup> have a high degree of molecular alignment in the fiber direction (57-60).



Kevlar<sup>R</sup> exhibits a three dimensional crystalline order whereas a two dimensional crystalline order is prevalent in as-spun PBT.

These as-spun rigid rod aromatic fibers demonstrate both high tensile modulus and tensile strength due to their molecular nature. The tensile stress-strain behavior for PBT and PBO is elastic-plastic with strain hardening characteristics. Allen et al. have proposed a residual stress model with compressively buckled elements to explain the tensile behavior of the as-spun PBT fiber (52). In this model, the enhancement in tensile moduli upon deformation has been attributed to the straightening of the buckled elements. The apparent plastic behavior is a result of the successive failure of overstressed elements within the fiber.

Heat treatment processing has a dramatic influence on the structure of the stiff chain polymeric fibers. From recent wide angle x-ray diffraction (WAXD) studies of PBT and PPTA after heat treating, evidence for the enhancement of three dimensional crystallinity has been reported (25,51,53). From spectroscopic characterization of PBT films, Hsu et al. have detected an improvement in axial orientation and an increase in the co-planarity of the phenyl and bisthiazole groups in the repeat units after post processing tension heat treatment (61). It is speculated that the alterations in the PBT chain and the development of three dimensional crystalline order are interrelated.

Both Allen (25) and Jaffee et al. (51) report that the mechanical properties of PBT and PPTA are further improved by post processing heat treatment (PPHT) under tension. The stress-strain behavior for PBT



becomes completely linear elastic after heat treatment processing. It has been suggested that the release of residual stresses and the removal of residual solvents/coagulants are responsible, in part, for the changes in the PBT fiber characteristics with post processing heat treatment. Both mechanical energy input (tension) and thermal energy input (temperature) have been determined to be requirements for property enhancement in these stiff chain aromatic fibers.

A major problem with these rigid rod aromatic fibers is their relatively poor transverse and compressive properties when compared to glass or graphite fibers. Due to their weak lateral interactions, the transverse and compressive properties are considerably lower than their axial properties (25,62,63).

DeTeresa et al. recently modeled the compressive buckling of extended chain polymers to allow for both predictions of compressive strengths and a further understanding of the buckling process (64). By modelling extended chain polymeric fibers with a collection of interacting rigid link-elastic hinge chains, the compressive strength is predicted to be proportional to the fiber's torsional shear modulus. Discrepancies which exist between the predicted and measured compressive strengths have been attributed, in part, to material imperfections such as the misalignment of fibrils and the presence of voids and residual stresses.

#### 1.4 Dissertation Overview

Previous processing studies on both extended flexible chain polymers and rigid rod aromatic polymers indicate that property alterations may be achieved by control of the fiber development during processing. The ability to manipulate fiber properties and control structure formation through its processing conditions is of technological importance. As previously discussed, the technology of high modulus/high strength aromatic fibers has not progressed to the level of the chemistry of these materials. In order to successfully engineer these fibers, a further understanding of the mechanisms which control property development and modifications are needed. Consequently, a study of the influence of drying in developing fiber properties in rigid rod aromatic systems, in particular, poly (p-phenylene benzobisthiazole), is undertaken in this dissertation.

In addition to providing insight on fiber formation for lyotropic liquid crystalline polymers, the information generated is intended to guide technological advancements in the PBT system. Development of the PBT fiber's tensile as well as compressive properties has been one of the main goals on the Air Force Ordered Polymers Research Program. Consequently, investigations concerning the influence of drying on the structure and mechanics of PBT fibers is necessary to adequately develop those particular fiber properties.

The structural and mechanical characteristics of PBT fibers from the coagulated state through the drying process to the as-spun and heat

treated state have been investigated herein. The findings of studies conducted on the coagulation fiber properties and their modifications during drying are analyzed in Chapter II. Through characterization of the macrostructure, microstructure, and mechanical properties of the coagulated state, the role of the coagulation process in fiber formation during the wet spinning of this PBT solution may be discerned. Studies on the alterations in the fiber properties due to the collapse process during drying is useful in the determination of the role of drying in property development during processing. A discussion of the dimensional changes associated with the collapse process of highly anisotropic materials is presented in both quantitative and qualitative terms. The results contained in Chapter II provide a basis for the remaining work described in Chapters III and IV.

In Chapter III, the influence of elevated temperature and high tension drying including subsequent post processing heat treatment on the morphology and the mechanics of the dried (as-spun) fiber is examined. These processing-structure property correlations are useful in determining which factors modify material imperfections which develop during coagulation and drying. These studies may also provide insight into structural basis for the weak transverse characteristics, that is, the compressive strength, of these high modulus/high strength fibers. Information of this kind will be invaluable for the improvement of both the compressive and tensile properties.

Force-Temperature studies to examine the thermal expansion properties (reversible thermoelastic behavior) of these rigid rod aromatic

polymers as well as material changes associated with the application of temperature and tension (irreversible thermoelastic behavior) are summarized in Chapter IV. Through this work, a better understanding of the effects of water removal to induce thermal stability and material alterations during the initial drying and heat treatment processes may be obtained.

The major findings of this dissertation work are highlighted in Chapter V. The current state of knowledge concerning fiber property formation and modifications in the PBT system is summarized with suggestions for future work.



## C H A P T E R   I I

### COAGULATED FIBER PROPERTIES: THE COLLAPSE PROCESS: MODIFICATIONS DURING DRYING

#### 2.1 Introduction

Due to the limitations in the dry jet wet spinning of PBT, the tensile as well as the compressive properties of the fibers fall short of their potential capabilities. In order to adequately engineer these fiber properties, knowledge on how these properties develop and what controls their modifications is needed. The processing and history of PBT prior to the as-spun state must then be examined to understand what dictates fiber development in these rigid rod systems. Therefore, the morphology and mechanics of the wet state and their alterations due to the collapse process during drying have been investigated. The information generated is intended to provide insight into the effects of water and its subsequent removal on the properties of rigid rod polymeric fibers. With a better fundamental understanding of the role of coagulation and drying in the fiber development process, modifications in the fiber properties through subsequent drying and heat treatment may be attempted in a more scientific and less empirical manner.

#### 2.2 Fiber Production

The PBT polymer used in this dissertation was synthesized by Dr. J. Wolfe at Stanford Research Institute International by the condensation of terephthalic acid with 2,5-dimercapto-1,4-phenylenediamine in

polyphosphoric acid (PPA) (18). Anisotropic solutions of 5.5% PBT and 15.5% PBT in PPA were used to produce fibers for this dissertation. The PBT in the 5.5% solution had an inherent viscosity (I.V.) of 18 dl/gm as determined by measurements in dilute methane sulfonic acid. Polymer contained in the high concentration PBT/PPA solution had an inherent viscosity of 25 dl/gm. From previously determined intrinsic viscosity-molecular weight relationships for a series of PBT polymers (65,66), the weight average molecular weight for the 18 I.V. and 25 I.V. polymer was estimated to be 30,400 g/mole and 36,500 g/mole respectively.

The PBT fibers examined in this dissertation were produced by dry jet wet spinning. A schematic of the spinning operation is depicted in Figure 3. After heating the anisotropic solutions for 24 hrs. at 120°C, the dopes were extruded through a single hole die, drawn in the dry-jet region and coagulated in water. The spin draw ratio was calculated as a ratio of the fiber's take up velocity to the extrusion velocity of the polymer solution. A variable ten speed transmission attached to a screw jactuator system allowed for the control of the ram speed and the rate of polymer extrusion. The take up velocity of the coagulated fiber was controlled by a Bodine DC motor speed control attached to a Bodine Series 200 gear motor. A water coagulant was used at a temperature of 15°C. These fibers were collected under water and kept submerged in the coagulant until further drying and heat treatment experiments were performed.

The processing parameters used in the spinning of the PBT fibers are outlined in Table 2. PBT fibers (I) & (II) were dry jet wet spun

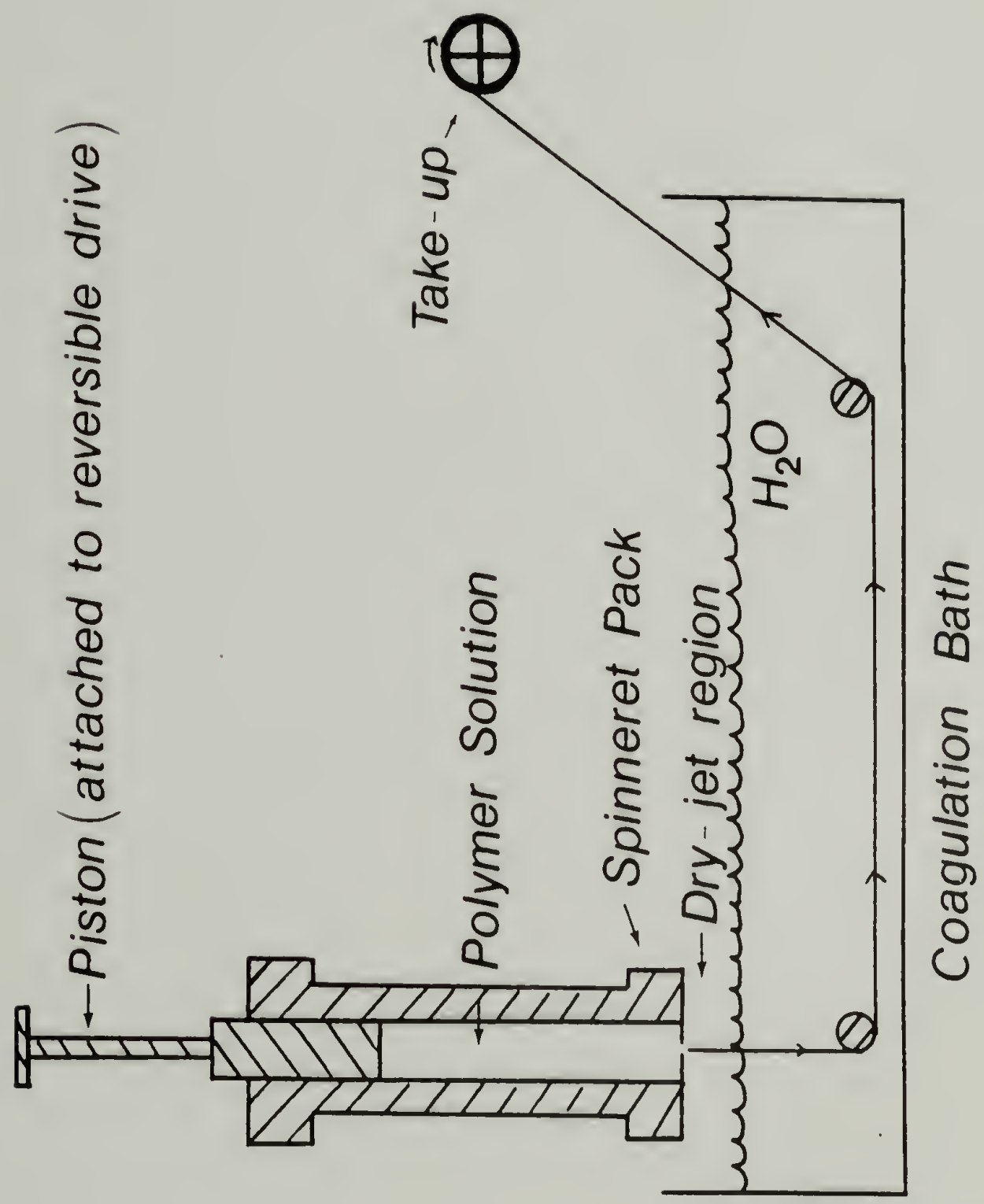


Figure 3. Schematic diagram of dry-jet wet spinning process

Table 2. Spinning conditions for PBT fibers.

Sample	I 5.5% PBT	II 5.5% PBT	III 15.5% PBT	IV 15.5% PBT	V 15.5% PBT	VI 15.5% PBT	VII 15.5% PBT	VIII 15.5% PBT	IX 15.5% PBT
Dope composition	(18 I.V.)/ PPA	(18 I.V.)/ PPA	(25 I.V.)/ PPA	(25 I.V.)/ PPA	(25 I.V.)/ PPA	(25 I.V.)/ PPA	(25 I.V.)/ PPA	(25 I.V.)/ PPA	(25 I.V.)/ PPA
Dope temperature	25	90	90	90	90	90	90	90	90
Extrusion rate (m/min)	.74	.74	.74	.74	.74	.74	.84	.84	.84
Take up rate (m/min)	1.83	4.6	2.2	6.1	9.6	12.4	1.28	4.15	7.8
Spin draw ratio	3:1	6:1	3:1	8:1	13:1	17:1	2:1	5:1	9:1
Die diameter ( $\mu$ )	330	330	330	330	330	330	100	100	100
Air gap (mm)	25	25	25	25	25	25	25	25	25
Coagulant/Wash bath temp. ( $^{\circ}$ C)	25	25	17	15	15	15	15	15	15



from an anisotropic solution of 5.5% PBT in PPA at a spin draw ratio of 3:1 and 6:1. Fibers (III), (IV), (V) and (VI) were spun from a 15.5% PBT/PPA solution with a spin draw ratio of 3:1, 8:1, 13:1 and 17:1 respectively. Fibers (I-VI) were spun from a 330 $\mu$ m die. Fibers (VII), (VIII) and (IX) were spun from the 15.5% PBT/PPA solution with spin draw ratio of 2:1, 5:1 and 9:1 respectively using a 100 $\mu$ m die.

Hollow fibers were supplied by Albany International Research Company. The PBT polymer (15% PBT/PPA solution) was reported to have an I.V. of 19 dl/gm which corresponds to a weight average molecular weight of 31,300 g/mole.

## 2.3 Experimental

### 2.3.1 Fiber Collapse Characterization

Dimensional changes which occur during drying were monitored both in the radial and longitudinal fiber direction. Laser light diffraction (67) was used to examine radial variations during the collapse process. The fiber, simulating an infinite slit of width,  $d$ , creates a laser diffraction pattern consisting of a series of maxima and minima on either side of a central maxima. The separation between the first corresponding pair of minima,  $\delta$ , is related to the diameter of the fiber through the Fraunhofer approximation

$$d = \frac{2\lambda s}{\delta} \quad (2.1)$$

where  $s$  = fiber to detector distance,  $\lambda$  = laser wavelength. To measure the radial collapse,  $\delta$  was monitored from the PBT fiber's laser diffraction pattern as a function of time.

Length changes were monitored by linear variable differential transformer (LVDT) measurements using the apparatus schematically shown in Figure 4. A PBT fiber, surrounded by water in a capillary pipet, was attached to the core of a Schaevitz E 2000 LVDT. By sealing the top of the pipet with a serum stopper, capillary forces prevented the disposal of water from within the pipet. To observe the axial changes during drying, the water was released from the pipet and the resulting displacement was monitored by a Schaevitz miniature digital transducer readout (350L) as a function of time.

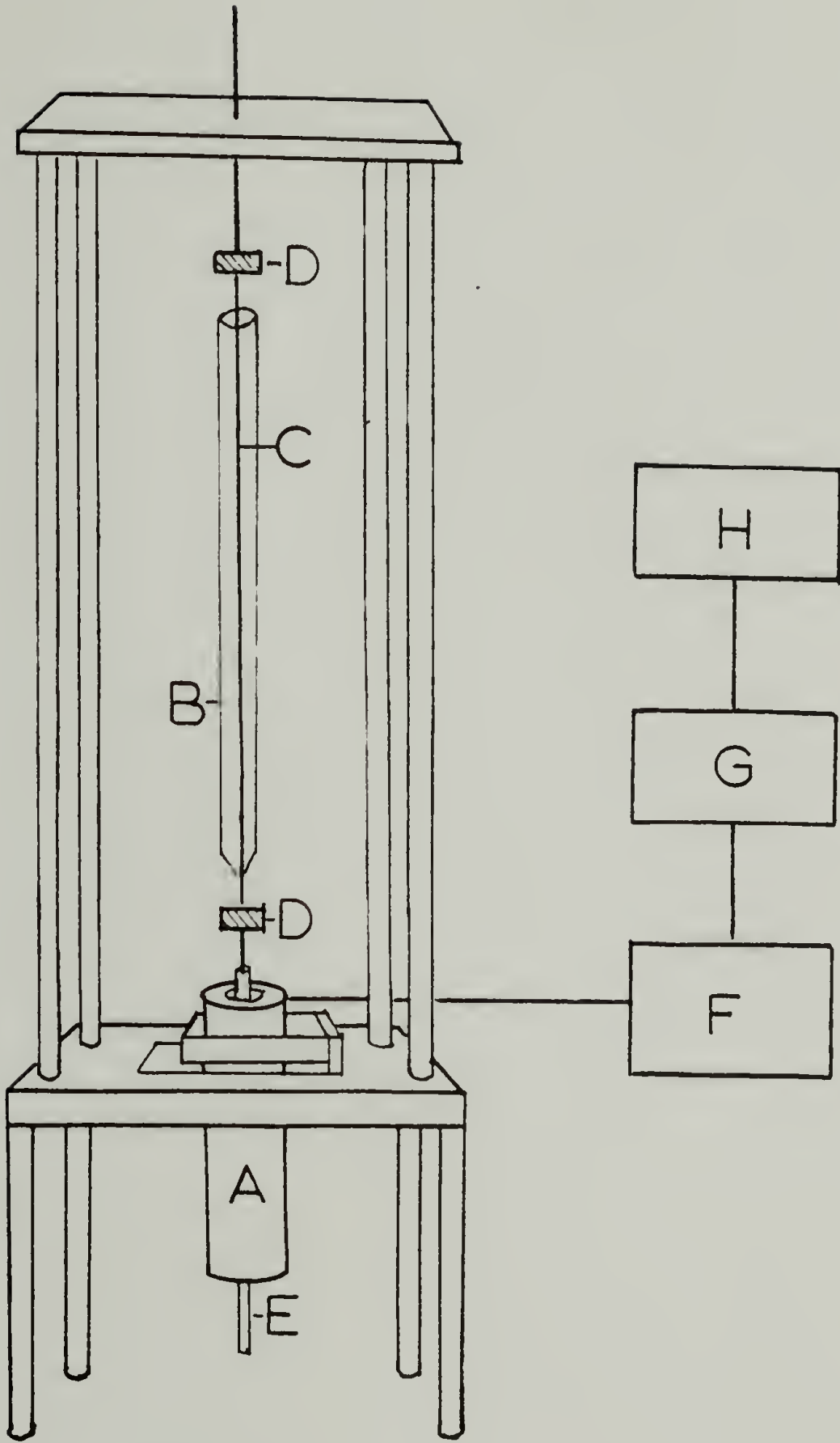
### 2.3.2 Morphology Characterization

The macrostructural and microstructural features of the PBT fiber reported in this chapter were examined by scanning electron microscopy (SEM) and wide angle x-ray diffraction (WAXD). To examine the wet PBT structure by SEM, the critical point method of drying (CPD) was employed to remove the water without collapsing or altering the structure which occurs with normal air drying. In this technique, the fiber was totally submerged in liquid ( $\text{CO}_2$ ) below its critical point in a Polaron E 300 critical point drying apparatus. The liquid and fiber were then taken to a temperature and pressure above the critical point. The  $\text{CO}_2$  liquid transformed to a gas without the formation of a gas/liquid interface because the densities of the liquid and the gas were equal at the critical point. By never allowing the liquid/gas interface to develop, capillary forces within the voids were minimized, thereby preventing the collapse of the fiber. Fiber samples dried for SEM observation were then sputter coated with a  $350 \text{ \AA}$  layer of gold in a Polaron E 5011 SEM

Figure 4

Experimental design for axial displacement measurements during drying.

- A. Linear Variable Differential Transformer
- B. Pipet with water
- C. PBT fiber
- D. Clamp
- E. Metallic Core
- F. Readout/Power source
- G. Amplifier
- H. Recorder





coating unit to minimize electron charging problems. An ETEC Autoscan operated at 20 KV was employed for the SEM studies.

WAXD results for both the wet and dry fiber were obtained from both diffractometric and flat film techniques. Flat film fiber patterns on a single PBT filament were obtained in a Warhus (Statton) camera employing pin-hole (0.2 mm) collimation and a sample to film distance of 53 mm. To obtain the flat film x-ray analysis on coagulated PBT, the wet fiber was sealed in a 200 $\mu$ m quartz capillary tube. Diffractometric ( $2\theta$ ) scans of equatorial reflections were obtained on a Siemens D-500 diffractometer utilizing line focus collimation. Incident beam diffractometer slits of  $0.3^\circ$  ( $2\theta$ ) with a final slit of  $0.15^\circ$  ( $2\theta$ ) were used for a scan rate of  $0.5^\circ$  ( $2\theta$ )/min. Two pieces of lead were placed onto the incident beam slit to provide a square x-ray source. For the diffractometer measurements, fiber samples were prepared by winding a 50 cm length of fiber around a cardboard mount. Wet fibers, after winding on a plastic mount, were sealed between two thin sheets (8-10 $\mu$ ) of mica to preserve their coagulated state. A lead aperture was placed over both the wet and dry fiber mounts in order to prevent any extraneous scattering from the cardboard and plastic mounts.  $\text{CuK}\alpha$  tubes were operated at 40 KV and 30 mA on the Warhus camera and Siemens diffractometer.

The interplanar spacing of molecules and the coherent scattering size of crystallites within both the wet and dry fibers were the microstructural features of interest. Through the Scherrer equation (2.2) (68), the coherent scattering size of the crystallite ( $L$ ) was assessed from the integral breadth at half maximum intensity of the equatorial

reflection profile,  $\beta_0$  or  $(FWHM)_s$

$$L_{hkl} = \frac{K\lambda}{(\beta_0)\cos\theta} \quad (2.2)$$

where  $K$  is a constant equal to one,  $\lambda$  = wavelength of CuK $\alpha$  x-ray,  $\theta$  = half the scattering angle.  $\beta_0$  or  $(FWHM)_s$  was corrected for instrumental peak broadening. Assuming Gaussian peak profiles, the instrumental effects could be separated from the total observed broadening using the following equation:

$$(FWHM)_s^2 = (FWHM)_{ob}^2 - (FWHM)_{ins}^2 \quad (2.3)$$

where  $(FWHM)_{ob}$  = observed peak width,  $(FWHM)_{ins}$  = peak width due to instrumental effects. D500 instrumental broadening was determined by measuring the FWHM of the 0.4968 nm spacing diffraction peak ( $2\theta=17.84$ ) of hexamethylene tetramine (HMTA) which should have negligible peak broadening because of its large crystal size.

The interplanar d-spacing values were calculated from Bragg's Law (2.4) (68):

$$\lambda = 2d \sin\theta \quad (2.4)$$

where  $\lambda$  = wavelength of CuK $\alpha$  x-ray,  $\theta$  = half the scattering angle.

### 2.3.3 Mechanics

The tensile properties for both the wet and dry materials were determined on single filaments in accordance with ASTM standards for testing high modulus single filament material (69). Reported tensile properties were corrected for the compliance of the testing machine. Detailed descriptions of the dry fiber sample preparation for mechanical

testing and machine compliance corrections are provided elsewhere (25). Single filament wet fibers were kept submerged in water during the sample preparation (mounting to plastic tabs) and testing. Tensile tests were performed on a Toyo Tensilon Model UTM-11 testing apparatus at a strain rate of .2%/minute using 100mm gauge length samples. Tensile properties represent an average  $\pm$  one standard deviation of at least ten test specimens.

Torsion (shear) moduli of the PBT fibers were obtained from free torsional oscillatory experiments as described earlier for these high modulus materials (25,62,63). After setting the fiber into torsional oscillation by twisting the disc pendulum, the period of oscillation of the single filament was measured. Equation (2.5) was used to calculate the torsion modulus from the torsional oscillations of the fiber:

$$G = \frac{8\pi I_d l}{r^4 \tau^2} \quad (2.5)$$

where  $I_d$  = moment of inertia of the pendulum disk  
 $l$  = sample length  
 $\tau$  = period of oscillation  
 $r$  = fiber radius

A disc pendulum was employed with a polar moment of inertia calculated to be  $357 \text{ g}\cdot\text{mm}^2$  using dimensions measured with a micrometer.

The shear modulus of the wet fiber was obtained using a torsional pendulum apparatus schematically depicted in Figure 5. The wet PBT fiber was submerged under water in a glass eyedropper and attached to a

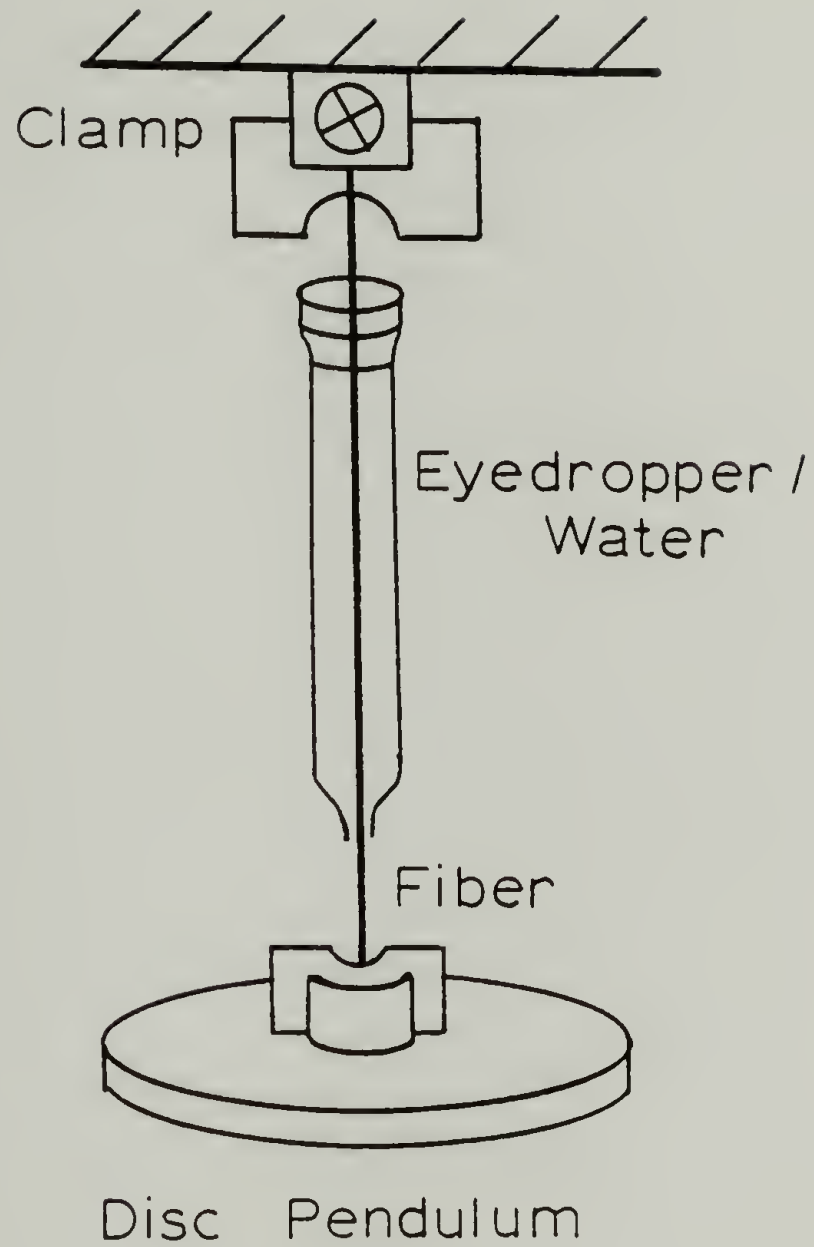


Figure 5. Schematic diagram of the torsional pendulum apparatus for wet PBT fibers



serum cap at one end. Again the capillary action of the liquid within the eyedropper prevented the loss of water from the opening at the bottom. Through this opening, the wet fiber was attached to the pendulum disc. Dry PBT fibers of known torsional rigidity were tested in this apparatus to verify its accuracy and reliability.

The compressive strength of the wet and dry PBT filaments was experimentally determined through two techniques: an elastica loop test (25) on solid filaments and an axial compression test on hollow fibers. In the elastica loop test, fiber loops were placed in water between glass slides. The loops were drawn down in size by pulling on the fiber ends to gradually increase the bending strains in the loop. The major (L) and minor (D) loop axis were measured with a calibrated 10x eyepiece. The critical strain to cause compressive buckling was determined as the point when the parameter  $L/D$  deviates from the elastic region ( $L/D=1.34$ ). The axial compressive strengths were calculated from the product of the compressive strain and the axial tensile modulus. A comparison of the axial tensile and compressive modulus of a hollow dry fiber in Table 10 shows that the stiffness in tension and compression are nearly the same.

A direct measure of the compressive strength was determined by means of an axial compression test on hollow PBT filaments. In this test, a fine wire (125 $\mu$ m diameter) was placed down the center and attached at one end of the hollow fiber (Figure 6). While clamping the outer edge of the fiber at the opposite end, the wire is slowly pulled out in tension. In this manner, the hollow fiber is placed into axial

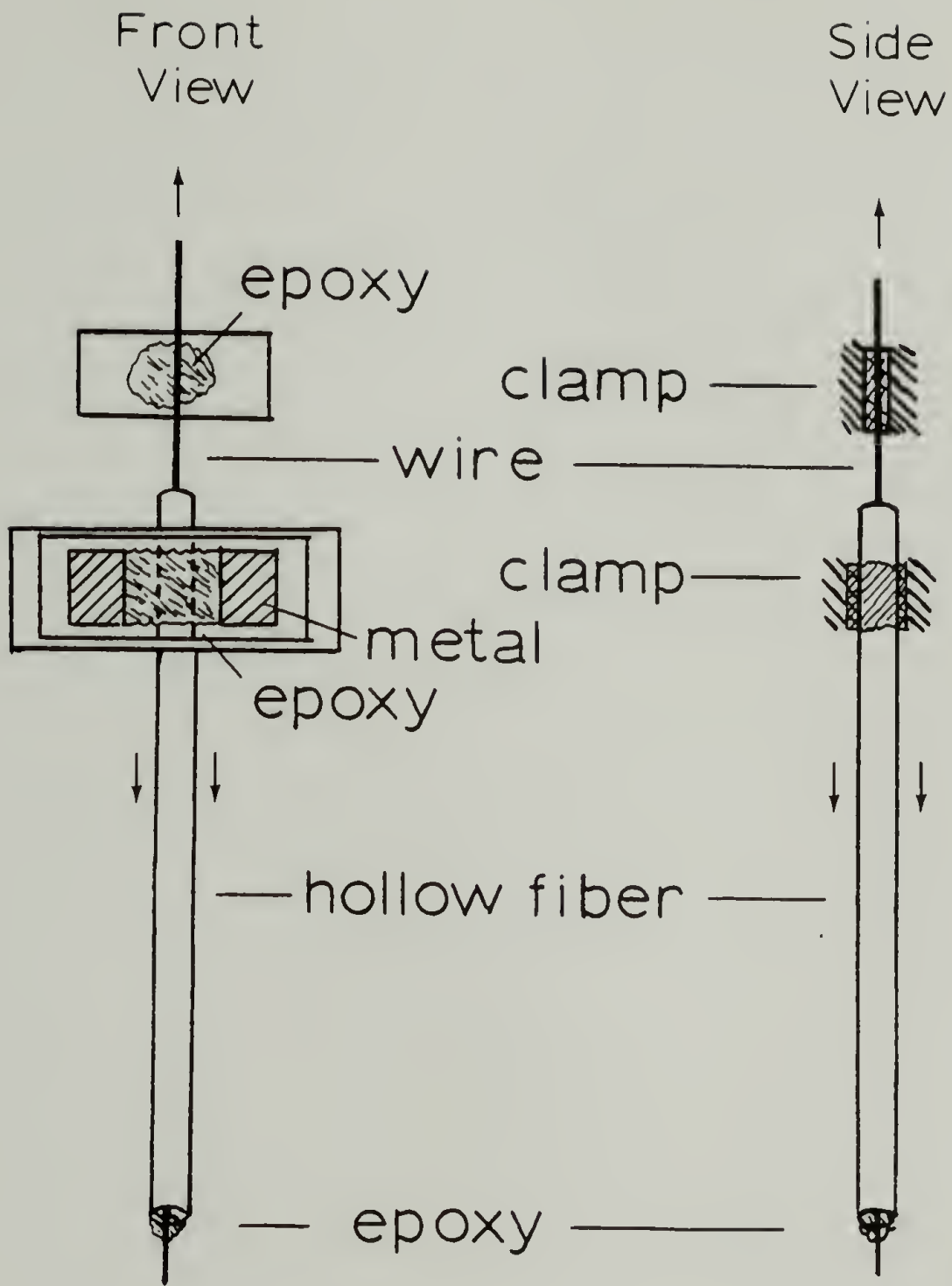


Figure 6. Mounting of hollow fibers for compression tests

compression. This sample geometry was selected because it is free of Euler column instabilities (70). The onset of buckling failure results in a complete loss of load. The compressive modulus, strength and strain may be discerned from the resulting stress-strain curve. To determine the compressive properties of the wet hollow fiber, these tests were performed with the fiber/wire assembly enclosed in a water-filled capillary tube.

Reported tensile, torsional, and compressive properties were based on cross sectional areas calculated from diameters measured by laser light diffraction (67) and optical microscopy. These techniques were implemented to directly measure the diameters of large PBT fibers ( $>180\mu\text{m}$ ) since these fibers of this size showed an induction period prior to drying. PBT fibers with diameters less than  $180\mu\text{m}$  began to collapse immediately, and thus the initial fiber diameter could not be measured directly. However the collapse of the PBT fiber at a given concentration of PBT/PPA appeared independent of the fiber diameter since the area reduction for fibers  $>180\mu\text{m}$  was equivalent (Table 5). Consequently, the wet diameters for fibers  $<180\mu\text{m}$  were calculated from knowledge of the dry diameter and the characteristic area reduction for a fiber spun from a given concentration of polymer.

## 2.4 Wet Fiber Properties

### Morphology

The microstructural features of the wet fiber are well characterized through WAXD flat film analysis. The WAXD patterns of the wet PBT

fiber, water and dry PBT fiber are shown in Figure 7. From a schematic of the coagulated PBT state without the background scattering from water in Figure 7, the sharp equatorial reflections are characteristic of a high degree of chain order in the direction normal to the fiber axis. The diffuse layer lines on the meridian and the absence of discrete  $h,k,l$  reflections indicate a random staggering of aligned chains along the fiber axis. Therefore, the coagulated fiber possesses lateral but no longitudinal molecular order. The two major equatorial reflections ( $e_1$  and  $e_2$ ) exhibited by the wet PBT fiber correspond to d-spacings of .572 nm and .341 nm respectively. The ratio of d-spacing values ( $e_1/e_2$ ) is 1.68 which according to Adams et al. (57) corresponds to an approximate hexagonal packing of these rodlike molecules. The chains in the wet fiber appear to be packed in a similar arrangement to that of the dried fiber. In addition, the meridional spacing of 1.25 nm corresponds to the monomer repeat unit of PBT. It is evident that the general microstructural characteristics of the as-spun PBT fiber are present in the wet state and appear to develop during the coagulation process.

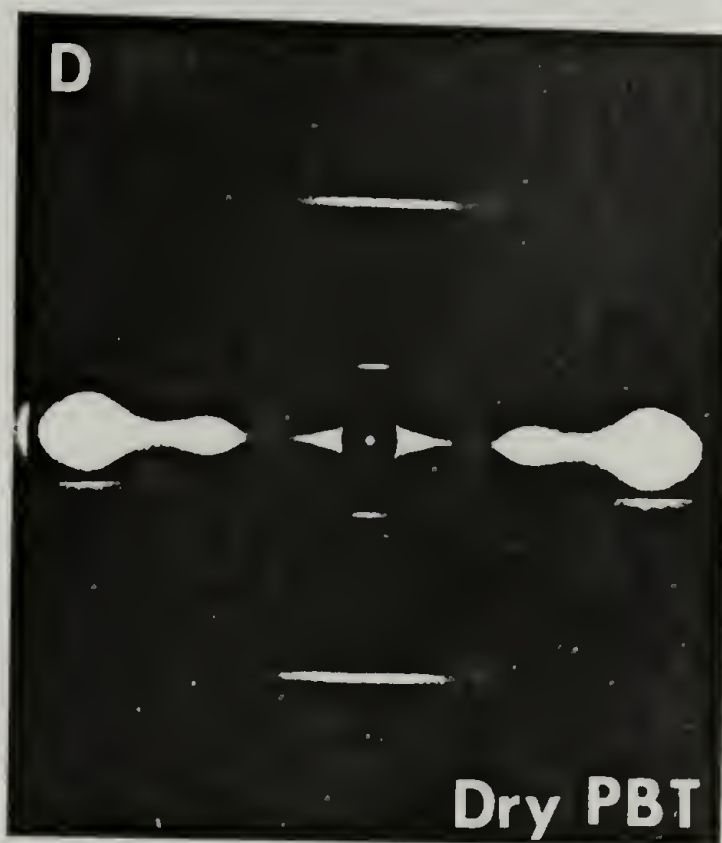
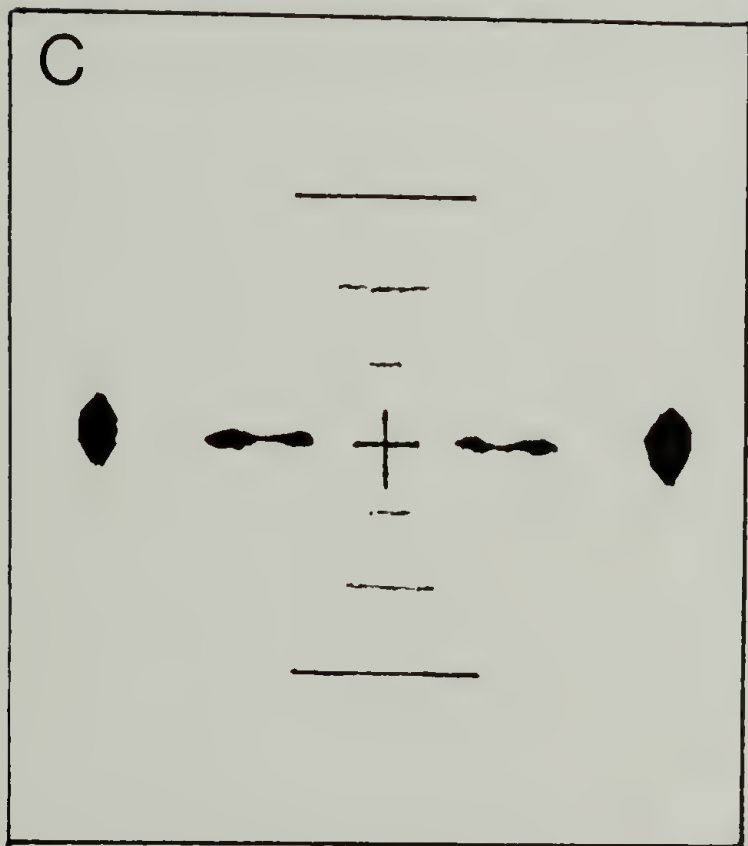
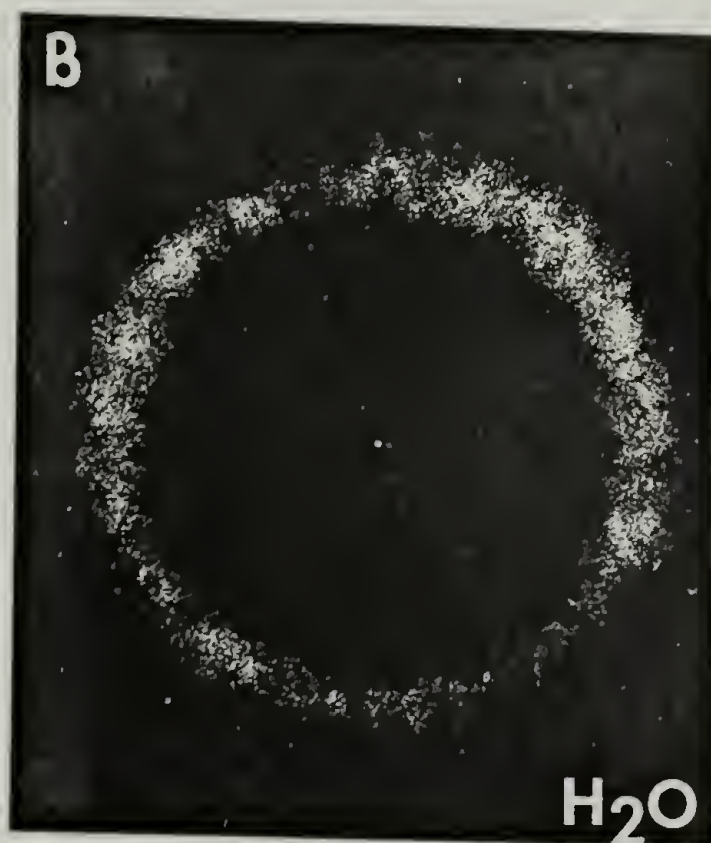
Recently, transmission electron microscopy (TEM) of a wet fiber impregnated with epoxy, cured and subsequently microtomed along the longitudinal axis has been investigated by Cohen and Thomas (71). From their results, the highly aligned chains are aggregated into a network of microfibrils in the coagulated state. From small angle x-ray analysis (SAXS) of the microvoids, the dimensions of the fibrils have been calculated to be approximately 7-10 nm (72).



## Figure 7

Wide angle x-ray diffraction patterns of

- (A) Wet PBT fiber
- (B) Water
- (C) Schematic of wet PBT fiber diffraction patterns without water scattering
- (D) Dry PBT fibers



On a more macroscopic level, the scanning electron micrograph of a peeled critical point dried fiber reveals a highly fibrillar internal structure (Figure 8). Although it may be argued that the fibrils are a consequence of the peeling process, it is believed that these macro-fibrils develop during coagulation.

The following model is proposed to account for all the structural observations on the wet fiber (Figure 9). Each PBT fiber consists of a highly swollen array of interconnected fibrils. Such a network had been suggested to account for the high load bearing capacity of the wet fiber (Section 2.4.2). In addition, it is proposed that each fibril is composed of a microfibrillar network of PBT chains as evidenced by the TEM studies described above (71). Within each microfibril, the PBT molecules are highly ordered in the two directions perpendicular to the fiber axis as evidenced by the WAXD fiber patterns. The water and/or residual acid is postulated to reside between the fibrils and microfibrils. Recently, Fourier transform infrared (FTIR) spectroscopy studies on dry PBT films have been performed by Chang and Hsu (73). Their results indicate that water has a preferred orientation. Consequently, there must be some association between the water and the PBT chain. In the microfibrillar model, an association between the PBT and coagulant can exist if the acid and/or water is located between chain aggregates and fibrils.

Evidence of a porous fibrillar structure for wet PBT is consistent with the previous data on the fibrillar nature of other solution spun fibers such as cellulose (30), PAN (35), PPTA (39,35) and PBA (11). In

Figure 8

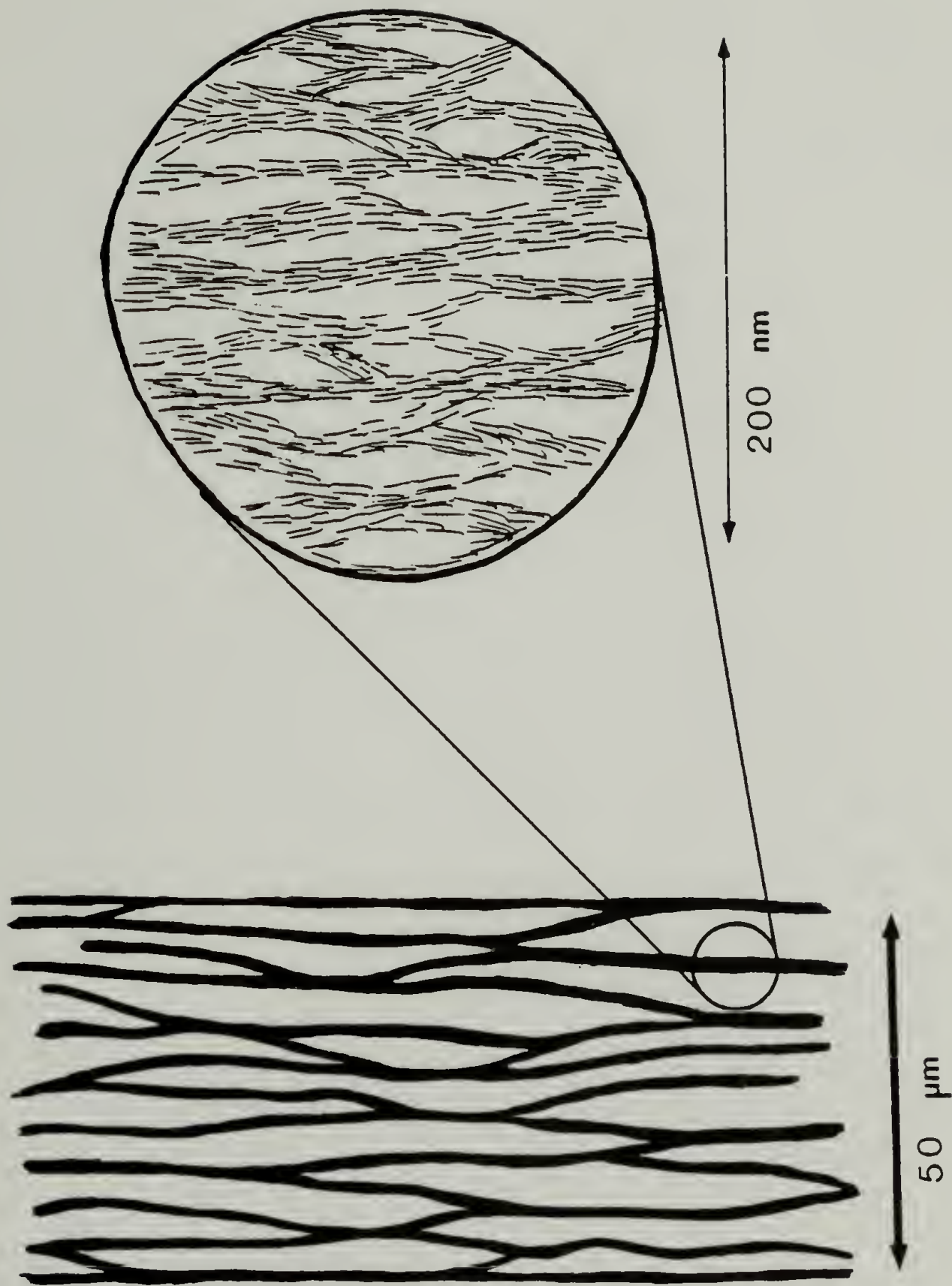
Scanning electron micrograph of a peeled  
critical point dried fiber.





Figure 9

Structural model for the coagulated (wet)  
PBT fiber.



addition, precipitation of polyaminoacids from relatively concentrated solutions (>0.5%) results in an interconnected fibrillar morphology (74).

At present, the mechanism responsible for the formation of the interconnected network observed for rigid rod polymers after coagulation is unclear. Cohen et al. (71,75) have considered the mechanism of spinodal decomposition and nucleation and growth in a solution of oriented rigid polymers and their relation to the structure of the coagulated state. They assume that the mobility of PBT molecules is highest along the longitudinal axis of the rod. By their approach, a one dimensional nucleation and growth mechanism may be associated with the formation of fibrils, whereas phase separation due to spinodal decomposition would most likely result in a lamellar morphology. Morgan et al. (76) have studied the structure of poly (p-phenylene terephthalamide) (PPTA) fibers, and have postulated a row nucleation mechanism whereby the extended chains crystallize into lamellae perpendicular to the fiber direction. However, the fibrillar nature of the coagulated PBT eliminates any mechanism which gives rise to a lamellar structure. Thus, Cohen and Thomas suggest that the origin of the microfibrillar network is controlled by a nucleation and growth process (71).

#### 2.4.2 Mechanics

The overall stress strain behavior of wet PBT is elastic-plastic with strain hardening characteristics (Figure 10). This tensile behavior is similar to that of the as-spun PBT. A relatively high modulus



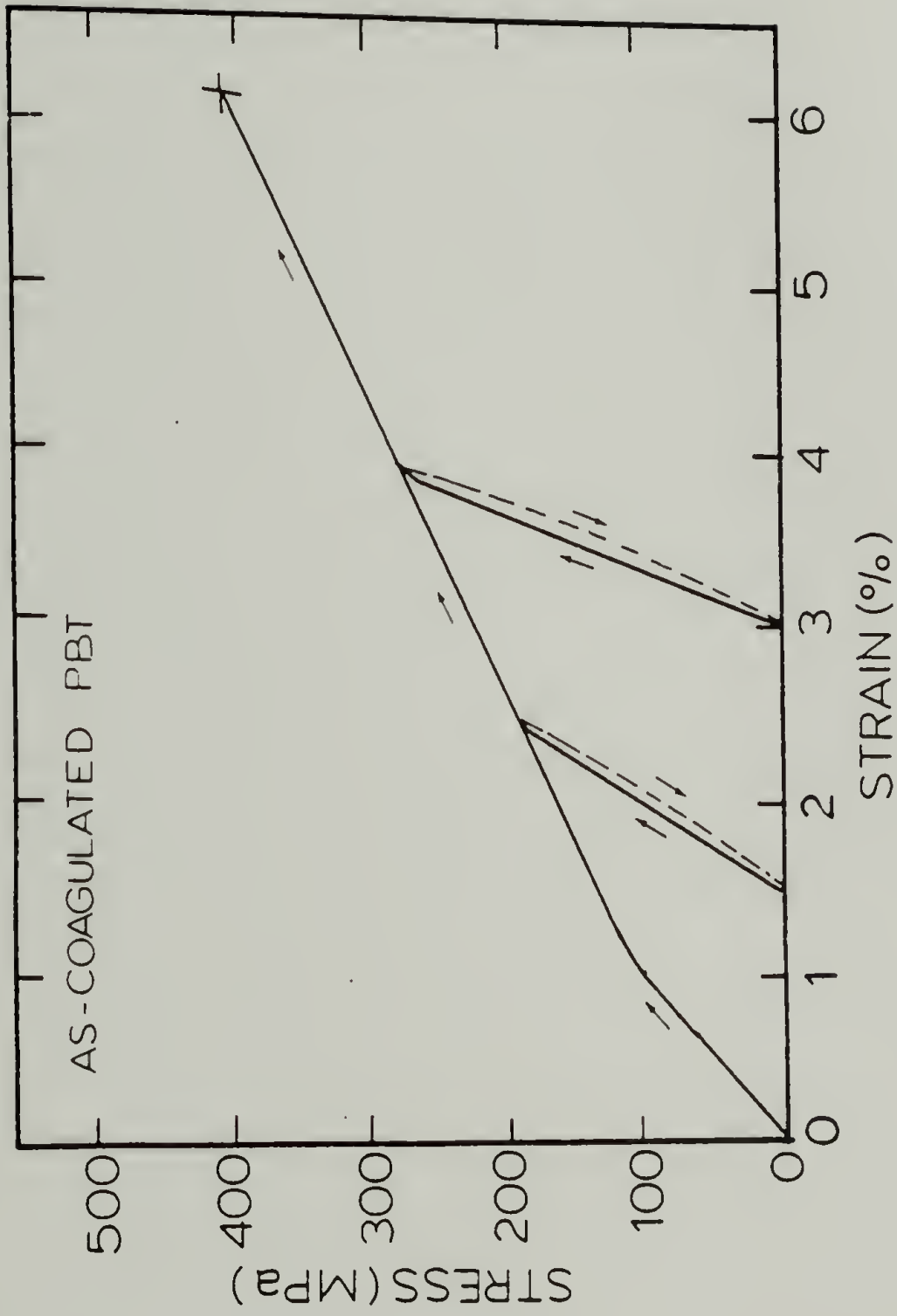


Figure 10. Typical stress-strain curve for wet PBT fiber

value is exhibited in the initial linear stress-strain region followed by a region of plastic deformation. The ultra stiff behavior exhibited by these wet fibers is attributed to the high degree of molecular orientation as evidenced by the WAXD studies.

With increasing spin draw ratio for each set of fibers spun from the same polymer concentration, there is an increase in the tensile modulus with a corresponding decrease in elongation (Table 3). From a closer examination of a plot of SDR vs. Tensile Modulus (Figure 11), fibers spun from a high concentration, high MW PBT exhibit higher properties and show a greater effect of SDR on the modulus than fibers spun from a low concentration, low MW PBT. Jaffee et al. have shown that for PPTA fibers, modulus development is a function of the total spinning strain and is essentially independent of inherent viscosity (51). Therefore, differences in the degree of property enhancement with increasing SDR for the wet PBT fiber is believed to be a concentration dependent phenomenon.

In general, spinning from low concentration dopes produces inferior properties compared to spinning from high polymer concentrations (51,77, 78). As discussed in Chapter I, increasing the polymer concentration reduces the coagulation rate. As a result, the fiber spun from a low concentration of PBT is believed to have a less homogeneous, more porous fibrillar network structure compared to the high concentration PBT fiber. The observed differences in tensile behavior and its dependence on spin draw ratio between these wet fibers spun from various dope

Table 3. Mechanical properties<sup>a</sup> of wet PBT fibers

Fiber	Spin Draw Ratio	% PBT / PPA	Tensile Moduli, E (GPa)	Tensile <sup>b</sup> Strength, $\sigma_b$ (MPa)	Elongation (%)	Shear Moduli (MPa)	E/G
I	3:1	5.5	1.5 $\pm$ 0.2	>60	4.5 $\pm$ 0.5	-	-
II	6:1	5.5	2.1 $\pm$ 0.2	60 $\pm$ 10	3.0 $\pm$ 0.7	-	-
III	3:1	15.5	15 $\pm$ 5	>110	-	-	-
IV	8:1	15.5	29 $\pm$ 7	>230	3.0 $\pm$ 0.5	125 $\pm$ 25	232
V	12:1	15.5	33 $\pm$ 3	410 $\pm$ 35	1.8 $\pm$ 0.3	120 $\pm$ 25	275
VI	17:1	15.5	41 $\pm$ 2	370 $\pm$ 35	1.5 $\pm$ 0.2	120 $\pm$ 10	342

<sup>a</sup>Calculations were based on a wet fibers cross sectional area.

<sup>b</sup>Fibers I, III and IV: tensile force exceeded the load cell capacity.

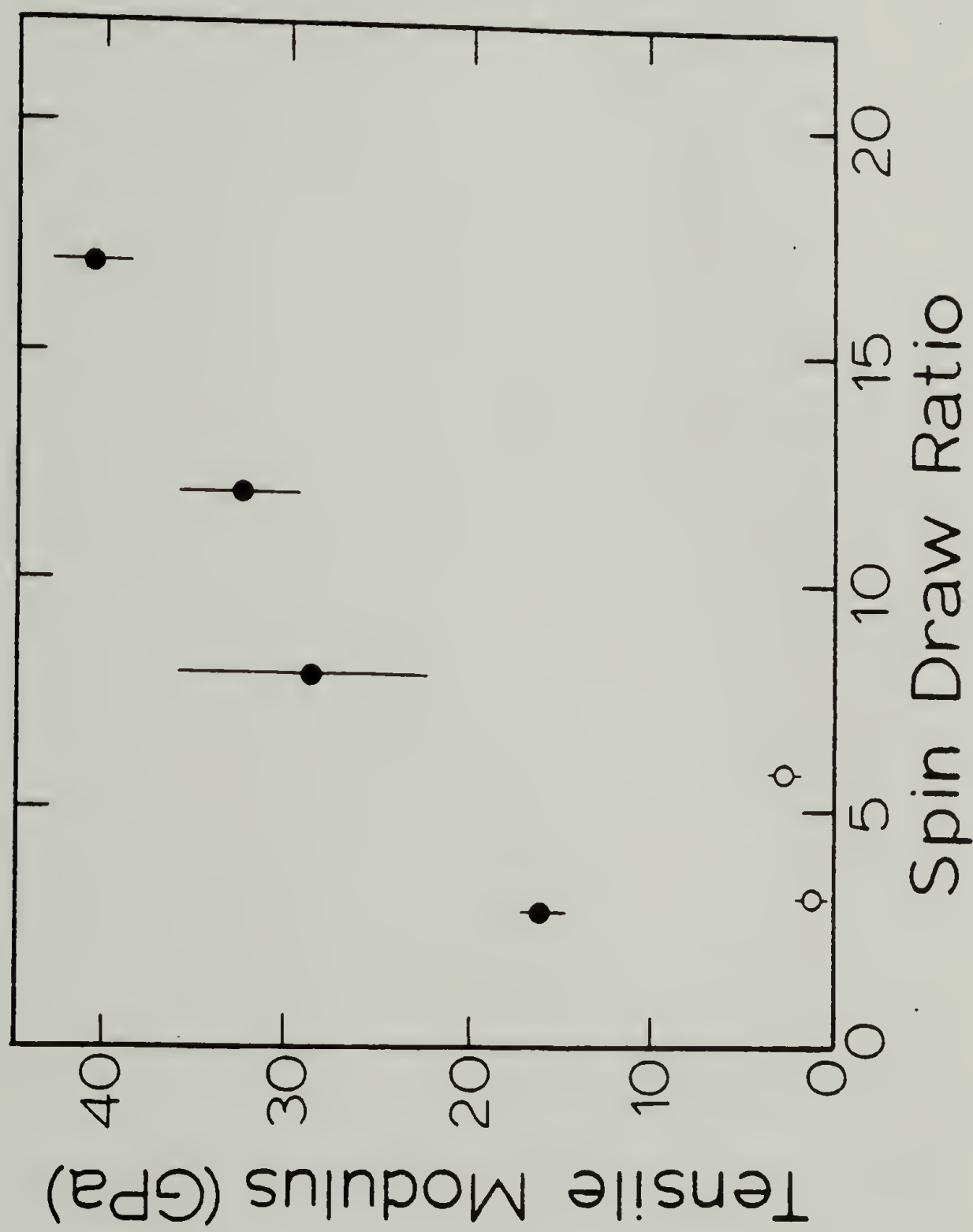


Figure 11. Tensile moduli for wet PBT fibers at different spin draw ratios  
( $\circ$  = 5.5 % PBT/PPA solution spun fiber;  $\bullet$  = 15.5% PBT/PPA solution spun fiber)



concentrations may be a result of different structures developed during coagulation.

The increase in modulus with re-extension after initial plastic deformation is most likely the result of the straightening of wavy regions within the fiber, thus increasing the overall chain orientation of the fibrillar network. The strain hardening characteristics in the wet fibers appear to be strongly dependent upon the extent of deformation, the fiber spin draw ratio and the concentration of polymer. From the data shown in Table 4, for PBT fiber (I), (II) and (III) the relative enhancement in modulus increases with increasing deformation. A comparison between SDR vs. modulus enhancement upon a 1% deformation for fibers spun from 5.5% and 15.5% PBT/PPA solutions has been made in Figure 12. For both sets of PBT fibers (I-VI), there is a reduction in strain hardening effects with increasing spin draw ratio. As the initial alignment of the molecules increases, further changes in chain alignment upon deformation are reduced.

Wet fibers spun from 5.5% PBT/PPA solution display larger strain hardening characteristics than fibers spun from 15.5% PBT/PPA solutions. This behavior is believed to be a direct result of the possible concentration dependent morphologies developed during coagulation. If, in fact, the low concentration fiber has a less homogeneous and more misaligned fibrillar structure, this network would exhibit a relatively greater change in alignment upon deformation.

Fibers traditionally dry-jet wet spun are not often wet stretched. Nonetheless, the previous results do indicate that wet stretching does

Table 4. Strain hardening effects versus spin draw ratio for wet PBT fibers

PBT Fiber	Draw Ratio	% PBT PPA	Initial Modulus, E (GPa)	Initial modulus after unloading and loading to strain $\epsilon_p$ (GPa)	$\epsilon_p$ (%)	Enhancement (%)
I	3:1	5.5	1.9	2.8	1	47
			1.5	2.9	2	93
II	6:1	5.5	2.1	3.0	1	44
			2.1	4.5	2	119
III	3:1	15.5	15	22	1	47
			14	26	2	86
IV	8:1	15.5	29	39	1	35
V	12:1	15.5	34	45	1	32
VI	17:1	15.5	31	36	1	16

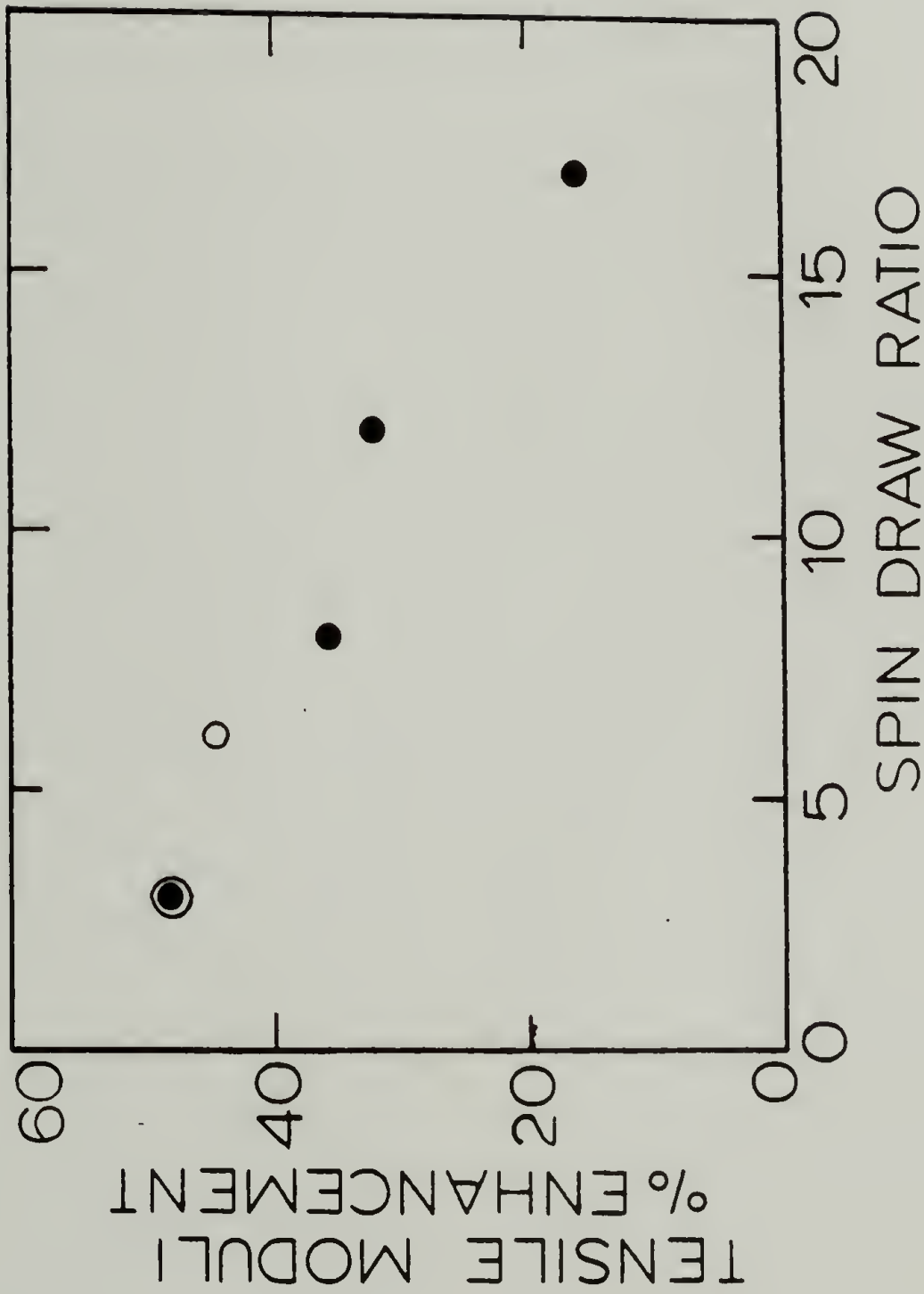


Figure 12. Relative enhancement in tensile moduli upon a 1% strain deformation for wet PBT fibers at different spin draw ratios (○ = 5.5% PBT/PPA solution spun fiber; ● = 15.5% PBT/PPA solution spun fiber)

provide certain advantages for fibers which are spun from low dope concentrations and low spin draw ratios. These results will be of further importance in Chapter III in the discussion of tension drying of these rigid rod polymers.

The apparent plastic behavior in the stress strain curve for the wet PBT fiber is similarly present in the dried state. Previously, it has been suggested that the apparent plastic behavior of the as-spun fiber is a result of the subsequent failure of overstressed elements within the fiber due to the presence of internal stresses (25). It is possible that during coagulation there is generation of internal stresses which would result in the non-linear stress-strain behavior of the wet fiber. Chenevey has determined that films extruded from PBT/PPA solutions exhibit a slight shrinkage (20%) in width upon coagulation (48). Thus, a slight contraction during the coagulation of the PBT fibers may produce internal stresses which may then result in the apparent plastic behavior in the stress strain curve.

Alternatively, the apparent yield stress may correspond to a critical load which effectively squeezes the water out of the fibrillar network, reducing the load bearing area of the fiber. A discussion of the yielding behavior as it pertains to the collapse of the PBT fiber is addressed in section 2.7.

The shear moduli for these wet fibers are summarized in Table 3. The torsional rigidity for these fibers is relatively low regardless of SDR. These wet fibers do possess a high degree of mechanical anisotropy based on calculations of the ratio of the tensile to torsion moduli. It



is concluded that the high degree of mechanical anisotropy present in the as-spun fibers appears to develop in the coagulation process.

## 2.5 Collapse Process

### 2.5.1 Observations

Although the PBT/PPA dope undergoes a slight shrinkage upon coagulation, most of the fiber's dimensional changes occur during the drying process. The collapse process is characterized by an enormous radial shrinkage. Typical radius versus time curves for large diameter PBT fibers I and III spun from 5.5% PBT/PPA and 15.5% PBT/PPA solution respectively are shown in Figure 13. The radial collapse for each of the fibers is observed over a short period ( $\sim 2$  minutes). For the fiber spun from a 5.5% PBT/PPA solution, a 90% reduction in cross sectioned area is evident whereas only a 66% reduction in cross sectional area is observed for fiber spun from a solution of higher polymer concentration (Table 5). This radial collapse is irreversible and when reexposing the fiber to water, no significant radial expansion is observed.

In addition to radial changes, these fibers exhibit longitudinal displacements upon drying as determined by linear variable differential transformer (LVDT) measurements at constant stress. These rigid rod polymers display a negative swelling coefficient whereby the fiber elongates up to 0.1%-0.2% during drying. Over the course of the experiment, the time dependent creep behavior accounted for half of the fiber's observed axial elongation (Figure 14). The remaining dimensional changes (0.05%-0.1%) are due to water removal.

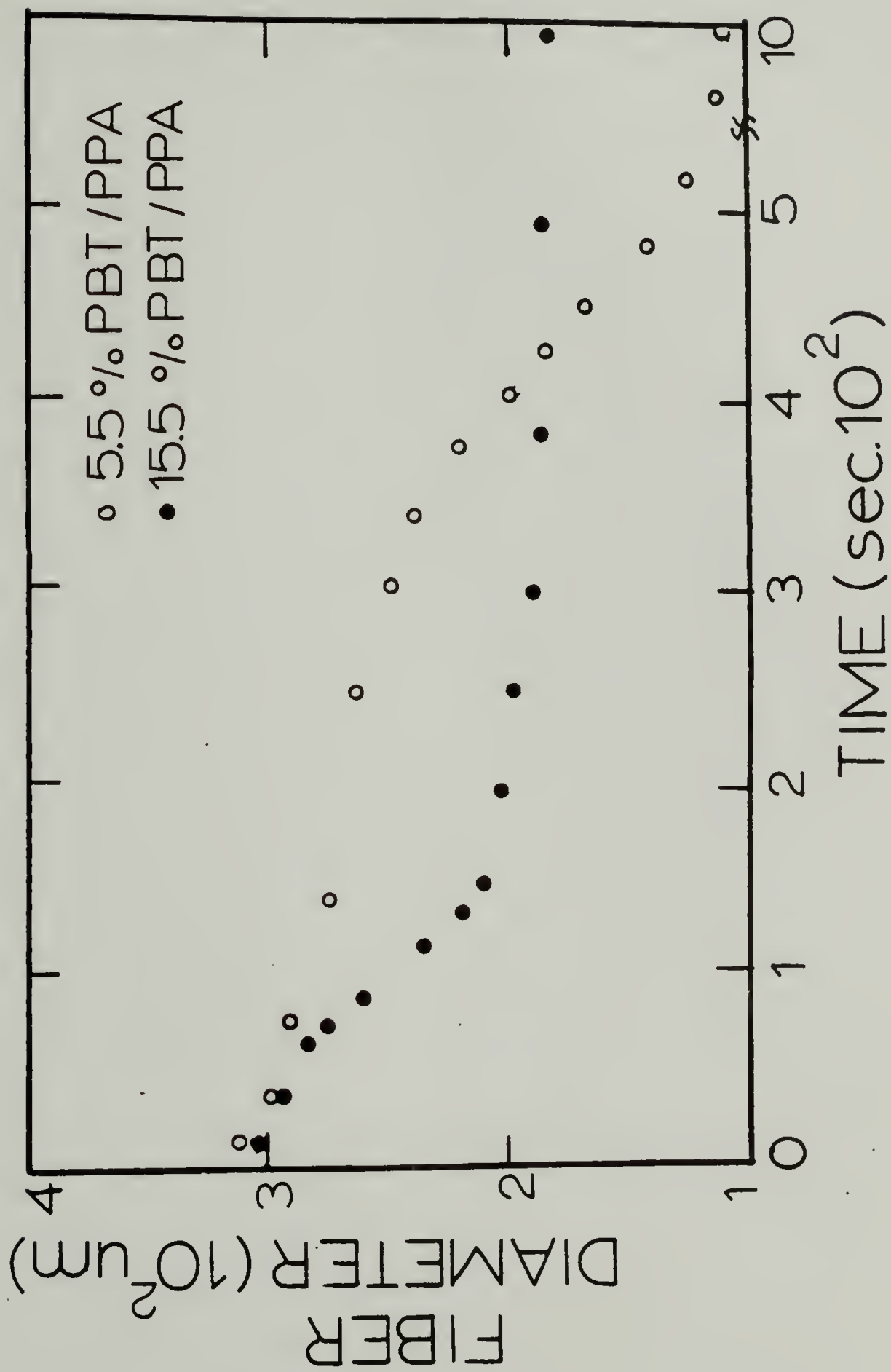


Figure 13. Radial changes for a PBT fiber during drying

Table 5. Diameter changes for various PBT fibers due to the drying process.

PBT in PPA (%)	Initial Diameter, $R_0$ ( $\mu\text{m}$ )	Final Diameter, $R_\infty$ ( $\mu\text{m}$ )	Cross Sectional Area Reduction (%)
5.5	310	109	-87
5.5	260	110	-82
5.5	185	80	-81
15.5	303	176	-66

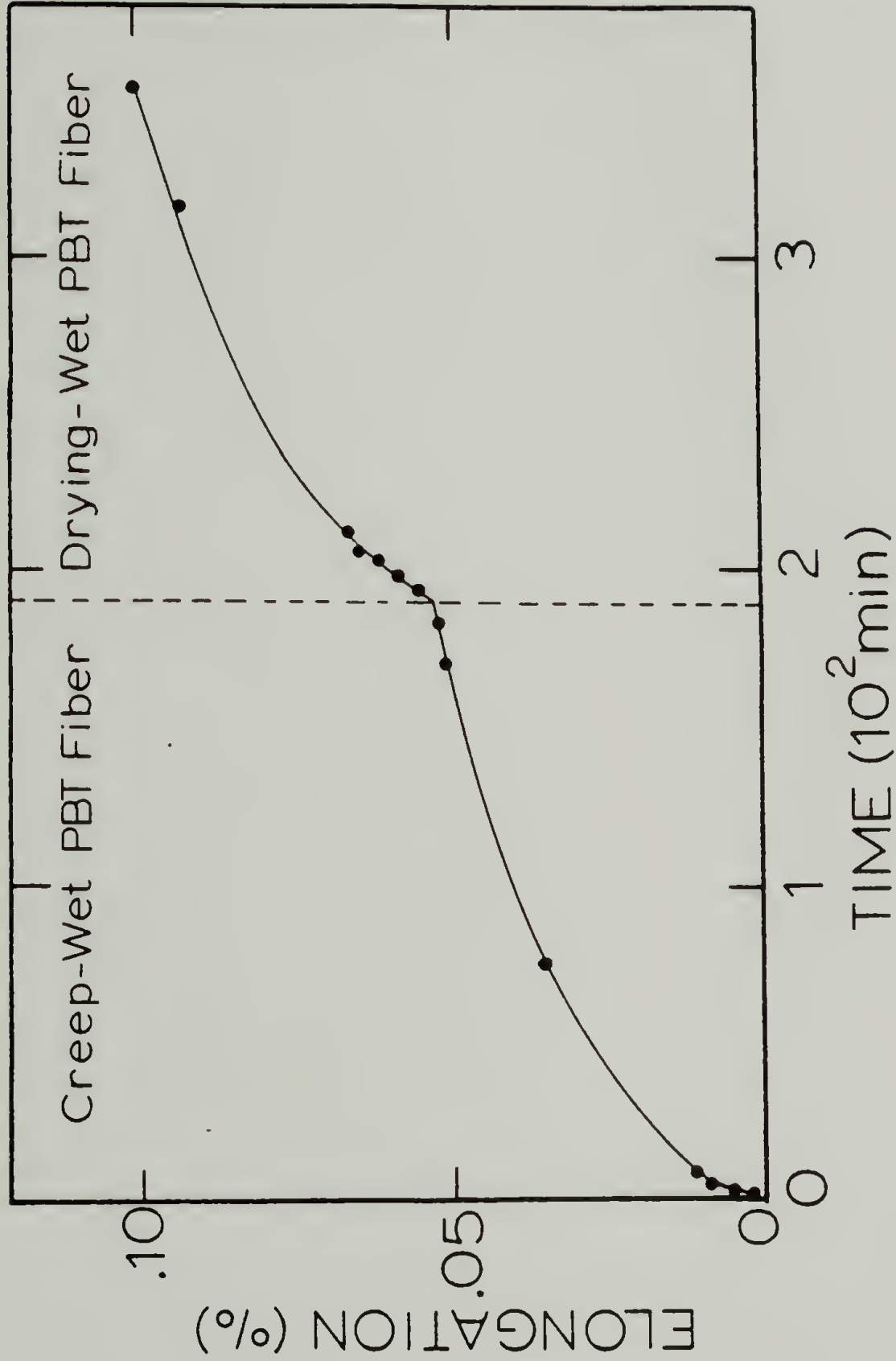


Figure 14. Axial changes for a PBT fiber during drying



### 2.5.2 Molecular Considerations

The observed dimensional changes which result from drying may be interpreted in light of the porous fibrillar nature of the wet fiber. It is speculated that capillary forces are created within the wet PBT fiber due to surface tensions present at the liquid/gas interface within the micro and macro voids as discussed in Chapter I for coagulated cellulose, PAN and wet wood. The capillary forces generated are described by Jurin's Law (2.6):

$$P_0 - P_1 = \frac{2\gamma\cos\theta}{r} \quad (2.6)$$

where  $P_0$  = pressure in gaseous phase

$P_1$  = pressure in liquid phase

$\theta$  = wetting angle

$r$  = radius of capillary

$\gamma$  = surface tension of liquid

Capillary tension arises when  $\Delta P$  is negative. It is believed that large capillary tensions can be formed in the swollen PBT network since the radii of the capillaries (the microvoids) are quite small ( $50\text{\AA}$ ) and the surface tension of the water is relatively high (72 dynes/cm). A radial collapse of the porous PBT network results if these internal forces exceed the transverse compressive strength of the wet fiber.

The effect of coagulation medium on the radial shrinkage of PBT fibers has been studied by investigators at DuPont (50). Based upon their results summarized in Table 6, the degree of radial shrinkage upon

Table 6. Air dried collapse of PBT coagulated by various non solvents

Coagulation Medium	Air Dried Shrinkage <sup>a</sup> (%)	Surface Tension $\gamma$ <sup>b</sup> dynes/cm
H <sub>2</sub> O	44	71.97
1% NaOH/H <sub>2</sub> O	32	72.02
30% MeOH/H <sub>2</sub> O	32	47.33
30% Acetone/H <sub>2</sub> O	26	42.03
0.5% NaOH/H <sub>2</sub> O	15	71.6
70% MeOH/H <sub>2</sub> O	15	31.60
70% Acetone/H <sub>2</sub> O	15	29.81
100% Acetone	11	23.0
100% MeOH	9	22.65
70% PPA	8	(15-40) <sup>c</sup>

<sup>a</sup>reference 50

<sup>b</sup>reference 79

<sup>c</sup>reference 80

drying may be ranked in decreasing order based on the coagulant employed.



H<sub>2</sub>O causing the highest collapse; PPA the lowest collapse. The variation in the collapse of PBT infiltrated with the different coagulants may be attributed to differing capillary tensions generated within the fiber. It is apparent from (2.6) that capillary tensions can be reduced with a decrease in  $\gamma$ . A comparison between the surface tension of the various coagulants and the % air dried shrinkage of PBT is shown in Table 6. The observed radial collapse decreases as the surface tension of the coagulant increases. From similar studies on hardwoods, Ellwood et al. have shown that the collapse is eliminated by replacing water with methanol and ethanol which have a lower surface tension (81).

A correlation between the surface tension of the coagulant and radial collapse of the fiber may be purely coincidental as the surface tension is not the only factor dictating the generation of capillary forces. For fibers coagulated with the different nonsolvents, various morphologies may result thereby generating different size microvoids. In addition, the wetting angle  $\theta$  between the coagulant and PBT may be considerably different for the various liquids. Variations in the wetting angle,  $\theta$ , and the void size,  $r$ , could conceivably contribute to the observed differences in the fiber shrinkage of PBT coagulated from various mediums.

The axial elongation of the PBT fiber during drying is unlike other solution spun fibers such as PAN and cellulose whereby the collapse

process is characterized by a contraction in all three principal directions (30,36,45). The collapse of the PBT fibrillar network radially and tangentially results in the alignment of the fibrils; thus, the observed elongation of the fiber.

## 2.6 Fiber Property Alterations During Drying

### 2.6.1 Structure

The effect of the collapse process on the microstructure has been investigated through both WAXD flat film and diffractometric techniques. The WAXS diffraction patterns of the PBT fiber before and after drying reveal few observable differences (Figure 7). However, microstructural alterations between the wet and dry PBT fiber were detected through line profile analysis of the equatorial reflections. The size of the lateral coherently scattering regions of PBT crystallites within the fiber are determined by the breadth of the equatorial reflection in the  $2\theta$  direction (measured as the full width at half maximum intensity above background (FWHM)).

A comparison of the WAXS diffractometric data between wet and dry PBT is provided in Table 7. From this data, a narrowing of the first equatorial reflection ( $e_1$ ) is detected after drying. This observation corresponds to an increase in the size of the lateral coherently scattering regions from 1.1 nm to 1.9 nm perpendicular to the chain axis. In addition, a shift in peak position to lower scattering angle (i.e., larger interplanar d-spacing) is observed. Such narrowing of equatorial peaks and the shifting of peak positions are characteristic of the



Table 7. Wide angle x-ray diffractometer data: Wet versus dry PBT

Sample	Peak	Position ( $2\theta$ ) (degrees)	d spacing (nm)	FWHM (rad.)	(Gaussian) Lateral Coherence Scattering Size (nm)
Wet PBT	e <sub>1</sub>	15.5	0.572	.140	1.1
	e <sub>2</sub>	26.1	0.341	.056	3.0
Dry PBT	e <sub>1</sub>	15.1	0.587	.084	1.9
	e <sub>2</sub>	25.9	0.344	.059	2.8

morphological changes associated with post processing heat treatment and indicate the existence of a higher degree of perfection in the lateral molecular order (25).

It is concluded that although the general microstructural details of PBT fibers are developed during coagulation, the drying process serves to improve the lateral molecular order.

### 2.6.2 Mechanics

A comparison between the tensile behavior of the wet and dry PBT is shown in Figure 15. The stress-strain curves for both fibers are initially elastic followed by an apparent plastic region. Upon drying, a dramatic increase in the tensile modulus and strength is observed with a reduction in elongation. This apparent increase in modulus and strength of the dried PBT fiber is attributed, in part, to the drastic reduction in cross-sectional area due to the collapse process. Therefore, a more meaningful comparison between the wet and dry tensile properties is obtained from the force versus strain curve (Figure 16). This result indicates that the wet fiber has the same load bearing capacity as the dried fiber and the force to yield is the same for both materials. However, the wet fiber's modulus in terms of gms/% strain is still less than the modulus of the dried fiber.

A comparison between the tensile properties of the wet and dry fibers with various spin draw ratios is summarized in Table 8. To calculate the wet fiber properties the final dried cross-sectional area was used to normalize for the cross sectional changes during drying. For

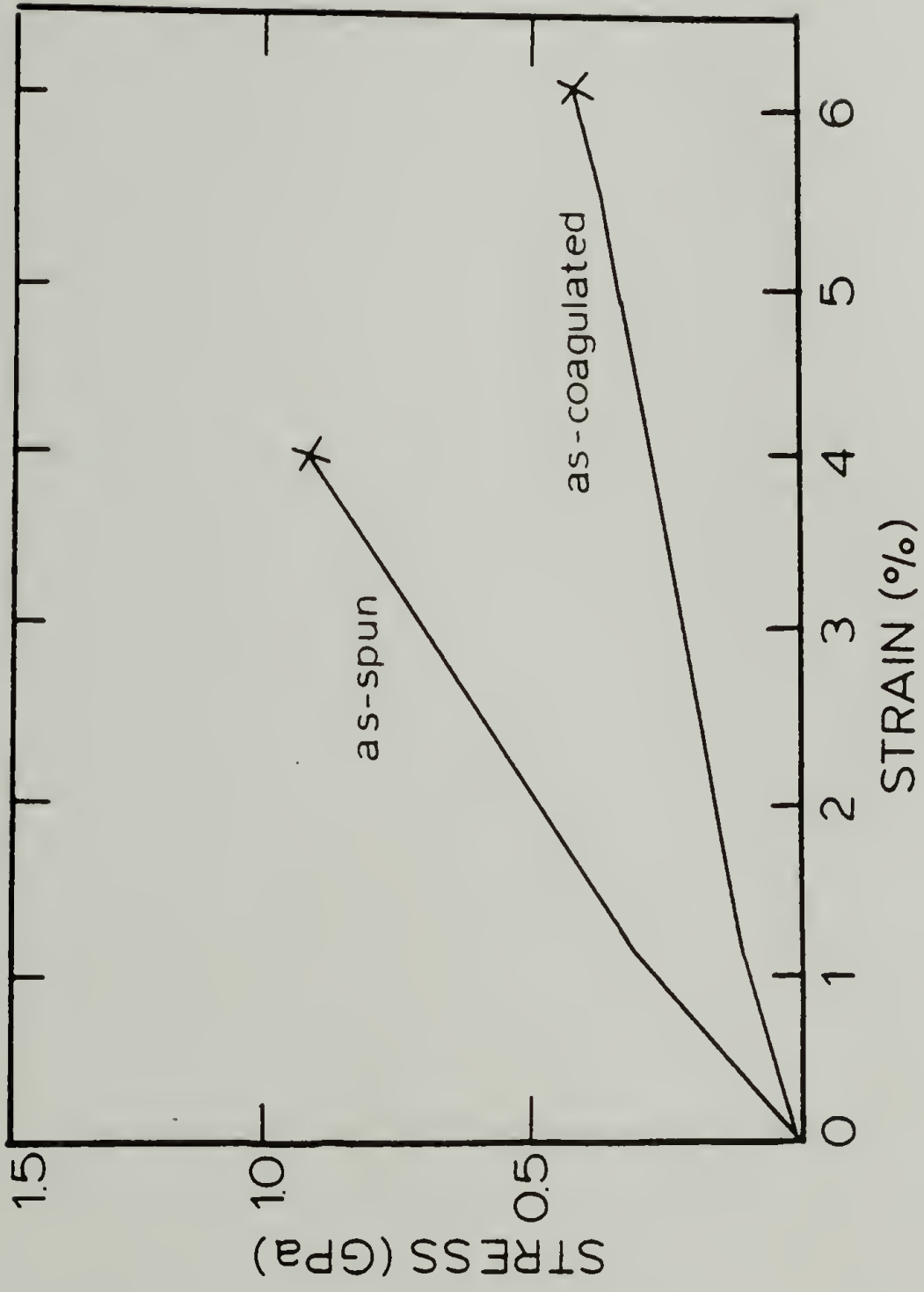


Figure 15. Typical stress-strain curves for wet vs. dry PBT fiber (I)

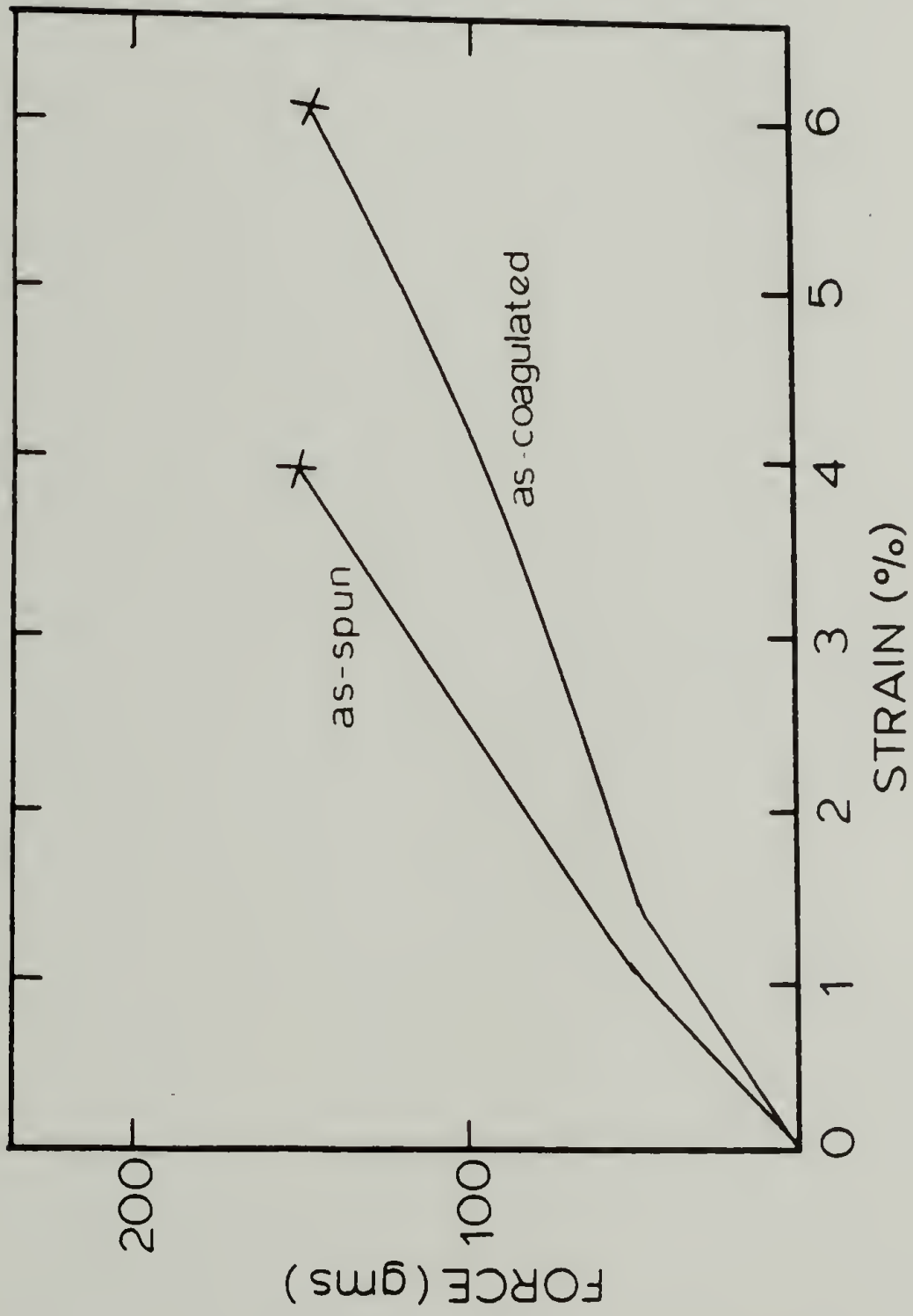


Figure 16. Typical force-strain curves for wet vs. dry PBT fiber (I)



Table 8. A comparison between the tensile properties of wet versus dry PBT fibers

PBT Fiber	PBT Content (%)	Spin Draw	Tensile Moduli, E (GPa)	Tensile Strength, $\sigma_b$ (GPa)	Elongation (%)	Tensile Moduli <sup>b</sup> Enhancement (%)
I Wet <sup>a</sup>	5.5	3:1	15 + 2	-	4.5 + 0.5	+165
I Dry			40 ± 5	-	3.5 ± 0.4	
II Wet <sup>a</sup>	5.5	6:1	20 + 2	0.6 + 0.1	3.0 + 0.7	+50
II Dry			30 ± 3	0.8 ± 0.1	2.9 ± 0.5	
III Wet <sup>a</sup>	15.5	3:1	43 + 8	-	-	+33
III Dry			57 ± 7	-	-	
IV Wet <sup>a</sup>	15.5	8:1	85 + 20	-	3.0 + 0.5	+35
IV Dry			115 ± 15	-	2.5 ± 0.4	
V Wet <sup>a</sup>	15.5	12:1	95 + 8	1.2 + 0.1	1.8 + 0.3	+26
V Dry			120 ± 10	1.2 ± 0.1	1.5 ± 0.2	
VI Wet <sup>a</sup>	15.5	17:1	120 + 5	1.1 + 0.1	1.5 + 0.2	+4
VI Dry			125 ± 10	1.4 ± 0.1	1.7 ± 0.2	

<sup>a</sup>Calculations were based on a "dried" cross sectional area.

<sup>b</sup>Comparisons were made between the Wet and Dry properties.

+ values are one standard deviation.

each PBT fiber, there is an enhancement in tensile modulus with a reduction in elongation after drying. The tensile strengths based on dried fiber diameters were not appreciably altered between the wet and dry state. However, with increasing spin draw ratio, the enhancement in tensile properties upon drying decreases (Figure 17).

These observed alterations in tensile properties are believed to be a direct consequence of the removal of water and the resulting fiber collapse. As the fibrillar network collapses during drying, the fibrillar elements become straightened as they elongate. Figure 18 illustrates a geometrical arrangement of two fibrils collapsing together. The original fiber length elongates by a distance  $\Delta L$  such that

$$L + \Delta L = L_0 \quad (2.7)$$

where  $L_0$  is the average fibril length. The corresponding change in average orientation angle,  $\Delta\theta$ , due to the collapse of the fibrils is calculated from equation (2.8).

$$\Delta\theta = \cos^{-1}\left(\frac{1}{1 + \frac{\Delta L}{L}}\right) \quad (2.8)$$

The average change in orientation angle is between  $1.8^\circ$ - $2.6^\circ$  when the fiber elongates  $\frac{\Delta L}{L}$  between .05%-.1%. Since the tensile modulus is controlled by the orientation of polymer chains, an enhancement of this tensile property occurs due to possible changes in the alignment of the fibrils after drying. A change of  $2^\circ$  could have considerable impact on the tensile modulus since these wet PBT fibers are initially so highly

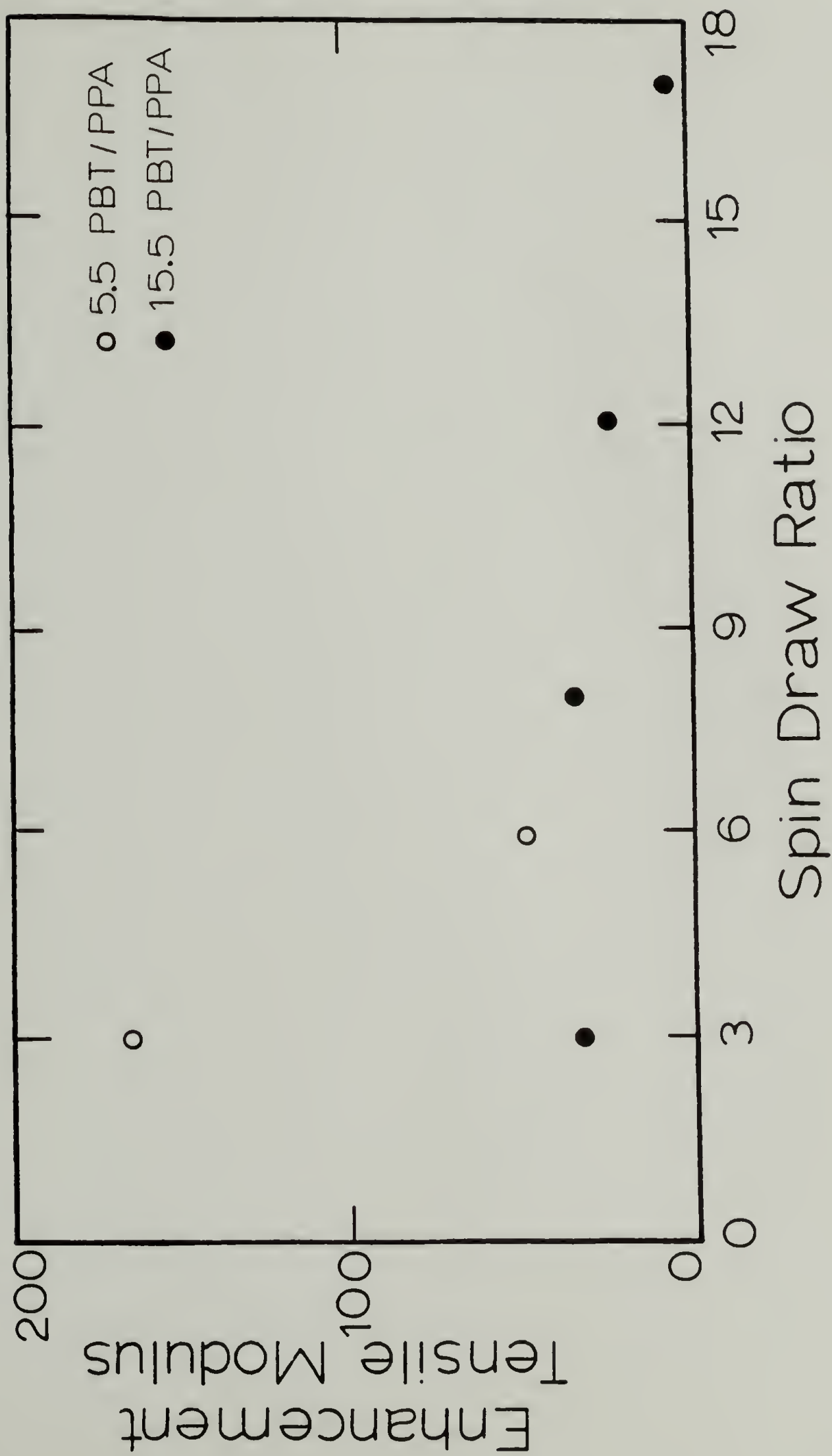
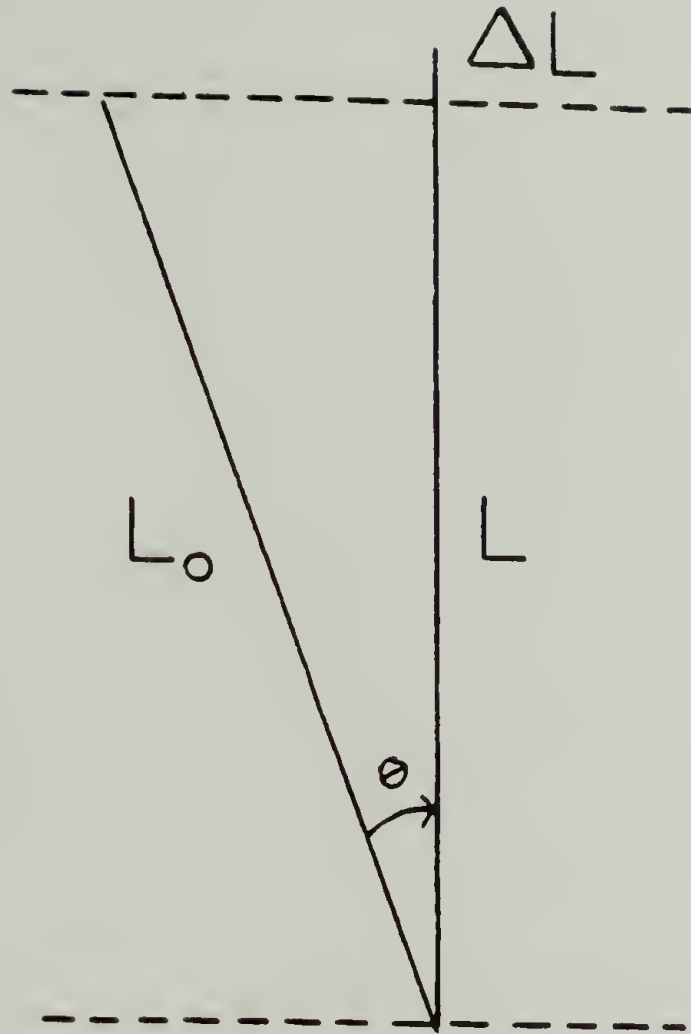


Figure 17. Enhancement in tensile moduli as determined from the force-deflection curves upon drying for PBT fibers of different spin draw ratios



$L$  = length of wet fiber  
 $L_0$  = length of fibril  
 $L + \Delta L$  = length of dry fiber  
 $\Delta \theta$  = change in fibril  
                   orientation angle

Figure 18. Representation of a fibril before and after the fiber's collapse



oriented. The observed decrease in the modulus enhancement with increasing fiber SDR may also be rationalized in terms of the collapse process. As the initial orientation of the wet fiber increases, the relative enhancement in further chain alignment decreases upon drying.

It appears that the magnitude of the collapse observed during drying is directly related to the relative enhancement in the tensile modulus upon drying. As mentioned previously, fibers spun from a low concentration of PBT in PPA exhibit the largest reduction in cross-sectional areas (Table 5). These same fibers exhibit the largest increase in Young's modulus upon drying (Table 8).

A comparison of the strain hardening characteristics between a wet and dry PBT fiber is shown in Table 9. For fibers spun from a low concentration of PBT/PPA, the strain hardening effects in a dry fiber are substantially greater than the wet fiber when deformed to 1% strain. The strain hardening effect in the wet fiber is a result of the straightening of the fibrillar network whereas in the dry fiber the increase in modulus upon deformation is attributed to both the straightening of the fibrils and the unbuckling of the compressed fibrillar elements which arise from internal stresses during shrinkage. Consequently, since fibers spun from a low concentration of PBT/PPA undergo a large radial collapse, the magnitude of the internal stresses and thus the degree of compressive buckling within the fiber is larger. Therefore, a more substantial difference in the strain hardening behavior between the wet and dry state is predicted and is observed in the fiber undergoing the greater radial shrinkage.

Table 9. Comparison between the strain hardening behavior of wet versus dry PBT at 1% strain

PBT Fiber	% PBT/PPA Solution	Draw Ratio	Initial Tensile Modulus <sup>a</sup> (GPa)	Initial Modulus After Loading and Unloading to 1% Strain (GPa)	Enhancement (%)
I Wet	5.5	3:1	1.9 + 0.3	2.8 + 0.3	47
I Dry			39 ± 7	63 ± 3	62
II Wet	5.5	6:1	2.1 + 0.3	3.0 + 0.4	44
II Dry			29 ± 3	51 ± 5	76
III Wet	15.5	3:1	15 + 3	22 + 3	47
III Dry			57 ± 7	87 ± 10	53
IV Wet	15.5	8:1	29 + 7	39 + 6	35
IV Dry			113 ± 14	156 ± 10	38
V Wet	15.5	12:1	34 + 2	45 + 3	32
V Dry			133 ± 11	176 ± 12	32
VI Wet	15.5	17:1	31 + 1	36 + 2	16
VI Dry			123 ± 8	142 ± 8	15

± values are one standard deviation.

<sup>a</sup>Calculations of wet fiber's tensile modulus are based on wet cross sectional area.

There is little difference in relative enhancement in tensile modulus between the wet and dry fiber for fibers spun from a high concentration of PBT. The magnitude of internal stresses generated and hence the compressive buckling of the dried fiber is speculated to be reduced for these PBT filaments which exhibit a smaller collapse process. Consequently, deforming the highly aligned network in either the swollen or collapsed state produces similar results.

The effects of the collapse process on the torsional and compressive characteristics are summarized in Table 10. Upon drying, there is an increase in the shear modulus whereas  $E/G$ , a measure of the degree of material anisotropy, decreases when the PBT fiber dries. In addition, the compressive strength as determined on both the solid and hollow filaments increases with the removal of water. A comparison of the compressive force-deflection curves between wet and dry hollow PBT fibers is shown in Figure 19. An increase in compressive force and compressive modulus (gms/% strain) is observed upon drying indicating that the mechanical alteration observed with the removal of water is not an artifact of the reduction in cross-sectional area. Moreover, the relatively high critical load to induce buckling in the wet fiber when compared to the dry fiber indicates that the compressive integrity of PBT appears to develop during coagulation.

For these wet rigid rod fibers, the observed enhancement in the shear modulus upon drying correlates to the enhancement in compressive strength. These observations correspond to the correlations predicted by DeTeresa et al. (63) between shear modulus and axial compressive

Table 10. Torsion and compressive properties of wet and dry PBT fibers

Sample	Tensile Modulus, E (GPa)	Torsion Modulus, G (MPa)	Compressive Modulus (GPa)	Critical Compressive Strain (%)	Compressive Strength (MPa)	E/G
Solid PBT Fiber (VII)						
Wet <sup>c</sup>	35 ± 5	115 ± 10	-	0.5 ± 0.05	170 ± 10 <sup>a</sup>	305
Dry	140 ± 15	820 ± 25	-	0.4 ± 0.05	575 ± 100	170
Hollow PBT Fiber						
Wet <sup>c</sup>	-	244 ± 30	2 ± .5	1.4 ± 0.2	22 ± 1 <sup>b</sup>	-
Dry	35 ± 10	847 ± 100	25 ± 10	0.6 ± 0.1	89 ± 27	-

± values are one standard deviation.

<sup>a</sup>Calculated compressive strength

<sup>b</sup>Measured compressive strength

<sup>c</sup>Wet properties calculated from wet cross sectional area



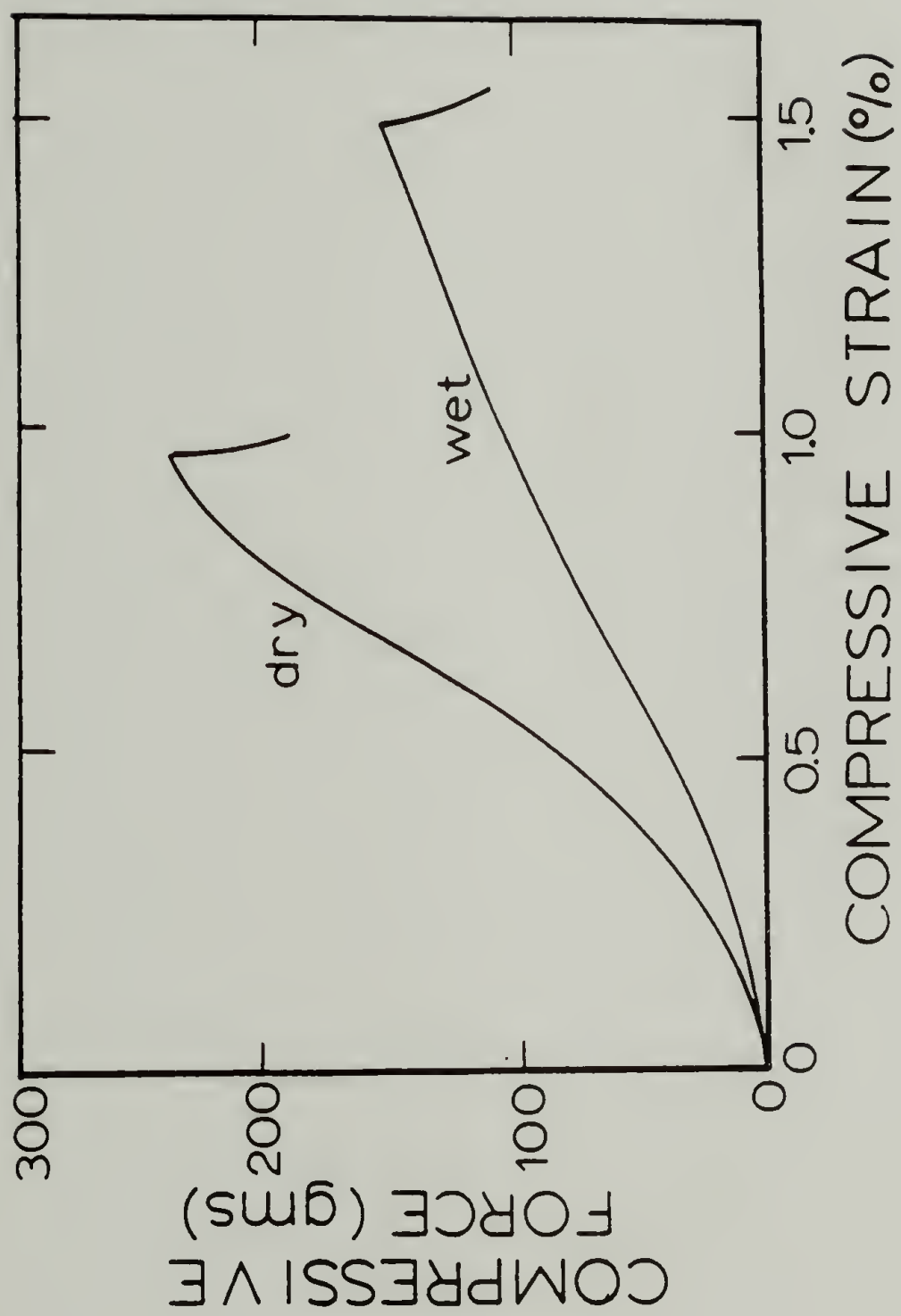


Figure 19. Compressive force-strain behavior for hollow wet vs. dry PBT fibers

strength for extended chain polymers. The results reported here suggest that the transverse structural interactions dictate the compressive behavior of PBT fiber.

Alterations in the shear and compressive characteristics of these fibers are easily interpreted in terms of the collapse of the wet fiber. The lateral interactions between the fibrils and microfibrils will be minimized when the fibrillar network is swollen with water. With the removal of water, these interactions on both the macroscopic and microscopic scale will increase. From WAXD measurements, an increase in the extent of lateral molecular order between chains is observed upon drying. This increase in chain and fibril interactions due to water removal is responsible, in part, to the observed enhancement in the transverse properties. It appears that improvements in the fiber's compressive strength can be achieved with the removal of water.

Alternatively, changes in the shear moduli and, in turn, the compressive strengths could be simple manifestations of the collapse of the fibrillar structure during drying. Assuming the PBT fiber is simply a collection of rods, the geometrical arrangement and rearrangement of these rods can strongly influence the shear modulus. The shear modulus is given as follows:

$$G = \frac{4\pi I_d \ell}{\tau^2 J} \quad (2.9)$$

where  $J$  = polar moment of inertia of a plane area  
 $I_d$  = moment of inertia of the pendulum disc  
 $l$  = fiber length  
 $t$  = period of oscillation

For simplicity, it is assumed that the PBT fiber consists of three non-interacting "fibrils" of radius  $R'$  tightly packed in the dry state. In the wet state, these rods are separated a distance  $R$  from the centroid of the collection of fibrils (Figure 20). Using the parallel axis theorem (82), the polar moment of inertia for these cross-sectional configurations is expressed as follows:

$$J = J_0 + A\bar{r}^2 \quad (2.10)$$

where  $J_0 = \int_0^R r^2 2\pi r dr$

$\bar{r}$  = distance from center to centroid of area  $A$

For the three rods in the dry PBT state where  $\bar{r}=R'$ , , the polar amount of inertia is determined to be

$$J = \frac{9}{2} \pi (R')^4 \quad (2.11)$$

Therefore, the shear modulus can be determined from (2.9).

$$G_{(\text{dry})} = \frac{8}{9} \frac{\pi}{t^2} \frac{I_d l}{(R')^4} \quad (2.12)$$

In the swollen PBT geometry where  $\bar{r}=2R$ ,  $J$  takes the following form.

$$J = \frac{27}{2} \pi R^4 \quad (2.13)$$

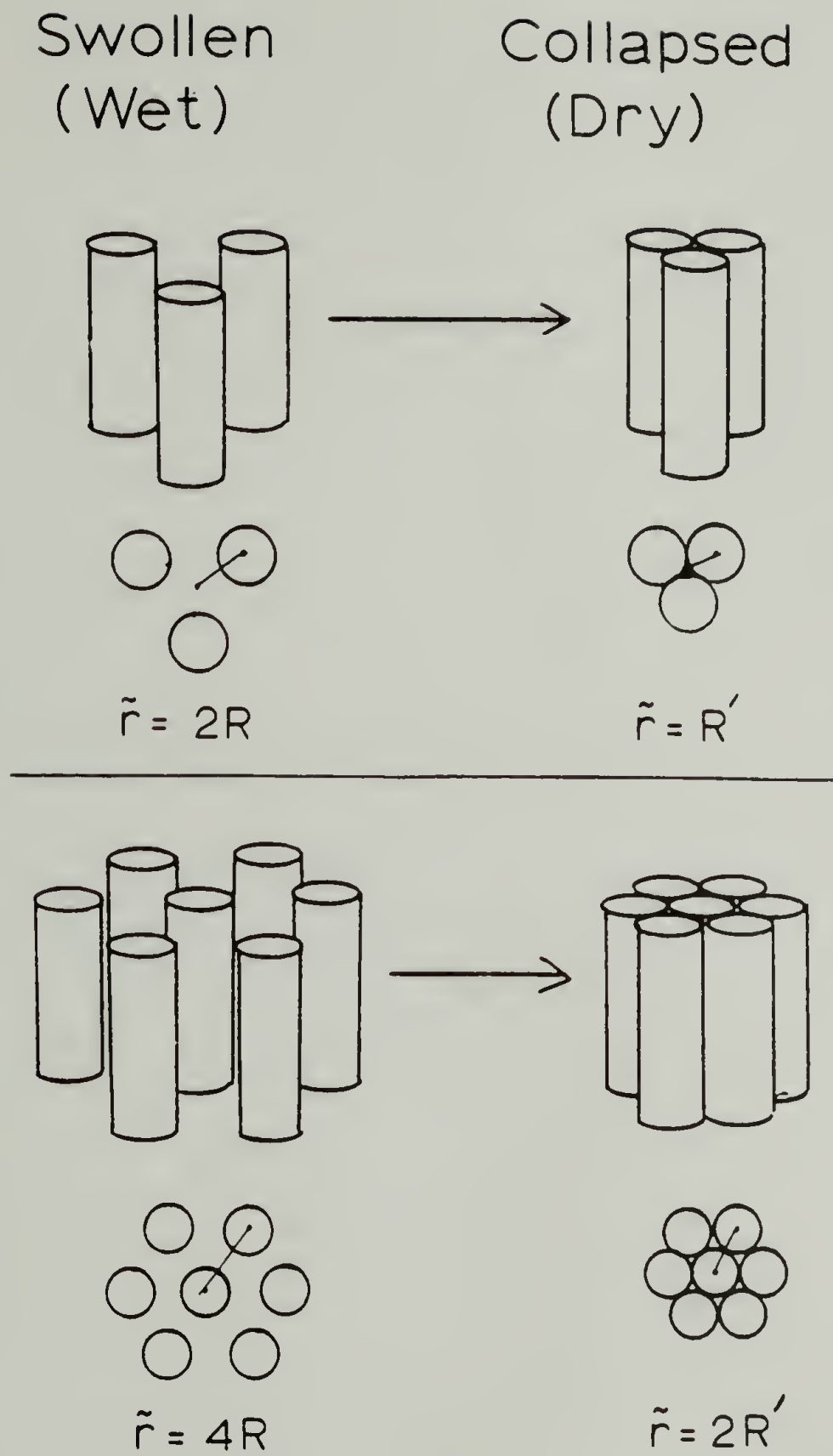


Figure 20. Representation of a PBT fiber composed of 3 and 7 fibrils in the wet and dry state



Thus, the shear modulus for this swollen array of fibrils is expressed as follows:

$$G_{(\text{wet})} = \frac{8}{27} \frac{\pi I_d \ell}{\tau R^4} \quad (2.14)$$

The ratio of  $G(\text{dry})/G(\text{wet})$  is approximately equal to  $3(\frac{R}{R'})^4$ . Although the period of oscillation is slightly greater for the wet fiber than the dry fiber, for purposes of this discussion it is assumed that they are nearly equal. However, a collapse of the microfibrillar network and hence the fibrils is expected, and the fibril radius in the wet state  $R$  may be greater than the fibril radius in the dry state,  $R'$ . The alterations in the fibril size upon drying contribute to an even larger difference between the predicted shear moduli in the wet and dry states.

Similar calculations have been made on a system of 7 "fibrils"; 6 equidistant from a central fibril in a swollen and collapsed state (Figure 20). The shear modulus for this geometry when in a swollen state is expressed as follows:

$$G_{(\text{wet})} = \frac{8\pi I_d \ell}{199\tau R^4} \quad (2.15)$$

For these same seven rods in a collapsed state, the shear modulus takes the following form.

$$G_{(\text{dry})} = \frac{8\pi I_d \ell}{55\tau (R')^4} \quad (2.16)$$

The ratio of  $G(\text{dry})/G(\text{wet})$  is approximately  $3.6(\frac{R}{R'})^4$ .

These calculations indicate that the apparent enhancement in the shear modulus upon drying may be strictly an artifact of the structural rearrangements of the fibrils.

### 2.7 Shrinkage Behavior in a Cylindrically Orthotropic Material

The different shrinkage behavior in the radial and longitudinal direction for PBT fibers is characteristic of the shrinkage phenomena observed in wood, a cylindrically orthotropic material. Cylindrically orthotropic materials possess three mutually orthogonal planes of symmetry along the radial ( $r$ ), tangential ( $\theta$ ), and longitudinal ( $z$ ) axis. The orthotropic nature of wood results from the organization of its cellular structure. Both softwood and hardwood are characterized by hollow longitudinally aligned tubular cells (tracheids and vessels) with the radial orientation of tubular cells (wood rays) (83). Because of this morphology the material properties differ in these three principal directions. In particular the shrinkage behavior may be ranked as follows:

$$\beta_{\theta} > \beta_r > \beta_z$$

where  $\beta_i$  = shrinkage coefficient defined as the total dimensional change between the green condition and 14% R.H.

The generation of stresses and strains due to orthotropic shrinkage is of particular interest. The magnitude of the radial and tangential collapse is believed to influence the observed longitudinal change in strain with concentration for such an orthotropic material. Therefore,

the change in strain,  $\epsilon_z$ , and the generation of internal stresses of a cylindrically orthotropic elastic solid undergoing isothermal concentration changes under a constant load has been derived from elasticity theory.

The mechanical properties of an elastic solid are defined by the generalized Hooke's Law (equation (2.17) for small strains.

$$\epsilon_{ij} = S_{ijkl} \sigma_{kl} \quad (ijkl = 1,2,3,4, \text{ etc.}) \quad (2.17)$$

where  $S_{ijkl}$  = compliance tensor

$\epsilon_{ij}$  = strain tensor

$\sigma_{kl}$  = stress tensor

Although the large radial and hoop contractions in wood do not constitute small strains, the non linear components in the above constitutive equation are ignored in this analysis. Through symmetry arguments where  $S_{ijkl} = S_{klij}$ , and energy restrictions on the material, the compliance tensor is reduced to 21 independent components. The number of independent compliance constants is reduced from 21 to 9 for a cylindrically orthotropic material since symmetry exists with respect to the three mutually orthogonal planes  $(r, \theta, z)$ . The matrix of compliance constants for an orthotropic solid is written as a six by six array  $a_{ij}$  instead of the fourth ranked tensor  $S_{ijkl}$  and is described as follows:

$$a_{ij} = \begin{vmatrix} a_{11} & a_{12} & a_{13} & 0 & 0 & 0 \\ a_{12} & a_{22} & a_{23} & 0 & 0 & 0 \\ a_{13} & a_{23} & a_{33} & 0 & 0 & 0 \\ 0 & 0 & 0 & a_{44} & 0 & 0 \\ 0 & 0 & 0 & 0 & a_{55} & 0 \\ 0 & 0 & 0 & 0 & 0 & a_{66} \end{vmatrix} \quad (2.18a)$$

For a cylindrical coordinate system, the compliance coefficients are expressed in terms of  $E_i$ , the Young's moduli,  $G_{ij}$ , the shear moduli, and  $\nu_{ij}$ , the Poisson coefficients.

$$a_{ij} = \begin{vmatrix} \frac{1}{E_r} & \frac{-\nu_{\theta r}}{E_\theta} & \frac{-\nu_{zr}}{E_z} & 0 & 0 & 0 \\ \frac{-\nu_{r\theta}}{E_r} & \frac{1}{E_\theta} & \frac{-\nu_{z\theta}}{E_z} & 0 & 0 & 0 \\ \frac{-\nu_{rz}}{E_r} & \frac{-\nu_{\theta z}}{E_\theta} & \frac{1}{E_z} & 0 & 0 & 0 \\ 0 & 0 & 0 & \frac{1}{G_{\theta z}} & 0 & 0 \\ 0 & 0 & 0 & 0 & \frac{1}{G_{rz}} & 0 \\ 0 & 0 & 0 & 0 & 0 & \frac{1}{G_{r\theta}} \end{vmatrix} \quad (2.18b)$$

The strains for a cylindrically orthotropic fiber are expressed by the following set of equations.



$$\epsilon_r = a_{11}\sigma_r + a_{12}\sigma_\theta + a_{13}\sigma_z$$

$$\epsilon_\theta = a_{12}\sigma_r + a_{22}\sigma_\theta + a_{23}\sigma_z$$

$$\epsilon_z = a_{13}\sigma_r + a_{23}\sigma_\theta + a_{33}\sigma_z$$

$$\gamma_{r\theta} = \frac{\tau_{r\theta}}{G_{r\theta}}$$

$$\gamma_{\theta z} = \frac{\tau_{\theta z}}{G_{\theta z}}$$

$$\gamma_{rz} = \frac{\tau_{rz}}{G_{rz}}$$

(2.19)

$\tau_{ij}$  and  $\gamma_{ij}$  are the shear stress and strain respectively. When a constrained body is subjected to a temperature change  $\Delta T$  or a change in concentration  $\Delta C$ , the material may develop strains without stresses. Thus, the tensile constitutive equations for an orthotropic solid are more accurately represented by equations (2.20).

$$\epsilon_r = a_{11}\sigma_r + a_{12}\sigma_\theta + a_{13}\sigma_z + \alpha_r\Delta T + \beta_r\Delta C \quad (2.20a)$$

$$\epsilon_\theta = a_{12}\sigma_r + a_{22}\sigma_\theta + a_{23}\sigma_z + \alpha_\theta\Delta T + \beta_\theta\Delta C \quad (2.20b)$$

$$\epsilon_z = a_{13}\sigma_r + a_{23}\sigma_\theta + a_{33}\sigma_z + \alpha_z\Delta T + \beta_z\Delta C \quad (2.20c)$$

where the coefficients of thermal expansion,  $\alpha_i$ , and the shrinkage coefficients  $\beta_i$  are defined as follows:

$$\alpha_r = \left(\frac{\partial \epsilon_r}{\partial T}\right)_{\sigma, c}; \quad \alpha_\theta = \left(\frac{\partial \epsilon_\theta}{\partial T}\right)_{\sigma, c}; \quad \alpha_z = \left(\frac{\partial \epsilon_z}{\partial T}\right)_{\sigma, c}$$

$$\beta_r = \left(\frac{\partial \epsilon_r}{\partial C}\right)_{\sigma, T}; \quad \beta_\theta = \left(\frac{\partial \epsilon_\theta}{\partial C}\right)_{\sigma, T}; \quad \beta_z = \left(\frac{\partial \epsilon_z}{\partial C}\right)_{\sigma, T}$$

In addition to the set of constitutive equations cited above, the equations of equilibrium, the strain displacement relations, and the compatibility equations are needed to predict the state of stress and the resulting strain of an orthotropic fiber undergoing a homogeneous change in concentration during drying. The equilibrium equations for an element in cylindrical coordinates are given in equation (2.21). It is assumed that the principal axis coincides with the three mutually orthogonal planes  $(r, \theta, z)$  and that the body forces are negligible.

$$\frac{\partial \sigma_r}{\partial r} + \frac{\sigma_r - \sigma_\theta}{r} = 0 \quad (2.21a)$$

$$\frac{\partial \sigma_\theta}{\partial \theta} = 0 \quad (2.21b)$$

$$\frac{\partial \sigma_z}{\partial z} = 0 \quad (2.21c)$$

The strain displacement relations for small strains in the three principal directions are denoted as follows:

$$\epsilon_\theta = \frac{u}{r}$$

$$\epsilon_r = \frac{\partial u}{\partial r} \quad (2.22)$$

$$\epsilon_z = \frac{\partial w}{\partial z}$$

where  $U$  and  $W$  are the components of displacement of a point in the deformed material along the  $r$  and  $z$  coordinates respectively.

In order to ensure the existence of a compatible strain distribution and a single valued displacement in a connected body, the compatibility equations are implemented in this elasticity problem. In cylindrical coordinates, the compatibility equations (2.23) reduce to the following form:

$$\frac{\partial \epsilon_z}{\partial r} = 0 \quad (2.23a)$$

$$\epsilon_r - \epsilon_\theta = r \frac{\partial \epsilon_\theta}{\partial r} \quad (2.23b)$$

Upon rearrangement of equation (2.20c), the axial stress generated under isothermal drying conditions is described as follows:

$$\sigma_z = \frac{\epsilon_z^o}{a_{33}} - \frac{a_{13}\sigma_r}{a_{33}} - \frac{a_{23}\sigma_\theta}{a_{33}} - \frac{\beta_z \Delta C}{a_{33}} \quad (2.24)$$

The axial strain is only a function of concentration and load.

$$\epsilon_z = \epsilon_z^o$$

Substituting (2.24) for  $\sigma_z$  into (2.20a) and (2.20b), the radial and hoop strains are expressed as follows:

$$\epsilon_r = \gamma_{11}\sigma_r + \gamma_{12}\sigma_\theta + \beta'_r \Delta C + \frac{a_{13}\epsilon_z^o}{a_{33}} \quad (2.25)$$

$$\epsilon_\theta = \gamma_{12}\sigma_r + \gamma_{22}\sigma_\theta + \beta'_\theta \Delta C + \frac{a_{23}\epsilon_z^o}{a_{33}} \quad (2.26)$$

where

$$\gamma_{11} = a_{11} - \frac{a_{13}^2}{a_{33}}$$

$$\gamma_{12} = a_{12} - \frac{a_{13}a_{23}}{a_{33}}$$

$$\gamma_{22} = a_{22} - \frac{a_{23}^2}{a_{33}}$$

$$\beta'_r = (\beta_r - \frac{a_{13}}{a_{33}} \beta_z) \Delta C$$

$$\beta'_\theta = (\beta_\theta - \frac{a_{23}}{a_{33}} \beta_z) \Delta C$$

The equations of equilibrium (2.21) are satisfied when

$$\sigma_r = \frac{\phi}{r} \quad (2.27)$$

$$\sigma_\theta = \frac{\partial \phi}{\partial r} \quad (2.28)$$

where  $\phi$  is an unspecified function of  $r$ . Inserting expressions for (2.27) and (2.28) for  $\sigma_r$  and  $\sigma_\theta$  into (2.25) and (2.26) for  $\epsilon_r$  and  $\epsilon_\theta$  and then substituting these expressions for  $\epsilon_r$  and  $\epsilon_\theta$  into the compatibility equation (2.23b), a single equation in terms of  $\phi$  results. In this derivation, it is assumed that  $\beta_i$ , the shrinkage coefficient, as well as  $\epsilon_z^0$  is not a function of  $r$ .

$$\phi'' + \frac{\phi'}{r} - \frac{\gamma_{11}}{\gamma_{22}} \frac{\phi}{r^2} = \frac{(\beta'_r - \beta'_\theta) \Delta C}{\gamma_{22} r} + \left( \frac{a_{13} - a_{23}}{a_{33}} \right) \frac{\epsilon_z^0}{\gamma_{22} r} \quad (2.29)$$



The expression for  $\phi$  which satisfies (2.29) is written as follows:

$$\phi = C_1 r^\lambda + C_2 r^{-\lambda} + (P_\beta \Delta C + K \epsilon_z^\circ) r \quad (2.30)$$

where

$$K = \frac{(a_{13} - a_{23})}{a_{33} \gamma_{22} (1 - \lambda^2)}$$

$$P_\beta = \left( \frac{\beta_r - \beta_\theta}{\gamma_{22} (1 - \lambda^2)} - K \beta_z \right)$$

$$\lambda = \left( \frac{\gamma_{11}}{\gamma_{22}} \right)^{1/2}$$

The radial and tangential stresses which arise from the fiber shrinkage are derived from (2.30) using (2.27) and (2.28).

$$\sigma_r = C_1 r^{\lambda-1} + C_2 r^{-\lambda-1} + P_\beta \Delta C + K \epsilon_z^\circ \quad (2.31)$$

$$\sigma_\theta = \lambda C_1 r^{\lambda-1} - \lambda C_2 r^{-\lambda-1} + P_\beta \Delta C + K \epsilon_z^\circ \quad (2.32)$$

Substituting  $\sigma_r$  and  $\sigma_\theta$  into (2.24), the axial stress generated during drying may be expressed as follows:

$$\begin{aligned} \sigma_z = & \frac{\epsilon_z^\circ}{a_{33}} - C_1 r^{\lambda-1} \left( \frac{a_{13} + \lambda a_{23}}{a_{33}} \right) - C_2 r^{-\lambda-1} \left( \frac{a_{13} - \lambda a_{23}}{a_{33}} \right) - \\ & \left( \frac{a_{13} + a_{23}}{a_{33}} \right) P_\beta \Delta C - \left( \frac{a_{13} + a_{23}}{a_{33}} \right) K \epsilon_z^\circ - \frac{\beta_z \Delta C}{a_{33}} \end{aligned} \quad (2.33)$$

Assuming that an infinitely small hole exists at the inside core of the fiber, the radial stresses vanish at the outer edge  $r=R$  and at the

inside core  $r=0$ . The coefficients  $C_1$  and  $C_2$  are then uniquely determined.

$$C_1 = \frac{-K\epsilon_z^o}{R^{\lambda-1}} - \frac{P_\beta \Delta C}{R^{\lambda-1}}$$

$$C_2 = 0$$

The principal stresses then take the following form:

$$\begin{aligned} \sigma_z = & \frac{\epsilon_z^o}{a_{33}} - \frac{(a_{13}+a_{23})}{a_{33}} K\epsilon_z^o - \frac{(a_{13}+a_{23})}{a_{33}} P_\beta \Delta C \\ & - \frac{\beta_z \Delta C}{a_{33}} + \left( \frac{a_{13}+\lambda a_{23}}{a_{33}} \right) (K\epsilon_z^o + P_\beta \Delta C) \frac{r^{\lambda-1}}{R^{\lambda-1}} \end{aligned} \quad (2.34)$$

$$\sigma_r = P_\beta \Delta C \left( 1 - \left( \frac{r}{R} \right)^{\lambda-1} \right) + K\epsilon_z^o \left( 1 - \left( \frac{r}{R} \right)^{\lambda-1} \right) \quad (2.35)$$

$$\sigma_\theta = P_\beta \Delta C \left( 1 - \lambda \left( \frac{r}{R} \right)^{\lambda-1} \right) + K\epsilon_z^o \left( 1 - \lambda \left( \frac{r}{R} \right)^{\lambda-1} \right) \quad (2.36)$$

Although  $\sigma_z$  is a function of  $r$ , it is assumed that the average stress over the fiber area is constant.

$$\int_0^R \sigma_z dA = P \quad (2.37)$$

Substituting (2.34) for  $\sigma_z$  into (2.37),  $\epsilon_z^o$  can be determined.

$$\epsilon_z^o = \frac{Pa_{33}}{\pi R^2 (1-\psi K)} + \frac{P_\beta \Delta C \psi}{(1-\psi K)} + \frac{\beta_z \Delta C}{(1-\psi K)}$$

where 
$$\psi = \frac{\lambda-1}{\lambda+1} (a_{13}-a_{23}) \quad (2.38)$$

By taking the derivative of  $\epsilon_z^0$  with respect to concentration, an explicit form describing the axial change during drying is obtained.

$$\frac{\partial \epsilon_z}{\partial C} = \frac{\beta_z}{1-\psi K} + \frac{P_\beta \psi}{1-\psi K} \quad (2.39)$$

Substituting in for  $P_\beta$ ,

$$\frac{\partial \epsilon_z}{\partial C} = \beta_z + (\beta_r - \beta_\theta) \chi \quad (2.40)$$

where 
$$\chi = \frac{\psi}{\gamma_{22}(1-\lambda^2)(1-\psi K)}$$

The second term in (2.40) is highly sensitive to the difference between  $a_{13}$  and  $a_{23}$ . For an isotropic material, the shrinkage coefficients are all equal. Thus, the change in axial strain with respect to concentration is adequately characterized by the axial shrinkage coefficient. However, for an orthotropic elastic solid, differences between  $a_{13}$  and  $a_{23}$  as well as  $\beta_r$  and  $\beta_\theta$  exist, and the change in strain versus concentration is no longer a simple function of the axial shrinkage coefficient. Depending on the magnitude of the elastic constant and the hoop and radial shrinkage, the second term of equation (2.40) may become instrumental in controlling the observed axial dimension changes upon drying.

It is of interest to determine the predictions made by this model for several types of wood, a material for which the elasticity coefficients are known. The shrinkage behavior and compliance coefficients for three hardwoods, American beech, Black walnut and Sweet gum, as well

as one softwood, Sitka spruce, have been well characterized (83,84). Defining the shrinkage coefficient as the percent shrinkage observed from the green condition to 14% relative humidity and utilizing the known compliance coefficients in Table 11, an expression for the observed change in axial strain under these drying conditions are obtained from equation (2.40) for each wood type.

$$\frac{\partial \epsilon_z}{\partial C} = \beta_z + .0001 \quad \text{American beech} \quad (2.41)$$

$$\frac{\partial \epsilon_z}{\partial C} = \beta_z + .00006 \quad \text{Black walnut} \quad (2.42)$$

$$\frac{\partial \epsilon_z}{\partial C} = \beta_z + .00006 \quad \text{Sweetgum} \quad (2.43)$$

$$\frac{\partial \epsilon_z}{\partial C} = \beta_z + .00005 \quad \text{Sitka spruce} \quad (2.44)$$

These results predict that the observed axial shrinkage for a cylindrical structure may be more than the actual longitudinal shrinkage for these particular orthotropic systems.

Equations (2.35)-(2.37) demonstrate that radial and hoop as well as axial stresses are generated for a cylindrically orthotropic fiber undergoing dimensional changes with drying. The radial and hoop stresses are highly dependent on the shrinkage behavior of the fiber and the parameter  $K$  which is a function of the differences in the  $a_{23}$  and  $a_{13}$  compliance constants. For a cylindrically isotropic fiber, no differentiation exists between the radial and hoop directions; thus  $\beta_r = \beta_\theta$  and



Table 11. Compliance coefficients<sup>a</sup> and shrinkage behavior<sup>b</sup> for various wood types

Wood	Beech	Walnut	Sweetgum	Sitka Spruce	
Compliance Coefficients (GPa <sup>-1</sup> )	a <sub>11</sub>	.446	.840	.741	1.111
	a <sub>22</sub>	.877	1.587	1.695	2.000
	a <sub>33</sub>	.073	.089	.085	.086
	a <sub>12</sub>	-.316	-.587	-.525	-.500
	a <sub>13</sub>	-.033	-.044	-.028	-.032
	a <sub>23</sub>	-.037	-.056	-.034	-.041
	Shrinkage <sup>c,d</sup>	radial	.055	.055	.053
tangential		.119	.078	.102	.075
longitudinal		-.002	-.005	.003	-.003
volumetric		.172	.128	.153	.115
$\gamma_{11}$ (GPa <sup>-1</sup> )		.431	.818	.732	1.099
$\gamma_{22}$ (GPa <sup>-1</sup> )		.858	1.552	1.681	1.98
$\lambda$		.709	.726	.660	.745
K (GPa)		.128	.184	.074	.119
$\Psi$ (GPa <sup>-1</sup> )		-.00068	-.0019	-.0012	-.0013
$\chi$		-.0016	-.0026	-.0013	-.0015

<sup>a</sup>reference 83<sup>b</sup>reference 82<sup>c</sup>shrinkage from green to oven dry moisture content<sup>d</sup>expressed as a percentage of green dimension

$a_{13}=a_{23}$ . The principal stresses subsequently reduce to the following form.

$$\sigma_z = \frac{P}{\pi R^2} \quad (2.45)$$

$$\sigma_r = \sigma_\theta = 0$$

It is informative to examine the stresses developed in wood during the shrinkage process. The radial ( $\sigma_r$ ), tangential ( $\sigma_\theta$ ) and longitudinal stresses which are formed during unrestrained ( $P=0$ ) isothermal drying have been calculated for the American Beech inserting the compliance and shrinkage constants in Table 11 into (2.34), (2.35) and (2.36). The predicted magnitude of the three stresses as a function of radial position is depicted in Figure 21. On the outer edge, the hoop and longitudinal stresses are compressive in nature while radial stress is zero. All three stresses become increasingly tensile progressing toward the inner core.

At present, there is no structural evidence that PBT fibers possess transverse symmetry such that the properties differ in the radial and tangential direction. If PBT fibers do possess such transverse symmetry, the characteristic shrinkage behavior predicted by equation (2.40) and the development of internal shrinkage stresses could have several important consequences on these rigid rod polymeric fibers. The development of compressive hoop stresses would enable the fibrillar network to collapse tightly together on the outside of the fiber which would then effectively squeeze the water out. However, the formation of such large tensile hoop and radial stresses internally would inhibit close

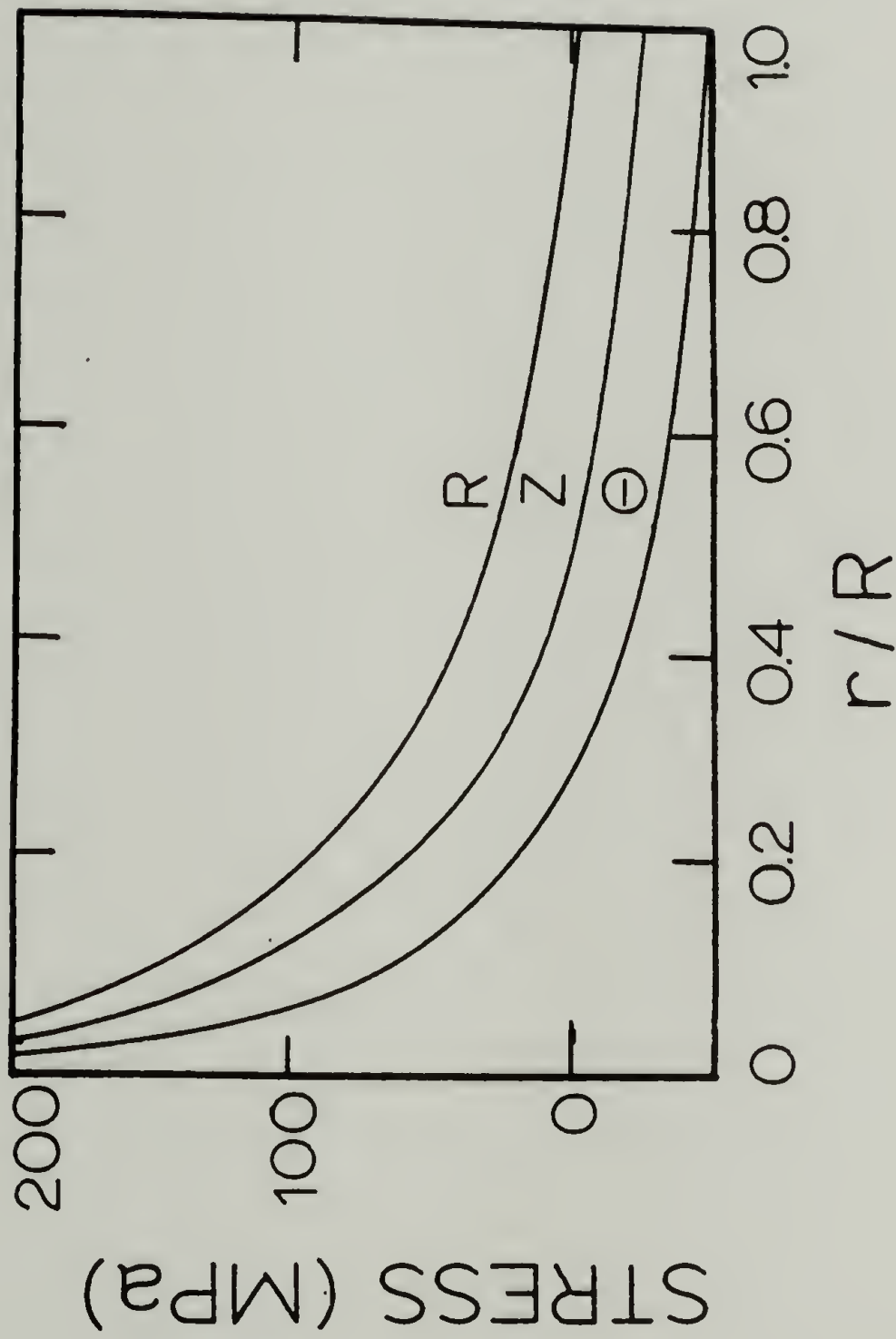


Figure 21. Predicted radial, longitudinal and hoop stress distributions after unrestrained drying in American Beechwood

packing of the fibrillar network during drying. The variation in hoop and radial stresses along the fiber's cross section would then be instrumental in the development of a skin-core morphology and in causing cavitation.

The apparent yield behavior of a wet PBT fiber under tensile deformation (Figure 10) may be a consequence of the potential stresses generated in this material. In this particular situation, the wet fiber is experiencing only a tensile load  $P$ . The equations for the radial and hoop stresses (2.36) and (2.37) simplify to:

$$\sigma_r = \frac{KPa_{33}}{\pi R^2(1-\psi K)} \left(1 - \left(\frac{r}{R}\right)^{\lambda-1}\right) \quad (2.46a)$$

$$\sigma_\theta = \frac{KPa_{33}}{\pi R^2(1-\psi K)} \left(1 - \lambda \left(\frac{r}{R}\right)^{\lambda-1}\right) \quad (2.46b)$$

These results are equivalent to the distribution of stresses predicted by Lekhnitskii (85) for a cylindrically orthotropic rod under the action of a tensile force  $P$  directed along the longitudinal axis. This set of equations indicates that the magnitude of these transverse stresses are proportional to the applied load  $P$ . Therefore, it is believed that during the tensile deformation of the wet fiber if orthotropic symmetry exists, the internal stresses may gradually increase. At a critical axial load, the transverse stresses may become large enough to effectively squeeze the water out of the fibrillar network and a collapse of the fiber will ensue. The apparent plastic behavior may



be a result of a gradual reduction in the load bearing cross sectional area due to a stress induced collapse mechanism.

## 2.8 Summary and Conclusions

Investigations on the morphology and mechanics of the wet fiber and their modifications during drying have enabled the formulation of a model for the coagulated fiber and the collapse process. This model postulates that the wet fiber consists of a swollen macro and microfibrillar structure with a high degree of two dimensional chain order. The wet fiber displays a high degree of mechanical anisotropy due to its relatively high tensile properties with low compressive and shear characteristics. The tensile behavior of the wet state is elastic-plastic with the same load bearing capacity of the dry fiber. The above described results suggest the existence of an interconnected fibrillar network for the wet fiber. The structural and mechanical characteristics of the wet state are similar to those features present in its dried counterpart, which suggests that the general structural and mechanical features of the dried fiber are developed during coagulation.

The collapse process of these anisotropic fibers is characterized by a distinct radial contraction with a slight axial elongation (.05-.1%). It is postulated that the nature of the dimensional changes are associated with the morphological characteristics of the coagulated fiber.

Alterations in the structure and mechanics of PBT fibers upon drying may be attributed to the removal of water and the resulting fiber

collapse. Therefore, while the characteristic mechanical and structural features of the dried fiber develop during coagulation, it is the drying process which causes structural rearrangements resulting in the enhancement of the mechanical properties.

There is a distinct difference in the wet fiber properties, the collapse process and alterations in the fiber properties after drying between fibers spun from a low and high concentration spinning dope at the various spin draw ratios. Gross differences in the wet fiber properties and their modification during drying are believed to be a consequence of various fiber morphologies which may develop during coagulation.

A theoretical analysis of the shrinkage behavior and the resulting internal stresses has been made for a cylindrically orthotropic material. The observed axial change in strain upon drying and the hoop, radial and longitudinal internal shrinkage stresses are determined to be a function of the shrinkage in all three principal directions. Although this analysis is applied to wood, these results may have important consequences for solution spun high modulus/high strength fibers found to be cylindrically orthotropic.

The implications of the work described in Chapter II are far reaching. Of particular significance is the finding that since the general features of the dried fiber develop during coagulation, any major alterations in the structure and properties of the final PBT fiber must be attempted during coagulation. The drying process will serve only to perfect the existing coagulated structure. However, the transverse and

compressive properties appear somewhat altered through the drying process. Although these changes are quite possibly a result of the collapse of the fibrillar network, suggestions that the lateral interactions between fibrils and microfibrils could conceivably be enhanced upon drying cannot be entirely eliminated. Based upon these findings, investigations to optimize the potential enhancement in the structure and mechanical properties of the PBT fiber through the drying process has been conducted. An analysis of the results is contained in Chapter III.

## C H A P T E R   I I I

### HIGH TENSION AND TEMPERATURE DRYING: POST PROCESSING HEAT TREATMENT INVESTIGATIONS

#### 3.1 Introduction

Unrestrained air drying of the PBT fiber leads to an increase in the molecular order and an enhancement in the fiber's mechanical properties. Despite these improvements, there is a tendency for internal stresses to develop due to the shrinkage of the fiber during drying as outlined in Chapter II. Earlier studies have demonstrated that the formation of material imperfections may severely alter the mechanical behavior, and thus limits the tensile capabilities of these rigid rod fibers (25,52). With post processing heat treatment of as-spun PBT, it is believed that these internal stresses are released along with the removal of residual solvents and coagulants resulting in a completely linear elastic stress strain behavior and an increase in tensile properties. It is postulated that through a more rigorous drying process, these material inhomogeneities can be minimized to produce a "better" as spun fiber. By heat treating this superior precursor, it is hoped that the properties will begin to achieve their potential as determined by the chemical nature of the rigid rod molecule. In an attempt to control the formation of internal shrinkage stresses while optimizing the driving force toward property enhancement through the removal of water and residual acid, high temperature and high tension have been employed



during drying. Subsequent studies on the post processing heat treatment (PPHT) of these variously dried fibers have been to determine whether the final fiber properties are dependent on the processing path.

The information derived from this research should provide a working knowledge of the precise way in which temperature and tension act to modify the fiber properties in both the drying and heat treatment processes.

### 3.2 Experimental

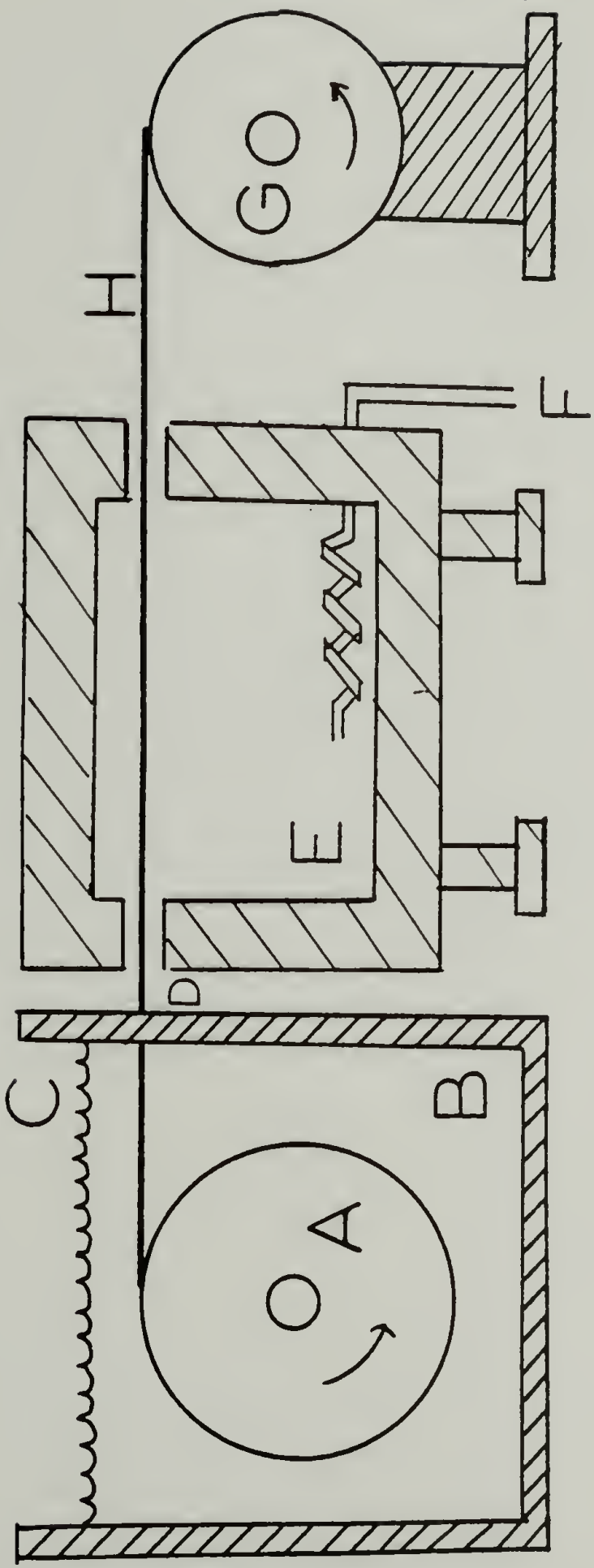
The PBT fibers I, III-VI (described in section 2.2) were employed for the high tension and temperature drying and heat treatment studies. These fibers were collected under water during the spinning process and kept submerged in water until further experiments were performed.

Monofilament PBT fibers were continuously dried using the apparatus illustrated in Figure 22. A fiber supply spool, which was submerged under water, was connected to a dynamometer (MAGTROL HD-500-1). A spring loaded teflon O-ring provided an adequate and nearly frictionless seal between the dynamometer and the fiber supply spool. The measurement and control of applied tension were accomplished through the use of the dynamometer. The axial force applied to the fiber was determined from dead weight calibrations of the dynamometer. Knowing the fiber's radius, the applied tension during drying was calculated. After each drying and heat treatment experiment residual magnetism on the dynamometer drum had to be removed to prevent torque oscillations on future processing experiments (25).

Figure 22

Schematic diagram of PBT fiber drying apparatus.

- A. Fiber supply spool
- B. Water
- C. Water bath
- D. Small opening
- E. Furnace
- F. Nitrogen supply
- G. Fiber take-up spool
- H. PBT fiber



Good control of the drying residence times under tension was obtained by means of a take up spool which was attached to a multiratio gear motor (APCOR 2202) and a ten speed transmission (APCOR 2415). In the studies conducted at room temperature a residence time of five minutes was employed while residence times of two and five minutes were implemented for the elevated temperature drying. Post processing heat treatment investigations were conducted with a residence time of two minutes.

A Grieve AC-493 furnace with an automatic temperature control was placed between the water bath and the take up spool to dry the PBT fibers at high temperatures. A short distance of two cm separated the furnace entrance from the exit point of the water bath. The internal furnace temperature was independently monitored with an Omega platinum resistant (RTD) element placed within the hearing chamber. Temperature variations in this oven have been reported to be minimal ( $10^{\circ}$ - $15^{\circ}$ C) (25). Nitrogen was purged through the furnace at a flow rate of 4 liter/minute to prevent oxidative degradation of the PBT fibers.

The heat treatment experiments on the variously tension and elevated temperature dried fibers were carried out as described previously by S.R. Allen (25).

The tensile properties for these materials were determined on single filaments in accordance with ASTM standards for testing high modulus materials (66) as discussed in Chapter II. Reported tensile properties were corrected for the compliance of the testing machine and were based on cross-sectional areas calculated from diameters measured



by light scattering (67). The tensile properties reported in this chapter were based on tensile tests performed on 30 mm gauge length samples at a pull rate of .5 mm/min on an Instron Floor Model Tensile Tester.

The axial compressive strengths for PBT fibers reported in this chapter were calculated from the product of the compressive strain to kink band formation and the axial tensile modulus. Similar to the elastic loop test calculations in Chapter II, it is assumed that the axial tensile and compressive moduli are the same. The critical compressive strains to kink band formation were measured employing a cantilever beam bending technique devised by S.J. DeTeresa (62). This technique involves bonding the fiber to an elastic rectangular beam and bending the beam in a cantilever configuration. This test sets up a linear distribution of compressive strains along the length of the fiber and beam length. The axial compressive strain is then determined at the region along the fiber where kink bands first form.

The macrostructure of the dried (as-spun) PBT fibers was examined by SEM as outlined in Chapter II. The microstructural characteristics of the variously dried and heat treated samples were investigated through both WAXD flat film and diffractometric techniques also described in Chapter II.

Thermal gravometric analyses (TGA) on PBT fibers were performed with a Perkin Elmer TGS-2 interfaced with a Perkin Elmer thermal analysis microprocessor. A scan rate of 10°C/min was employed with a nitrogen rate of 60 cc/minute.

### 3.3 Room Temperature Drying

The tensile stress-strain behavior of PBT fiber (I) dried under various tensions is depicted in Figure 23. The stress-strain behavior of the tension dried fibers (curves A and B) is elastic-plastic similar to the non-tension dried PBT fiber (curve C). However, with increasing levels of applied stress during drying, the moduli and yield stresses increase while the strains to break gradually decrease. The fiber strengths are not significantly altered by these drying conditions. Similar results have been reported on paper when shrinkage during drying is restricted (86).

The tensile properties for PBT fibers of different spin draw ratios dried under various tensions are summarized in Figures 24 and 25 and Table 12. For each spin draw ratio, the fiber exhibits an enhancement in tensile modulus and yield stress and a reduction in percent elongation with increasing levels of applied stress during drying. However, the relative differences in tensile properties between the non-tension and tension dried fibers is greatest for the PBT fiber with the lowest spin draw ratio spun from the lowest concentration of PBT/PPA. It appears that with sufficient tension applied during drying, the modulus of a minimally drawn fiber spun from a low concentration of PBT/PPA approaches that of a highly drawn fiber spun from a high concentration of PBT/PPA.

The mechanical alterations of the tension dried fibers are caused by a combination of two processes. As discussed in Chapter II, the

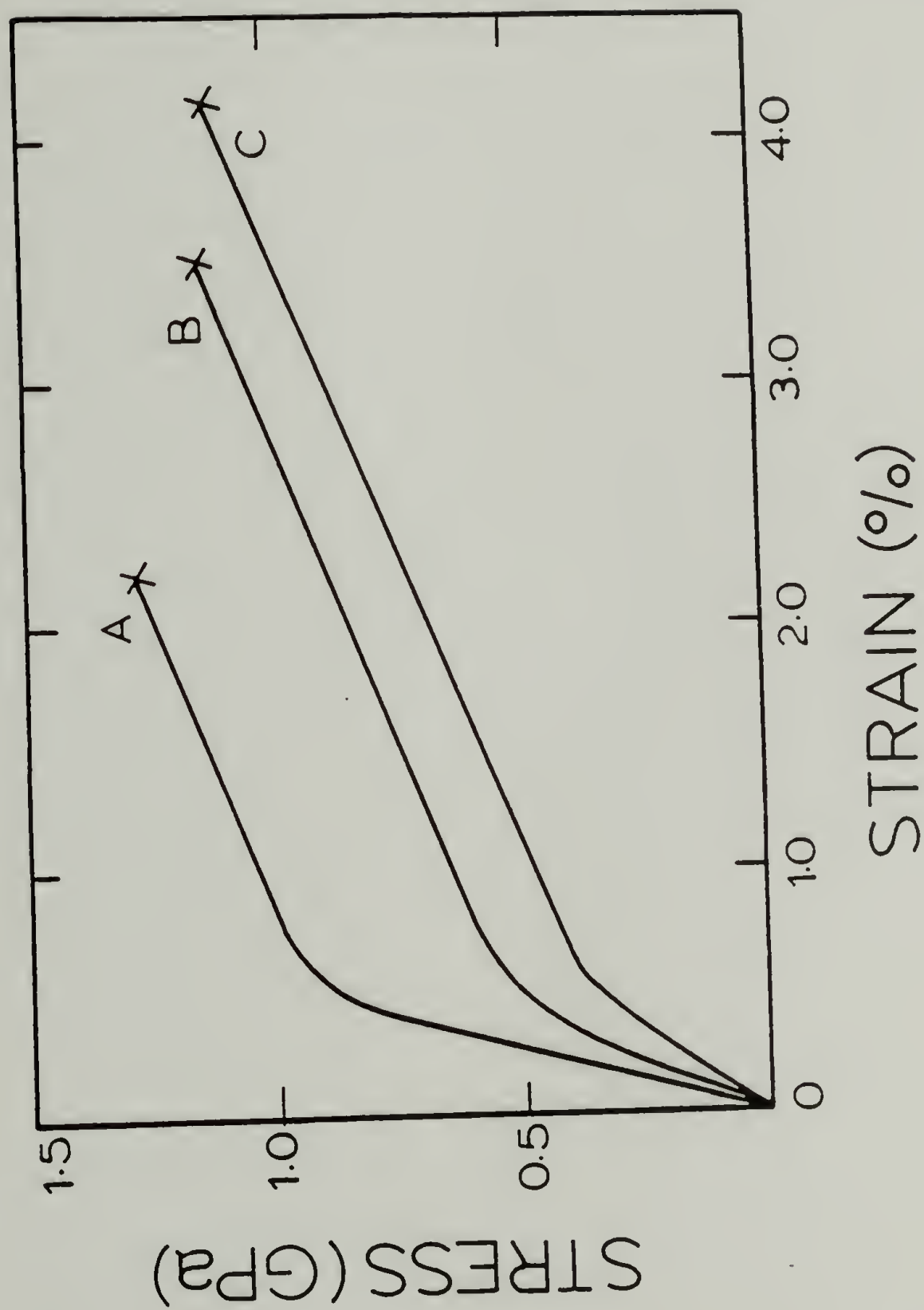


Figure 23. Typical stress-strain curves for as-spun PBT fiber (I): (A) tension dried (300 MPa); (B) tension dried (30 MPa) (C) non-tension dried

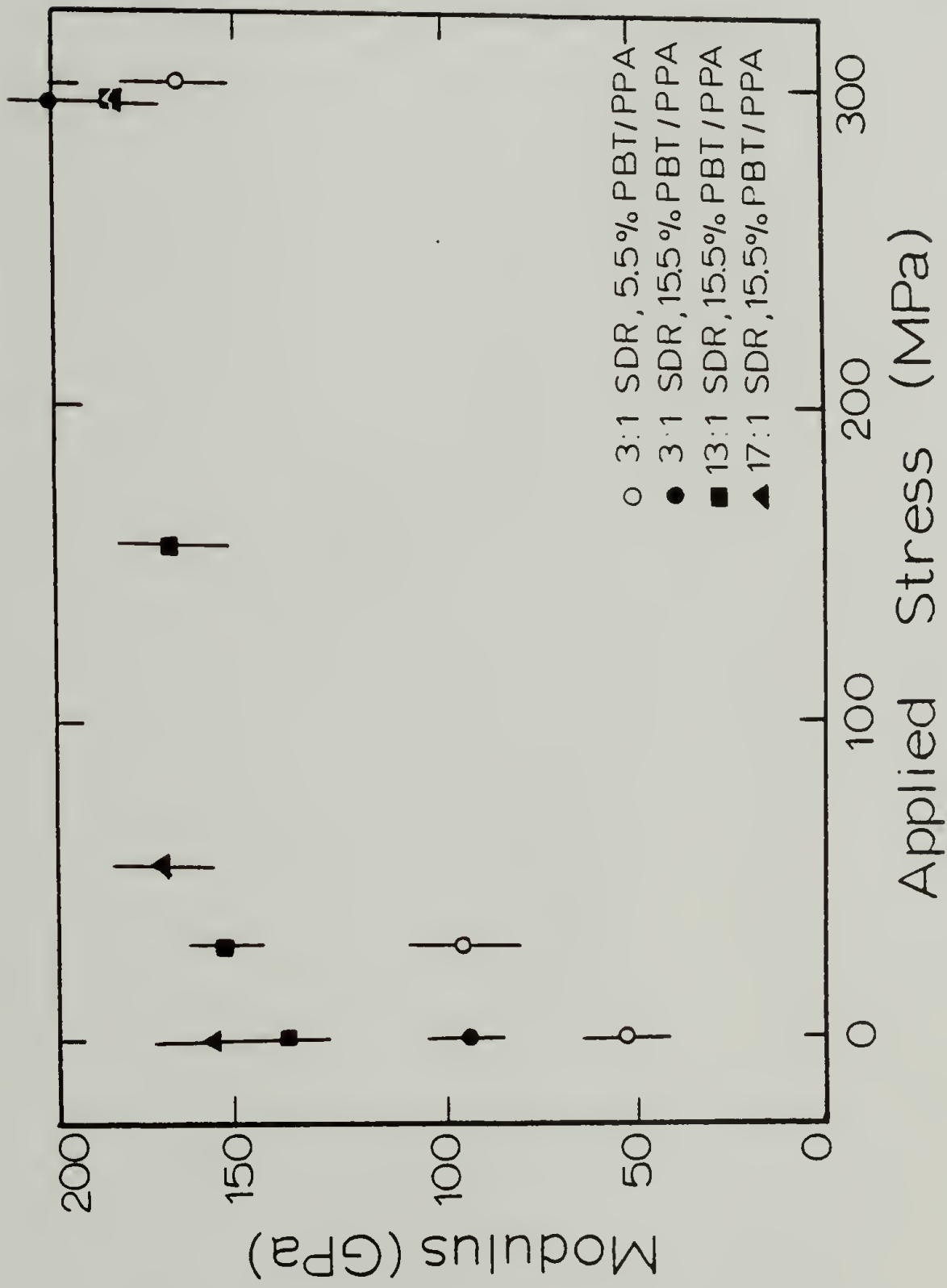


Figure 24. Tensile moduli of PBT fibers dried at various tensions at room temperature



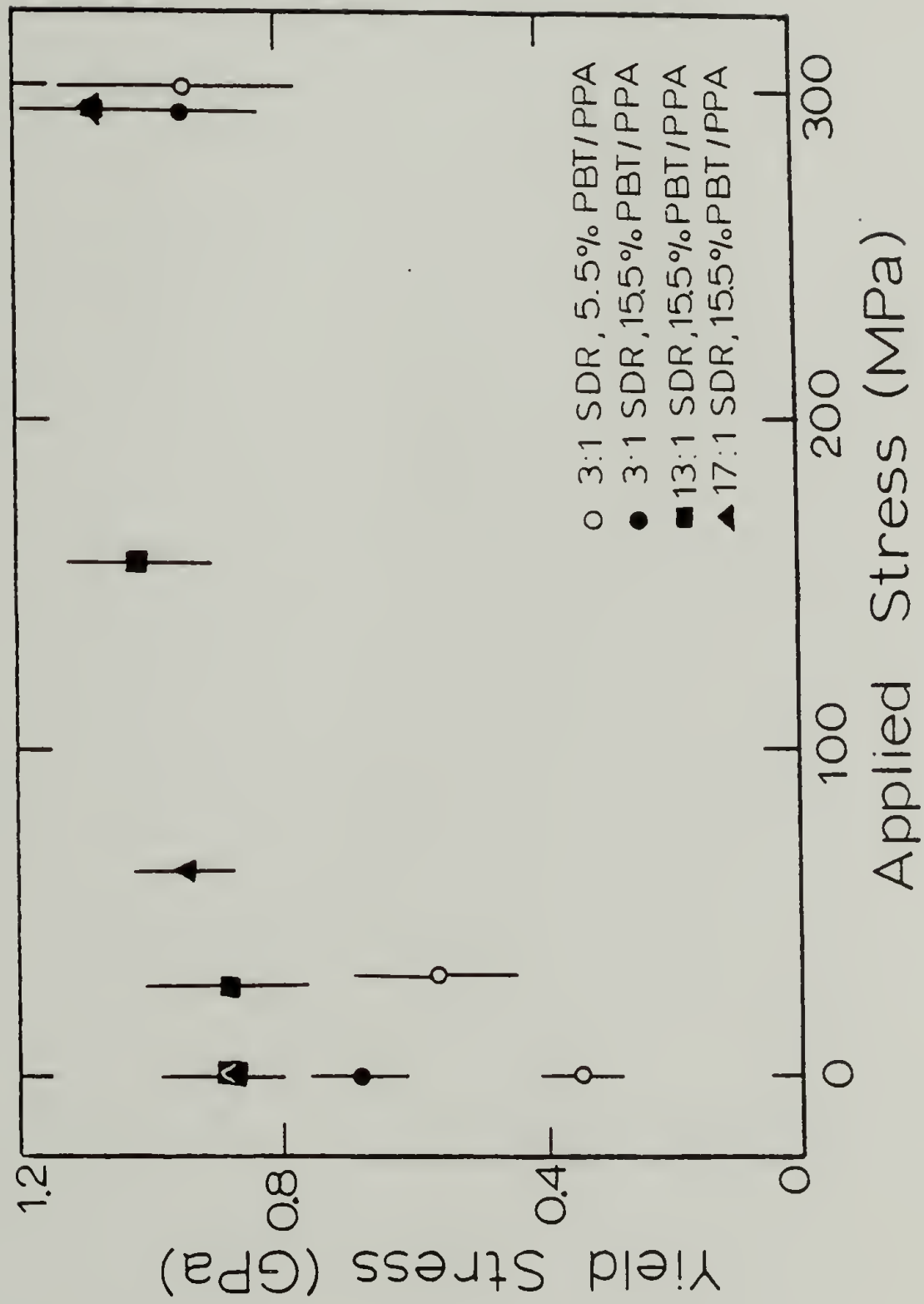


Figure 25. Yield stresses of PBT fibers dried at various tensions at room temperature

Table 12. Tensile properties<sup>a</sup> for differently drawn PBT fibers dried under various tensions

PBT Fiber	Dope Concentration PBT/PPA (%)	Spin Draw Ratio	Applied Load (MPa)	Tensile Modulus, E (GPa)	Tensile Strength, $\sigma_b$ (GPa)	Elongation $\epsilon_b$ (%)	Yield Strength $\sigma_y$ (MPa)
I	5.5	3:1	0	55 + 5	1.1 + .2	4.1 + .3	375 + 105
			30	95 + 10	1.1 + .1	3.4 + .6	570 + 100
			300	180 + 15	1.3 + .2	2.2 + .2	955 + 190
III	15.5	3:1	0	95 + 10	1.5 + .3	2.4 + .1	705 + 75
			294	205 + 20	1.7 + .1	2.1 + .1	900 + 70
IV	15.5	8:1	0	160 + 15	1.6 + .1	1.7 + .1	870 + 85
			30	175 + 20	1.7 + .2	1.7 + .1	955 + 75
			295	185 + 20	1.6 + .2	1.4 + .1	985 + 130
V	15.5	13:1	0	140 + 25	1.7 + .3	1.9 + .3	880 + 170
			30	155 + 10	1.7 + .1	1.8 + .2	880 + 130
			155	180 + 15	1.7 + .2	1.6 + .1	1010 + 170
			300	185 + 10	1.7 + .2	1.4 + .1	1070 + 130
VI	15.5	17:1	670	190 + 20	1.7 + .2	1.3 + .1	1070 + 190
			0	155 + 15	1.7 + .2	1.6 + .2	880 + 105
			55	170 + 15	1.7 + .2	1.6 + .1	955 + 90
			305	190 + 20	1.6 + .1	1.2 + .1	1060 + 90

<sup>a</sup>Data represents the average values  $\pm$  one standard deviation using 12 test specimens.

application of tension during drying in the wet fiber causes a straightening of the network structure as evidenced by the fiber's strain hardening response to static tensile deformation (Figure 10). Furthermore, a comparison of WAXD patterns of single filaments dried with and without tension reveals a narrowing of the azimuthal breadth of the equatorial reflections in the tension dried fiber (Figure 26) which is indicative of an improvement in chain orientation. Therefore, the increase in modulus with a reduction in strain to break within the tension dried fiber can be attributed to an increase in the molecular alignment.

The magnitude of property enhancement is believed to be a function of the ability to wet stretch the fiber. The strain hardening behavior of wet fibers spun from different PPA/PBT dope concentrations of different spin draw ratios at the tensions applied during the drying process is reported in Table 13. The relative increase in the elastic moduli upon cyclic deformation is greatest for the fiber spun from a low concentration of PBT. Moreover, the strain hardening effects diminish with increasing spin draw ratio for fibers spun from high concentration of PBT/PPA. Fibers spun from a low concentration and low spin draw ratio appear to be most responsive to wet stretching and further chain alignment prior to and during drying at a given tension. This data is consistent with the previous results showing that tension drying had a more pronounced effect on fibers spun from a low PBT/PPA concentration and low SDR.

In addition to wet stretching prior to drying, the observed modifications in the tensile behavior of the resulting tension dried fiber may

Figure 26

WAXD patterns for PBT Fiber I

- (A) Non-tension dried
- (B) Tension dried (300 MPa)





B

A

Table 13. Strain hardening effects of the coagulated PBT fibers

PBT Fiber	% PBT/PPA	Draw Ratio	Initial Modulus, E (GPa)	Initial Modulus After Loading and Unloading to $\sigma_B$ (GPa)	$\sigma_B^b$ (MPa)	% Enhancement
I	5.5	3:1	$1.5 \pm 0.3$	$2.9 \pm 0.6$	200	$65 \pm 15$
III	15.5	3:1	$15 \pm 1$	$19 \pm 1$	190	$27 \pm 2$
IV	15.5	8:1	$29 \pm 6$	$37 \pm 5$	280	$28 \pm 6$
V	15.5	12:1	$39 \pm 3$	$46 \pm 3$	460	$18 \pm 2$
VI	15.5	17:1	$32 \pm 2$	$36 \pm 2$	350	$13 \pm 1$

<sup>a</sup>Data represents an average  $\pm$  one standard deviation of at least 8 test specimens.

<sup>b</sup>Calculation of stress based on the final dried cross-sectional area.

be attributed to an offset in the axial compressive shrinkage stresses with the continued application of tension during the collapse process.

In order to obtain a qualitative measure of these compressive stresses, the effect of tension drying on the strain hardening behavior of the dried fiber has been investigated. As stated earlier, the as-spun fiber exhibits a strain hardening effect if the compressive internal stresses are high enough to cause the buckling of the outer fibrillar elements. A reduction in the strain hardening behavior of the dried fibers is expected by offsetting the compressive residual stresses with tension during drying, thereby eliminating the buckling of the fibrillar elements.

A comparison of the stress-strain hysteresis behavior of the tension dried (300 MPa) and non-tension dried fibers illustrates that strain hardening upon deformation occurs in the non-tension dried fiber but is virtually absent in the tension dried material (Figures 27 and 28, Table 14). Furthermore, a comparison of SEM micrographs of a single filament dried with and without tension shows the elimination of surface undulations in the tension dried fiber (Figure 29).

Both the mechanical and morphological studies indicate that applied tension during drying does eliminate the buckling of the outer fibrillar elements. It is believed that by tensioning the fiber during drying, the resulting shrinkage stresses are not self equilibrating. Rather, the total force across the cross section is tensile in nature. As indicated in Chapter II:

$$\int \sigma_z dA = P \quad (3.1)$$

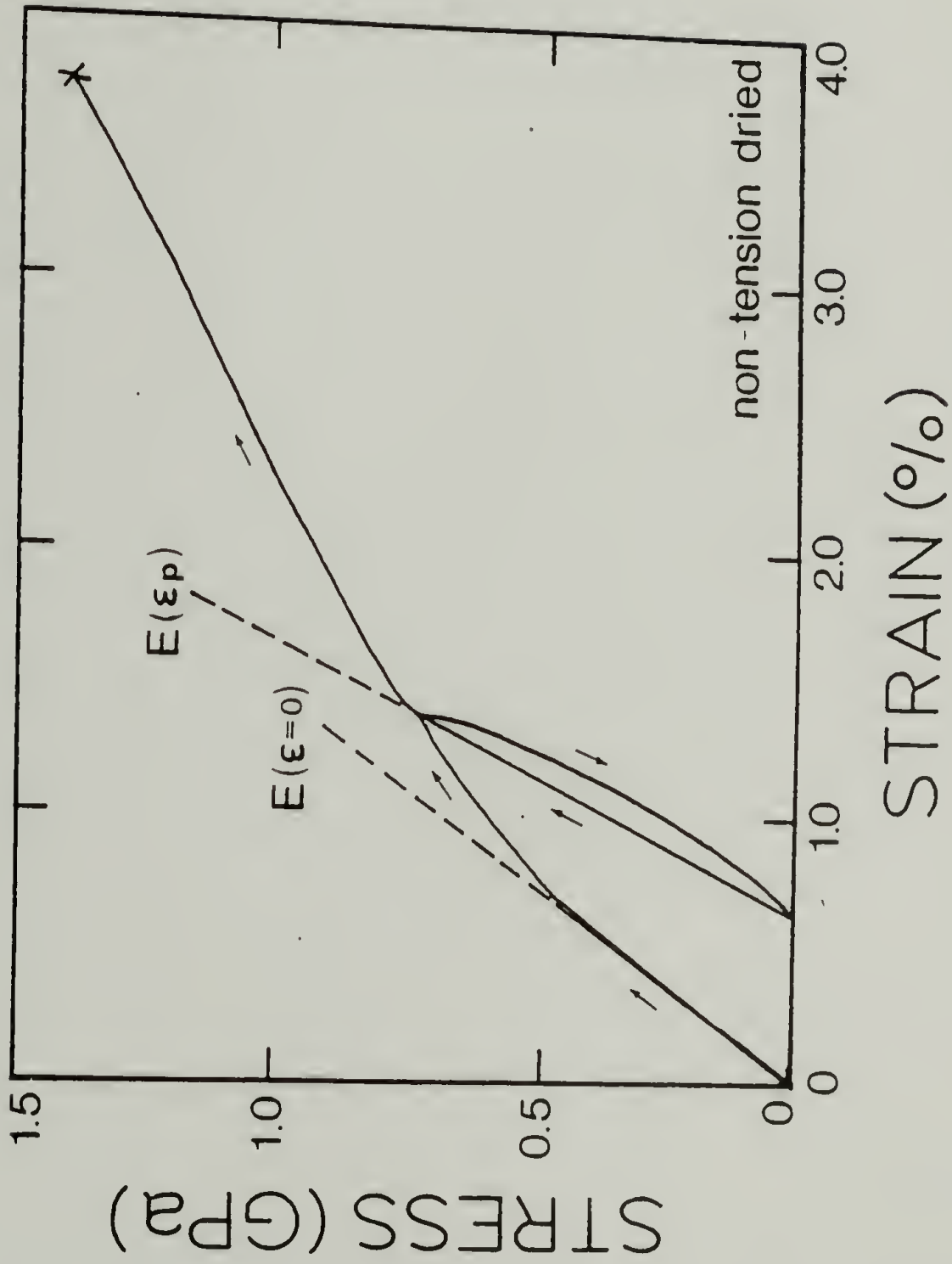


Figure 27. Stress-strain curve displaying strain hardening effects for a non-tension room temperature dried PBT fiber



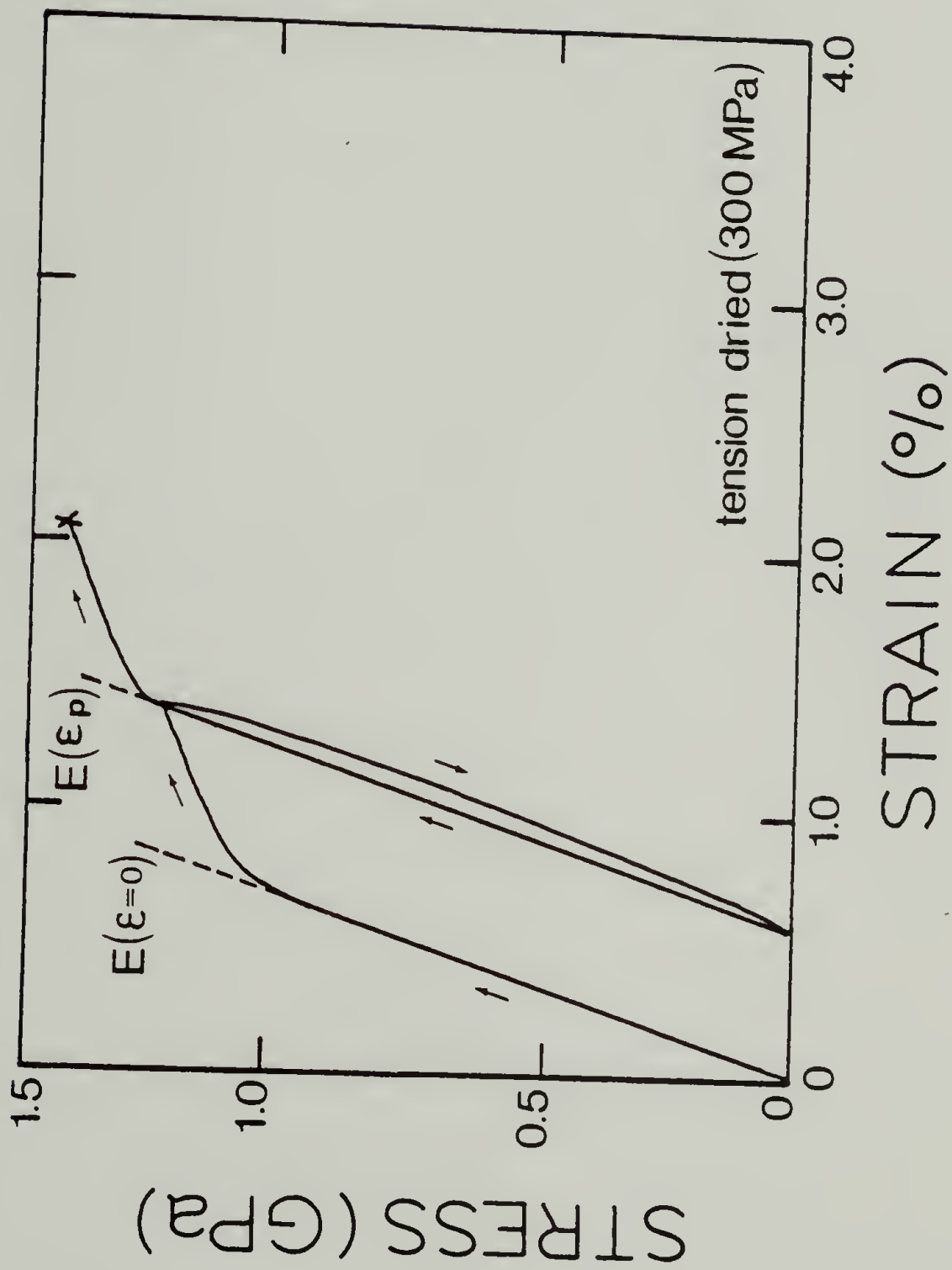


Figure 28. Stress-strain curve displaying strain hardening effects for a room temperature tension dried PBT fiber

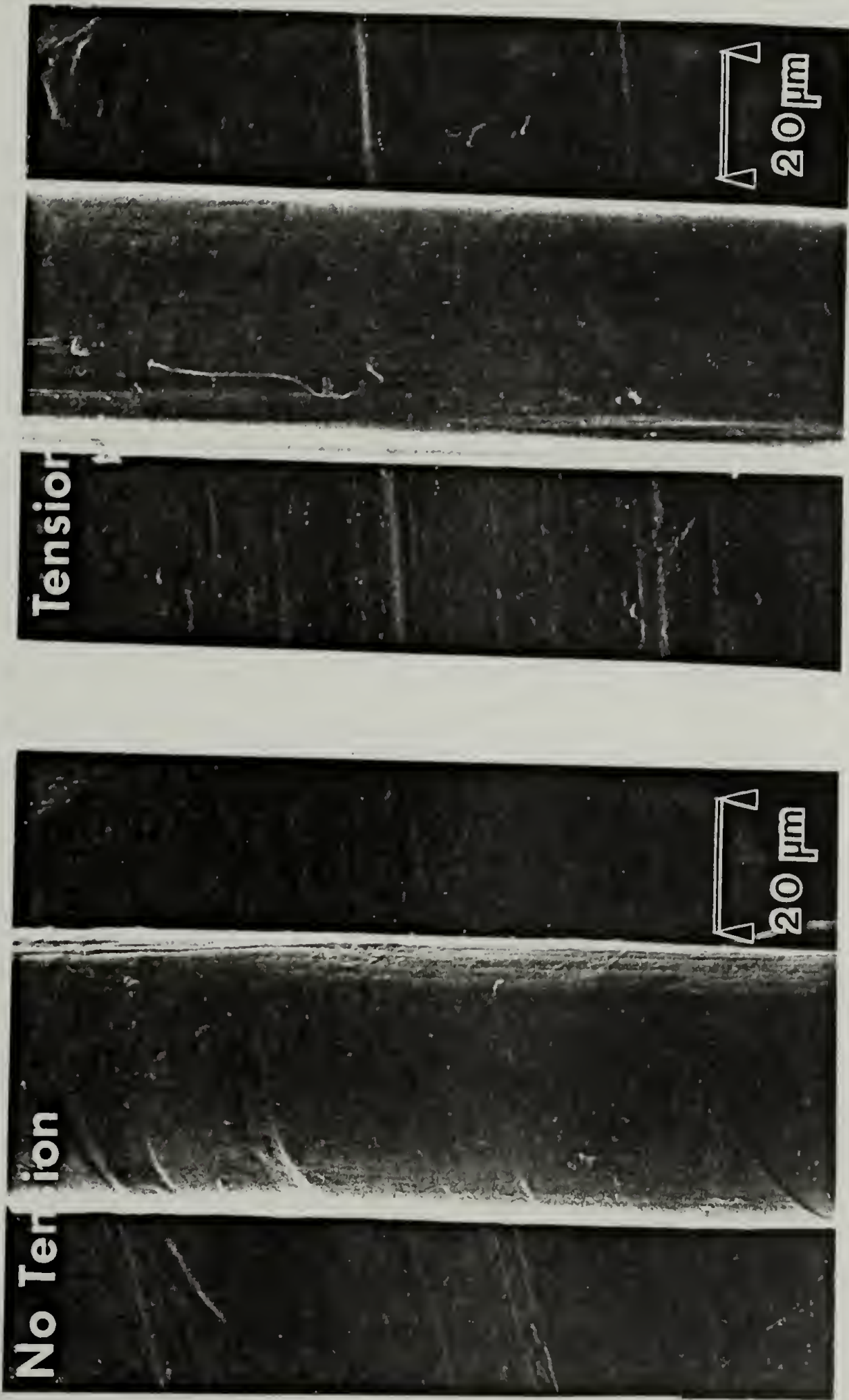
Table 14. Strain hardening<sup>a</sup> behavior of PBT fiber (I)

Applied Tension During Drying (MPa)	Initial Modulus (GPa)	Initial Modulus After Unloading and Loading to 1.7% Strain (GPa)	% Enhancement
0	57 ± 6	85 ± 5	49
30	102 ± 7	112 ± 12	10
300	184 ± 5	183 ± 2	0

<sup>a</sup>Data represents an average ± one standard deviation for 6 test specimens.

## Figure 29

Scanning electron micrographs of a non tension dried fiber displaying surface undulations and a tension dried fiber void of buckling defects.





However, upon removal of the applied load, the internal stresses become self-equilibrating whereby

$$\int \sigma_z dA = 0 \quad (3.2)$$

An increase in the compressive internal stress occurs with a corresponding decrease in the tensile internal stress (Figure 30). Since the compressive strength of the dried fiber is higher than that of the wet fiber as indicated in section 2.6, the dried fiber can now withstand these compressive forces so that the critical conditions necessary for buckling to occur are never achieved. Thus, modifications in the mechanical behavior due to tension drying results from an offset in the compressive shrinkage stresses as well as the increased ordering of the microstructure.

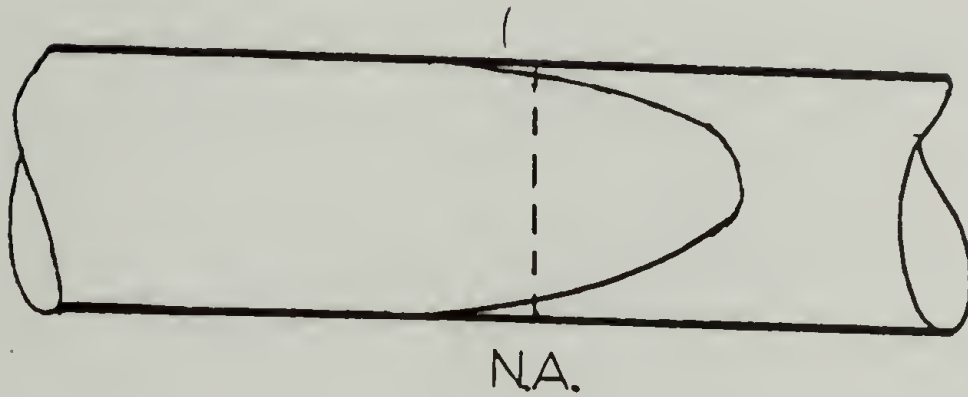
Based upon the data in Figure 25, there is an increase in yield stress with increasing amounts of applied load during the drying process. Allen et al. have proposed previously that the yielding behavior in the as-spun PBT fiber corresponds to the onset of fracture of overstressed fibrillar elements (52). Allen has postulated that the failure process begins when a critical stress  $\sigma_i$ , a sum of the maximum axial internal stress and the applied stress during deformation, is reached (25).

$$\sigma_i = \sigma_i^{\max} + \sigma_y \quad (3.3)$$

Assuming the critical stress to initiate the fracture of fibrils is constant for each set of PBT fibers, a lower yield stress corresponds to a higher maximum internal stress from (3.3). Therefore, in addition to

Fiber Under Tension - Drying

$$\int \sigma_z dA = P$$



Fiber After Removal of Tension

$$\int \sigma_z dA = 0$$

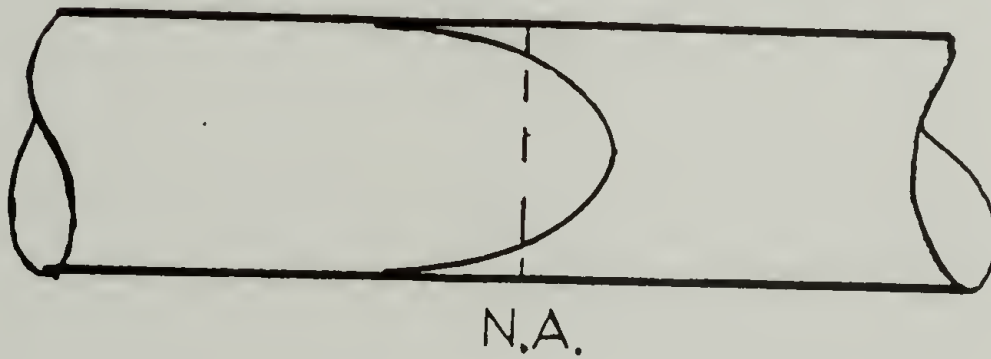


Figure 30. Schematic representation of axial internal stress distribution during and after tension drying

offsetting the compressive internal stresses, the distribution of residual stresses may be modified through tension drying.

It is proposed that in order to fully attain these structural and mechanical changes, tension must be applied to the wet swollen fiber prior to any drying. To substantiate this claim, a comparison of the microstructure and mechanics of the following three fibers has been made: (1) a fiber dried without tension; (2) a fiber non-tension dried then subsequently tensioned; and (3) a fiber which was tension dried. The tension dried fiber displays a higher modulus and yield strength and a lower strain to break than the non-tension dried fiber which was subsequently tensioned (Figure 31, Table 15). Additionally, a comparison of the WAXD patterns of the three above described PBT fibers (Figure 32) reveals that the tension dried fiber displays the highest narrowing of the aximuthal breadth of the equatorial reflections indicative of the highest degree of molecular orientation.

These observations indicate that the wet fiber is more receptive to lateral and longitudinal chain alignment leading to a greater enhancement in the tensile modulus than a dried/collapsed fiber under similar applied loads. When the strain hardening behavior under cyclic deformation of a wet fiber is compared to its dried counterpart, it is observed that the relative increase in the elastic moduli upon deformation for the wet fiber is higher than the dried fiber (Table 16). Both the microstructural and mechanical data suggest that tensioning the fiber in the wet state is more effective in modifying the tensile behavior and

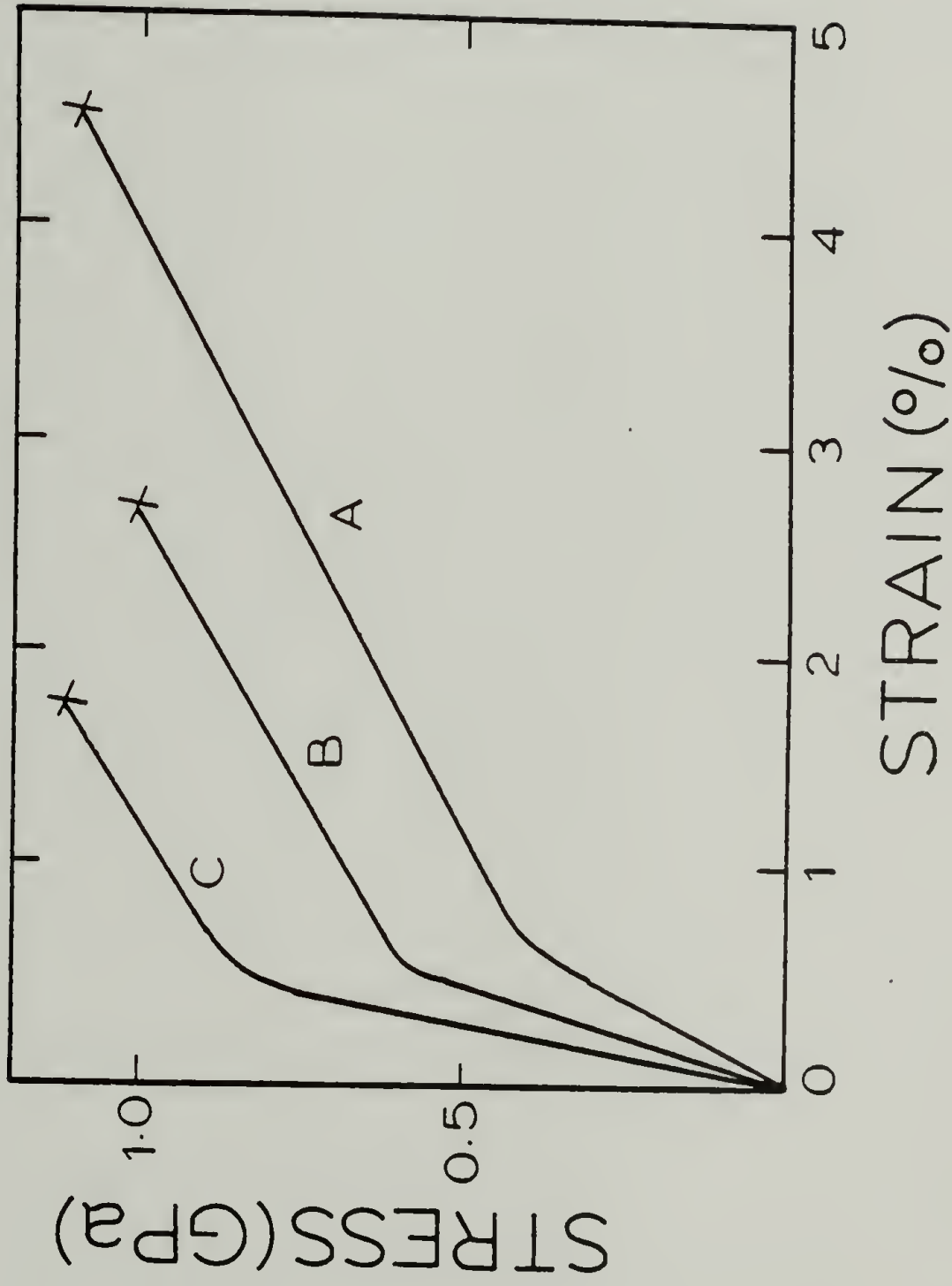


Figure 31. Stress-strain behavior for PBT fiber I: (A) non-tension dried, (B) non-tension dried then subsequently tensioned, (C) tension dried

Table 15. Mechanical properties<sup>a</sup> of PBT fibers dried at room temperature

PBT Fiber	Drying Conditions	Tensile Modulus, E (GPa)	Tensile Strength, $\sigma_b$ (GPa)	Strain at Break, $\epsilon_b$ (%)	Yield Strength, $\sigma_y$ (MPa)
I	Stress free	35 ± 2	1.1 ± .1	4.4 ± .8	480 ± 100
	Stress free then tensioned in dry state (400 MPa)	150 ± 10	1.0 ± .1	2.7 ± .3	600 ± 30
	Tensioned during drying (400 MPa)	175 ± 15	1.1 ± .2	1.8 ± .5	835 ± 40

<sup>a</sup>Data represents an average ± one standard deviation using six test specimens.



Figure 32

WAXD patterns of PBT Fiber I

- (A) Non-tension dried
- (B) Non-tension dried then subsequently tensioned
- (C) Tension dried

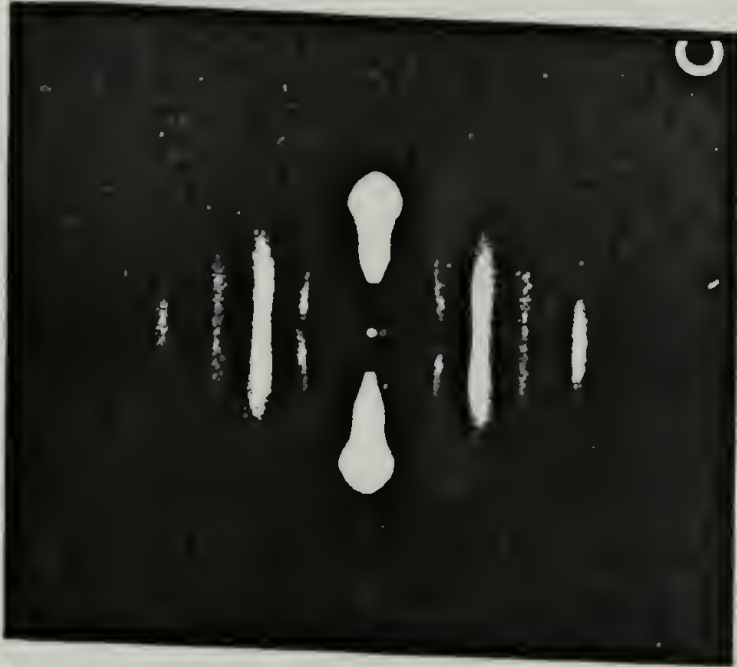


Table 16. Strain hardening effects<sup>a</sup> of wet vs. dry PBT fiber (I)

PBT Fiber	Draw Ratio	Initial Modulus (GPa)	Initial Modulus After Loading and Unloading to $\sigma^b$ (GPa)	$\sigma^b$ (MPa)	% Enhancement
(I) wet	3:1	1.5 $\pm$ 0.3	2.5 $\pm$ 0.6	200	67 $\pm$ 15
(I) dry	3:1	39 $\pm$ 7	53 $\pm$ 7	233	36 $\pm$ 6

<sup>a</sup>Data represents an average of 6 test samples  $\pm$  one standard deviation.

<sup>b</sup>Calculation based on dried cross sectional area.

properties than tensioning the fiber in the dried (as-spun) or collapsed state.

The effect of room temperature tension drying on the lateral molecular order as depicted by the lateral coherent scattering size of the crystallites and the fiber's compressive and shear characteristics have also been investigated. From the results summarized in Table 17, increasing levels of applied load during drying has no effect on these fiber properties. A meaningful quantitative evaluation of the molecular alignment within each tension dried fiber could not be assessed since D-500 diffractometer measurements require the stacking of several filaments which introduces misorientation. However previously reported WAXD flat film results on single filaments indicate that high tension drying improved chain orientation. Consequently, the use of high tension during drying serves only to modify the molecular alignment and internal shrinkage stresses thus altering only the tensile properties.

The work per unit volume (strain energy) required to break each of the room temperature dried fibers may be determined from the following relationship:

$$u = \int \sigma d\epsilon \quad (3.4)$$

where  $u$  = strain energy  
 $\sigma$  = uniaxial stress  
 $\epsilon$  = uniaxial strain

The work was calculated to be between  $2-3 \times 10^{-3}$  joules for the various

Table 17. Comparison of PBT fibers (VA) dried under various tensions at room temperature

Applied Load (MPa)	Tensile Modulus, E (GPa)	Shear Modulus, G (MPa)	(Gaussian) Lateral Coherence Scattering Size (nm)		Compressive Strength $\sigma_c$ (MPa)
			$e_1$	$e_2$	
0	140 $\pm$ 25	650 $\pm$ 65	2.0	2.9	170 $\pm$ 45
30	155 $\pm$ 10	570 $\pm$ 60	2.2	2.8	195 $\pm$ 20
155	180 $\pm$ 15	670 $\pm$ 90	2.0	2.7	210 $\pm$ 40
300	185 $\pm$ 10	540 $\pm$ 30	1.9	2.7	220 $\pm$ 25
520	190 $\pm$ 20	650 $\pm$ 50	2.0	3.0	-
670	190 $\pm$ 20	670 $\pm$ 40	2.1	3.0	-



tension and non-tension dried fibers by integrating the areas under the stress-strain curves in Figure 23. The work appears independent of the tension level during drying.

The apparent plastic behavior and the complete failure for each fiber is a result of the gradual breakage of microfibrils and fibrils. Moreover, the number of broken fibrils per unit time varies depending on the molecular and fibrillar orientation of the fiber and is exemplified in the tensile stress strain behavior. For example, the non-tension dried fiber experiences fewer broken fibrils per unit time as compared to the tension dried fiber which is more highly oriented. However, the work equivalence for the variously dried fibers implies that the work required to break all the fibrils (i.e., the fiber) appears independent of the rate of fibril rupture.

#### 3.4 Elevated Temperature Drying

High tension drying at room temperature has proven effective in modifying the structure and mechanics of the as-spun fiber. However, the extent of lateral molecular order and the shear and compressive properties are unaffected by room temperature drying. Furthermore, internal stresses are still present in the tension dried fiber. It has been speculated from earlier work on the heat treatment processing of PBT fibers that residual stresses may be removed while increasing the extent of the lateral chain order with the application of heat (25). Therefore, the presence of high temperature in conjunction with high

tension during drying is expected to produce further alterations in the material properties of the PBT fiber.

The tensile stress-strain behavior of PBT fiber V dried at 150°C, 320°C, and 500°C under various applied tensions is shown in Figure 33. At each temperature range examined, with increasing levels of applied stress during drying, the modulus increases while the elongation to break decreases (Table 18).

A comparison between the tensile behavior of PBT Fiber V dried at two levels of tension (40 MPa and 450 MPa) under various temperatures (25°C, 150°C, 320°C, and 500°C) is depicted in Figures 34 and 35 respectively. At both levels of tension, the stress-strain behavior gradually becomes linear elastic with increasing temperature. The tensile moduli increase with a reduction in percent elongation with higher drying temperatures. Therefore the modifications in tensile properties caused by high tension drying are further improved with a concurrent application of high temperatures.

With the exception of fibers non-tension dried at 150°C, all of the stress-strain curves become linear elastic with high temperature drying. With tension at a drying temperature of 150°C, the tensile behavior becomes completely linear elastic. Allen et al. has suggested that the elimination of internal stresses within the PBT fiber is detected by the absence of a yield point (52). Defining the interaction stress,  $\Psi$ , as the stress necessary to move a fibrillar element with respect to its neighbor, the internal stresses can be modified when

Figure 33

Typical stress-strain curves for PBT fibers  
dried at 150°C, 320°C, and 500°C at:

- A. 45 MPa tension
- B. 440 MPa tension

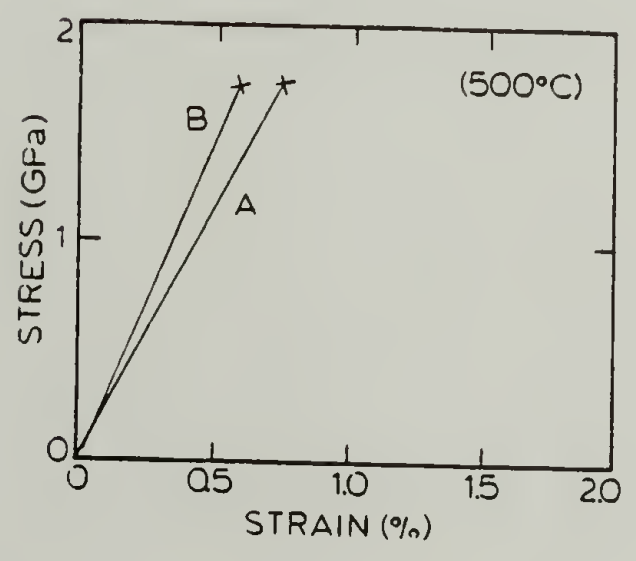
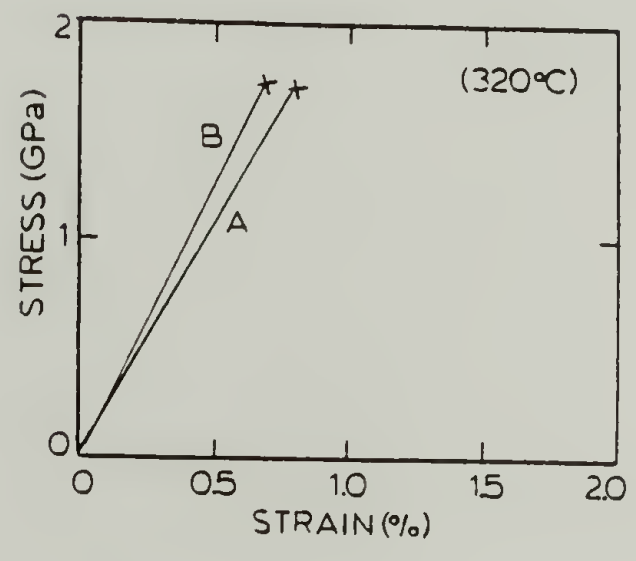
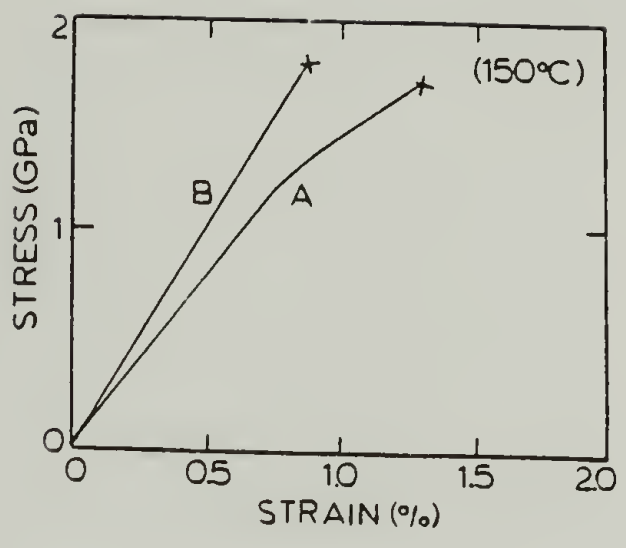


Table 18. Tensile properties<sup>a</sup> of PBT fibers continuously dried at various temperatures

PBT Fiber	Temperature <sup>b</sup> (°C)	Applied Load <sup>b</sup> (MPa)	Tensile Modulus, E (GPa)	Tensile Strength, $\sigma_b$ (GPa)	Elongation (%)
VA	25	0	140 + 25	1.7 + 0.3	1.9 + 0.3
		30	160 + 10	1.7 + 0.1	1.8 + 0.2
		300	185 + 10	1.7 + 0.2	1.4 + 0.1
		520	190 + 20	1.7 + 0.1	1.4 + 0.2
	150	45	175 + 10	1.6 + 0.1	1.3 + 0.1
		440	230 + 5	1.8 + 0.1	0.9 + 0.1
		45	205 + 20	1.6 + 0.1	0.8 + 0.1
		420	255 + 10	1.7 + 0.1	0.7 + 0.1
500	35	275 + 20	1.8 + 0.1	0.7 + 0.1	
	465	285 + 20	1.7 + 0.1	0.6 + 0.1	
VB	25	0	150 + 5	1.7 + 0.1	1.8 + 0.1
		30	145 + 5	1.7 + 0.1	1.8 + 0.1
		315	150 + 15	1.5 + 0.1	1.4 + 0.1
		800	165 + 20	1.8 + 0.2	1.5 + 0.1
	320	50	202 + 10	1.3 + 0.1	0.7 + 0.1
		360	225 + 10	1.4 + 0.1	0.7 + 0.1
		50	206 + 10	1.5 + 0.2	0.7 + 0.1
		310	266 + 20	1.7 + 0.2	0.9 + 0.1

<sup>a</sup>Reported values represent an average  $\pm$  one standard deviation for a minimum of 12 samples.

<sup>b</sup>Drying residence time 5 minutes



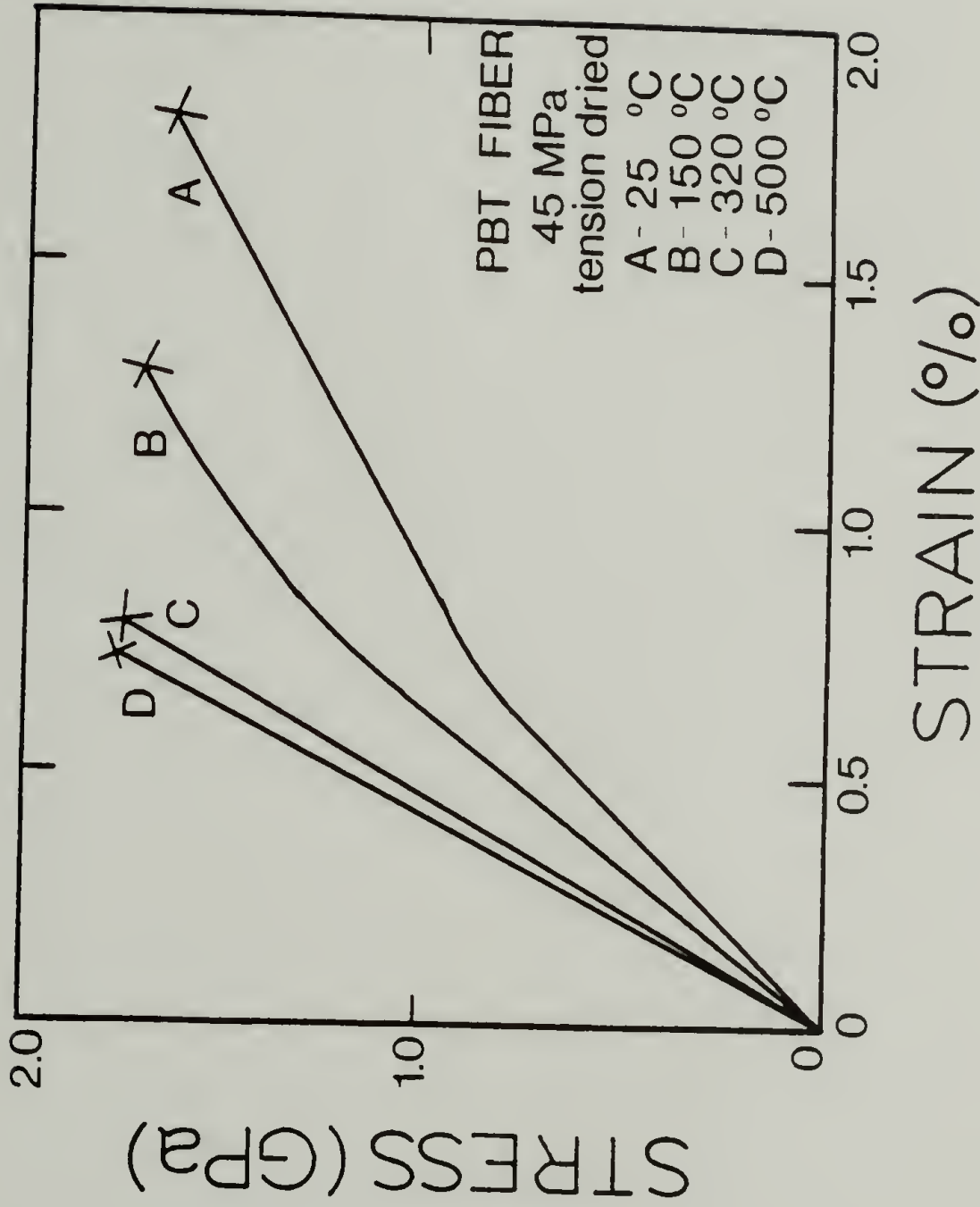


Figure 34. Comparison of the stress-strain behavior for PBT fiber (VA) dried under 45 MPa (minimal) tension at (A) 25 C, (B) 150 C (C) 320 C, (D) 500 C

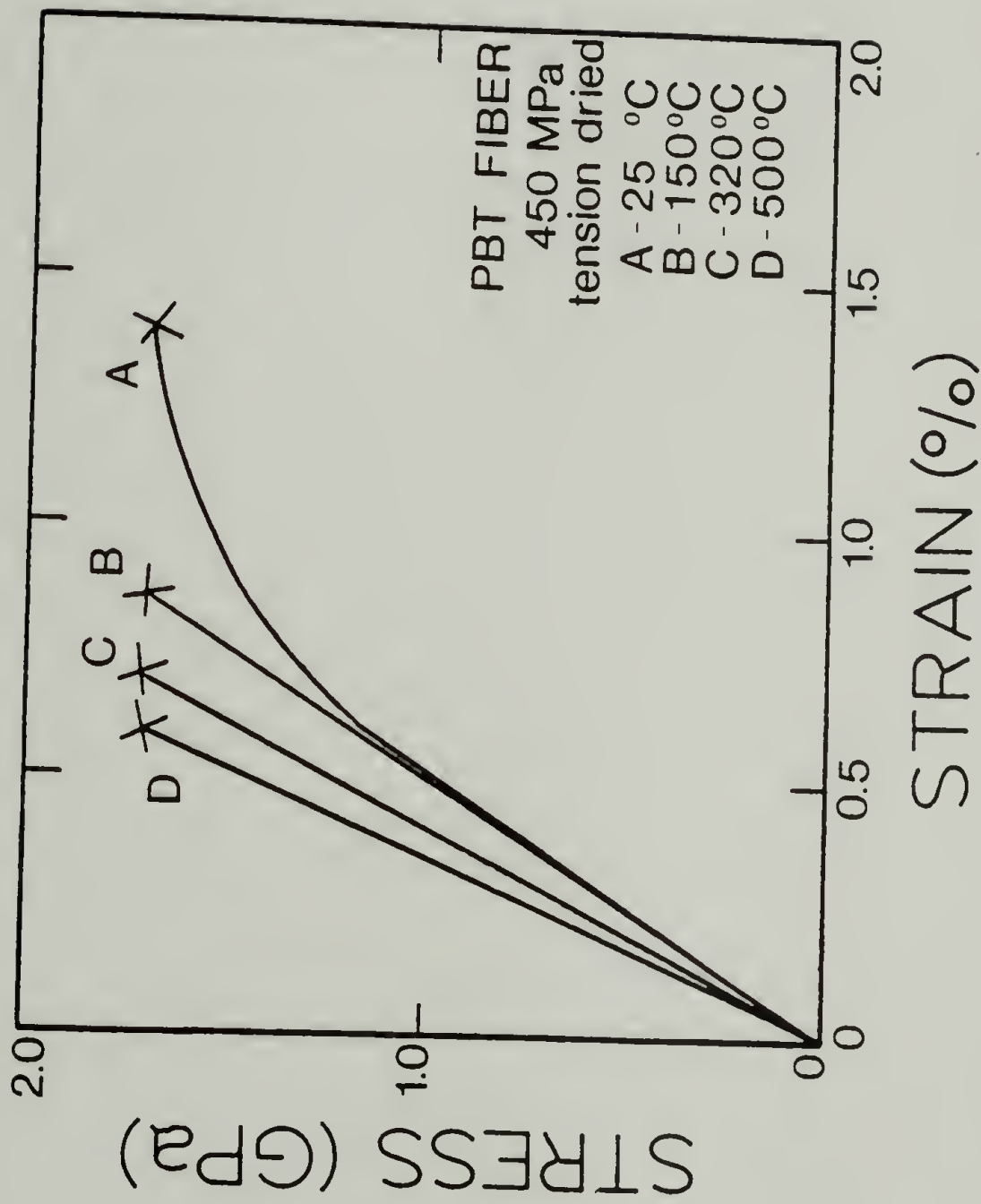


Figure 35. Comparison of the stress-strain behavior of PBT fibers (VA) dried under 450 MPa tension at (A) 25 C, (B) 150 C, (C) 320 C (D) 500 C

$$\sigma_i^{(\max)} \geq \psi(AT_0) \quad (3.5)$$

where  $A$  = fibrillar element's lateral area of interaction

$T_0$  = drying temperature

$\sigma_i^{\max}$  = maximum residual stress.

The interaction stress is a function of the element's lateral area of interaction and has been found to be temperature dependent (25,52). However, the application of tension may also serve to displace a fibrillar element with respect to its neighbors (25,52).

$$\sigma_i^{\max} = \psi(A, T_0) - \sigma_{\text{app}} \quad (3.6)$$

For fibers dried at 150°C with no tension, the interaction stress,  $\psi$ , was greater than  $\sigma_i^{\max}$  and the relative displacement of elements to eliminate the internal stresses was not possible. The absence of a yield point for fibers tension dried at 150°C suggests that the internal stresses may be eliminated as the interaction stress is offset by the tension applied during drying.

The application of both temperature and tension during drying serves two important but different functions. As previously stated, the application of tension (work contribution) during drying causes a straightening of the wet fibrillar network and offsets the formation of compressive shrinkage stresses. The use of high temperature supplies the appropriate thermal energy (heat contribution) to drive off the water and/or residual solvent which would not be removed by ordinary

diffusion at room temperature. The spectroscopic analysis measuring the amount of residual acid and/or water molecules and variously dried PBT films have been carried out by Chang and Hsu (73). No observable absorbance bands at 3300 cm corresponding to the OH stretching vibration of water molecules are reported in samples dried at 109°C, whereas the room temperature dried films show a distinct band at this frequency. It is postulated that the removal of water with high temperature drying facilitates the molecular ordering and results in improved tensile properties.

The effect of elevated temperature drying with minimal and high tension on the lateral molecular ordering and their transverse properties has been investigated. The coherent scattering size of the crystallites is enlarged as expected for both the non-tension and tension dried fibers with increasing temperature (Table 19). Furthermore, high tension drying produces slightly larger crystallites than non-tension drying at a given elevated temperature. Figure 36 and Table 19 summarize the compressive strengths and shear moduli for the various temperature dried fibers without and with tension. The shear moduli and the compressive strengths are not appreciably altered for the elevated temperature non-tension dried fibers. However, high tension drying under high temperatures results in a slight increase in the fiber's shear modulus and compressive strength.

Alterations in the shear and compressive characteristics appears to depend on the degree to which lateral interactions are developed. Since the microfibrils have been reported to be approximately 70Å-100Å (71),

Table 19. Transverse properties of PBT fibers (VB) dried at various temperatures

Applied Load (MPa)	Applied Temperature (°C)	Tensile Modulus (GPa)	(Gaussian) Lateral Coherence Scattering Size (nm)	Shear <sup>b</sup> Moduli, G (MPa)	Compressive Strain (%)	Compressive Strength (MPa)
			$e_1$			
			$e_2$			
30	25	140 ± 5	2.1	670 ± 140	0.139 ± .005	195 ± 20
35	320	200 ± 15	6.9	670 ± 100	0.123 ± 0.17	245 ± 50
50	500	225 ± 35	10.1	800 ± 100	0.096 ± .013	215 ± 60
300	25	165 ± 15	1.8	650 ± 185	0.112 ± .015	185 ± 55
375	320	250 ± 25	8.2	675 ± 285	0.110 ± .032	275 ± 100
355	500	245 ± 20	11.4	860 ± 270	0.138 ± .021	340 ± 80

<sup>a</sup>Residence time in oven = 2 minutes

<sup>b</sup>Average of 6 tests ± one standard deviation



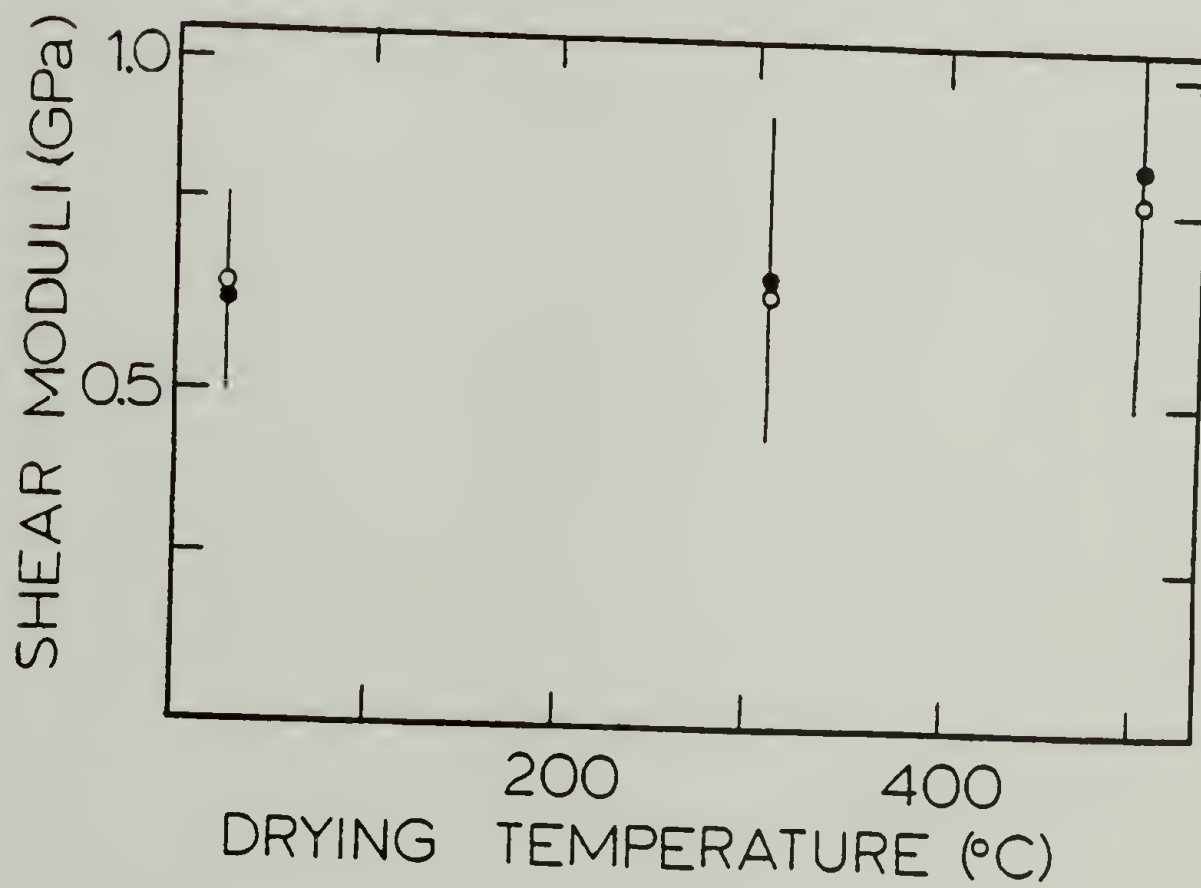
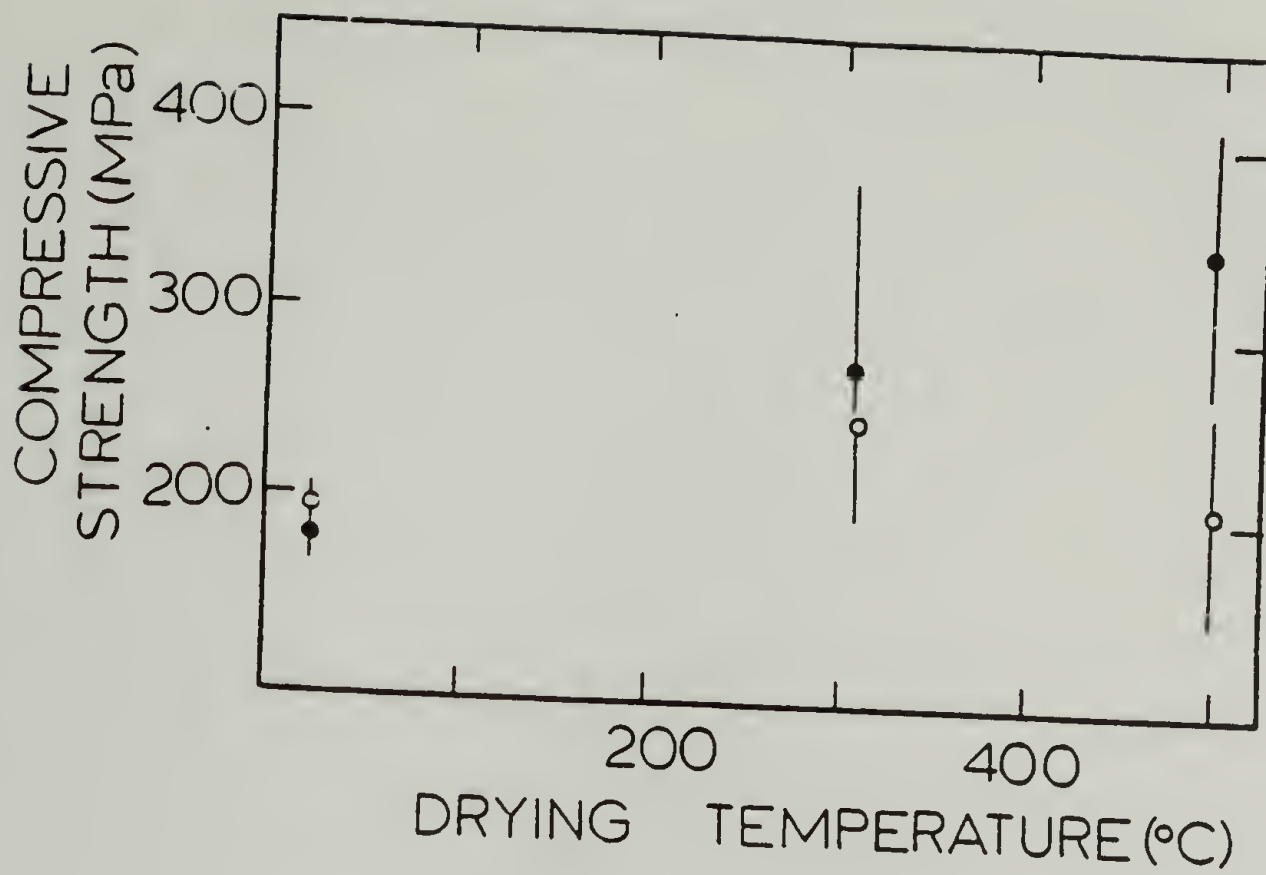


Figure 36. Shear moduli and compressive strengths for PBT fibers (VB) dried at various temperatures

enlarging the crystallite size within the microfibrils ( $100\text{\AA}$ ) does not alter the transverse mechanical properties as evidenced by the results generated on non-tension elevated temperature dried PBT fibers. However a slight enhancement in the compressive and shear characteristics of a high temperature and tension dried fiber coincides with the development of larger crystallites ( $\sim 114\text{\AA}$ ). These coherently scattering regions slightly exceed the average dimensions of the microfibril which suggests that alterations in the compressive and shear behavior of PBT fibers may be achieved by intermicrofibrillar and interfibrillar associations.

### 3.5 Post Processing Heat Treatment Investigations

Many of the observed changes in the structure and properties of the PBT fiber through elevated temperature drying resemble the fiber changes evident with post processing heat treatment. In order to explore the potential difference in the two processing techniques, a comparative study between "heat treating" a wet fiber (i.e., elevated temperature drying) and "heat treating" a dry fiber has been performed. To determine the relevance of a rigorous drying process in producing an "as-spun" fiber with high properties, post processing heat treatment investigations have been performed on the different high temperature and tension dried samples.

Table 20 summarizes the tensile properties which are produced from heat treating in the wet versus the dry state at  $320^{\circ}\text{C}$  and  $500^{\circ}\text{C}$ . Within statistical error, there is no detectable difference between the tensile moduli of fibers processed by the two methods. All fibers tested

Table 20. Comparison between the tensile properties of a "heat treated" wet and dry PBT fiber (VB)

Initial Fiber State	Heat Treatment <sup>a</sup> Conditions		Tensile Modulus, E (GPa)	Tensile Strength, $\sigma_b$ (GPa)
	Temperature (°C)	Tension (MPa)		
Wet	320	35	200 + 15	1.3 + 0.1
Dry	320	65	180 $\pm$ 15	1.8 $\pm$ 0.2
Wet	320	235	250 + 25	1.5 + 0.1
Dry	320	375	240 $\pm$ 60	1.9 $\pm$ 0.1
Wet	500	50	225 + 35	1.6 + 0.3
Dry	500	55	190 $\pm$ 10	1.7 $\pm$ 0.2
Wet	500	370	245 + 20	1.7 + 0.1
Dry	500	355	270 $\pm$ 60	2.1 $\pm$ 0.3

<sup>a</sup>Residence time = 2 minutes

exhibit a linear elastic stress strain curve. Note that the tensile strength of the elevated temperature dried sample is slightly inferior to the strengths of the PPHT fibers. Scanning electron micrographs of the various dried and heat treated fibers in Figure 37 reveal no observable differences on a macrostructural level.

A comparison between the microstructural features of "heat treated" wet and dry fibers has been made. From the data summarized in Table 21, the crystallite size increases for both sets of fibers with increasing levels of applied temperature and tension during processing. However, the coherent scattering size of the crystallites is slightly larger for the elevated temperature dried fiber. It is possible that the water may be more effectively removed during elevated temperature drying which results in the enhancement in the lateral molecular order.

The compressive strengths and shear moduli for these variously processed fibers have been analyzed. From the results in Table 21, within statistical error there appears to be little difference between heat treating a wet versus a dry fiber on the above mentioned mechanical properties. The observed microstructural changes less than  $100\text{\AA}$  have little effect on the fiber's compression or shear behavior.

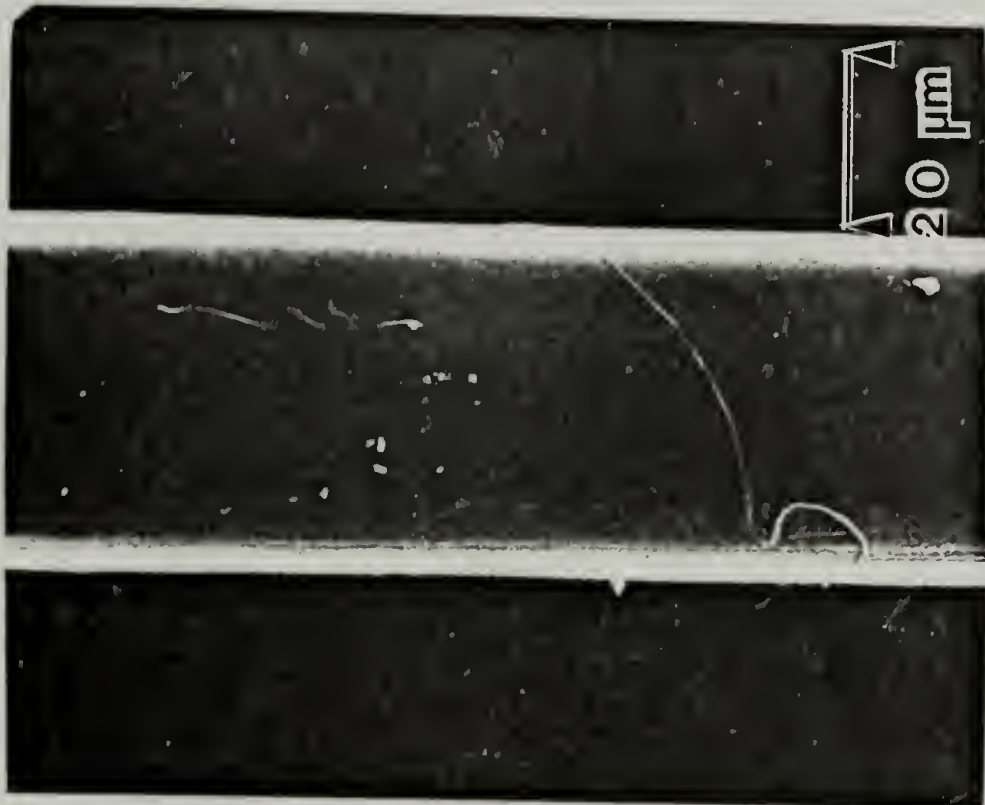
A logical extension of this work is to examine the effects of subsequent post processing heat treatment on the various tension dried fibers. A comparison between the properties of a non-tension and tension dried fiber which was subsequently heat treated is summarized in Table 22. For each series of differently dried fibers, heat treatments were conducted at  $320^{\circ}\text{C}$  and  $500^{\circ}\text{C}$  with and without tension. There is an

Figure 37

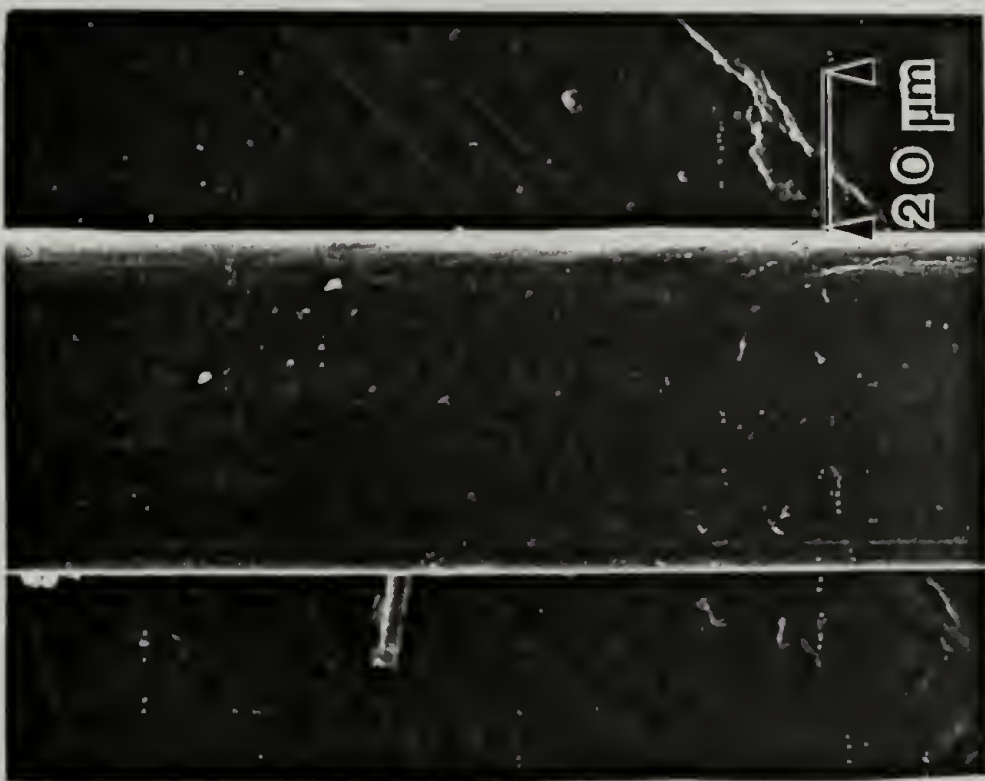
Scanning electron micrographs of a PBT fiber:

- (A) dried at 320°C
- (B) heat treated at 320°C





B



A

Table 21. Comparison between the transverse properties of a "heat treated" wet and dry PBT fiber (VB)

Initial Fiber State	Heat Treatment Conditions <sup>a</sup>		(Gaussian)		Shear Moduli, G (MPa)	Compressive Strain (%)	Compressive Strength ( $\sigma_c$ )
	Applied Temperature (°C)	Applied Load (MPa)	Lateral Coherence Scattering Size (nm)				
Wet	320	35	$\underline{e_1}$	$\underline{e_2}$	670 + 100	.119 ±	240 + 45
Dry	320	65	6.9	4.8	970 ± 70		
Wet	320	375	6.8	5.1			
Dry	320	375	8.2	4.8	675 + 285	.092 +	230 + 55
Wet	500	50	6.5	4.5	585 ± 125	.071 ±	170 ± 70
Dry	500	50	10.1	4.2	800 + 100	.096 ±	200 ± 30
Wet	500	355	9.0	4.7	945 ± 90		
Dry	500	355	11.4	6.5	860 + 270	.138 +	340 + 80
			10.1	5.7	860 ± 270	.093 ±	250 ± 90

<sup>a</sup>Residence time = 2 minutes

<sup>b</sup>Average of 6 test specimens ± one standard deviation

Table 22. Summary of heat treated properties of tension versus non-tension room temperature dried fibers (VB)

Applied Tension (Drying) (MPa)	Heat Treatment Conditions		Tensile Modulus, E (GPa)	Tensile Strength (GPa)	Shear Modulus, G (MPa)	Lateral Coherent Scattering Size (nm)
	Temperature (°C)	Tension (MPa)				
30	-	-	145 + 5	1.7 + 0.1	685 + 145	$\frac{e_1}{e_2}$ 2.1 / 2.9
30	320	30	180 + 15	1.8 + 0.2	965 + 70	6.8 / 5.1
30	320	300	240 + 60	1.9 + 0.1	677 + 30	6.5 / 4.5
30	500	30	190 + 10	1.7 + 0.1	945 + 175	9.0 / 4.7
30	500	300	279 + 60	2.1 + 0.3	860 + 270	10.1 / 5.7
800	-	-	165 + 15	1.8 + 0.2	755 + 85	2.2 / 2.7
800	320	30	170 + 15	1.5 + 0.2	865 + 100	6.4 / 4.5
800	320	300	235 + 20	1.6 + 0.2	995 + 160	6.4 / 8.3
800	500	30	210 + 15	2.0 + 0.3	620 + 30	9.0 / 4.4
800	500	300	290 + 25	2.0 + 0.2	1140 + 65	12.6 / 6.1

increase in the tensile modulus and strength as well as increase in the lateral molecular order with increased levels of temperature and tension for both the non-tension and tension dried fibers. Observed microstructural changes have little influence on the shear modulus as detected in previous studies herein. It is apparent that within statistical error, the final fiber properties attained after post processing heat treatment are equivalent and are independent of whether or not the precursor had been tension dried.

The effects of post processing heat treatment on variously elevated temperature dried fibers with and without tension have also been investigated. From the results in Table 23, without tension during heat treatment processing, the precursor having the higher tensile properties results in higher heat treated tensile properties. Conversely, the final tensile modulus is independent of the initial precursor when the fibers are tension heat treated. The tensile strengths do increase with post processing heat treatment, but the ultimate values are again independent of the as-spun precursor.

The similarities between elevated temperature drying and heat treatment processing suggest that post processing heat treatment is simply a second stage drying process. Thermal gravimetric analysis of an as-spun and heat treated PBT fiber have been performed. From the results in Figure 38, the as-spun PBT fiber displays a 12% weight loss prior to a 310°C whereas the heat treated fiber remains virtually unaffected until thermal degradation begins at 750°C. From thermal degradation studies of the as-spun fiber, Jones et al. have found that water is

Table 23. Summary of heat treated properties<sup>a</sup> of elevated temperature dried fibers (VB)

Drying Condition		Heat Treatment Conditions		Tensile Modulus (GPa)	Tensile Strength (GPa)
Tension (MPa)	Temperature (°C)	Tension (MPa)	Temperature (°C)		
30	R.T.	-	-	140 + 5	1.7 + 0.1
30	R.T.	30	320	180 + 15	1.8 + 0.2
30	R.T.	300	320	240 + 60	1.9 + 0.1
30	R.T.	30	500	190 + 10	1.7 + 0.1
30	R.T.	300	500	270 + 60	2.1 + 0.3
30	320	-	-	205 + 20	1.3 + 0.2
30	320	30	320	210 + 20	1.7 + 0.2
30	320	300	320	240 + 15	1.7 + 0.1
30	320	30	500	225 + 10	2.0 + 0.1
30	320	300	500	265 + 10	1.9 + 0.1
30	500	-	-	213 + 15	1.5 + .3
30	500	30	320	213 + 10	1.8 + .3
30	500	300	320	213 + 40	1.8 + .2
30	500	30	500	225 + 30	1.5 + .2
30	500	300	500	225 + 20	1.8 + .2

<sup>a</sup> Average values  $\pm$  one standard deviation for a minimum of 12 test samples.



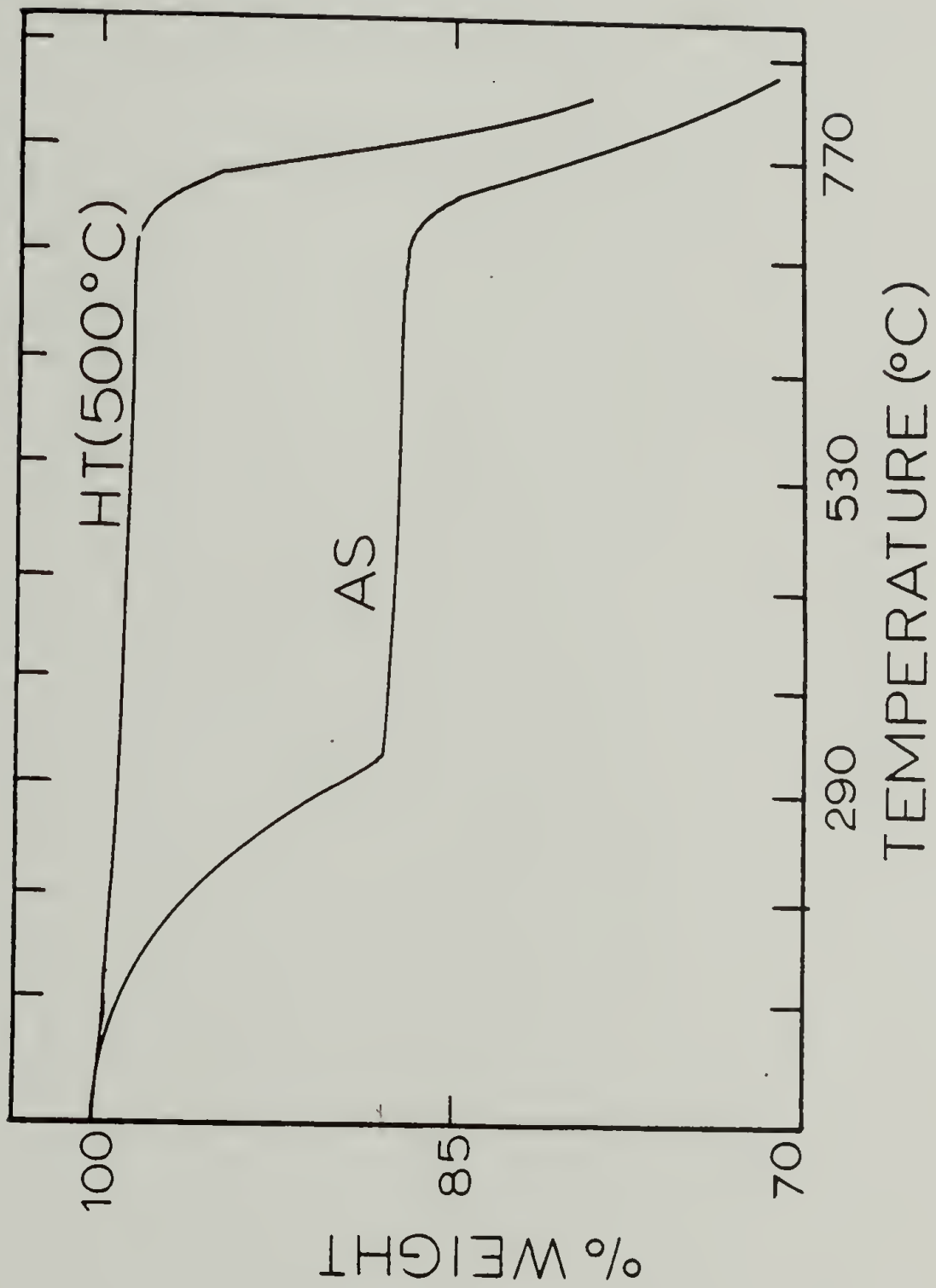


Figure 38. Thermal gravimetric behavior for (A) as-spun PBT fiber, (B) tension heat treated PBT fiber (800 MPa; 500 C)

eliminated at 120°C and the residual acid is totally removed by 320°C (87). Fourier transform infrared spectroscopic studies conducted by Hsu et al. of an as-spun film undergoing a heat treatment process support these findings (73). Upon annealing, they report a complete elimination of water and acid absorption bands at 110°C and 310°C respectively. The apparent weight loss on the thermal gravimetric thermogram for the as-spun PBT fiber can be attributed to the removal of water and residual solvents.

As indicated in Chapter I, post processing heat treatment is associated with an increase in the molecular orientation corresponding to an enhancement in the tensile properties. It is postulated that the structural alterations may be a result of the water and solvent removal. This would suggest that the elimination of residual water/acid is crucial in the development of the fiber properties for PBT.

### 3.6 Conclusions

Modifications in the structure and mechanics of PBT fibers have been attempted through high tension and temperature drying and subsequent post processing heat treatment experiments. The application of tension during drying on PBT fibers spun from anisotropic solutions of PBT/PPA results in an enhancement of tensile modulus and yield strength with a reduction in strain to break. Modifications in the mechanical behavior of PBT fibers through tension drying can be achieved regardless of the initial spin draw ratio of the fiber. Furthermore, tension drying provides a means by which to maximize the potential stiffness of PBT

fibers which are spun from low concentrations of PBT/PPA and have a low spin draw ratio. Alterations in the tensile properties can be attributed to the straightening of the wet fibrillar network. Also, the axial compressive stress which develops during drying is offset thus eliminating the buckling of the fibrillar elements. These investigations show that in the processing of PBT fibers, preventing the onset of axial buckling and aligning the wet fibrillar network with tension during drying is more effective in enhancing the tensile properties than straightening the dried buckled fibers.

High temperature drying with tension results in a further enhancement in tensile properties in these fibers which is attributed to the observed increase in the crystallite size and molecular orientation. These microstructural changes can be associated with the removal of water/residual solvents which are not removed by ordinary diffusion during room temperature drying.

The torsional rigidity and compressive strengths appear only slightly altered by the rigorous drying process. There is no conclusive correlation between these mechanical properties and the extent of lateral molecular order on a scale  $< 10$  nm. However a slightly higher compressive strength for the PBT fiber is observed when the coherently scattering crystalline regions exceed the reported dimensions of the microfibrils. These observations suggest that the fiber's compressive strength as well as the shear modulus may be influenced by interfibrillar and intermicrofibrillar interactions.

A summary of the range of fiber properties at various stages during fiber development abstracted from the results in Chapters II and III is presented in Table 24. Based on this information, the fibers at various stages during the dry-jet wet spinning process can be ranked in order of increasing lateral molecular order and enhancement in tensile properties as follows:

Coagulated fiber < non-tension dried fiber < tension-dried fiber < heat and tension dried fiber < heat treated fiber

From these observations, various conclusions can be drawn regarding the development of these fiber properties during the spinning process.

The gradual development of the tensile properties can be interpreted in terms of the imposed spinning strain. According to Jaffee and Jones, the tensile modulus and strength are highly dependent on the total spinning strain (51). In dry-jet wet spinning, this strain can be implemented in the dry-jet region manifested in the spin draw ratio, in the coagulation bath through a wet stretching process and in the drying and heat treatment processes. The ultimate tensile modulus and strength attainable is simply a function of the total strain in all four processes.

Table 24. Overview of properties during PBT fiber spinning process

	Tensile Modulus (GPa)	Shear Modulus (MPa)	Maximum Coherent Scattering Size From $e_1$ Peak (nm)
Coagulated Fiber	15-120 <sup>a</sup>	115	1.1
Non-tension Dried As-Spun Fiber	30-140	650	2.0
Tension Dried As-Spun Fiber	180-190	540-670	2.2
Heat and Tension Dried As-Spun Fiber	265-285	675-860	11.4
Heat Treated Fiber	265-285	585-860	10.5

<sup>a</sup>Value reported based on dried fiber diameter.



$$\epsilon_{(sp)} = f(\epsilon_{(ag)}) + f(\epsilon_{(cb)}) + f(\epsilon_{(d)}) + f(\epsilon_{(ht)}) \quad (3.8)$$

where

$\epsilon_{(sp)}$  = total spinning strain

$\epsilon_{(ag)}$  = strain imposed in the air gap or dry jet region

$\epsilon_{(cb)}$  = strain imposed during wet stretch process in coagulation bath

$\epsilon_{(d)}$  = strain imposed during drying

$\epsilon_{(ht)}$  = strain imposed during post processing heat treatment

This concept is consistent with many of the observations pertaining to property development during drying and heat treatment. For example, a fiber with a low spin draw ratio, when sufficiently wet stretched and tension dried, had approximately the same modulus as a fiber spun from a high spin draw and subsequently wet stretched and tension dried. It is speculated that the sum of the strains imposed in the air gap, during coagulation and during drying for the two fibers are equal.

$$\begin{aligned} f(\epsilon_{(ag)}) + f(\epsilon_{(cb)}) + f(\epsilon_{(d)})_{\text{fiber I}} &= f(\epsilon_{(ag)}) \\ &+ f(\epsilon_{(cb)}) + f(\epsilon_{(d)})_{\text{fiber VI}} \end{aligned} \quad (3.9)$$

Furthermore, the properties of the non-tension dried (NT) and tension dried (T) fiber become identical with subsequent tension during heat treatment because the total strain imposed on the two fibers during coagulation, drying and heat treatment is the same.

$$\begin{aligned} f(\epsilon_{(cb)}) + f(\epsilon_{(d)}) + f(\epsilon_{(ht)})_{\text{NT}} &= f(\epsilon_{(cb)}) \\ &+ f(\epsilon_{(d)}) + f(\epsilon_{(ht)})_{\text{T}} \end{aligned} \quad (3.10)$$

It appears that the attainment of the optimal fiber properties is independent of the processing pathway and determined solely by the ability to orient the polymer through deformation during processing. Unfortunately, defects such as voids and internal stresses may limit the amount of strain which can be imposed during spinning, thus limiting the attainment of their theoretically predicted properties.

The removal of water and acid is believed to contribute substantially to the development of the fiber properties after coagulation. It is implied that post processing heat treatment is simply a continued drying process. It is speculated that both tension and temperature play two important and synergistic roles during drying and PPHT. The applied tension (mechanical energy input) functions to improve chain alignment while preventing the fiber from buckling during the collapse process. The application of heat (thermal energy) is believed to facilitate the removal of water while relieving internal stresses. However quantitative relationship between these two parameters can be deduced from the empirical observations on their influence on the fiber properties. An attempt to closer correlate these two processing parameters during fiber development is one of the subjects addressed in Chapter IV.

CHAPTER IV  
FORCE TEMPERATURE BEHAVIOR OF  
RIGID ROD POLYMERIC FIBERS

4.1 Introduction

In the Force-Temperature (F-T) experiments, the generation of thermal stresses or shrinkage force in materials held at constant strain is monitored as a function of temperature. Thermal expansion properties of material may be readily examined from this experimental technique.

Writing the total differential for force,  $f$ , in terms of length,  $L$ , and temperature,  $T$ , the following relation is obtained

$$\left(\frac{\partial f}{\partial T}\right)_{L,P} = -\left(\frac{\partial f}{\partial L}\right)_{T,P} \left(\frac{\partial L}{\partial T}\right)_{f,P} \quad (4.1)$$

Normalizing the equation by a reference area,  $A_0$ , and length,  $L_0$ , equation (4.1) becomes

$$\left(\frac{\partial \sigma}{\partial T}\right)_{\epsilon,P} = -\left(\frac{\partial \sigma}{\partial \epsilon}\right)_{T,P} \left(\frac{\partial \epsilon}{\partial T}\right)_{\sigma,P} = -E\alpha \quad (4.2)$$

where  $\sigma$  = uniaxial stress  
 $\epsilon$  = uniaxial strain  
 $E$  = isothermal Young's Modulus  
 $\alpha$  = linear axial thermal expansion coefficient

The slope of the axial stress versus temperature plot is, the negative of the product of the axial modulus and the axial thermal expansion coefficient. The thermal expansion coefficient,  $\alpha$ , is ascertainable

from the slope of the (F-T) curve if the modulus is determined independently. The preceding thermodynamic arguments are only valid on materials which behave reversibly with temperature variations.

The F-T technique has also proven to be a useful thermal analysis probe to assess molecular phenomena in polymers associated with the application of stress and temperature (88-92). From the early F-T studies by Stein et al. (88) and more recently by DeCandia et al. (89) on deformed polyethylene, an observed irreversible stress drop has been associated to the structural modifications of the non-equilibrium morphology frozen in during deformation. Conversely, Buchanan et al. (90) have observed the generation of stress in the F-T profiles for Nylon 6,6, poly (ethylene terephthalate), and polypropylene textile yarns. These authors postulate that a shrinkage stress develops as the contraction of molecules from an extended chain conformation is restricted. The irreversible F-T behavior on natural rubber reported by Luch et al. (91) has been attributed to the melting of stress induced crystalline regions. More recently, Wang et al. have studied the F-T behavior of polyurethane elastomeric fibers (92). They suggest that a shrinkage stress develops below the glass transition of the soft segment whereas the observed stress softening behavior at high temperatures is a consequence of structural perfection and eventual melting of the hard segment domains. The generation of irreversible shrinkage and retractive forces with increasing temperature for semi-crystalline polymers may be attributed to one or more of the following processes: (1) relaxation of oriented amorphous polymers, (2) molecular restructuring and perfecting



(crystallization), (3) melting, (4) solvent and moisture removal. Thus, the F-T technique has proven to be a unique way to monitor the effective material changes with the application of stress and temperature.

In this chapter, experiments examining the F-T behavior of Kevlar<sup>R</sup> and various as-spun and heat treated PBT fibers have been conducted. The data generated is intended to provide insight into the relative degree of thermal stability as detected by a reversible F-T profile induced in their initial processing. Secondly, an assessment of the effectiveness of the initial drying and heat treatment processing may be obtained by examination of the irreversible F-T effects.

From the processing-property investigations reported in Chapter III, temperature and tension are important factors in controlling the alterations in material properties. However, a complete understanding of the relationship between the mechanical energy input (tension) and the thermal energy input (temperature) is still lacking. The F-T technique on these rigid rod fibers has been studied to explore any possible correlation between temperature and tension during processing.

## 4.2 Experimental

### 4.2.1 F-T Design and Procedures

The PBT yarns investigated in this chapter were dry-jet wet spun at the Celanese Research Company. These same PBT yarns were then heat treated at 600°C for 8 seconds and designated PBT-HT. F-T experiments were also carried out on dried and HT single filaments reported in Chapter III. For comparative purposes, Kevlar<sup>R</sup> 29 and Kevlar<sup>R</sup> 49 yarns were



also investigated. Both aramid yarns were obtained commercially from DuPont. Steel yarn, obtained from Bekeart Steelwire Corporation, was examined to determine the reliability of the instrumentation.

A schematic of the force-temperature apparatus employed in this work is shown in Figure 39. A 30 cm sample was fed through the oven; one end was clamped to an Interphase 5 kg load cell while the other end was attached to a movable clamp. The sample was stretched to a fixed length by adjustment of the movable clamp and the temperature of the oven was controlled manually with a variac at a rate of approximately 5°C/min. Subambient temperatures were achieved by forcing liquid nitrogen vapor through the oven. The temperature was monitored by an Omega platinum resistance (RDT) thermocouple situated in the middle of the oven. The resulting fiber's stress and its change with temperature were monitored on a Houston Instruments X-Y recorder. Nitrogen was continuously flushed through the oven to prevent degradation of the material at the high temperatures achieved.

#### 4.2.2 Fiber Physical and Mechanical Characterization

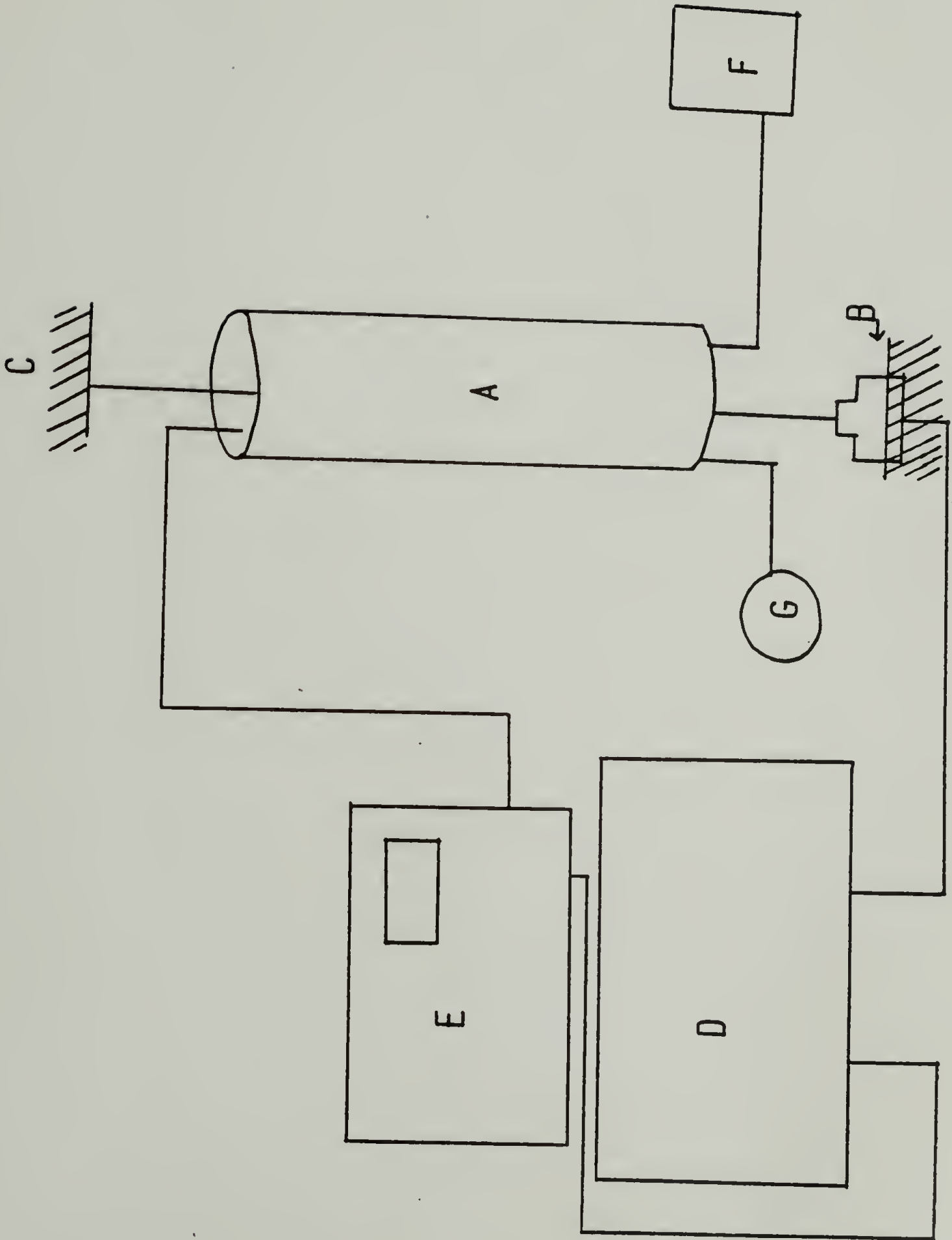
The tensile properties of Kevlar<sup>R</sup>, PBT and steel were determined on single filaments as described in Chapter III. The reported moduli were corrected for machine compliance and were based on diameters measured by light scattering (66).

Wide angle x-ray diffractions results were obtained from both diffractometric and flat film techniques as discussed in Chapter II.

Figure 39

Schematic diagram of force-temperature experiment.

- A. Oven
- B. Load cell
- C. Adjustable clamp
- D. X-Y recorder
- E. Temperature readout/thermocouple
- F. N<sub>2</sub> source
- G. Variac



A thermal gravometric analysis (TGA) on PBT fibers was performed with a Perkin Elmer TGS-2 interfaced with a Perkin Elmer thermal analysis microprocessor. A scan rate of 10°C/min was employed with a nitrogen flow rate of 60 cubic centimeters/min.

#### 4.2.3 Fiber Denier Characterization

A newly devised technique for linear density or denier measurements during on line fiber processing has been devised by Farris et al. (93). This technique is based on determining the propagation velocity of a transverse wave along the length of fiber with the simultaneous application of heat. The relationship between the velocity of the transverse wave along the fiber,  $v$ , the tension on the fiber,  $F$ , and the mass per unit length,  $M_\mu$ , is expressed by the following equation (4.3):

$$v = \left(\frac{F}{M_\mu}\right)^{1/2} \quad (4.3)$$

Thus, the measurement of the time it takes for a wave to propagate a specified distance under a known tension allows for the determination of  $M_\mu$ .

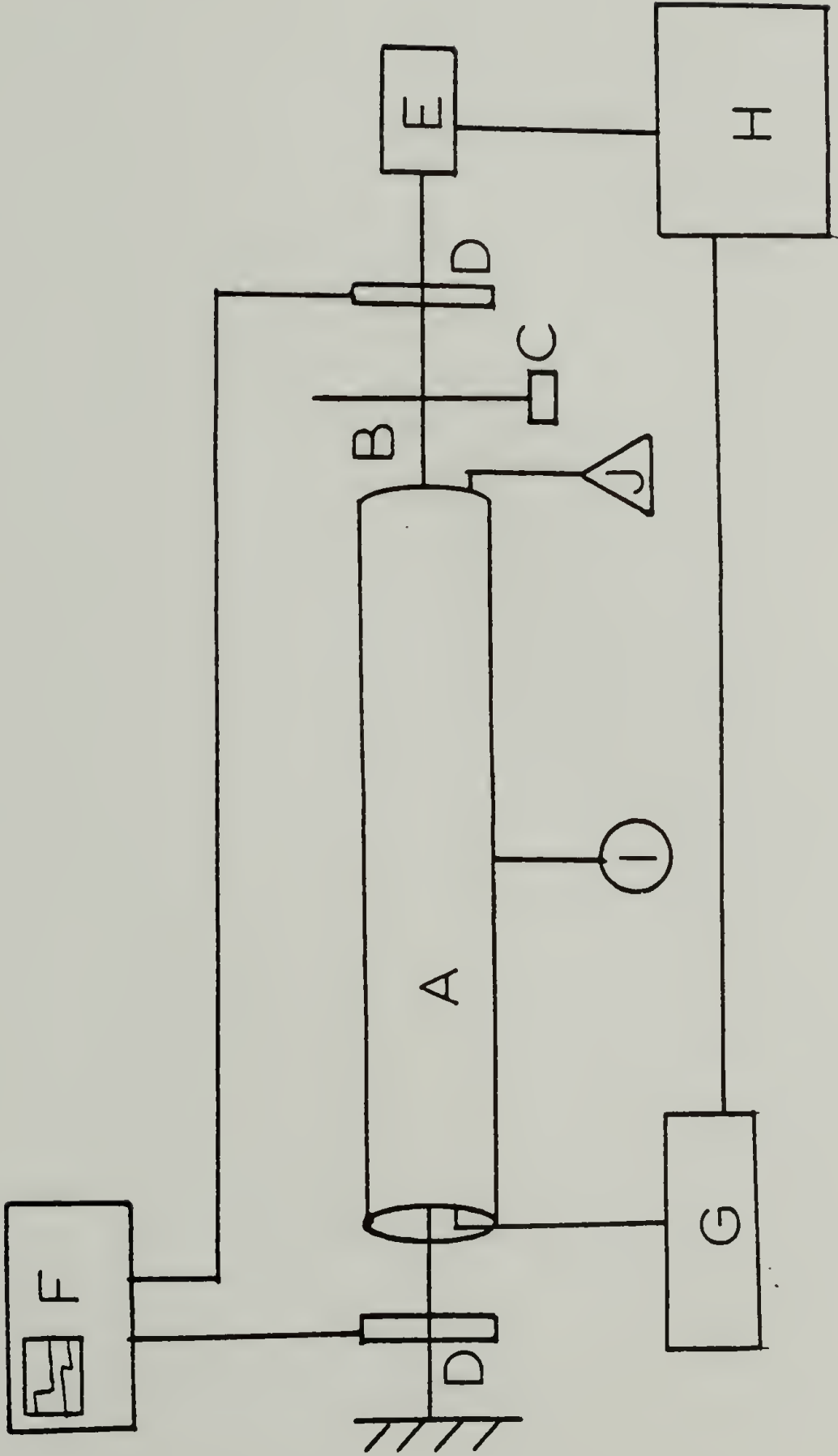
A schematic of the apparatus employed is depicted in Figure 40. The fiber, surrounded by a tubular heating element, was held under constant strain between a fixed support and a Toyo 550 gm load cell. The temperature of the oven was controlled manually with a variac at a rate of 5°C/min and monitored by an Omega platinum thermal sensing probe. A striker was used to initiate a transverse wave in the fiber. While slowly heating the fiber (5°C/min), the sample was periodically tapped.

Figure 40

Schematic diagram of the force-temperature/  
denier-temperature apparatus.

- A. Oven
- B. Fiber
- C. Striker
- D. Sensor
- E. Load cell
- F. Oscilloscope
- G. Temperature readout/thermocouple
- H. X-Y recorder
- I. Variac
- J. Nitrogen





The resulting wave velocity was subsequently detected by two sensing devices situated a known distance apart and recorded on a Nicolet Digital oscilloscope. The linear density was then calculated as a function of temperature. The resulting force was independently monitored with increasing temperature on a Houston Instruments X-Y recorder so a direct comparison between the fiber's denier and the F-T behavior could be assessed. Nitrogen was continuously flushed through the oven to prevent thermal oxidative degradation of the material.

#### 4.3 Reversible Thermal Elastic Behavior

According to equation (4.2), material possessing a positive thermal expansion coefficient will experience a stress drop with increasing temperature when maintained at constant length. To test the validity of this equation and the accuracy of the F-T apparatus, a steel yarn was first examined. A stress drop with increasing temperature is observed for the steel yarn (Figure 41) indicating a positive thermal expansion coefficient as expected. The F-T behavior is reversible on cooling and the thermal expansion coefficient calculated from the slope of the F-T curve is approximately  $7 \times 10^{-6} / ^\circ\text{C}$  based on a temperature independent modulus of 202 GPa. Since steel is known to have a thermal expansion coefficient of  $(9-11) \times 10^{-6} / ^\circ\text{C}$  (94), the calculated value for  $\alpha$  is in reasonable agreement considering the experimental errors inherent in the apparatus such as a  $30^\circ\text{C}$  temperature distribution within the oven, possible load cell compliance, neglect of any thermal expansion of the clamps as well as anisotropy in the highly drawn steel wire.

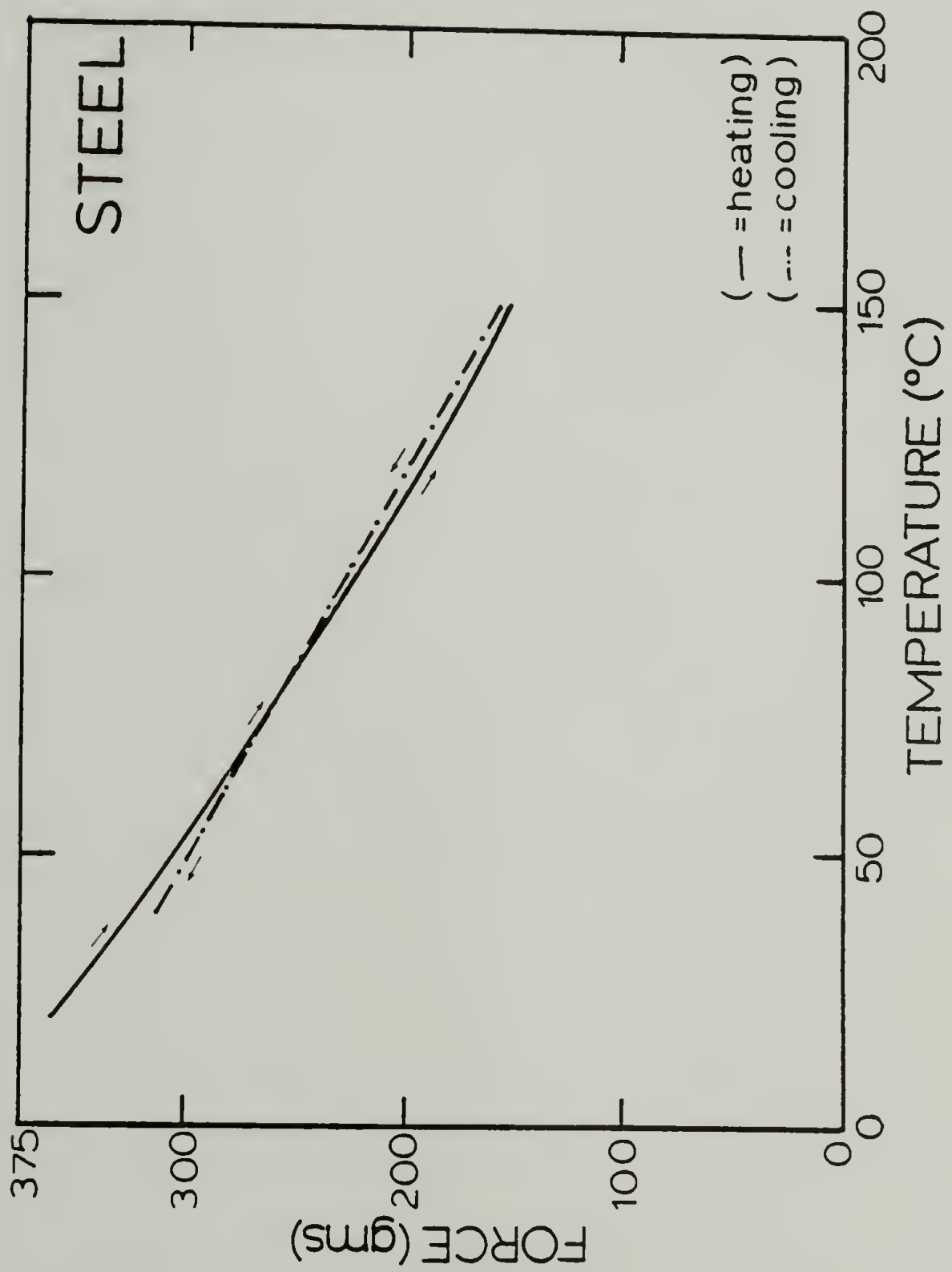


Figure 41. Force versus temperature profile for steel yarn

The F-T behavior of the heat treated PBT and Kevlar<sup>R</sup> 49 yarn is shown in Figure 42. The stress increases with increasing temperature indicating the existence of a negative thermal expansion coefficient for both materials. Although the modulus of PBT and Kevlar<sup>R</sup> is known to vary with temperature (23,25), the thermal expansion coefficient approximated using the room temperature modulus values of 215 GPa for PBT-HT and 125 GPa for Kevlar<sup>R</sup> 49. In these calculations, the yarn modulus is approximated by the single filament modulus. The calculated thermal expansion coefficient for PBT-HT and Kevlar<sup>R</sup> are approximately  $-1 \times 10^{-6}$  and  $-3 \times 10^{-6}/^{\circ}\text{C}$ , respectively. This value of  $\alpha$  for Kevlar<sup>R</sup> 49 is in close agreement with reported values of  $-(2-4) \times 10^{-6}/^{\circ}\text{C}$  (23).

From examination of the F-T behavior of Kevlar<sup>R</sup> 49 (Figure 42), the stress does not increase linearly with temperature between 50°C-100°C. The stress is observed to vary linearly over this same temperature range after the sample is cooled and subsequently reheated. In order to understand this initial behavior, a sample of Kevlar<sup>R</sup> 49 was heated to 200°C, cooled and then allowed to relax at room temperature at atmospheric conditions for 24 hours. Upon reheating, the initial non-linear behavior returns as shown in Figure 43. A similar sample which was heated to 200°C, cooled then placed in a desiccated environment for 24 hours, exhibited a linear increase in stress with temperature upon reheating (Figure 43).

Therefore, it appears that moisture absorption by Kevlar<sup>R</sup> 49 causes this initial irreversible non-linearity of the stress versus temperature curve. The removal of residual moisture is accomplished by the

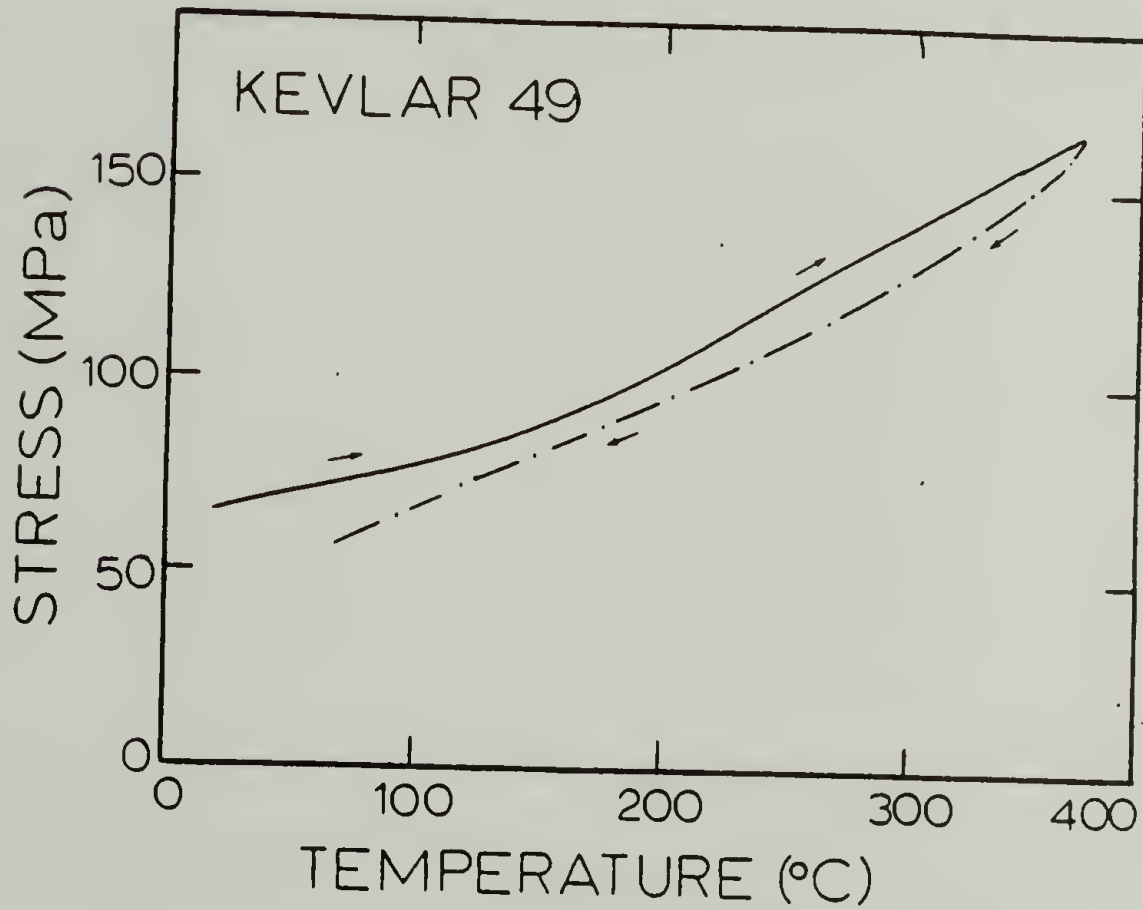
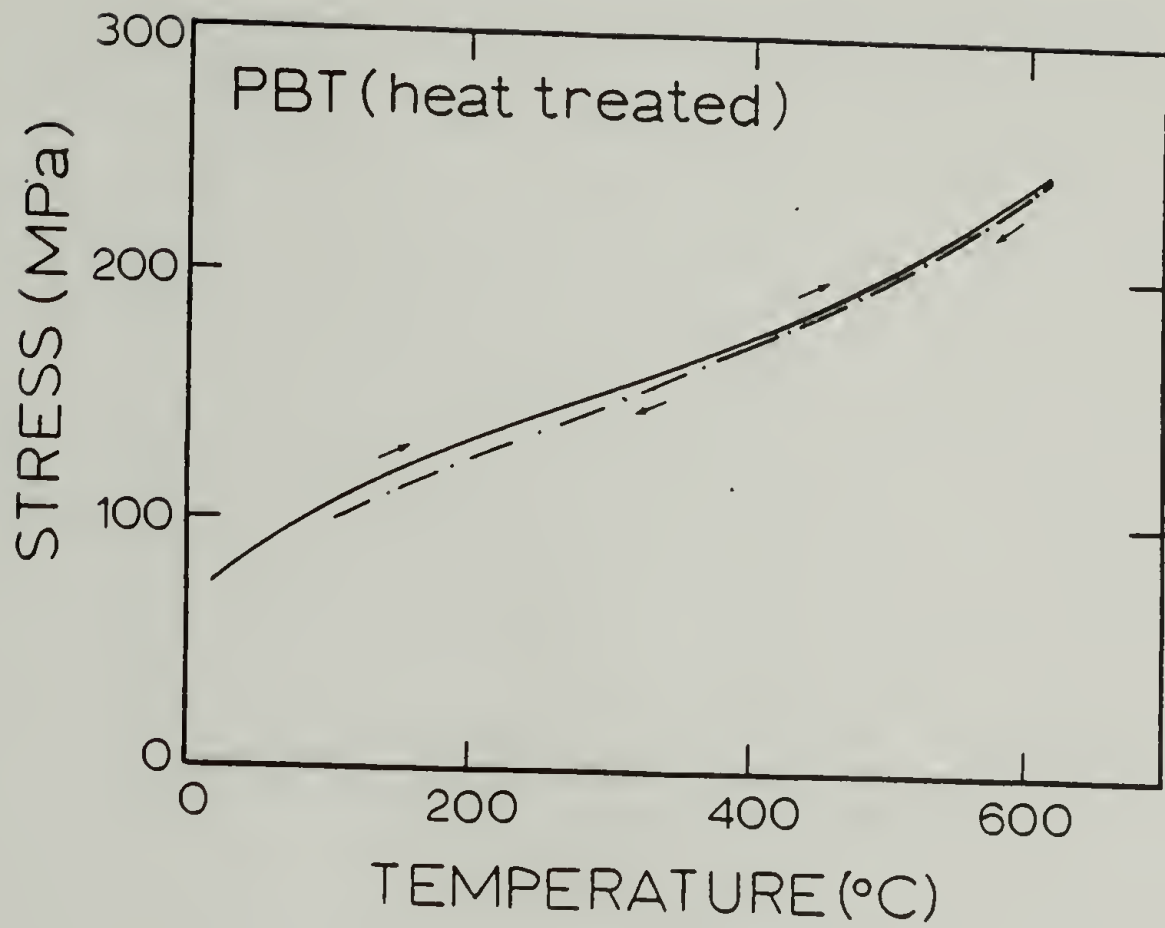


Figure 42. Stress-temperature profiles for tension heat treated PBT and Kevlar 49 yarns



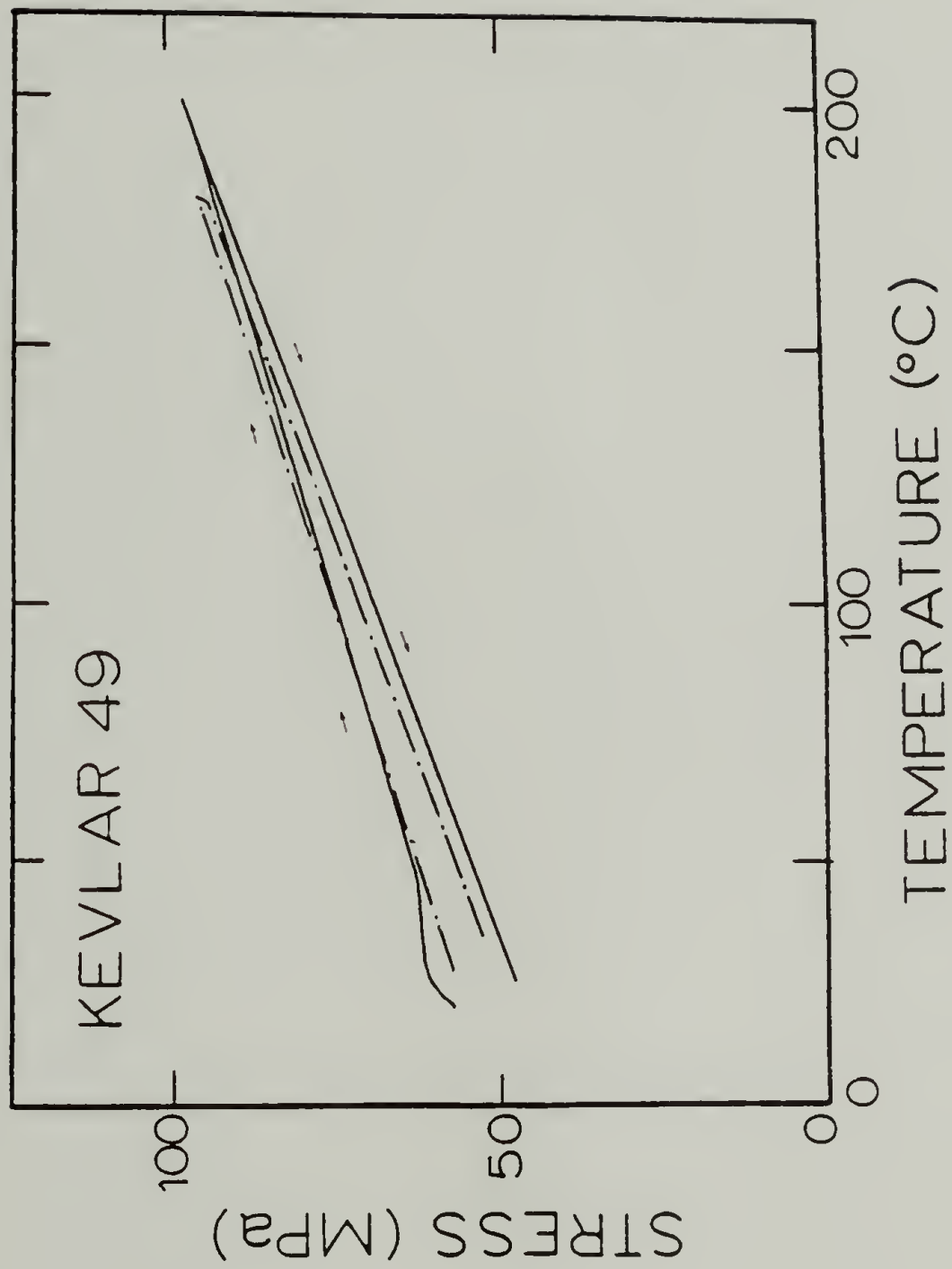


Figure 43. Stress-temperature profiles for Kevlar<sup>R</sup> 49 yarn 24 hours after the first heating cycle (— = undesiccated; - - - = desiccated)

application of heat as evidenced by the linearity of the cooling curve. After removing the residual moisture, the stress level at room temperature is lower than the stress level at room temperature before the application of heat. This result is consistent with the possibility that Kevlar<sup>R</sup> has a negative axial swelling coefficient whereby the material elongates when it dries.

Since the F-T profile for the PBT-HT is linear and completely reversible, PBT-HT yarn appears less moisture sensitive than Kevlar<sup>R</sup> 49.

The negative thermal expansivity of these rigid rod aromatic fibers is typical of other highly oriented polymers such as high chain extended polyethylene (PE), polyethylene terephthalate (PET) and polyacrylonitrile (PAN) (95-97). It is possible to interpret this negative thermal expansion phenomena several ways. For one, oriented materials do exhibit a positive volume expansion which results due to increased molecular vibration with increasing temperature. For highly oriented fibers, the molecular bending and torsional vibration of these rigid rod chains effectively produce a contraction along the chain axis while expanding in the radial and hoop directions as shown in Figure 44. Such thermally induced molecular motion results in a negative longitudinal thermal expansion behavior with a positive transverse thermal expansion coefficient. For example, the resulting thermal expansivity for Kevlar<sup>R</sup> 49 is positive in the radial direction ( $\alpha_{\perp} = 59 \times 10^{-6} / ^\circ\text{C}$  (23)) and negative along the fiber longitudinal axis.

The effects of orientation on thermal expansivity of various amorphous and crystalline polymers have been reported by Jaffe (95), Kimmel

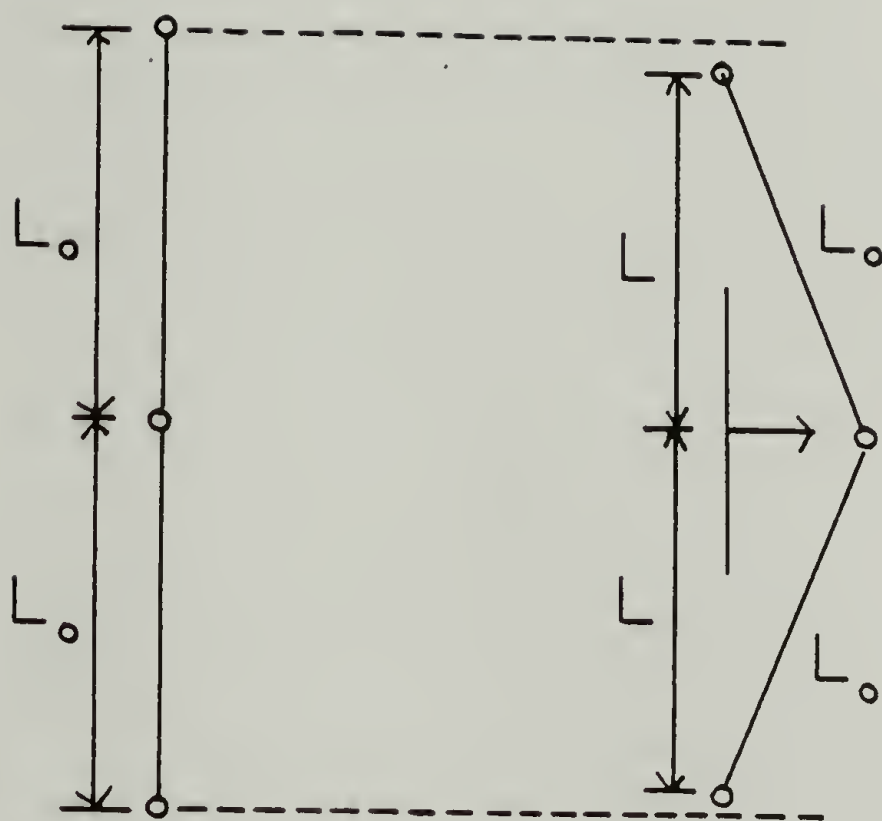


Figure 44. Lateral motion of an atom in an inextensible chain (reference 98)

(96) and Porter et al. (97). From their results, the axial thermal expansion coefficient decreases from a positive to a negative value with increasing spin draw ratio.

In the determination of the axial thermal expansion coefficient for Kevlar<sup>R</sup> and HT-PBT it is assumed that  $E$  and  $\alpha_z$  are temperature independent functions. In reality, the tensile moduli for both Kevlar<sup>R</sup> 49 and PBT have been reported to decrease with increasing temperature up to 200°C (23,25). Furthermore, the axial coefficient of thermal expansion for thermal expansion for Kevlar<sup>R</sup> 49 is observed to increase from  $-2 \times 10^{-6}/^{\circ}\text{C}$  between 0°-100°C to  $-4 \times 10^{-6}/^{\circ}\text{C}$  in the temperature range between 100°C and 200°C (23). Although both  $E$  and  $\alpha$  are temperature dependent quantities, their product is independent of temperature as evidenced by the constant F-T slope for both Kevlar<sup>R</sup> 49 and H-T PBT over the temperature range examined. A constant proportionality between  $E$  and  $\alpha$  appears to exist for these rigid rod aromatic fibers.

The inverse relationship between  $E$  and  $\alpha$  also exists in elastomeric materials such as natural rubber which exhibits a linearly reversibly F-T profile (99). This behavior has been used by Lyon (100) to predict the strain required to induce the thermoelastic inversion phenomena in such elastomers.

The origin of the temperature dependent behavior of the coefficient of thermal expansion for these rigid rod polymers may be interpreted in light of their anisotropic nature. Similar to the shrinkage behavior exhibited by these fibers upon drying, the observed change in strain

with temperature can be expressed as follows:

$$\frac{\partial \epsilon_z}{\partial T} = \alpha_{zz} + (\alpha_{rr} - \alpha_{\theta\theta})\chi \quad (4.4)$$

where

$$\alpha_{zz} = \left(\frac{\partial \epsilon_z}{\partial T}\right)_\sigma; \quad \alpha_{rr} = \left(\frac{\partial \epsilon_r}{\partial T}\right)_\sigma; \quad \alpha_{\theta} = \left(\frac{\partial \epsilon_{\theta}}{\partial T}\right)_\sigma$$

$$\chi = \frac{\Psi}{\gamma_{22}}(1-\lambda^2)(1-\Psi K)$$

$$\Psi = \frac{\lambda-1}{\lambda+1} (a_{13}-a_{23})$$

$$K = \frac{a_{13}-a_{23}}{a_{33}\gamma_{22}} (1-\lambda^2)$$

$$\lambda = \left(\frac{\gamma_{11}}{\gamma_{22}}\right)^{1/2}$$

$$\gamma_{22} = a_{22} - \frac{a_{23}^2}{a_{33}}$$

$$\gamma_{11} = a_{11} - \frac{a_{13}^2}{a_{33}}$$

For a transversely isotropic fiber, the compliance constants  $a_{13}$  and  $a_{23}$  are equal; in which case the second term in (4.4) vanishes. However, for an orthotropic fiber,  $\chi$ , which is highly sensitive to differences in the  $a_{13}$  and  $a_{23}$  compliance coefficients, becomes pronounced.  $\chi$  will vary with temperature since the compliance coefficients are likely to be temperature sensitive and a temperature dependent expression for  $d\epsilon_z/dT$  results.



It is instructive to examine the predicted axial change in length with temperature in a model graphite fiber although graphite possesses only two mutually perpendicular planes of symmetry with unique elastic constants whereas Kevlar<sup>R</sup> is truly cylindrically orthotropic. The compliance coefficients and thermal expansion coefficients for single crystal graphite (101,102) are utilized in the analysis of radial and onion skin morphology (Table 25). Substitution of the appropriate compliance and thermal expansion coefficients in (4.4), the apparent change in strain with temperature for both morphologies is calculated to be:

$$\frac{\partial \epsilon_z}{\partial T} = -.5 \times 10^{-6} + .12 \times 10^{-6} = -.38 \times 10^{-6} \quad (4.5)$$

This result suggests that the observed thermal expansion of the fiber is less negative than the single crystal's axial coefficient of expansion. In general axial thermal expansion coefficients for graphite fibers are reported in the range of  $-.5 \times 10^{-6}$  to  $+.5 \times 10^{-6}$  (102) which is consistent with the above theoretical predictions.

A temperature dependent coefficient of axial expansion has been observed by Bacon and Williams (103) for Thornel carbon fibers. They report a value which is negative below 400°C, zero at 400°C and positive above 400°C. The coefficient of thermal expansion becomes less negative with increasing temperature unlike the case for Kevlar<sup>R</sup> 49 fibers. From examination of equation (4.5), the generation of the  $\chi$  dependent term for graphite inherently reduces the actual  $\alpha_z$ . Therefore, if the second term in (4.4) becomes sufficiently large with increasing temperature for

Table 25. Compliance and thermal expansion coefficients for model single crystal graphite fibers (101,102)

$a_{ij}$ (GPa <sup>-1</sup> )	Radial Morphology	Onion-Skin Morphology
$a_{11}$	0.00098	0.0275
$a_{22}$	0.0275	0.00098
$a_{33}$	0.00098	0.00098
$a_{13}$	-0.00016	-0.00033
$a_{23}$	-0.00033	-0.00016
$\gamma_{11}$ (GPa <sup>-1</sup> )	0.000954	0.02739
$\gamma_{22}$ (GPa <sup>-1</sup> )	0.2739	0.000954
$\lambda$	0.187	5.36
$K$ (GPa)	6.56	6.56
$\psi$ (GPa <sup>-1</sup> )	-0.00012	0.00012
$\chi$	-0.0045	0.0045
$\alpha_i$ (°C <sup>-1</sup> )		
$\alpha_r$	$-.5 \times 10^{-6} / ^\circ\text{C}$	$27 \times 10^{-6} / ^\circ\text{C}$
$\alpha_\theta$	$27 \times 10^{-6} / ^\circ\text{C}$	$-.5 \times 10^{-6} / ^\circ\text{C}$
$\alpha_z$	$-.5 \times 10^{-6} / ^\circ\text{C}$	$-.5 \times 10^{-6} / ^\circ\text{C}$

these carbon fibers, the apparent axial thermal expansion coefficient may increase from a negative to a positive value.

The observed inverse relationship between  $E$  and  $\alpha$  for Kevlar<sup>R</sup> 49 may also be rationalized in terms of the predictions made in (4.4).  $\chi$  may be written more explicitly as follows:

$$\chi = \frac{(a_{23}-a_{13})a_{33}}{(\lambda+1)^2(a_{33}\gamma_{22}-(\lambda-1)^2)} \quad (4.6)$$

Since  $a_{33} = \frac{1}{E_z}$ ,  $\chi$  is inversely proportional to the axial modulus.

Therefore, a decrease in tensile modulus or increase in  $a_{33}$ , increases the magnitude of  $\chi$ . An increase in the observed coefficient of thermal expansion is then predicted to occur from (4.4).

#### 4.4 Irreversible Thermal Elastic Behavior

The F-T behavior of the as-spun PBT and Kevlar<sup>R</sup>29 yarns are most interesting. For both materials, there is a dramatic stress drop with increasing temperature once the fiber has reached a critical temperature denoted as  $T_T$  (Figures 45 and 46). The behavior of these fibers appears to be dependent on their thermal history whereby the material upon cooling and subsequent reheating displays a linear reversible F-T behavior up to the maximum temperature to which it has been previously exposed. The material once again exhibits a drop in stress when exceeding the maximum temperature.

It is suggested that the observed stress drop with increasing temperature is associated with two different but not mutually exclusive

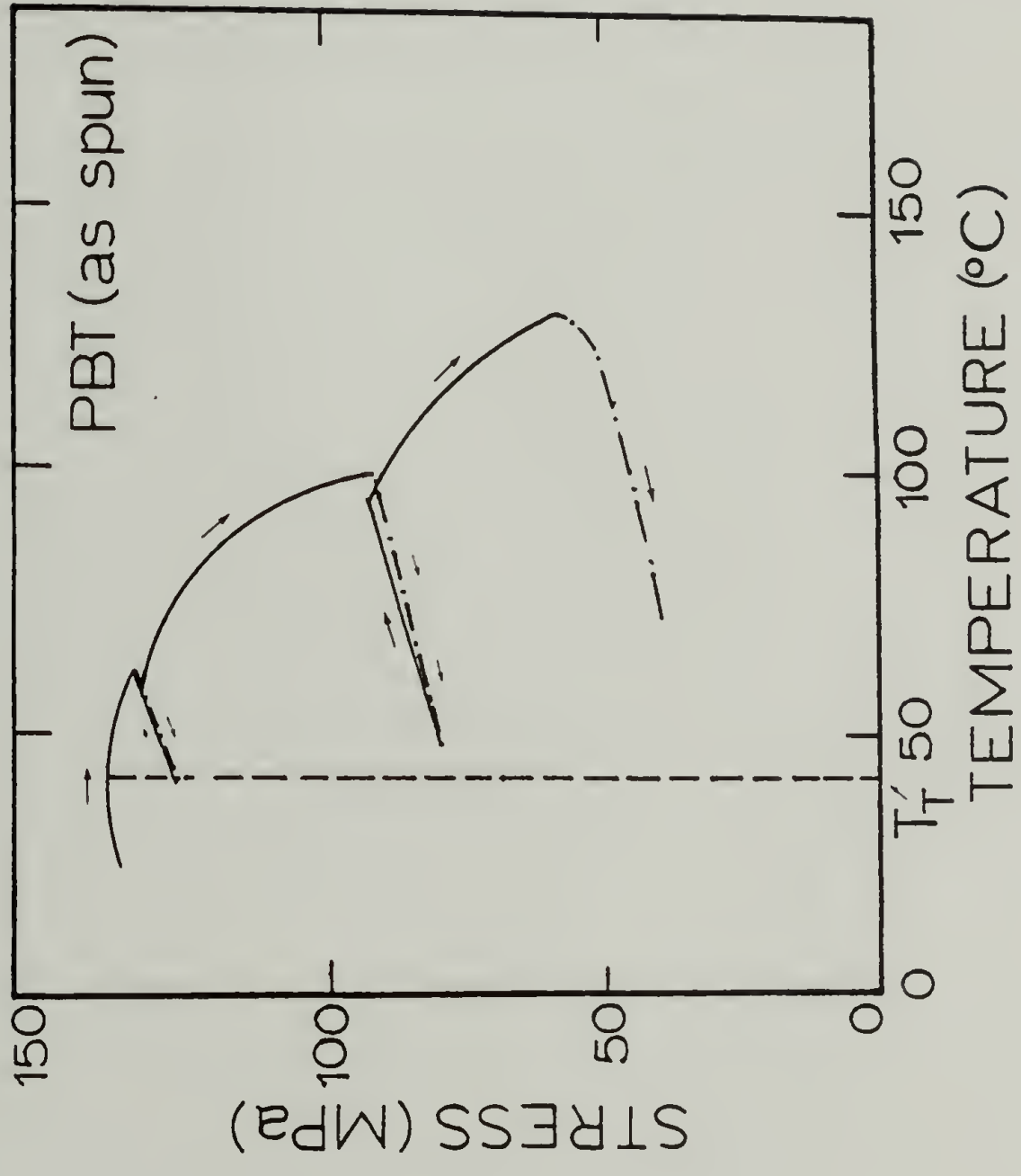


Figure 45. Stress-temperature profile for as-spun PBT yarn ( — = heating; -.- = cooling)

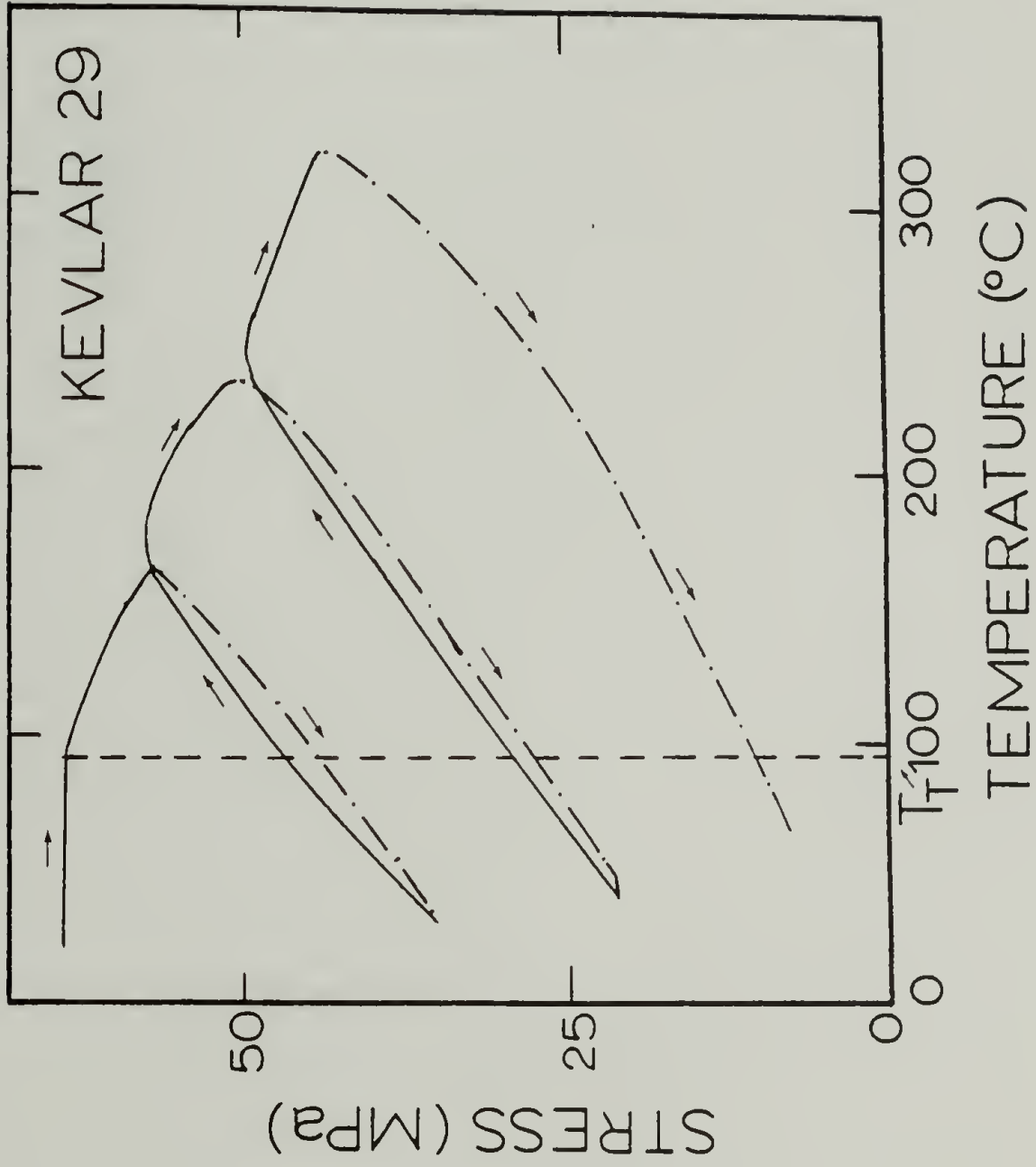


Figure 46. Stress-temperature profile for Kevlar<sup>R</sup> 29 yarn  
( — = heating; - · - = cooling)



mechanisms. The observed stress drop may be a manifestation of the material changes associated with post processing heat treatment. If this correlation holds true, then a fiber would be expected to exhibit enhanced mechanical properties and increased molecular order if it has undergone a force-temperature history where  $T_T$  is observed.

A comparison of the wide angle x-ray diffraction patterns of Kevlar<sup>R</sup> 29 and Kevlar<sup>R</sup> 29 force-temperature cycled (FTC) shows a sharpening of the equatorial reflections in the FTC-Kevlar<sup>R</sup> 29 (Figure 47). The FTC sample was subjected to a load of 675 MPa, heated to 300°C and cooled to room temperature. The WAXD results are indicative of an improvement in the extent and perfection of the lateral molecular order. In addition, there is a sharpening of the meridional reflections. The appearance of sharp meridional and distinct  $hkl$  reflections are quite similar to those observed for Kevlar<sup>R</sup> 49.

The WAXD diffraction line profile analysis of the equatorial reflections of as-spun PBT yarn before and after the force-temperature cycling reveal some observable differences. From the results in Table 26, the FTC-PBT exhibits a narrowing of the equatorial reflections and a shift in the peak position to lower scattering angles. As discussed earlier, such a narrowing of the peaks and the shifting of the peak positions indicate the existence of a higher degree of perfection of the lateral molecular order.

The tensile properties of Kevlar<sup>R</sup> 29, FTC-Kevlar<sup>R</sup> 29, as-spun PBT and FTC-PBT are shown in Table 27. There is an enhancement in the measured moduli with a reduction in elongation for the FTC-Kevlar<sup>R</sup> 29 and

Figure 47

Wide angle x-ray diffraction patterns of

- (A) Kevlar<sup>R</sup> 29
- (B) FTC Kevlar<sup>R</sup> 29
- (C) Kevlar<sup>R</sup> 49

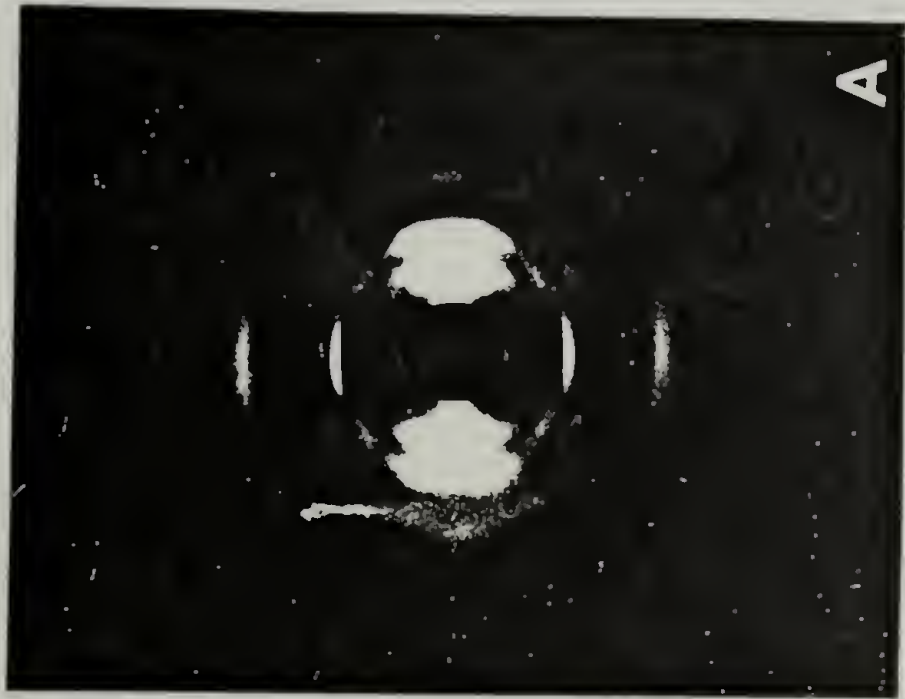
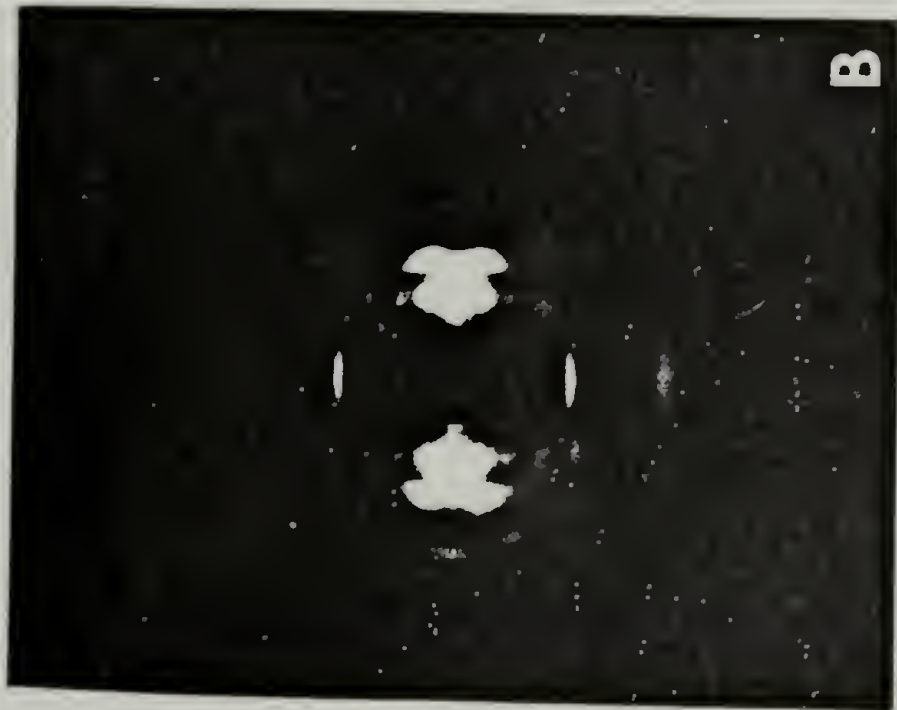
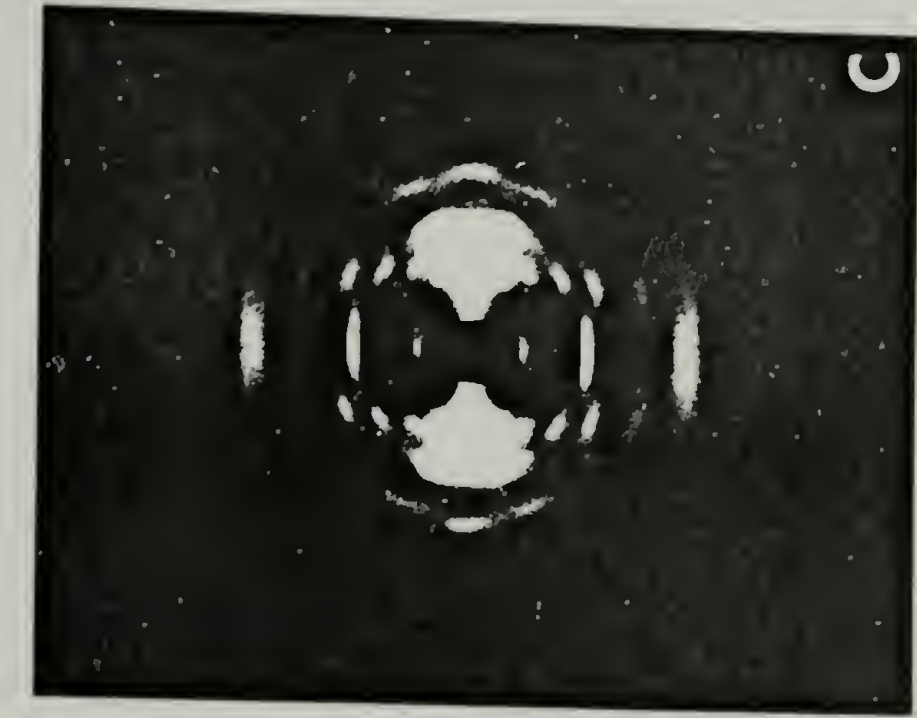


Table 26. WAXS diffractometric data of as-spun PBT yarn

Sample	As-spun PBT		Cycled PBT	
	$e_1$	$e_2$	$e_1$	$e_2$
Peak Number				
Position	16.3°	25.9°	15.4°	25.6°
d-spacing (nm)	.544	.344	.575	.348
Peak Width	5.0°	4.5°	3.2°	3.8°
Gaussian Coherent Scattering Crystallite Size (nm)	1.8	1.9	2.7	2.3

Table 27. Mechanical properties of PBT and Kevlar<sup>R</sup> 29 before and after force temperature cycling

Sample	As-spun PBT	F-T Cycled PBT	Kevlar <sup>R</sup> 29	F-T Cycled Kevlar <sup>R</sup> 29
Modulus (GPa)	95 ± 15	190 ± 10	75 ± 10	145 ± 25
Strength (GPa)	1.05 ± 0.1	1.3 ± 0.2	3.3 ± 0.6	2.9 ± 0.4
Elongation (%)	2.1 ± 0.2	0.7 ± 0.1	3.9 ± 0.4	2.5 ± 0.8



FTC-PBT material. For PBT, the strength also increases when cycled whereas for Kevlar<sup>R</sup> 29, the strength is the same within experimental error. This data agrees with known changes in mechanical properties due to the heat treatment of PBT and Kevlar<sup>R</sup> (25,104).

Both Kevlar<sup>R</sup> and as-spun PBT exhibit enhanced mechanical properties and increased molecular order after they have undergone a force-temperature history in excess of  $T_T$ . Thus, the dramatic stress drop observed in the force temperature behavior of these materials depicts the onset of material changes or of effective heat treatment.

The observed stress drop may also be a manifestation of a continued drying process with the application of heat during the F-T experiment. Since these rodlike polymers display a negative swelling behavior, the fiber elongates resulting in a subsequent drop in stress if drying is occurring. It is of interest to determine if the stress drop in the F-T curve coincides with alterations in the fiber's linear density or denier and a weight loss.

A comparison between the F-T curve, TGA thermogram and denier-temperature curve is depicted in Figure 48. The majority of the weight loss by TGA measurements corresponds to the temperature range over which the greatest stress drop in the F-T profile exists. The most dramatic decrease in linear density for a fiber undergoing the F-T cycling is observed in the same temperature range. A comparison of the F-T, denier-temperature, and TGA thermograms of heat treated PBT Fiber V (500°C, 60 sec) is shown in Figure 49. The absence of any weight loss or denier changes over the course of the F-T experiment contributes to the fiber's

Figure 48

A comparison between

- (A) Force-Temperature Profile
- (B) Denier-Temperature Profile
- (C) Thermal Gravimetric Profile

for as-spun PBT fiber.

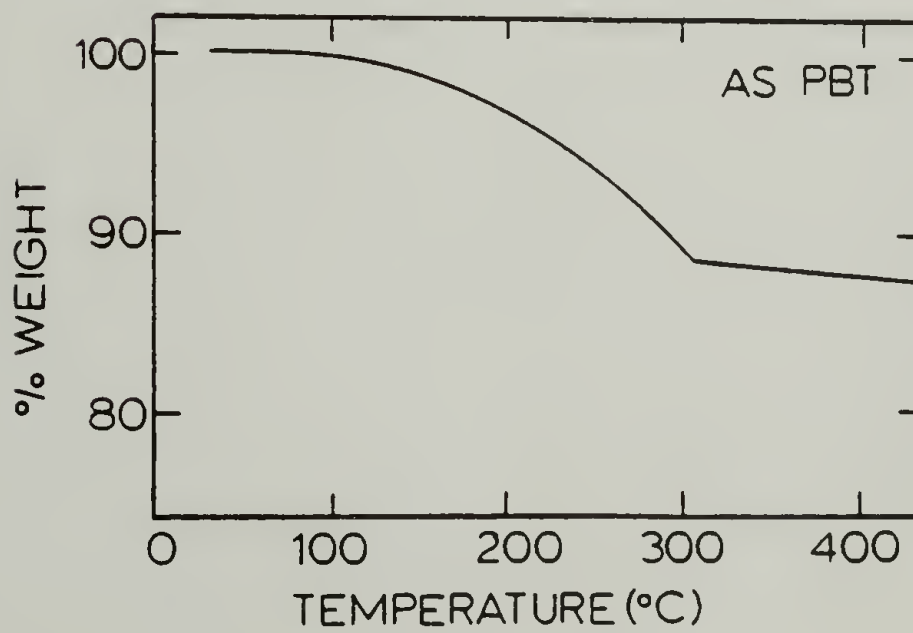
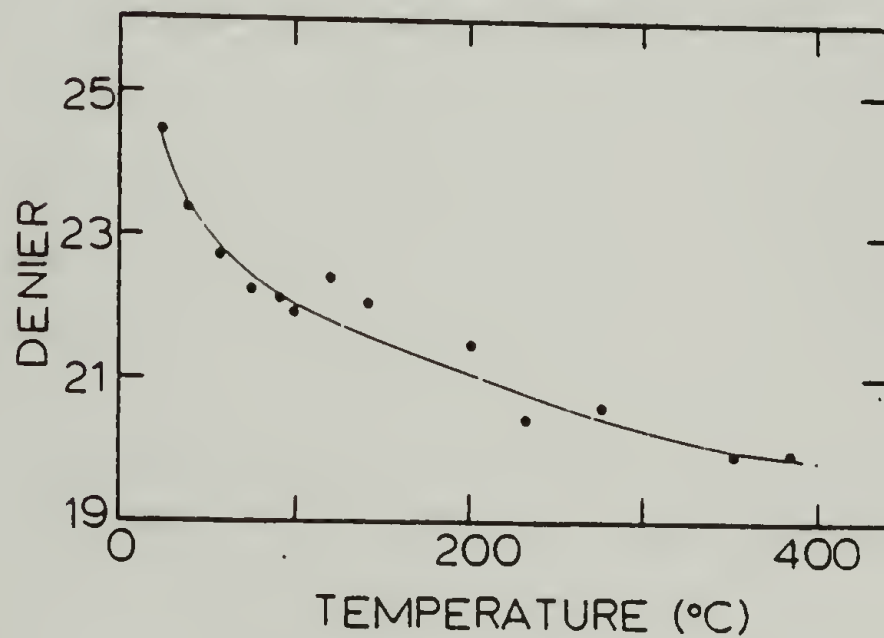
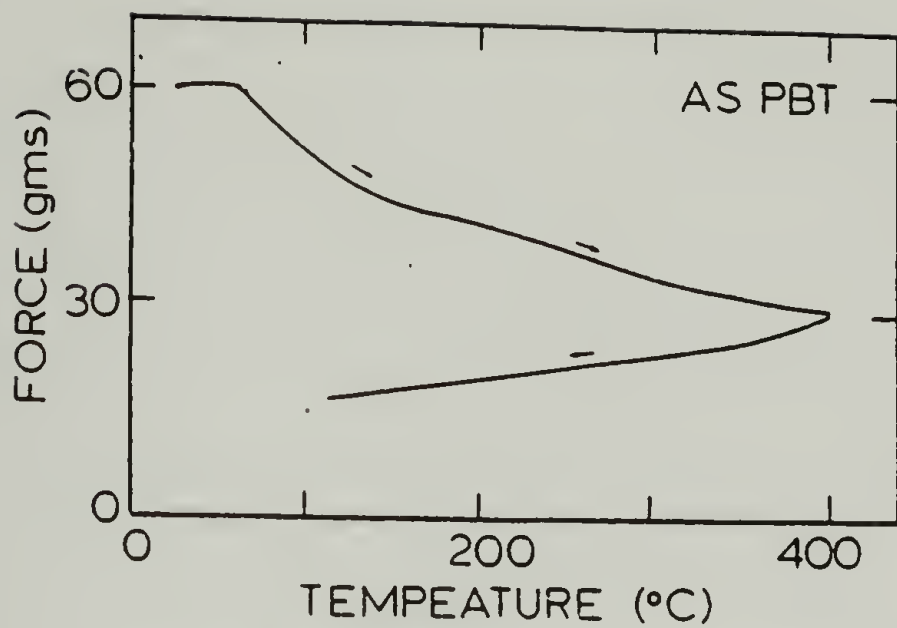
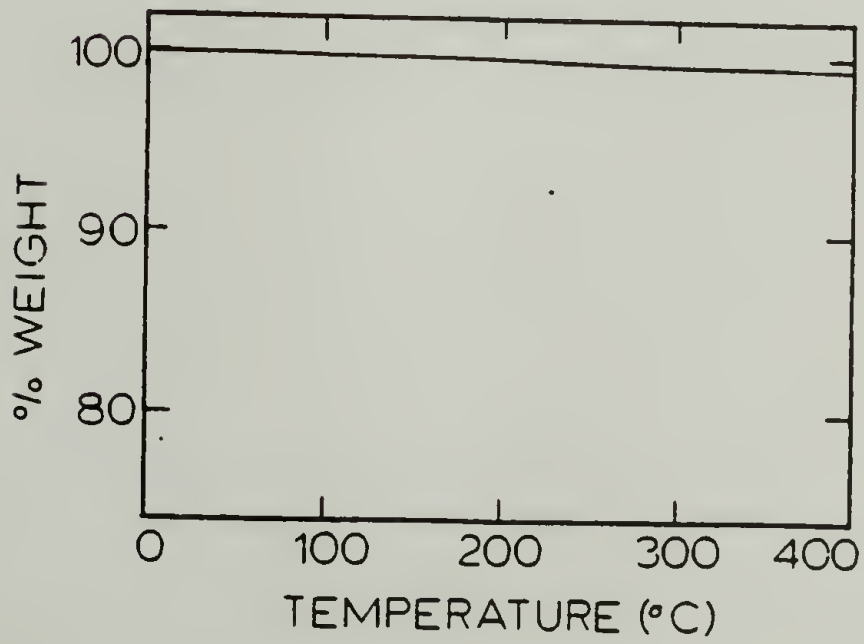
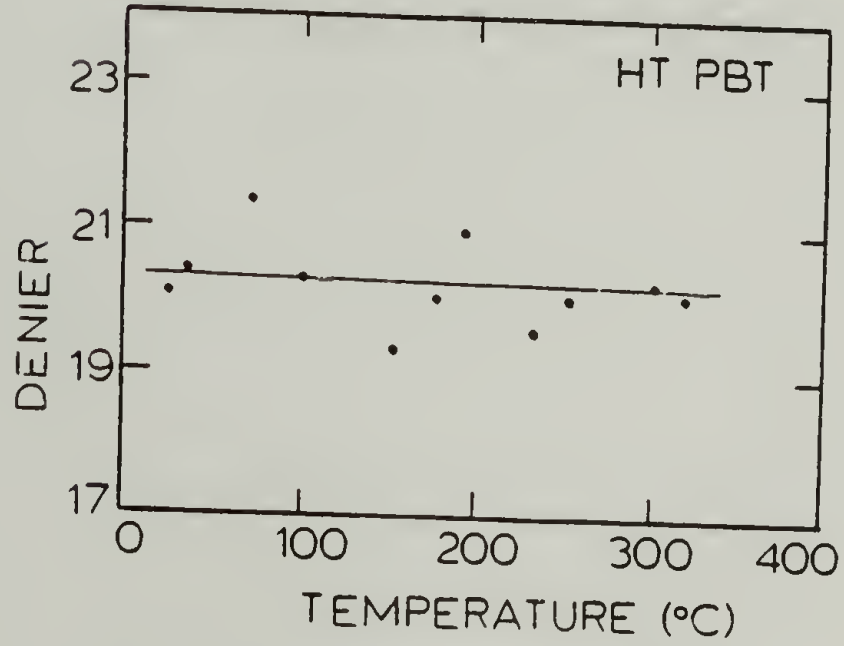
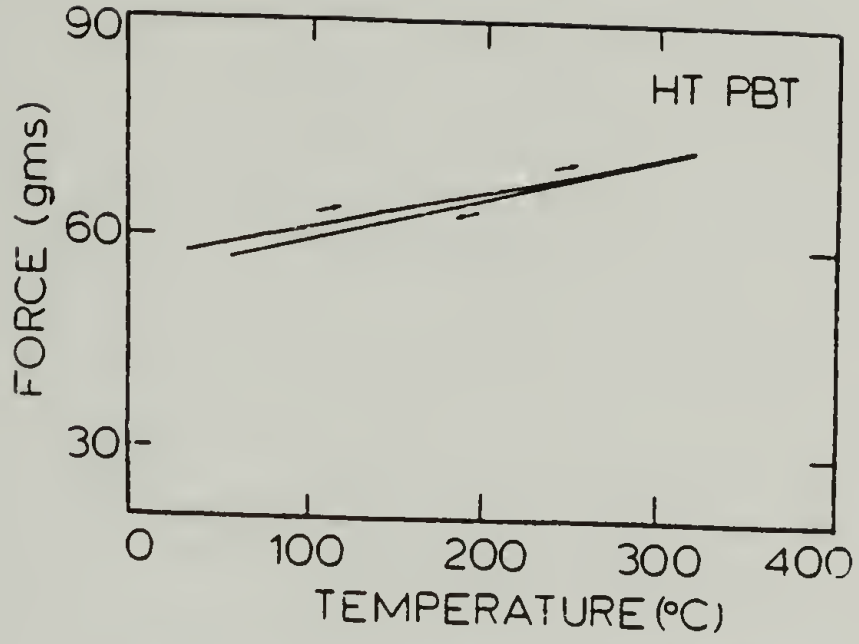


Figure 49

A comparison between

- (A) Force-Temperature Profile
- (B) Denier-Temperature Profile
- (C) Thermal Gravimetric Profile

for heat treated PBT fiber.





thermal stability. The fiber denier determined by this technique corresponds to the denier determined by a weight method.

These results suggest that the observed stress softening behavior is a result of the removal of water and/or solvents as exhibited by the weight and denier changes during the F-T experiment. It is speculated that the mass changes and alterations in the fiber's microstructure and mechanics are related.

The F-T experiments on these rigid rod systems depicted two different processes, thermal expansion effects and material changes with temperature (time). Equation (4.2) does not describe the change in axial stress from strains caused by isothermal swelling or drying. Therefore, the uniaxial stress,  $\sigma_z$ , may be more adequately described by (4.7)

$$d\sigma_z = E_z(d\varepsilon_z - \alpha dT - \beta dC) \quad (4.7)$$

where  $\sigma_z$  = uniaxial stress

$E_z$  = tensile modulus

$\varepsilon_z$  = uniaxial strain

$\alpha_z = \left(\frac{\partial \varepsilon_z}{\partial T}\right)_\sigma$  = axial thermal expansion coefficient

$\beta = \left(\frac{\partial \varepsilon_z}{\partial C}\right)_\sigma$  = axial shrinkage coefficient

For simplicity, it is assumed that hoop and radial components do not contribute to the axial stress. Equation (4.7) is differentiated to generate an expression for the change in axial stress with respect to temperature at constant strain.

$$\left(\frac{d\sigma}{dT}\right)_\epsilon = -E\alpha - E\beta \frac{dC}{dT} \quad (4.8)$$

Thus, the irreversible force temperature behavior of the as-spun PBT and Kevlar<sup>R</sup> 29 fibers is described by two different components: (1) thermal expansion effects ( $-E\alpha$ ), and (2) material changes associated with mass loss ( $-E\beta\left(\frac{dC}{dT}\right)_\epsilon$ ). The thermal expansion effects are most evident prior to  $T_T$ , the onset of material changes. After  $T_T$ , the stress drop is described by  $-E\beta\left(\frac{dC}{dT}\right)_\epsilon$ .

The temperature of the onset of heat treatment,  $T_T$ , is dependent upon the applied stress as shown in Figure 50 for both the as-spun PBT and Kevlar<sup>R</sup> 29. With increased applied stress,  $T_T$  decreases. By increasing the mechanical input (applied stress), less thermal input (oven temperature) is required to reach the required energy to induce material changes. The experimental data indicates that there is a linear correspondence between these two heat treatment parameters: stress and temperature. In addition, the slope of  $T_T$  vs. applied stress for Kevlar<sup>R</sup> 29 is greater than that of as-spun PBT. Thus, the onset of material changes for Kevlar<sup>R</sup> 29 is much more sensitive to the application of tension than as-spun PBT, while the onset of material changes in as-spun PBT is more sensitive to temperature.

#### 4.5 Force-Temperature Processing Correlations

The irreversible F-T behavior of the as-spun fibers allows for the detection of the temperature range for which the fibers are linearly thermoelastic. The magnitude of further material changes which are

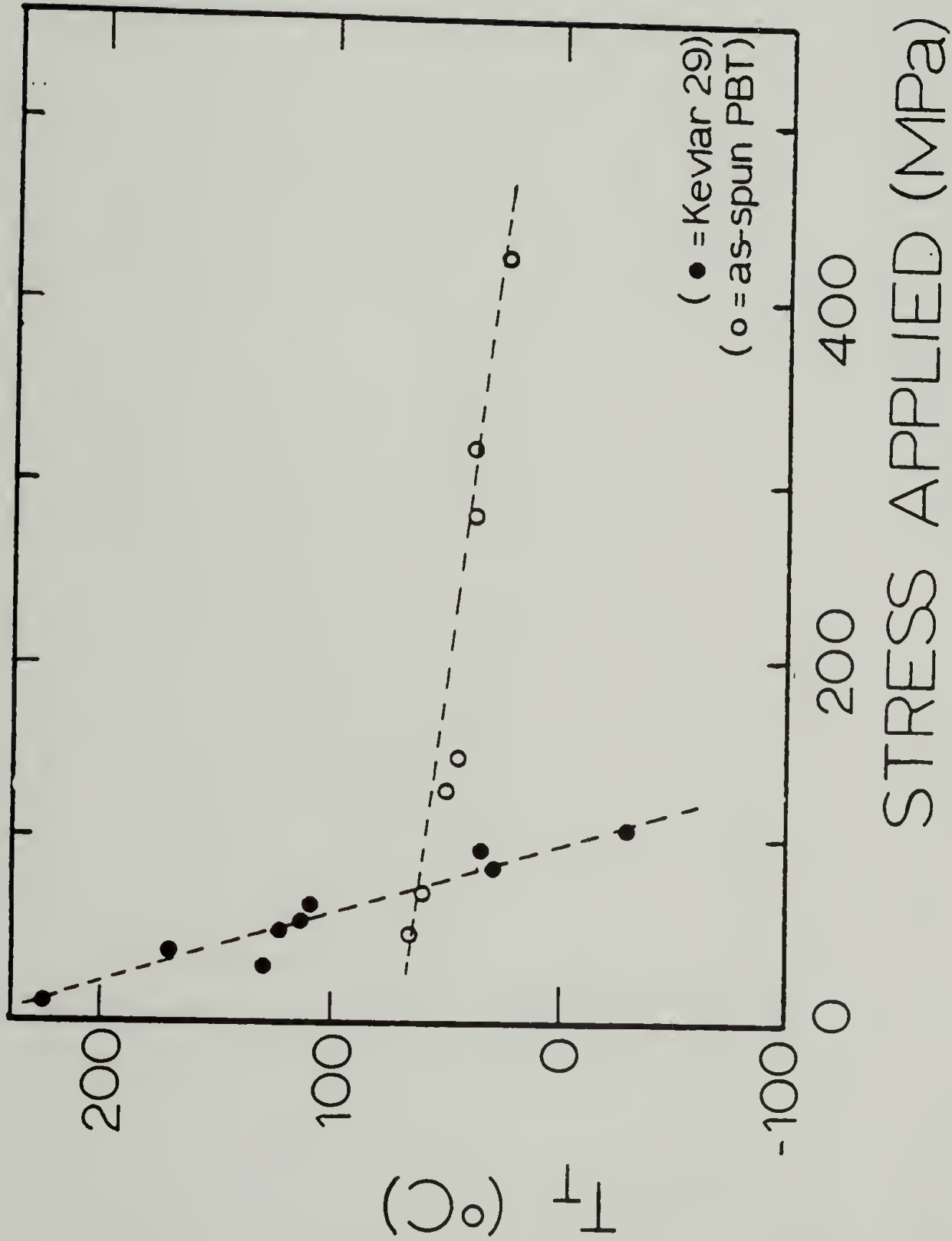


Figure 50. Temperature of onset of stress drop,  $T_T$ , versus applied stress during the F-T experiment

induced by the F-T technique is reflected in the magnitude of the stress drop. The F-T profile of variously dried and heat treated fibers have, therefore, been assessed. From these investigations, some insight can be gained into the effectiveness of tension and temperature in causing material changes and thermal stability during the initial processing of these fibers.

Typical stress-temperature profiles for PBT fibers dried at room temperature are depicted in Figure 51. The application of tension during drying does not introduce significant thermoelastic stability within the PBT fiber. However, the magnitude of the stress drop decreases slightly with increasing levels of applied tension during drying. Assuming that the stress drop is associated with water removal and subsequent material alterations, this data suggests that with the application of tension during drying the fiber may become more efficiently dried and result in modifications in the fiber properties.

A comparison between the F-T behavior of variously elevated temperature dried fibers with minimal tension is shown in Figure 52. The dramatic stress drop present in the as-spun fiber is eliminated provided the maximum temperature under which the fiber was dried is not exceeded. Beyond this temperature, the fiber exhibits a sharp stress drop. However, prior to  $T_T$ , the F-T behavior is still not completely reversible. Alterations in the fiber properties which are associated with a stress drop occur to a very slight degree at temperatures for which the fiber has already been exposed. This behavior is not surprising since the fiber is experiencing a stress level which it had not previously been

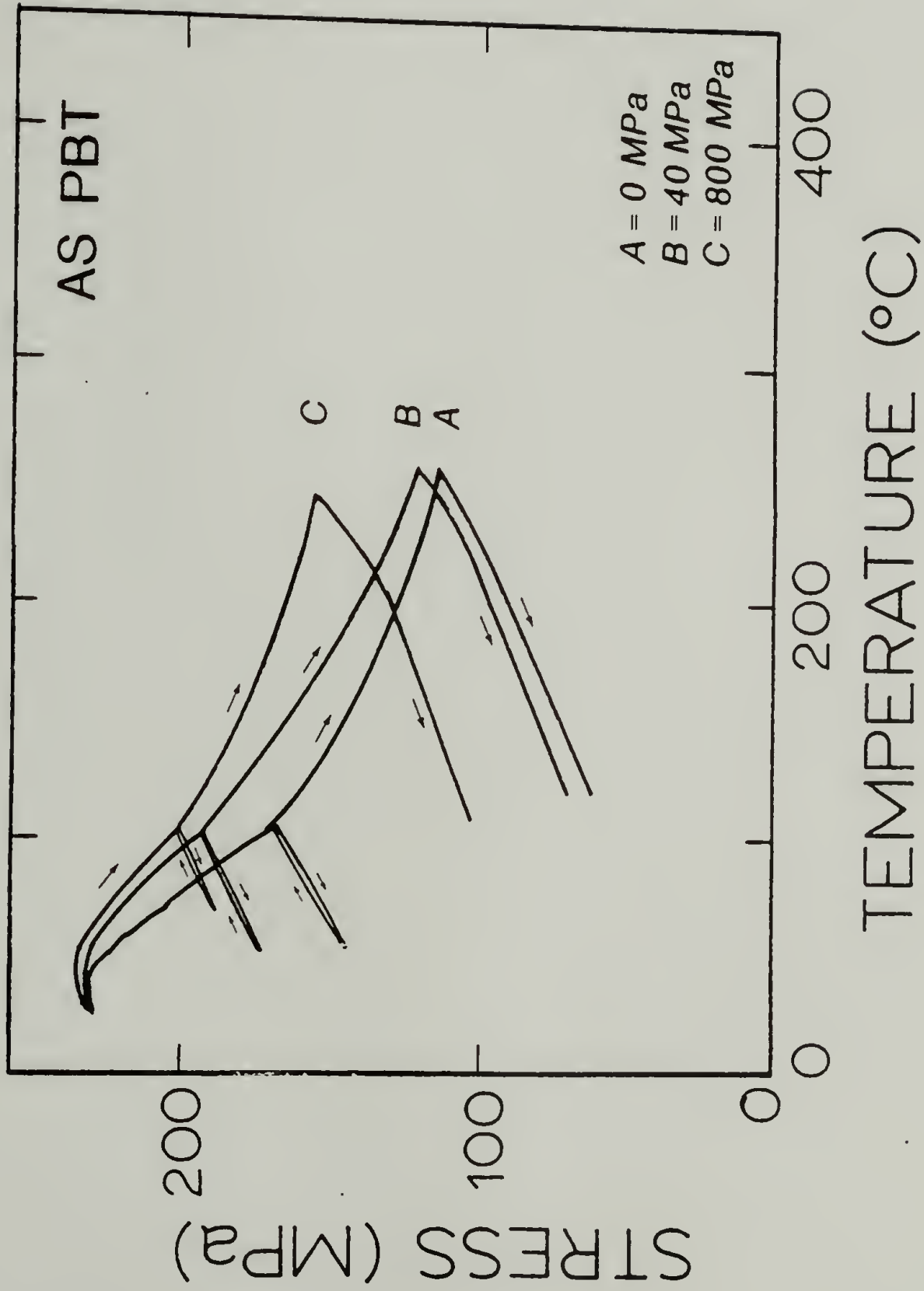


Figure 51. Typical stress-temperature profiles for PBT fiber dried at room temperature (A) no tension, (B) 40 MPa tension, (C) 800 MPa tension



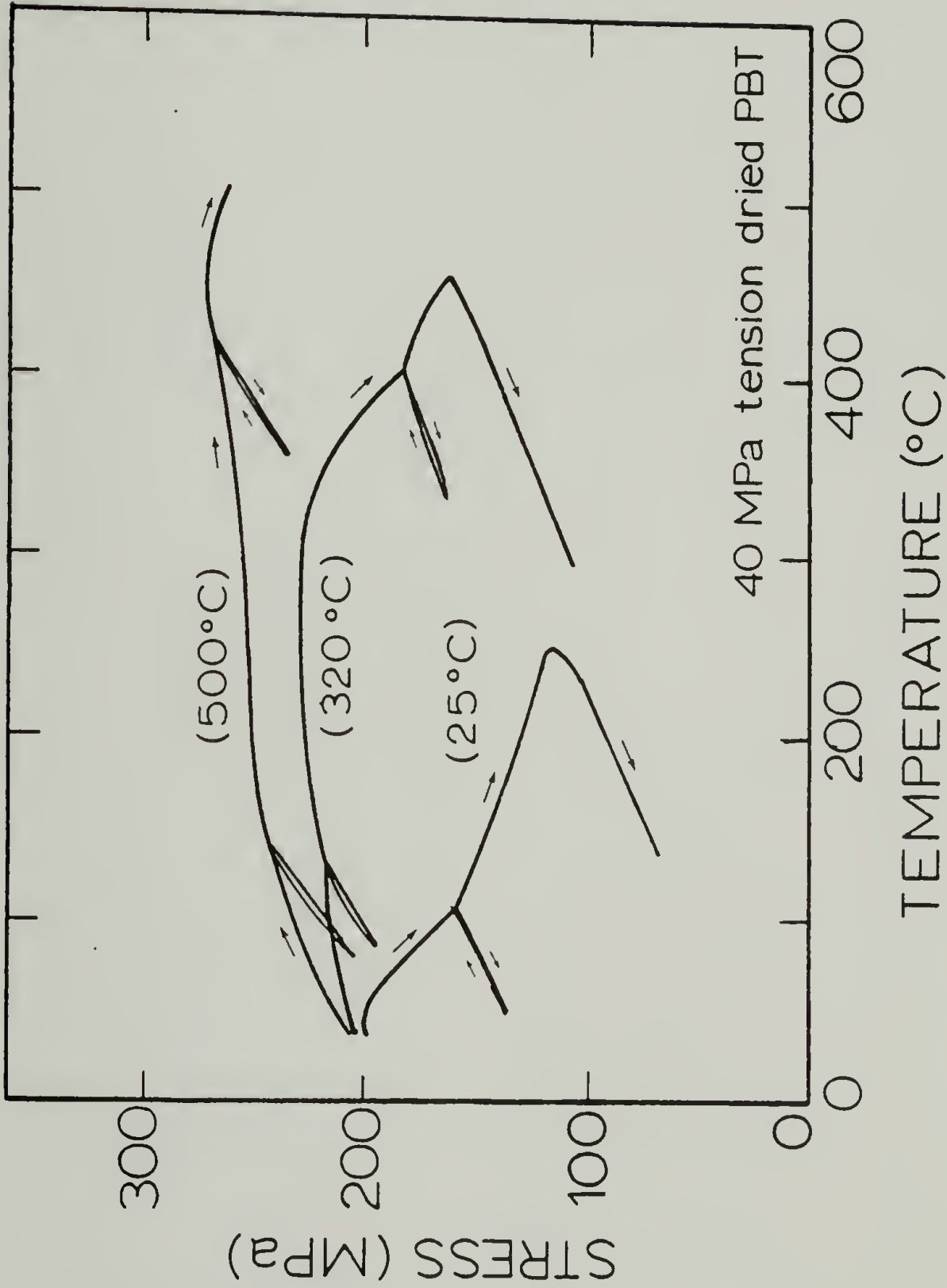


Figure 52. Typical stress- temperature profiles for PBT fibers dried under minimal load at various temperatures

exposed to in the F-T experiment. The application of tension during the F-T experiment appears to contribute to the irreversible behavior in the initial portion of the F-T profile.

The magnitude of the stress drop prior to  $T_T$  is observed to decrease with increasing temperature. A reduction in the magnitude of the stress drop suggests that with increasing temperature during the initial drying, the fibers may be more efficiently dried with increasingly altered fiber properties. These inductions are consistent with the structure and mechanical property enhancements observed with increasing temperature during the drying process (Chapter III).

Similar results have been obtained through F-T investigations on the non-tension dried PBT fibers which have been subsequently heat treated. A comparison between the stress-temperature profiles of PBT fibers non-tension and tension heat treated at 320°C and 500°C and the as-spun fiber is shown in Figures 53 and 54. Similar to the F-T studies on the high temperature dried fibers, the non-tension heat treated fibers show increasing levels of thermal stability with increased processing temperature. Again, the initial portion of heat treated fiber's F-T curve is not reversible due to the 225 MPa tension imposed during the experiment to which the fiber has never previously been exposed. Conversely, the tension heat treated fibers display a linear thermoelastic behavior up to the maximum temperature in which they had been heat treated. The tension heat treated fibers have previously been exposed to this stress level, and under the conditions imposed in this experiment, the F-T profile becomes reversible. These findings suggest that

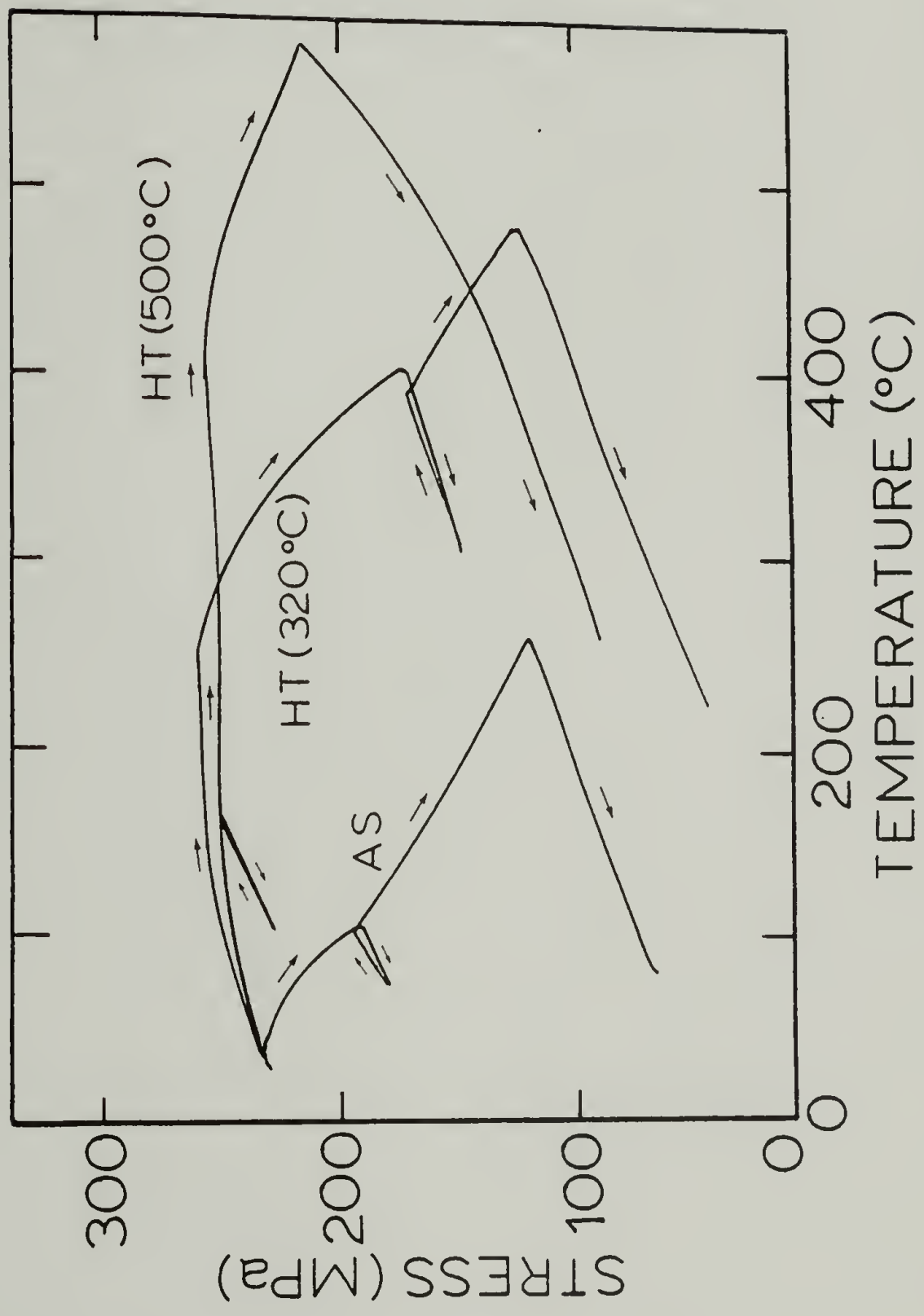


Figure 53. Typical stress-temperature profiles for PBT fibers initially non-tension dried then heat treated at 320 C and 500 C

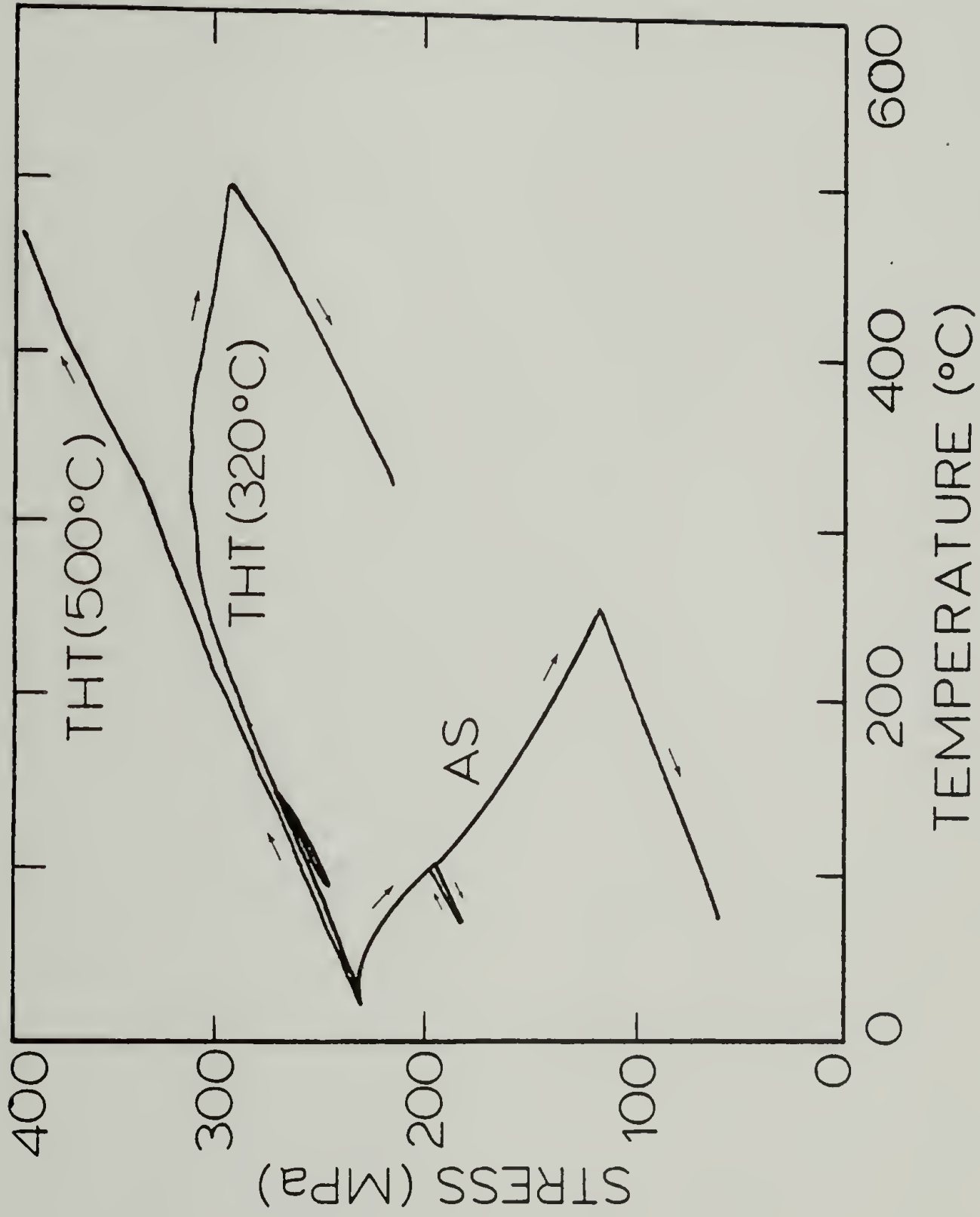


Figure 54. Typical stress-temperature profiles for PBT fibers initially non-tension dried then tension (80MPa) heat treated at 320 C and 500 C

these PBT fibers are only thermally stable in the temperature and tension ranges to which they have been exposed during the initial processing.

It is evident that both temperature and tension are necessary in the attainment of thermoelastic stability in PBT fibers. Although the application of tension during the initial processing does serve to reduce the stress drop, temperature provides a greater source of internal energy to introduce thermal stability.

The question still remains as to what advantages are there in heat treating the wet fiber (elevated temperature drying) as opposed to heat treating a dry fiber (post processing heat treatment). Observations in Chapter III indicate that elevated temperature drying provides little observable advantage in improving the macroscopic structural and mechanical properties. Since thermomechanical stability is of prime importance in many applications, a comparison between the F-T curves of fibers dried and heat treated at 320°C and 500°C has been made.

It is evident that from the F-T profiles for fibers dried at 320°C (Figure 55) and 500°C (Figure 56) with minimal tension, the magnitude of the stress drop in the F-T profile for the elevated temperature dried fiber is less than their heat treated counterparts. High temperature drying appears to be more effective in inducing thermal stability than post processing heat treatment.

The thermal expansion coefficients for the variously processed fibers are calculated from the slope of the reversible portion of the F-T profile having independently determined the tensile moduli. From a



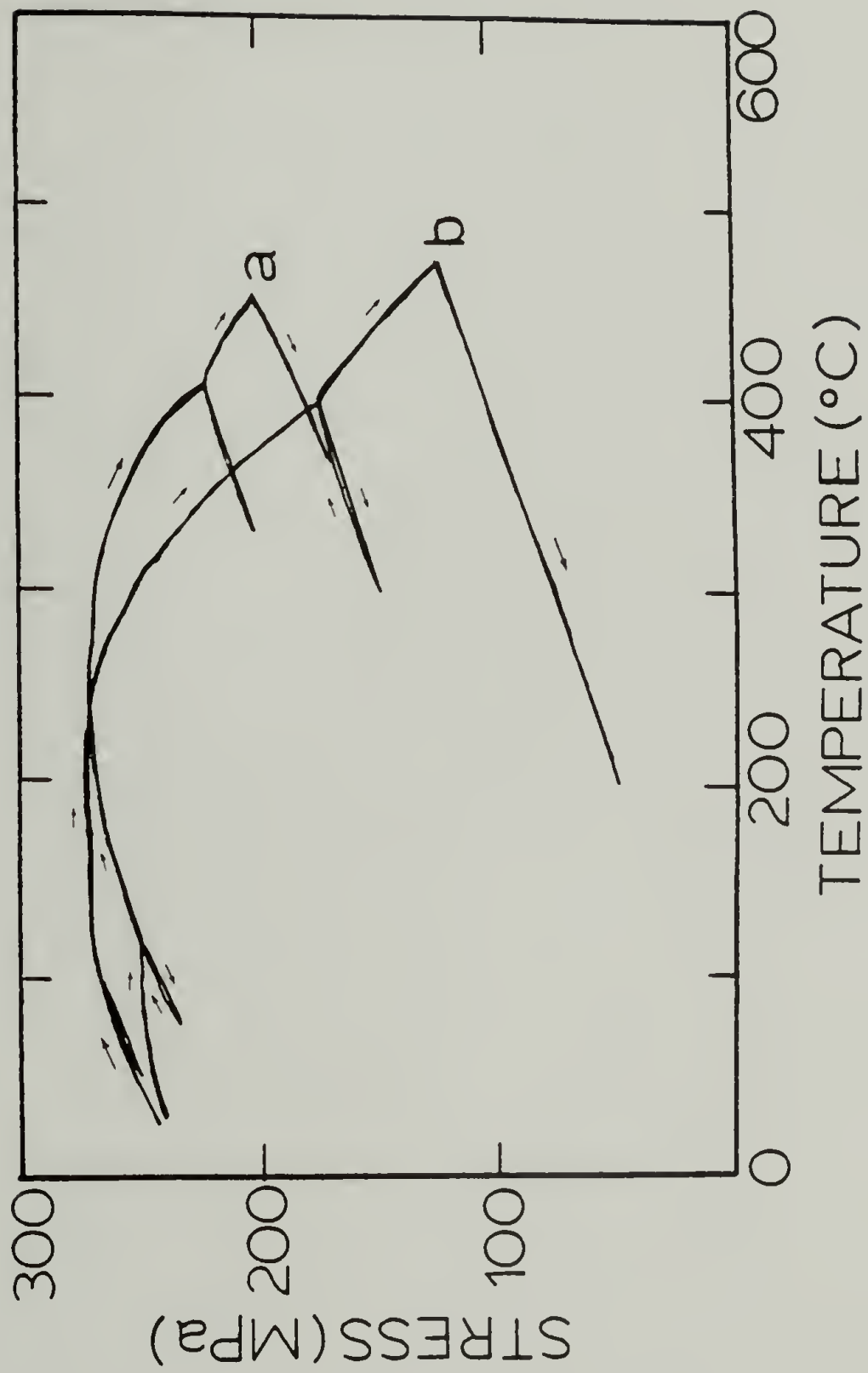


Figure 55. Typical stress-temperature profiles for PBT fiber: (a) non-tension dried 320 C, (b) heat treated 320 C with no tension

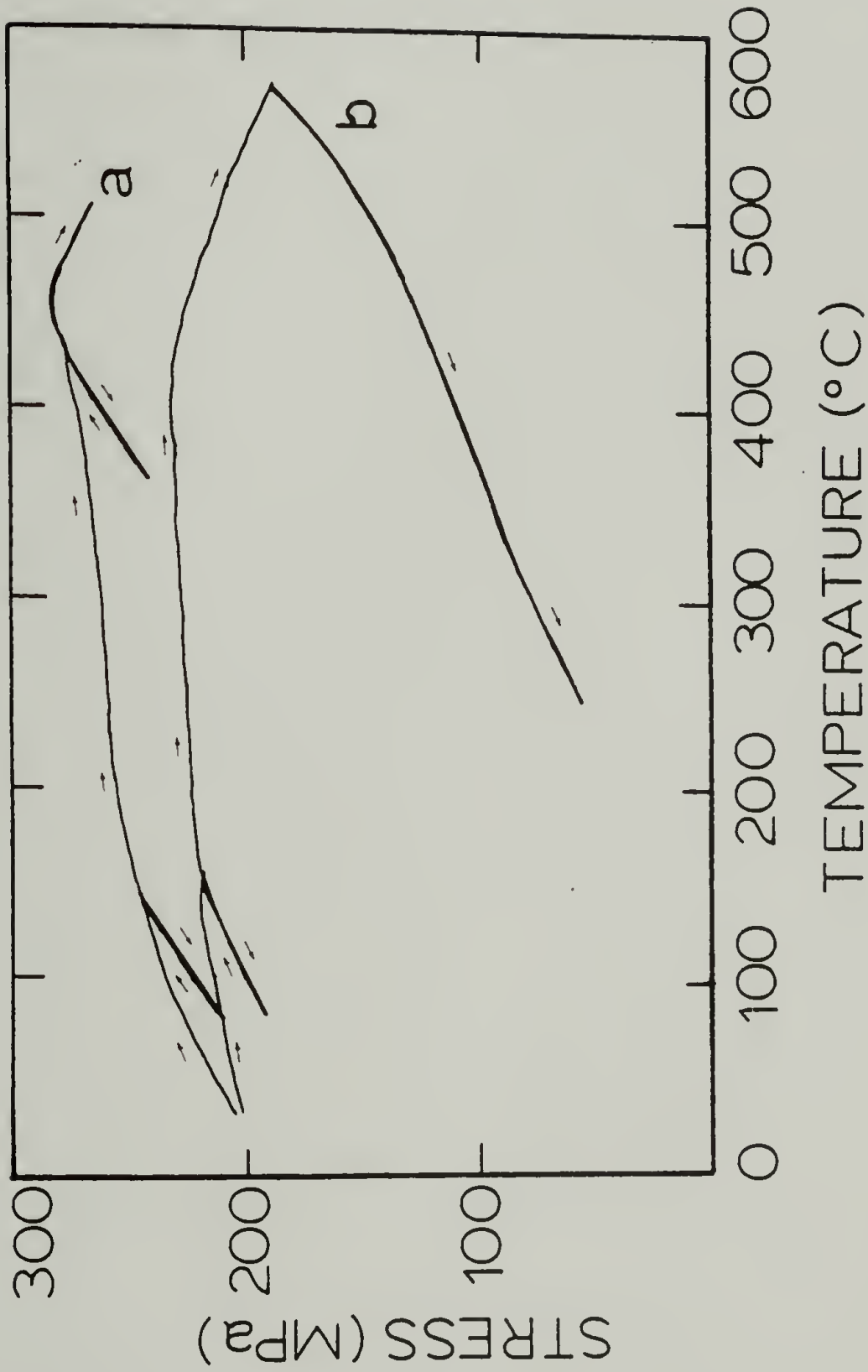


Figure 56. Typical stress-temperature profiles for PBT fiber; (a) non-tension dried 500 C, (b) heat treated at 500 C with no tension

summary of the results in Table 28, the magnitude of the negative axial thermal expansion coefficient for the heat treated fiber is less than the as-spun PBT fiber. These results may be attributed to the increased lateral packing into ordered crystallite domains; thus reducing lateral chain mobility after heat treatment processing. A reduction in thermal expansivity both perpendicular and parallel to the fiber axis may then result.

#### 4.6 Conclusions

The force-temperature (F-T) technique provides a unique way to characterize the thermal stability of variously processed rigid rod aromatic fibers. It is evident that Kevlar<sup>R</sup> 29 and as-spun PBT do not exhibit a linear thermal elastic behavior whereas Kevlar<sup>R</sup> 49, PBT-HT and steel do exhibit such behavior. For as-spun PBT and Kevlar<sup>R</sup> 29, a dramatic stress drop is observed from the F-T curves which is associated to mechanical and structural changes in addition to denier changes with water and acid removal due to the subsequent application of heat and tension.

By implementation of the F-T technique, the processing of these rigid rod fibers can be uniquely analyzed. Increasing the temperature and tension during the initial drying and heat treatment processing increases the degree of thermal stability. However, these fibers do not behave in a thermally reversible manner when subjected to temperatures and tensions in excess of their initial processing conditions. This

Table 28. Calculated thermal expansion coefficients for differently processed PBT fiber VB

Tension applied During Drying	Heat Treatment Temperature (°C)	Conditions Tension (MPa)	Axial Thermal Expansion Coefficients ( $\times 10^{-6} \text{ } ^\circ\text{C}^{-1}$ )
0	-	-	-2.5 $\pm$ .5
0	320	30	-2.0 $\pm$ .5
0	320	300	-2.0 $\pm$ .5
0	500	30	-1.5 $\pm$ .5
0	500	30	-1.0 $\pm$ .5
30	-	-	-2.0 $\pm$ .5
30	320	30	-1.5 $\pm$ .5
30	320	300	-1.0 $\pm$ .5
30	500	30	-1.5 $\pm$ .5
30	500	300	-1.5 $\pm$ .5
800	-	-	-2.5 $\pm$ .5
800	320	30	-1.5 $\pm$ .5
800	320	300	-1.5 $\pm$ .5
800	500	30	-1.0 $\pm$ .5
800	500	300	-1.0 $\pm$ .5

complex history dependent behavior should be carefully considered in any engineering use of Kevlar<sup>R</sup> 29 and as-spun PBT.

F-T investigations provide an indirect analysis of water removal if it is assumed that the magnitude of the stress drop is a direct measure of the water removal. The elimination of water while the fiber is still in a swollen wet state induces better thermal stability as manifested by a reduction in the stress drop in the F-T curve compared to the F-T behavior of a dried fiber heat treated under similar conditions. Although no differences between the macroscopic structural and mechanical properties are detected between elevated temperature dried fibers and PPHT fibers, the increased thermal stability exhibited by the elevated temperature dried fibers may prove advantageous, for example, in composite applications.

A linear correspondence between the temperature at which the stress drop begins,  $T_t$  (thermal input), and the initial stress applied (mechanical input) to induce material changes is found.

The thermal expansion properties have been deduced. For fibers which behave reversibly in this F-T technique the thermal expansion coefficients are evaluated to be approximately  $-(1-2) \times 10^{-6}/^{\circ}\text{C}$  and  $-3 \times 10^{-6}/^{\circ}\text{C}$  for PBT-HT and Kevlar<sup>R</sup> 49, respectively. Furthermore, the product  $E\alpha$  is constant over the temperature ranges examined which suggests that  $E$  and  $\alpha$  are inversely temperature dependent. It is postulated that the temperature dependence of  $\alpha$  and its relationship to the tensile modulus may be related to the anisotropic nature of the fiber. Heat treated PBT has a slightly less negative thermal expansion



coefficient as compared to as-spun PBT. This is possibly a result of decreased chain mobility with increased lateral order upon heat treatment processing.

CHAPTER V  
CONCLUDING REMARKS AND RECOMMENDATIONS

5.1 Overview

Considerable effort has been expended over the last twenty years towards the development of polymeric materials with engineering properties comparable to those of structural metals and ceramics. The U.S. Air Force Materials Lab has been actively involved in the development of polymeric fibers with "high performance" characteristics. A sizable research effort has focused on poly (p-phenylene benzobisthiazole) because of its high thermal and oxidative stability. As a result of the extensive research efforts by scientists at the University of Massachusetts (25), Celanese Research Corp. (43,105,106) and DuPont Co. (50,107) the processing technology has been continually advancing for PBT resulting in fibers with a tensile modulus of approximately 300 GPa and strengths of 3 GPa. Still, these properties fall short of the properties as determined by the polymer's chemical structure. In addition, the PBT fibers possess a maximum compressive strength of approximately 250 MPa which is considerably less than ceramic, glass and graphitic materials. In order to further develop these particular fiber properties for the lyotropic liquid crystalline system, a more thorough understanding of the fiber formation processes is needed.

Thus, the structure and mechanical characteristics of PBT fibers have been investigated from the coagulated state through the drying

process to the as-spun and heat treated state in this dissertation. The major findings of this work are reviewed in the subsections to follow. The role of the coagulation, drying and heat treatment processes on structure and property formation is summarized with suggestions for future work in these three areas of fiber spinning.

## 5.2 Coagulation Process

During coagulation, the polymer system phase separates accompanied by a crystallization process. The resulting wet fiber consists of a swollen macro and microfibrillar crystalline structure composed of highly oriented molecules with axial chain disorder. The existence of an interconnected fibrillar network has been suggested based on the high load bearing capacity of the wet fiber.

A high degree of mechanical anisotropy as evidenced by the relatively high tensile properties with low compressive and shear characteristics is present in the wet fiber. The high tensile modulus is a result of high chain alignment while the weak compressive and shear characteristics are a consequence of the weak lateral interactions between fibrils within the network. The potential for compressive deformation to induce buckling instabilities is enhanced with water serving as the "matrix" for the fibrillar network. In addition, differences observed in the wet tensile properties between fibers spun from low and high concentration spinning solutions at various spin draw ratios may be attributed to different morphologies that develop during coagulation. The swollen fibrillar structure formed during coagulation

appears instrumental in controlling the fiber properties in the wet state.

The morphology and mechanical characteristics of the wet fiber are quite similar to the dry or as-spun fiber. Based on this observation, the coagulation process appears to be a critical step in the development of the fiber properties in the PBT system. Consequently, one approach in which to improve the mechanical properties of PBT fibers is by adequately controlling the initial morphology developed during the coagulation process. At present, a complete understanding concerning the physical aspects of structure formation and its effect on the fiber properties is lacking. Studies on both the thermodynamic and kinetic effects of the phase separation process on the resulting fiber properties are warranted.

### 5.3 Drying Process

The drying process for these rigid rod aromatic solution spun fibers is associated with a distinct radial collapse and axial elongation. The observed change in axial strain with concentration has been predicted to be a function of the hoop and radial shrinkage coefficients as well as axial shrinkage coefficients for fibers which dry under constant stress. The generation of radial, hoop and axial internal stresses are predicted for cylindrically orthotropic materials due to the dimensional changes incurred during the drying process. The predicted internal stresses correspond to axial internal stresses which have been postulated to exist in the as-spun fiber (25).



Despite the formation of internal stresses, structural improvements and enhancements in the mechanical properties in PBT fibers are observed upon drying and may be attributed to removal of water and the resulting collapse of the fibrillar network. While the characteristic mechanical and structural features of the dried fiber develop during coagulation, the drying process serves, then, to perfect the existing coagulated structure.

In an attempt to control the formation of internal shrinkage stresses while optimizing the driving force toward property enhancement with the removal of water, the use of high temperature and high tension has been employed during drying. Through high tension drying, alterations in the tensile properties have been achieved by straightening the wet fibrillar network thus improving the molecular alignment while offsetting compressive internal stresses and preventing the formation of buckles on the fiber. The application of temperature during the drying process serves to improve the lateral molecular order while minimizing internal stresses. Both temperature and tension contribute to a further enhancement in tensile modulus and strength, and play two separate but synergistic roles during the fiber modification stage.

A slight improvement in the shear and compressive characteristics for the PBT system is achieved through the use of high temperature and tension drying. However this property enhancement has only been achieved when the crystalline regions within the fiber are larger than  $100\text{\AA}$ , the average width of the microfibril. Improving the lateral order on a scale less than  $100\text{\AA}$  has only a minimal effect on the transverse



behavior of PBT fiber. These results imply that intermicrofibrillar lateral interactions may be crucial in the development of the compressive strength of PBT. It is believed that by modifying the lateral dimension of the fibrils and microfibrils such that larger crystallite regions may be induced, the compressive and shear characteristic may be significantly altered. Coagulation studies geared toward the generation of larger microfibrils of PBT with the characterization of the final fiber's shear and compressive characteristics are necessary.

The ultimate fiber properties achieved through the rigorous drying process are independent of the processing pathway and appear controlled by the initial properties developed in coagulation. If the compressive and tensile properties of the coagulated fiber are improved, the ultimate fiber properties may be improved. Studies on the effects of high temperature and tension drying on PBT fibers spun utilizing different coagulation conditions would be useful.

The hypothesis above appears to contradict the results of drying studies which compared fibers spun from a 5.5% PBT/PPA and 15.5% PBT/PPA. Although the wet tensile properties of the fibers spun from the low PBT concentration are considerably less than fibers spun from a 15.5% polymer concentration, high tension drying of these two fibers has produced equivalent results. However, fibers spun from a low concentration of PBT undergo a larger collapse (increased enhancement in chain orientation). An increased enhancement in tensile modulus upon drying is observed since the modulus is controlled by the alignment of the molecules. Therefore, the lower tensile moduli initially obtained from

spinning from a low concentration of PBT/PPA may be overcome by utilizing the greater collapse process to improve their tensile moduli. However, studies concerning the influence of the drying process on distinctly different fibrillar networks generated by spinning from different polymer concentrations warrant further attention.

Although the collapse process functions to improve fibrillar alignment, the internal stresses generated do limit the tensile capabilities of the as-spun fiber. Thus, it is desirable to minimize the collapse process; thus eliminating the generation of internal stresses. As discussed in Chapter II, Uy et al. have shown the air dried shrinkage of PBT fiber could be virtually eliminated if the coagulant is carefully selected (50). However, a more detailed study is needed to determine what effect the elimination of internal stresses has on the tensile behavior of these fibers in general.

It is of interest to determine how various morphologies developed during different coagulation processes affect the collapse process. Based upon theories relating to the collapse of wood, the capillary forces generated within the porous structure contribute substantially to this collapse process. Thus by generating different morphologies with varying degrees of porosity, this model may be tested.

Investigations on the collapse process of hollow PBT filaments and its effects on fiber properties would be of interest since it is speculated that residual stresses due to drying may be significantly different in these fibers. Assuming internal stresses in PBT fibers result from shrinkage constraints, modifications in these tensile residual

stresses are expected by inserting a hole down the PBT fiber's center thus removing some of the internal constraint. Studies on the effects of high tension and temperature drying on the properties of hollow PBT filament may be quite interesting and useful in developing a PBT fiber with "improved" properties.

Preliminary studies on the shear moduli for PBT fibers of different diameters have shown that the modulus increases with decreasing fiber size (Table 29). Similar results have been found on poly (p-phenylene benzobisoxazole) (PBO) fibers by M. Hansager (108). The increased shear modulus is believed to be attributed to different skin-core morphologies developed during coagulation and/or drying. Panar et al. (55) have suggested that the "skin" in PPTA fibers is more homogeneous than the core, and consequently, this densely packed skin may exhibit increased torsional rigidity. If a skin in fact exists in the PBT fiber, an increase in shear properties results if the skin comprises a larger cross-section of the fiber and is located on the outer edge of the fiber. The existence of a high volume of a "skin" morphology may be instrumental in the development of the shear and compressive characteristics. The skin-core effects in the PBT fibers and the resulting fiber properties warrant further study.

Due to the structural changes and possible skin formation accompanying the collapse process, the transport processes during the drying of PBT become quite complex. The effects of the collapse process on heat and mass transport phenomena merit further attention. A more complete understanding of how drying occurs in this complex system would

Table 29. Shear characteristics versus diameter size for PBT fiber

PBT Fiber	Diameter ( $\mu\text{m}$ )	Shear Modulus (MPa)
IV	68	675 $\pm$ 50
V	49	602 $\pm$ 40
VI	41	665 $\pm$ 40
VII	35	740 $\pm$ 30
VIII	21	885 $\pm$ 50
VIII	18	925 $\pm$ 60



allow for better control of the drying process and hence the fiber properties.

It has been determined that tension and heat during drying strongly influence the final fiber properties. However, the present understanding of the effects of high tension and temperature on the rate of drying is incomplete. The kinetics of the drying process may be analyzed by monitoring the rate of radial and longitudinal dimensional changes during the fiber's collapse. Investigations monitoring the rate of collapse under hydrostatic pressure, axial tension and high temperature may be useful in assessing the stress and temperature dependent drying behavior.

#### 5.4 Post Processing Heat Treatment

Allen has demonstrated that the PBT fiber's tensile properties may be greatly enhanced by increasing the extent lateral molecular order and chain alignment upon post processing heat treatment (PPHT) (25). Others have found that PPHT results in the elimination of water and residual acid (72,89). Essentially, PPHT is simply a continued drying process. No detectable differences are observed on the tensile, shear, compressive and microstructural characteristics between fibers subjected to a one stage drying process (elevated temperature drying) and those fibers exposed to a two stage drying process (drying and PPHT).

PPHT investigations on the variously dried fibers show that the final fiber properties attained by heat treatment at the highest levels of temperature and tension are equivalent and independent of the



state of the precursor. It is speculated that the final fiber properties achieved through PPHT are controlled by the structure and properties developed during coagulation rather than the properties of the as-spun fiber. It must be noted that producing a "better" as-spun fiber through the drying process does not necessarily produce a "better" tension heat treated fiber. It would be of interest to determine the ultimate achievable properties with PPHT of as-spun fibers attained through different coagulation processes and then implementing high tension and temperature drying processes.

A novel way by which to examine the heat treatment processing of rigid rod fibers has been developed through a Force-Temperature (F-T) technique. For heat treated PBT and Kevlar<sup>R</sup> 49, the F-T behavior is dictated exclusively by thermal expansion effects, whereas for Kevlar<sup>R</sup> 29 and as-spun PBT, a dramatic stress drop is observed. After a sample has been F-T cycled to a given temperature, the subsequent cooling and heating behavior is governed by thermal expansion effects up to the maximum temperature and tension it has seen previously. Force-temperature cycling appears to increase the fiber's denier or linear density, increase the lateral microstructural order and molecular orientation, and enhance the tensile properties. A direct correspondence between the observed stress drop in the F-T profile and mass changes with temperature have been observed. Thus, the dramatic stress drop may be attributed to possible water and acid removal and material alterations with the application of heat and temperature in the F-T experiment. A linear correspondence between the temperature at which the stress drop begins

$T_t$  (thermal input) and the initial stress applied (mechanical input) has been found to induce the material changes.

The above described technique has been used to "fingerprint" the various PBT fibers which underwent various processing conditions. The fibers behave thermally linear elastic when exposed to stresses and temperatures previously experienced. When subjected to temperatures and tension in excess of their initial processing conditions, the F-T profile exhibits the complex history dependent behavior. Based upon the F-T results, it is apparent that both temperature and tension are necessary to induce thermal stability.

### 5.5 Summary

The influence of water and residual acid and their subsequent removal in developing and modifying the fiber properties has been examined herein. The research described is intended to provide further insight into the processing and history of the PBT system prior to the dried and heat treated state. The findings on PBT fibers reported herein further reinforce the importance of the coagulation and drying processes in the development and modification of fiber properties during the solution spinning of rigid rod aromatic systems in general. Such information is invaluable in tailoring the final properties of "high performance" fibers. Although this work focuses on the PBT system, the research reported in this dissertation has intended to provide greater knowledge and further insight into the drying processes during the solution spinning of high polymers overall.

## REFERENCES

1. W.B. Black, "High Modulus/High Strength Organic Fibers," *Ann. Rev. of Mat. Sci.* 10, 311 (1980).
2. A. Cifferi and I.M. Ward, Ultra High Modulus Polymers, Applied Science, London (1979).
3. W.B. Black, "Stiff Chain Aromatic Polymer Solutions, Melts and Fibers," in Flow Induced Crystallization, R.L. Miller (ed.), Gordon Breach, N.Y. (1977).
4. D.C. Prevorsek, "Recent Advances in High Strength Fibers and Molecular Composites," in Polymer Liquid Crystals, A. Ciferri (ed.), Academic Press, N.Y. (1982).
5. G. Capaccio and I.M. Ward, "Properties of Ultra High Modulus Linear Polyethylene," *Nature Phys. Sci.* 243, 143 (1973).
6. M.T. Mead and R.S. Porter, "Recent Developments in Ultramolecular Orientation of Polyethylene by Solid State Extrusion," in Ultra High Modulus Polymers, A. Cifferi (ed.), Applied Science, London (1979).
7. A.J. Pennings and K.E. Meihyzen, "Polyethylene Fibers with Ultra-High Modulus and Strength Produced by Flow Controlled Crystallization," in Ultra High Modulus Polymers, A. Cifferi (ed.), Applied Science, London (1979).
8. P. Smith and P.J. Lemstra, "Ultra High Strength Polyethylene Filaments by Solution Spinning/Drawing," *J. Mater. Sci.*, 15, 505 (1980).
9. T. Kanomoto, A. Tsuruta, K. Tanaka, M. Takeda and R.S. Porter, "On Ultra High Modulus by Drawing Single Crystal Mats of High Molecular Weight Polyethylene," *Polymer J.*, 15, 327 (1983).
10. S.L. Kwolek, "Optically Anisotropic Aromatic Polyamide Dopes," U.S. Patent 3,671,542 (1972). Assigned to DuPont Co.
11. S.L. Kwolek, "Synthesis, Anisotropic Solutions and Fibers of Poly (1-4 Benzamide)," *Macromolecules* 10, 1390 (1977).
12. J. Preston, "Linear Condensation of Polymers Containing Carbonamide and Heterocyclic Linkages," U.S. Patent 3,484,407 (1969). Assigned to Monsanto.



13. J. Preston, W.B. Black and W.L. Hofferbert Jr., "High Modulus Wholly Aromatic Fibers II. Partially Ordered Polyamide-Hydrazides," *J. Macromol. Sci.-Chem.*, 147, 67 (1973).
14. A.J. Sicree, F.E. Arnold and R.L. Van Deusen, "New Imidazoisoquinoline Ladder Polymers," *J. Poly. Sci. Poly. Chem. Ed.*, 12, 265 (1974).
15. R.F. Kovar and F.E. Arnold, "Para-Ordered Polybenzimidazole," *J. Poly. Sci. Poly. Chem. Ed.* 14, 2809 (1976).
16. J.F. Wolfe and F.E. Arnold, "Rigid Rod Polymers 1. Synthesis and Thermal Properties of Para-Aromatic Polymers with 2,6 Benzobisoxazole Units in the Main Chain," *Macromolecules*, 14, 909 (1981).
17. E.W. Choe and S.N. Kim, "Synthesis, Spinning and Fiber Mechanical Properties of Poly(p-phenylene benzobisoxazole), *Macromolecules*, 14, 920 (1981).
18. J.F. Wolfe, B.H. Loo and F.E. Arnold, "Rigid Rod Polymers 2. Synthesis and Thermal Properties of Para-Aromatic Polyamides with 2,6, Benzothiazole Units in the Main Chain," *Macromolecules*, 14, 915 (1981).
19. T.E. Helminiak, "The Air Force Ordered Polymers Research Program: An Overview," *ACS Org. Coat. and Plast. Preprints*, 4, 475 (1979).
20. W.B. Black, J. Preston, H.S. Morgan, G. Raumann, M.R. Lilyquist, "Some Physical and Mechanical Properties of High Modulus Fibers Prepared from All-Para Aromatic Polyamide-Hydrazides," *J. Macromol. Sci. Chem.*, A7, 137 (1973).
21. H. Blades, "Dry-Jet Wet Spinning Process," U.S. Patent 3,767,756 (1973) assigned to duPont.
22. H. Blades, "High Modulus, High Tenacity Poly (p-phenylene terephthalamide) Fiber," U.S. Patent 3,869,430 (1975) assigned to duPont.
23. Kevlar Aramid Data Manual, DuPont Textile Fibers Department (October 1976).
24. E.C. Chenevey, T.E. Helminiak, "The Process of Preparing Shaped Articles of Rigid Rod Heterocyclic Liquid Crystalline Polymers," U.S. Patent Appl.
25. S.R. Allen, Mechanical and Morphological Correlations in Poly (p-phenylene benzobisthiazole) Fibers, Ph.D. Thesis, University of Massachusetts, Amherst, (1983).

26. P.K. Kim, C. Chang and S.L. Hsu, "Normal Vibrational Analysis of a Rigid Rod Polymer: Poly (p-phenylene terephthalamide), submitted to Polymer (1985).
27. W.W. Adams, personal communication.
28. I.M. Ward, "Mechanical Anisotropy at Low Strains," in Developments in Oriented Polymers Vol. 1, I.M. Ward (ed.), Appl. Sci. Pub., Ltd., London (1982).
29. A. Ziabiacki, Fundamentals of Fibre Formation, Wiley Interscience, N.Y. (1976).
30. P.H. Hermans, Physics and Chemistry of Cellulose Fibers, Elsevier Publishing Co. Inc., N.Y. (1949).
31. J.L. White and J.E. Spruiell, "Structure Development in Fiber Formation from Aliphatic Polyamides and Polypeptides," in Fiber Structure and Properties, J. Appl. Poly. Sci. Applied Polymer Symposium, 33, 91 (1976).
32. W.G. Miller, L. Kou, K. Tohyama and V. Voltaggio, "Kinetic Aspects of the Formation of the Ordered Phase in Stiff Chain Helical Polyamino Acids," J. Poly. Sci.: Poly. Symp. 65, 91 (1978).
33. D.R. Paul, "Diffusion During the Coagulation Step of Wet Spinning," J. Appl. Poly. Sci., 12, 383 (1968).
34. V. Groebe and H.J. Heyer, "Diffusion in Wet Spinning of Polyacrylonitrile Filaments IV. Results obtained using aliphatic alcohols as precipitating media," Faserforschung U. Textiltech., 19, 398 (1968).
35. J.P. Knudsen, "The Influence of Coagulation Variables on the Structure and Physical Properties of Acrylic Fiber," Text. Res. J., 33, 13 (1963).
36. J.P. Craig, J.P. Knudsen and V.F. Holland, "Characterization of Acrylic Fiber Structure," Text. Res. J., 32, 435 (1962).
37. J.H. Dumbleton, "The Collapse Process in Acrylic Fibers," J. Appl. Poly. Sci., 14, 2402 (1970).
38. J.P. Bell and J.H. Dumbleton, "Changes in the Structure of Wet Spun Acrylic Fibers During Processing," Text. Res. J., 41, 196 (1971).
39. T.A. Hancock, J.E. Spruiell and J.L. White, "Wet Spinning of Aliphatic and Aromatic Polyamides," J. Appl. Poly. Sci., 21, 1227 (1977).



40. T.A. Hancock, J.L. White and J.E. Spruiell, "Mechanism of Formation of Fluted Void Superstructures in the Coagulation of Wet Spun Fibers and Applications to Membranes," *Poly. Eng. Sci.*, 20, 1126 (1980).
41. J.F. Siau, Transport Processes in Wood, Springer-Verlag, N.Y. (1984).
42. C. Skaar, Water in Wood, Syracuse University Press, N.Y. (1972).
43. H.H. Bosshard, "Shrinkage and Swelling Anisotropy," FOA Fifth Conference on Wood Technology, U.S. Forestry Prod. Lab., Madison, Wisconsin (1963).
44. N.F. Barbes, "A Theoretical Model of Shrinking Wood," *Holzforschung*, 22, 97 (1968).
45. G.J. Ritter and R.L. Mitchell, "Fiber Studies Contributing to the Differential Shrinkage of Cellulose," *Paper Indust.*, 33, 1189 (1952).
46. W.G. Kaufman, "The Influence of Drying Stresses and Anisotropy on Collapse in Eucalyptus Regnan," *Div. of For. Prod. Tech.*, Paper No. 3, CSIRO (1958).
47. J.M. McMillen, "Stress in Wood During Drying," U.S. Dept. Agr. For. Serv. For. Prop. Lab. Report No. 1652 (1958).
48. E.C. Chenevey, "Processing of Rod-Like Polymers, Part II," ARWAL-TR-80-4142 (October 1981).
49. E.L. Thomas, R.J. Farris and S.L. Hsu, "Mechanical Properties versus Morphology of Ordered Polymers," AFML-TR-80-4045 Vol. II (July 1981).
50. W.C. Uy, "Exploratory Development of High Strength, High Modulus Polybenzotiazole Fibers Part I," AFWAL-TR-82-4145 (August 1982).
51. M. Jaffee and R.S. Jones, "High Performance Aramid Fibers," in *Handbook of Fiber Science and Technology Vol. III: High Technology Fibers Pt. A.*, M. Lewin and J. Preston (eds.), Marcel Dekker Inc., N.Y. (1985).
52. S.R. Allen, A.G. Filippov, R.J. Farris and E.L. Thomas, "Macrostructure and Mechanical Behavior of Fibers of Poly-p-phenylene benzobisthiazole," *J. Appl. Poly. Sci.*, 26, 291 (1981).
53. J.R. Minter, Structural Investigations of Fibers and Films of Poly (p-phenylene benzobisthiazole), Ph.D. Thesis, University of Massachusetts, Amherst (1982).

54. M.G. Dobb, D.J. Johnson, A. Majeed and B.P. Saville, "Microvoids in Aramid Type Fibrous Polymers," *Polymer*, 20, 1284 (1979).
55. M. Panar, P. Avakian, R.C. Blume, K.H. Gardner, T.D. Gierke and H.H. Yang, "Morphology of Poly (p-phenylene terephthalamide) Fibers," *J. Poly. Sci. Poly. Phys. Ed.*, 21, 1955 (1983).
56. L.S. Li, L.F. Allard and N.C. Biegelow, "On the Morphology of Aromatic Polyamide Fibers (Kevlar, Kevlar 49, PRD-49)," *J. Macromole. Sci. Phys.*, 22, 269 (1983).
57. W.W. Adams, L.V. Azaroff and A.K. Kulshreshtha, "X-ray Diffraction by a Nematic Polybenzothiazole Fiber," *Zeit. Krist.*, 150, 321 (1979).
58. E.J. Roche, T. Takahashi, and E.L. Thomas, "Structure of High Modulus Fibers of Poly-p-phenylene benzobisthiazole," *Amer. Chem. Soc. Symp.*, Fiber Diffraction Methods, 141, 303 (1980).
59. M.G. Northolt, "X-ray Diffraction Study of Poly (p-phenylene therphthalamide) Fibers," *European Polymer Journal*, 10, 799 (1974).
60. M.G. Dobb, D.J. Johnson and B.P. Saville, "Direct Observation of Structure in High Modulus Aromatic Fibers," *J. Poly. Sci. Pol. Symp.* 58, 237 (1977).
61. E.L. Thomas, R.J. Farris and S.L. Hsu, "Mechanical Properties Versus Morphology of Ordered Polymers," AFML-TR-80-4045, Vol. III (August 1982).
62. S.J. DeTeresa, S.R. Allen, R.J. Farris, and R.S. Porter, "Compressive and Torsional Behavior of Kevlar 49 Fiber," *J. Mat. Sci.*, 19, 57 (1984).
63. S.J. DeTeresa, Axial Compressive Strength of High Performance Polymer Fibers, Ph.D. Thesis, University of Massachusetts (1985).
64. S.J. DeTeresa, R.S. Porter, R.J. Farris, "A Model for the Compressive Buckling of Extended Chain Polymers," *J. Mat. Sci.* (in press 1985).
65. C.R. Crosby III, N.C. Ford, F.E. Karasz, K.H. Langley, "Depolarized Dynamic Light Scattering of a Rigid Rod Macromolecule PBT," *J. Chem. Phys.* 79, 4298 (1981).
66. G.C. Berry, P. Metzger, S. Venkatramen, D.B. Cotts, "Properties of Rodlike Polymers in Solution," *ACS Polymer Preprints Polymer Chemistry Division* 20, 42 (1979).

67. A.J. Perry, B. Ineichen, and B. Eliasson, "Fibre Diameter Measurements by Laser Diffraction," *J. Mat. Sci.* 9, 1376 (1974).
68. L.E. Alexander, X-ray Diffraction Methods in Polymer Science, Robert E. Kreiger Publishing Co., N.Y. (1979).
69. ASTM D3379-75e Standard Test Method for Tensile and Young's Modulus of High Modulus Single Filament Materials, ASTM, Philadelphia (1975).
70. R.J. Farris, private communication.
71. Y. Cohen and E.L. Thomas, "Structure Formation During Spinning of Poly p-phenylenebenzobisthiazole Fiber" (submitted to *Polymer Engineering and Science* 1985).
72. R.J. Farris, M.F. Malone, E.L. Thomas, "Molecular Composites: Processing Post Treatment and Properties," Air Force Quarterly Report, Oct. 1-Dec. 30, 1984.
73. C. Chang and S.L. Hsu, "Spectroscopic Analysis of Poly (p-phenylene benzobisthiazole) Films," *J. Polym. Sci., Polym. Phys. Ed.* (in press 1985).
74. K. Tohyama and W. Miller, "Network Structure in Gels of Rod-like Polypeptides," *Nature*, 289, 813 (1981).
75. E.L. Thomas, Y. Cohen, H. Frost and L.A. Pottick, "Phase Transformation and Structure Development in Rigid Rod Solutions," presented at International Fiber Conference, Japan, August 19-23 (1985).
76. R.J. Morgan, C.O. Pruneda, W.J. Steele, "The Relationship between the Physical Structure and the Microscopic Deformation and Failure Processes of Poly (p-phenylene terephthalamide) Fibers," *J. Poly. Sci. Polym. Phys. Ed.*, 21, 1757 (1983).
77. G.C. Alfonso, E. Bianchi, A. Ciferri, S. Russo, F. Salaris, and B. Valenti, "Ultra High Modulus Fibers from Rigid and Semirigid Aromatic Polyamides," *J. Pol. Sci.: Polym. Symp.* 65, 213 (1978).
78. P.W. Morgan, "Synthesis and Properties of Aromatic and Extended-Chain Polyamides," *Polymer Preprints, Amer. Chem. Soc. Div. Polym. Chem.* 17, 47 (1976).
79. R.C. Weast and M.J. Astle, CRC Handbook of Chemistry and Physics, 61st edition, CRC Press Inc. (1981).
80. J. Brandrup and E. Immergut, Polymer Handbook, Interscience, N.Y. (1966).



81. E.L. Ellwood, P.A. Ecklund, E. Zavarin, "Collapse of Wood and Exploratory Experiments to Prevent Its Occurrence," Univ. of Cal. For. Prod. Lab. Report (1959).
82. A.P. Boressi, O.M. Sidebottom, F.B. Seely, and J.O. Smith, Advanced Mechanics of Material, John Wiley and Sons, N.Y. (1978).
83. J. Bodig and B.A. Jayne, Mechanics of Wood and Wood Composites, Van Nostrand Reinhold Company (1982).
84. R.F.S. Hearman, The Elasticity of Wood and Plywood, Department of Scientific and Industrial Research, Forest Products Research, Special Report #7, His Majesty Stationery Office, London (1948).
85. S.G. Lekhnitskii, Theory of Elasticity of an Anisotropic Elastic Body, Holden Day, Inc., San Francisco (1963).
86. M. Htun, "The Influence of Drying Strategies on Paper Strength," in Progress in Paper Physis Seminar, Design Criteria for Paper Performance, Swedish Forest Products Research Lab., Stockholm, Sweden, June 25-29, 1984.
87. E.G. Jones, J.M. Pickard and D.L. Pedrick, "Thermal Degradation of Polymers and Mechanisms of Curing in AT-Polymer Systems," AFWAL-TR-80-4154 (1980).
88. R.S. Stein, S. Krimm and A.V. Tobolsky, "An Investigation of the Relationship Between Polymer Structure and Mechanical Properties. III. A Thermodynamic and Optical Analysis of the Behavior of Polyethylene, Polyvinyl Chloride and Lactoprene," Text. Res. J., 19, 325 (1949).
89. F. DeCandia, R. Russo, V. Vittoria, A. Peterlin, "Shrinkage and Retractive Forces During the Annealing of Drawn Low-Density Polyethylene," J. Polym. Sci.: Polym. Phys. Ed., 20, 1175 (1982).
90. D.R. Buchanan and C.L. Hardegree, "Thermal Stress Analysis of Textile Yarns," Text. Res. J., 47, 732 (1977).
91. D. Luch and G.S.Y. Yeh, "Morphology of Strain Induced Crystallization of Natural Rubber. 1. Electron Microscopy on Uncrosslinked Thin Film," J. Appl. Phys., 43, 4326 (1972).
92. D.X. Wang, R.E. Lyon, R.J. Farris, "Force-Temperature Behavior of Polyurethanes Elastomeric Fibers Under Statis Stretching Detonation" (submitted to Journal of Macromolecular Science (1983)).
93. M. Chipalkatti, J. Hutchinson and R.J. Farris, private communication.

94. L.H. Van Vlack, Elements of Material Science and Engineering, Addison Wesley Publishing Co. (1975), Appendix C.
95. M. Jaffee, "Chapter 6: Fibers," Thermal Characterization of Polymeric Materials (ed. E.A. Turi), Academic Press (1981).
96. R.M. Kimmel, Fiber Society Lecture data presented in Thermal Characterization of Polymeric Materials, Chapter 7, ed. E. Turi, Academic Press, N.Y. (1981).
97. R.S. Porter, N.E. Weeks, N.J. Capiati, R.J. Krzcuki, J. Therm. Anal. 8, 547 (1975).
98. C.L. Choy, "Thermal Expansivity of Oriented Polymers," in Developments in Oriented Polymers, I.M. Ward (ed.), Applied Science Publishers, London (1982).
99. J.J. Aklonis, W.J. MacKnight, and M. Sahen, Introduction to Polymer Viscoelasticity, Wiley Interscience, N.Y. (1972).
100. R.E. Lyon, Thermodynamics of Deformation, Ph.D. Thesis, University of Massachusetts, Amherst (1985).
101. O.L. Blakslee, D.G. Proctor, E.L. Seldin, G.B. Spence and T. Weng, "Elastic Constants of Compression Annealed Pyrolytic Graphite," J. Appl. Physics 41, 3373 (1970).
102. J.T. Meers, "Properties of Manufactured Graphite," in Encyclopedia of Chemical Technology, 3rd ed. (ed. M. Grayson), Chapter 4, Vol. 4, John Wiley and Sons, N.Y. (1978).
103. R. Bacon, "Carbon Fibers From Rayon Precursors," in Chemistry and Physics of Carbon, Vol. 9 (eds. P.L. Walker Jr. and P.A. Throver), Marcel Dekker Inc., N.Y. (1973).
104. duPont Technical Information Report, "Characteristics and Uses of Kevlar 29 Aramid," (1976).
105. E.C. Chenevey, "Processing of Rod-Like Polymers, Part I," AFWAL-TR-80-4142 (July 1980).
106. E.C. Chenevey, "Processing of Rod-Like Polymers, Part III," AFWAL-TR-80-4142 (December 1982).
107. J.F. Mammone and W.C. Uy, "Exploratory Development of High Strength, High Modulus Polybenzothiazole Fibers, Part II: Fiberization Scale-Up and Optimization," AFWAL-TR-82-4154, Part II, May 1984.
108. M. Hansager, private communication.



## BIBLIOGRAPHY

- Adams, W.W., Azaroff, L.V., and Kulshreshth, A.K., "X-ray Diffraction by a Nematic Polybenzothiazole Fiber," *Zeit. Krist.*, 150, 321 (1979).
- Aklonis, J.J., MacKnight, W.J., and Sahen, M., Introduction to Polymer Viscoelasticity, Wiley Interscience, N.Y. (1972).
- Alexander, L.E., X-ray Diffraction Methods in Polymer Science, Robert E. Kreiger Publishing Co., N.Y. (1979).
- Alfonso, G.C., Bianchi, E., Ciferri, A., Russo, S., Salaris, F., and Valenti, B., "Ultra High Modulus Fibers from Rigid and Semirigid Aromatic Polyamides," *J. Pol. Sci.: Poly. Symp.* 65, 213 (1978).
- Allen, S.R., Filippov, A.G., Farris, R.J., and Thomas, E.L., "Macrostructure and Mechanical Behavior of Fibers of Poly-p-phenylene benzobisthiazole," *J. Appl. Poly. Sci.*, 26, 291 (1981).
- Allen, S.R., Mechanical and Morphological Correlations in Poly (p-phenylene benzobisthiazole) Fibers, Ph.D. Thesis, University of Massachusetts, Amherst (1983).
- ASTM D3379-75e Standard Test Method for Tensile and Young's Modulus of High Modulus Single Filament Materials, ASTM, Philadelphia (1975).
- Bacon, R., "Carbon Fibers From Rayon Precursors," in Chemistry and Physics of Carbon, Vol. 9 (eds. P.L. Walker Jr. and P.A. Thrower), Marcel Dekker Inc., N.Y. (1973).
- Barbes, N.F., "A Theoretical Model of Shrinking Wood," *Holzforschung*, 22, 97 (1968).
- Bell, J.P. and Dumbleton, J.H., "Changes in the Structure of Wet Spun Acrylic Fibers During Processing," *Textile Research Journal*, 41, 196 (1971).
- Berry, G.C., Metzger, P., Venkatramen, S., and Cotts, D.B., "Properties of Rodlike Polymers in Solution," *ACS Polymer Preprints Polymer Chemistry Division* 20, 42 (1979).
- Black, W.B., Preston, J., Morgan, H.S., Raumann, G., and Lilyquist, M.R., "Some Physical and Mechanical Properties of High Modulus Fibers Prepared from All-Para Aromatic Polyamide-Hydrazides," *J. Macromol. Sci. Chem.*, A7, 137 (1973).
- Black, W.B., "Stiff Chain Aromatic Polymer Solutions, Melts and Fibers," in Flow Induced Crystallization, R.L. Miller (ed.), Gordon Breach, N.Y. (1977).

- Black, W.B., "High Modulus/High Strength Organic Fibers," *Annual Review of Material Science*, 10, 311 (1980).
- Blades, H., "Dry-Jet Wet Spinning Process," U.S. Patent 3,767,756 (1973) assigned to duPont.
- Blades, H., "High Modulus, High Tenacity Poly (p-phenylene terephthalamide) Fiber," U.S. Patent 3,869,430 (1975) assigned to duPont.
- Blakslee, O.L., Proctor, D.G., Seldin, E.L., Spence, G.B., and Weng, T., "Elastic Constants of Compression Annealed Pyrolytic Graphite," *J. Appl. Physics* 41, 3373 (1970).
- Bodig, J. and Jayne, B.A., Mechanics of Wood and Wood Composites, Van Nostrand Reinhold Company (1982).
- Boressi, A.P., Sidebottom, O.M., Seely, F.B., and Smith J.O., Advanced Mechanics of Material, John Wiley and Sons, N.Y. (1978).
- Bosshard, H.H., "Shrinkage and Swelling Anisotropy," FOA Fifth Conference on Wood Technology, U.S. Forestry Prod. Lab., Madison, Wisconsin (1963).
- Brandrup, J. and Immergut, E., Polymer Handbook, Interscience, N.Y. (1966).
- Buchanan, D.R. and Hardegree, C.L., "Thermal Stress Analysis of Textile Yarns," *Text. Res. J.*, 47, 732 (1977).
- Capaccio, G. and Ward, I.M., "Properties of Ultra High Modulus Linear Polyethylene," *Nature Phys. Sci.* 243, 143 (1973).
- Chang, C. and Hsu, S.L., "Spectroscopic Analysis of Poly (p-phenylene benzobisthiazole) Films," *J. Polym. Sci., Polym. Phys. Ed.* (in press 1985).
- Chenevey, E.C., "Processing of Rod-Like Polymers, Part I," AFWAL-TR-80-4142 (July 1980).
- Chenevey, E.C., "Processing of Rod-Like Polymers, Part II," ARWAL-TR-80-4142 (October 1981).
- Chenevey, E.C., "Processing of Rod-Like Polymers, Part III," AFWAL-TR-80-4142 (December 1982).
- Chenevey, E.C., and Helminiak, T.E., "The Process of Preparing Shaped Articles of Rigid Rod Heterocyclic Liquid Crystalline Polymers," U.S. Patent Appl.

- Choe, E.W. and Kim, S.N., "Synthesis, Spinning and Fiber Mechanical Properties of Poly (p-phenylene benzobisoxazole), *Macromolecules*, 14, 920 (1981).
- Choy, C.L., "Thermal Expansivity of Oriented Polymers," in Developments in Oriented Polymers, I.M. Ward (ed.), Applied Science Publishers, London (1982).
- Cifferi, A. and Ward, I.M., Ultra High Modulus Polymers, Applied Science, London (1979).
- Cohen, Y. and Thomas, E.L., "Structure Formation During Spinning of Poly p-phenylenebenzobisthiazole Fiber" (submitted to *Polymer Engineering and Science* 1985).
- Craig, J.P., Knudsen, J.P., and Holland, V.F., "Characterization of Acrylic Fiber Structure," *Textile Research Journal*, 32, 435 (1962).
- Crosby, C.R. III, Ford, N.C., Karasz, F.E., and Langley, K.H., "Depolarized Dynamic Light Scattering of a Rigid Rod Macromolecule PBT," *J. Chem. Phys.* 79, 4298 (1981).
- DeCandia, F., Russo, R., Vittoria, V., and Peterlin, A., "Shrinkage and Retractive Forces During the Annealing of Drawn Low-Density Polyethylene," *J. Polym. Sci.: Polym. Phys. Ed.*, 20, 1175 (1982).
- DeTeresa, S.J., Allen, S.R., Farris, R.J., and Porter, R.S., "Compressive and Torsional Behavior of Kevlar 49 Fiber," *J. Mat. Sci.*, 19, 57 (1984).
- DeTeresa, S.J., Axial Compressive Strength of High Performance Polymer Fibers, Ph.D. Thesis, University of Massachusetts (1985).
- DeTeresa, S.J., Porter, R.S., and Farris, R.J., "A Model for the Compressive Buckling of Extended Chain Polymers," *J. Mat. Sci.* (in press 1985).
- Dobb, M.G., Johnson, D.J., and Saville, B.P., "Direct Observation of Structure in High Modulus Aromatic Fibers," *J. Poly. Sci. Pol. Symp.*, 58, 237 (1977).
- Dobb, M.G., Johnson, D.J., Majeed, A., and Saville, B.P., "Microvoids in Aramid Type Fibrous Polymers," *Polymer*, 20, 1284 (1979).
- Dumbleton, J.H., "The Collapse Process in Acrylic Fibers," *J. Appl. Poly. Sci.*, 14, 2402 (1970).
- duPont Technical Information Report, "Characteristics and Uses of Kevlar 29 Aramid" (1976).



- Ellwood, E.L., Ecklund, P.A., and Zavarin, E., "Collapse of Wood and Exploratory Experiments to Prevent Its Occurrence," Univ. of Cal. For. Prod. Lab. Report (1959).
- Farris, R.J., Malone, M.F., and Thomas, E.L., "Molecular Composites: Processing Post Treatment and Properties," Air Force Quarterly Report, Oct. 1-Dec. 30, 1984.
- Groebe, V., and Beyer, H.J., "Diffusion in Wet Spinning of Polyacrylonitrile Filaments IV. Results Obtained Using Aliphatic Alcohols as Precipitating Media," *Faserforschund U. Textiltech.*, 19, 398 (1968).
- Hancock, T.A., Spruiell, J.E., and White, J.L., "Wet Spinning of Aliphatic and Aromatic Polyamides," *J. Appl. Poly. Sci.*, 21, 1227 (1977).
- Hancock, T.A., White, J.L., and Spruiell, J.E., "Mechanism of Formation of Fluted Void Superstructures in the Coagulation of Wet Spun Fibers and Applications to Membranes," *Poly. Eng. Sci.*, 20, 1126 (1980).
- Hearman, R.F.S., The Elasticity of Wood and Plywood, Department of Scientific and Industrial Research, Forest Products Research, Special Report #7 His Majesty Stationery Office, London (1948).
- Hermans, P.H., Physics and Chemistry of Cellulose Fibers, Elsevier Publishing Co. Inc., N.Y. (1949).
- Helminiak, T.E., "The Air Force Ordered Polymers Research Program: An Overview," *ACS Org. Coat. and Plast. Preprints*, 4, 475 (1979).
- Hunt, M., "The Influence of Drying Strategies on Paper Strength," in *Progress in Paper Physis Seminar, Design Criteria for Paper Performance* Swedish Forest Products Research Lab., Stockholm, Sweden, June 25-29, 1984.
- Jaffee, M., "Chapter 6: Fibers," Thermal Characterization of Polymeric Materials (ed. E.A. Turi), Academic Press (1981).
- Jaffee, M. and Jones, R.S., "High Performance Aramid Fibers," in *Handbook of Fiber Science and Technology Vol. III: High Technology Fibers Pt. A.*, M. Lewin and J. Preston (eds.), Marcel Dekker Inc., N.Y. (1985).
- Jones, E.G., Pickard, J.M. and Pedrick, D.L., "Thermal Degradation of Polymers and Mechanisms of Curing in AT-Polymer Systems," AFWAL-TR-804154 (1980).
- Kanomoto, T., Tsuruta, A., Tanaka, K., Takeda, M., and Porter, R.S., "On Ultra High Modulus by Drawing Single Crystal Mats of High Molecular Weight Polyethylene," *Polymer J.*, 15, 327 (1983).

Kaufman, W.G., "The Influence of Drying Stresses and Anisotropy on Collapse in Eucalyptus Regnan," Div. of For. Prod. Tech., Paper No. 3, CSIRO (1958).

Kevlar Aramid Data Manual, duPont Textile Fibers Department (October 1976).

Kim, P.K., Chang, C., and Hsu, S.L., "Normal Vibrational Analysis of a Rigid Rod Polymer: Poly (p-phenylene terephthalamide), submitted to Polymer (1985).

Kimmel, R.M., Fiber Society Lecture data presented in Thermal Characterization of Polymeric Materials, Chapter 7, ed. E. Turi, Academic Press, N.Y. (1981).

Knudsen, J.P., "The Influence of Coagulation Variables on the Structure and Physical Properties of Acrylic Fiber," Textile Research Journal, 33, 13 (1963).

Kovar, R.F. and Arnold, F.E., "Para-Ordered Polybenzimidazole," J. Poly. Sci. Poly. Chem. Ed. 14, 2809 (1976).

Kwolek, S.L., "Optically Anisotropic Aromatic Polyamide Dopes," U.S. Patent 3,671,542 (1972).

Kwolek, S.L., "Synthesis, Anisotropic Solutions and Fibers of Poly 1-4 Benzamide," Macromolecules 10, 1390 (1977).

Lekhnitskii, S.G., Theory of Elasticity of an Anisotropic Elastic Body, Holden Day, Inc., San Francisco (1963).

Li, L.S., Allard, L.F., and Biegelow, N.C., "On the Morphology of Aromatic Polyamide Fibers (Kevlar, Kevlar 49, PRD-49)," J. Macromole. Sci. Phys., 22, 269 (1983).

Luch, D. and Yeh, G.S.Y., "Morphology of Strain Induced Crystallization of Natural Rubber. 1. Electron Microscopy on Uncrosslinked Thin Film," J. Appl. Phys., 43, 4326 (1972).

Lyon, R.E., Thermodynamics of Decormation, Ph.D. Thesis, University of Massachusetts, Amherst (1985).

Mammone, J.F. and Uy, W.C., "Exploratory Development of High Strength, High Modulus Polybenzothiazole Fibers, Part II: Fiberization Scale-Up and Optimization," AFWAL-TR-82-4154, Part II, May 1984.

McMillen, J.M., "Stress in Wood During Drying," U.S. Dept. Agr. For. Serv. For. Prop. Lab. Report No. 1652 (1958).



Mead, M.T. and Porter, R.S., "Recent Developments in Ultramolecular Orientation of Polyethylene by Solid State Extrusion," in Ultra High Modulus Polymers, A. Cifferi (ed.), Applied Science, London (1979).

Meers, J.T., "Properties of Manufactured Graphite," in Encyclopedia of Chemical Technology, 3rd ed. (ed. M. Grayson), Chapter 4, Vol. 4, John Wiley and Sons, N.Y. (1978).

Miller, W.G., Kou, L., Tohyama, K., and Voltaggio, V., "Kinetic Aspects of the Formation of the Ordered Phase in Stiff Chain Helical Polyamino Acids," *J. Poly. Sci.: Poly. Symp.* 65, 91 (1978).

Minter, J.R., Structural Investigations of Fibers and Films of Poly (p-phenylene benzobisthiazole), Ph.D. Thesis, University of Massachusetts, Amherst (1982).

Morgan, P.W., "Synthesis and Properties of Aromatic and Extended-Chain Polyamides," *Polymer Preprints, Amer. Chem. Soc. Div. Polym. Chem.* 17, 47 (1976).

Morgan, R.J., Pruneda, C.O., and Steele, W.J., "The Relationship Between the Physical Structure and the Microscopic Deformation and Failure Processes of Poly (p-phenylene terephthalamide) Fibers," *J. Poly. Sci. Polymer Physic. Ed.*, 21, 1757 (1983).

Northolt, M.G., "X-ray Diffraction Study of Poly (p-phenylene terphthalamide) Fibers," *European Polymer Journal*, 10, 799 (1974).

Panar, M., Avakian, P., Blume, R.C., Gardner, K.H., Gierke, T.D., and Yang, H.H., "Morphology of Poly (p-phenylene terephthalamide) Fibers," *J. Poly. Sci. Poly. Phys. Ed.*, 21, 1955 (1983).

Paul, D.R., "Diffusion During the Coagulation Step of Wet Spinning," *J. Appl. Poly. Sci.*, 12, 383 (1968).

Pennings, A.J. and Meihyzen, K.E., "Polyethylene Fibers with Ultra-High Modulus and Strength Produced by Flow Controlled Crystallization," in Ultra High Modulus Polymers, A. Cifferi (ed.), Applied Science, London (1979).

Perry, A.J., Ineichen, B., and Eliasson, B., "Fibre Diameter Measurements by Laser Diffraction," *J. Mat. Sci.* 9, 1376 (1974).

Porter, R.S., Weeks, N.E., Capiati, N.J., and Krzcuki, R.J., *J. Therm. Anal.* 8, 547 (1975).

Preston, J., U.S. Patent 3,484,407 (1979), assigned to Monsaoto, "Linear Condensation of Polymers Containing Carbonamide and Heterocyclic Linkages."

- Preston, J., Black, W.B., and Hofferbert, W.L. Jr., "High Modulus Wholly Aromatic Fibers II. Partially Ordered Polyamide-Hydrazides," *J. Macromol. Sci.-Chem.*, 147, 67 (1973).
- Prevorsek, D.C., "Recent Advances in High Strength Fibers and Molecular Composites," in *Polymer Liquid Crystals*, A. Ciferri (ed.), Academic Press, N.Y. (1982).
- Ritter, G.J. and Mitchell, R.L., "Fiber Studies Contributing to the Differential Shrinkage of Cellulose," *Paper Indust.*, 33, 1189 (1952).
- Roche, E.J., E.J., Takahashi, T., and Thomas, E.L., "Structure of High Modulus Fibers of Poly-p-phenylene benzobisthiazole," *Amer. Chem. Soc. Symp., Fiber Diffraction Methods*, 141, 303 (1980).
- Siau, J.F., *Transport Processes in Wood*, Springer-Verlag, N.Y. (1984).
- Sicree, A.J., Arnold, F.E., and Van Deusen, R.L., "New Imidazoisquinoline Ladder Polymers," *J. Poly. Sci. Poly. Chem. Ed.*, 12, 265 (1974).
- Skaar, C., *Water in Wood*, Syracuse University Press, N.Y. (1972).
- Smith, P. and Lemstra, P.J., "Ultra High Strength Polyethylene Filaments by Solution Spinning/Drawing," *J. Mater. Sci.*, 15, 505 (1980).
- Stein, R.S., Krimm, S., and Tobolsky, A.V., "An Investigation of the Relationship Between Polymer Structure and Mechanical Properties. III. A Thermodynamic and Optical Analysis of the Behavior of Polyethylene, Polyvinyl Chloride and Lactoprene," *Text. Res. Journal*, 19 (1949).
- Thomas, E.L., Farris, R.J., and Hsu, S.L., "Mechanical Properties Versus Morphology of Ordered Polymers," AFML-TR-80-4045 Vol. II (July 1981).
- Thomas, E.L., Farris, R.J., and Hsu, S.L., "Mechanical Properties Versus Morphology of Ordered Polymers," AFML-TR-80-4045, Vol. III (August 1982).
- Thomas, E.L., Cohen, Y., Frost, H., and Pottick, L.A., "Phase Transformation and Structure Development in Rigid Rod Solutions," presented at International Fiber Conference, Japan, August 19-23 (1985).
- Tohyama, K. and Miller, W., "Network Structure in Gels of Rod-like Polypeptides," *Nature* 289, 813 (1981).
- Uy, W.C., "Exploratory Development of High Strength, High Modulus Polybenzotiazole Fibers Part I," AFWAL-TR-82-4145 (August 1982).
- Van Vlack, L.H., *Elements of Material Science and Engineering*, Addison Wesley Publishing Co. (1975), Appendix C.

- Wang, D.X., Lyon, R.E., and Farris, R.J., "Force-Temperature Behavior of Polyurethanes Elastomeric Fibers Under Static Stretching Detonation" (submitted to Journal of Macromolecular Science (1983)).
- Ward, I.M., "Mechanical Anisotropy at Low Strains," in Developments in Oriented Polymers Vol. 1, I.M. Ward (ed.), Appl. Sci. Pub., Ltd., London (1982).
- Weast, R.C. and Astle, M.J., CRC Handbook of Chemistry and Physics, 61st edition, CRC Press Inc. (1981).
- White, J.L. and Spruiell, J.E., "Structure Development in Fiber Formation from Aliphatic Polyamides and Polypeptides," in Fiber Structure and Properties, J. Appl. Poly. Sci. Applied Polymer Symposium, 33, 91 (1976).
- Wolfe, J.F. and Arnold, F.E., "Rigid Rod Polymers 1. Synthesis and Thermal Properties of Para-Aromatic Polymers with 2,6 Benzobisoxazole Units in the Main Chain," Macromolecules, 14, 909 (1981).
- Wolfe, J.F., Loo, B.H., and Arnold, F.E., "Rigid Rod Polymers 2. Synthesis and Thermal Properties of Para-Aromatic Polyamides with 2,6 Benzothiazole Units in the Main Chain," Macromolecules, 14, 915 (1981).
- Ziabiacki, A., Fundamentals of Fibre Formation, Wiley Interscience, N.Y. (1976).

## APPENDIX

### LIST OF PUBLICATIONS

Parts of this dissertation appear in the open literature in the following publications:

L.A. Pottick, S.R. Allen and R.J. Farris, "Force-Temperature Behavior of Rigid Rod Polymeric Fibers," J. Appl. Poly. Sci., 29, 3915 (1984).

L.A. Pottick and R.J. Farris, "Linear and Non-Linear Thermoelastic Behavior of High Modulus/High Strength Poly (p-phenylene benzobisthiazole) and Kevlar Fibers," Polymer Preprints, ACS Division of Polymer Chemistry, 25, 209 (1984).

L.A. Pottick and R.J. Farris, "The Effect of Tension During Drying on the Structure and Mechanics of Poly (p-phenylene benzobisthiazole) Fibers," Poly. Eng. Sci., 25, 284 (1985).

L.A. Pottick and R.J. Farris, "Alterations in the Structure and Mechanics of Poly (p-phenylene benzobisthiazole) Fibers Due to the Collapse Process During Drying," TAPPI Proceeding: 1985 Non Wovens Symposium, 85, 65 (1985).



